Hyaluronan (HA) glycopolymers and self-assembling HA-binding peptides: a synthetic toolbox for probing HA-peptide/protein interactions and creating supramolecular HA biomaterials

Dominic W. P. Collis

School of Engineering and Material Science, Queen Mary University of London

Primary Supervisor: Dr Helena S. Azevedo

Secondary Supervisor: Dr C. Remzi Becer

Date: 28th September 2018

Required statement of originality

I, Dominic W. P. Collis, confirm that the research included within this thesis is my own work or that where it has been carried out in collaboration with, or supported by others, that this is duly acknowledged below, and my contribution indicated. Previously published material is also acknowledged below.

I attest that I have exercised reasonable care to ensure that the work is original and does not to the best of my knowledge break any UK law, infringe any third party's copyright or other Intellectual Property Right, or contain any confidential material.

I accept that the College has the right to use plagiarism detection software to check the electronic version of the thesis.

I confirm that this thesis has not been previously submitted for the award of a degree by this or any other university.

The copyright of this thesis rests with the author and no quotation from it or information derived from it may be published without the prior written consent of the author.

Signature:

Date:

Abstract

Hyaluronan (HA) is a highly abundant anionic polysaccharide found throughout mammalian connective tissues. Unlike other glycosaminoglycans, HA is non-sulfated and its alternating chemical structure is invariable. Despite its simplicity, HA is involved in the extracellular matrix organization and many other aspects of cell behaviour. Using HA as a model polymer, we took inspiration to design and synthesize glycopolymers based on HA and self-assembling HA-binding peptides.

Glycopolymers provide an alternative to conventional polysaccharides by offering the possibility to display sugars across the polymer at defined densities, while providing a robust polymer backbone rather than the glycosidic bonds, potentially forming more stable biomaterials with similar biological activity. The synthesis of alternating, homo and statistical HA neoglycopolymers was achieved via reversible addition fragmentation chain transfer (RAFT) polymerisation. The monosaccharides are grafted onto the polymers backbone by post-polymerisation click reactions to achieve the desired glycopolymers. These glycopolymers share some properties of native HA, such as water solubility and negative charge. Binding studies showed the ability of these glycopolymers to interact with HA-binding peptides and proteins, whilst not presenting any cytotoxicity behaviour. This approach provides control over the type and variation of saccharides, not be possible using natural HA, suggesting their potential use in mechanistic studies to understand HA binding processes.

Peptides, on the other hand, have received increasing interest as potential biomaterials due to their inherent biocompatibility and biodegradability. Peptides can be engineered to drive their self-assembly into defined nanostructures, such as micelles and fibers. By designing HA-binding peptides with self-assembling properties, their combination with natural HA resulted in the formation of supramolecular hydrogels or membranes. Whilst the synthesis of large molecules like proteins is still a challenge, peptide synthesis is relatively simple and their self-assembly can result in nanomaterials with structures and functions resembling proteins.

The synthetic molecules described in this thesis can be used as probes to better understand the role and binding of HA as well as reveal new applications.

Acknowledgement

Table of Contents

List of Figures

List of Tables

List of Schemes

Abbreviations

ζ	Zeta
$(CH_3)_3SiN_3$	Trimethylsilyl Azide
% .wt	Weight Percentage
2OST	2-O-sulfotransferase
6OST	6-O-sulfotransferases
Ac_2O	Acetic Anhydride
AcOH	Acetic Acid
AcONa	Sodium Acetate
Ada	Adamantane
AEA	Azidoethyl Acrylate
Al_2O_3	Aluminium Oxide
aPTT	Activated Partial Thromboplastin Time
Ar	Argon
AROP	Anionic Ring-opening Polymerisation
AT	Antithrombin
atm	Atmosphere
ATRP	Atom Transfer Radical Polymerisation
Au	Gold
Au-NP	Gold Nanoparticle
BDTMP	Butyl 2-(((dodecylthio)carbonothioyl)thio)2-methyl propionate
BEA	Bromoethyl Acrylate
$BF_3.OEt_2$	Boron Trifluoride Etherate
Boc	tert-Butyloxycarbonyl
BSPP	Bis(p-Sulfonatophenyl) Phenylphosphine
C4ST	Chondroitin 4-O-sulfotransferase
C6ST-1	Chondroitin 6-O-sulfotransferase
Ca^{2+}	Calcium
CAC	Critical Aggregation Concentration
Cd	Cyclodextrin
CD	Circular Dichroism
CD44	Cluster of Differentiation 44
Chst1	Gal 6-O-sulfotransferase
Cit	Citrate
Cl	Chloride
COSY	Correlation Spectroscopy (COSY)
CROP	Cationic Ring-opening Polymerisation
CRP	Controlled Radical Polymerisation
CS	Chondroitin Sulfate
CTA	Chain Transfer Agent
Cu(I)Br	Copper (I) Bromide
CuAAC	Copper Azide Alkyne Cycloaddition
CuI	Copper (I) iodide
$CuSO_4.5H_2O$	Copper Sulphate Pentahydrate
Đ	Polydispersity
Da	Dalton
DBU	1,8-Diazabicyclo[5.4.0]undec-7-ene
DC	Dendritic Cell

DC-SIGN	Dendritic Cell-Specific Intercellular adhesion molecule-3-Grabbing Non-integrin
DCC	N,N'-Dicyclohexylcarbodiimide
DCM	Dichloromethane
DDR	Discoidin Domain Receptors
DIAD	Diisopropyl Azodicarboxylate
DIC	N,N′-Diisopropylcarbodiimide
DIEA	N,N-Diisopropylethylamine
DIFO	Difluorinated Cyclooctyne
Dil-PA	Diluent Peptide Amphiphile
DLS	Dynamic Light Scattering
DMAP	4-Dimethylaminopyridine
DMF	Dimethyl Formaldehyde
DMSO	Dimethyl Sulfoxide
DP	Degree of Polymerisation
DRI	Differential Refractive Index
DS	Dermatan Sulfate
ECM	Extrasellar Matrix
EDC	1-Ethyl-3-(3-dimethylaminopropyl)carbodiimide
EDX	X-ray spectroscopy
ELISA	Enzyme-Linked Immunosorbent Assay
ESI-MS	Electrospray Ionisation Mass Spectroscopy
Et_2O	Diethyl ether
EtOAc	Ethyl Acetate
EXT	Exostosin-like
F/I	Fluorescent Intensity
FGF	Fibroblast Growth Factor
FRP	Free Radical Polymerisation
FT-IR	Fourier Transform Infrared
G	Glycine
GAG	Glycosaminoglycan
Gal	Galactose
GalNAc	N-acetylgalactosamine
GalNAc4S-6ST	4-sulfate 6-O-sulfotransferase
GalNAcT-I	GalNAc transferase I
GalNAcT-II	GalNAc transferase II
GDNF	Glial Cell-Derived Neurotrophic Factor
GF	Growth Factor
Glc	Glucose
GlcA	Glucuronic Acid
GlcAT-II	GlcA transferase II
GlcNAc	N-Acetyl-Glucosamine
GPC	Gel Permeation Chromatography
H_2NNH_2	Hydrazine
H_2O	Water
H_2O_2	Hydrogen Peroxide
H_2O_2	Hydrogen Peroxide
H_2SO_4	Sulphuric Acid
HA	Hyaluronic Acid
HABP	Hyaluronic Acid Binding Protiens

HABPA	Hyaluronic Acid-Binding Peptide Amphiphiles
HABPep	Hyaluronic Acid-Binding Peptides
HAS	Hyaluronic Acid Synthase
HBTU	(2-(1H-benzotriazol-1-yl)-1,1,3,3-tetramethyluronium hexafluorophosphate
HCII	Heparin Cofactor II
HCl	Hydrochloric Acid
HCV	Hepatitis C virus
HDA	Hetero-Diels alder
HIV	Human Immunodeficiency Virus
HMDI	Methylene bis(4-cyclohexyl isocyanate)
HOBt	Hydroxy benzotriazole
HOMO	Highest Occupied Molecular Orbital
HS	Heparan Sulfate
Hs2st	HS 2-O-sulfotransferase
HYAL	Hyaluronidases
I	Iodine
IC_{50}	Half Maximal Inhibitory Concentration
IdoA	Iduronic acid
iGnT	β-1,3-N-acetylglucosaminyltransferase
IPA	Isopropan-2-ol
IPDI	Isophorone Diisocyanate
ITC	Isothermal Titration Calorimetry
K_2CO_3	Potassium Carbonate
k_a	Association Constant
K_a	Equilibrium association constant
K_{act}	Rate of activation
K_{ATRP}	Rate of Atom Transfer Radical Polymerisation
K_D	Equilibrium dissociation constant
k_d	Dissociation Constant
K_{deact}	Rate of deactivation
KOH	Potassium hydroxide
k_p	Rate of Polymerisation
K_p^{app}	Rate of Consumption
KS	Keratin Sulfate
LPO	Lauroyl Peroxide
LUMO	Lowest Unoccupied Molecular Orbital
LYVE-1	Lymphatic Vessel Endothelial Hyaluronan Receptor 1
MAh	Maleic Anhydride
MALDI-ToF	Matrix-Assisted Laser Desorption Ionization Time of Flight
Man	Mannose
ManA	Mannuronic acid
ManNAc	N-acetyl-D-mannose
MASP	MBL-associated serine protease
MB	Membrane Bound
MB	Membrane Bound
MBL	Mannose Binding Lectin
Me_6Tren	Tris[2-(dimethylamino)ethyl] amine
MeI	Methyl Iodide
MeOH	Methanol

MgSO$_4$	Magnesium Sulphate
MIC	Minimum Inhibitory Concentration
M$_n$	Number Average Molecular Weight
M$_p$	Peak Molecular Weight
MS	Mass Spectroscopy
Mtt	4–methyltrityl
M$_w$	Weight Average Molecular Weight
n-BuLi	n-Butyl Lithium
N$_2$	Nitrogen
N$_3$	Azide
Na	Sodium
NaBH$_4$	Sodium Borohydride
NaHCO$_3$	Sodium Carbonate
NaN$_3$	Sodium Azide
NaOMe	Sodium Methoxide
NBu$_4$Br	Tetra-n-Butylammonium Bromide
NDST	N-deacetylase/N-sulfotransferase-1
NGF	Nerve Growth Factor
NK	Natural Killer
NMP	Nitroxide Mediated Polymerisation
NMR	Nuclear Magnetic Resonance
NOE	Nuclear Overhauser Effect
OH	Hydroxide
PA	Peptide Amphiphile
PAPS	3′-phosphoadenyl-5′-phosphosulfate
Pbf	2,2,4,6,7-Pentamethyldihydrobenzofuran-5-sulfonyl
PE	Polyelectrolyte
PFS	Pentaflurostyrene
PG	Proteoglycan
pI	Isoelectric Point
pKa	Dissociation constant
PMI	N-propargyl maleimide
ppm	Parts per million
PT	Prothrombin Time
pVBAz	Poly (Vinylbenzyl) azide
pVBC	Poly (Vinylbenzyl) chloride
QCM	Quartz Crystal Microbalance
RAFT	Reversible Addition Fragmentation Chain-Transfer
RHAMM	Receptor for Hyaluronan Mediated Motility
RI	Refractive Index
RIP	Relative Inhibitory Potency
ROMP	Ring-opening Metathesis Polymerisation
ROP	Ring-opening Polymerisation
Ru	Ruthenium
SA	Self-assembly
SAXS	Small Angle X-ray Scattering
SEM	Scanning Electron Microscopy
SET-LRP	Single-Electron Transfer Living Radical Polymerisation
SnCl$_4$	Tin (IV) Chloride

SP	Soluble Protein
SP-A	Surfactant Protein-A
SP-D	Surfactant Protein-D
SPAAC	Strain-promoted azide-alkyne [3+2] cycloaddition
SPPS	Solid Phase Peptide Synthesis
SPR	Surface Plasmon Resonance
St	Styrene
TBA	Tetrabutylammonium Ion
TDI	Toluene 2,4-Diisocyanate
TEM	Transmission Electron Microscope
Temp	Temperature
TEMPO	2,2,6,6-tetramethyl-1-piperidynyl-N-oxy
TFA	Trifluoracetic Acid
THF	Tetrahydrofuran
Thiol-HABPep	Thiolated-Hyaluronic Acid Binding Peptides
TIS	Triisopropylsilane
TLR	Toll-Like Receptor
TMS	Trimethylsilyl
TMS-Cl	Trimethylsilyl Chloride
TMS-PMI	N-Trimethylsilyl propargyl maleimide
Trt	Trityl
TSG-6	Tumour necrosis factor-inducible gene 6
TT	Thrombin Time
UDP	Uridine Diphosphate
UST	Uranyl 2-O-sulfotransferase
UV	Ultraviolet
V601	Radical Initiator
VBAz	Vinylbenzyl Azide
VBC	Vinylbenzyl Chloride
Vis	Visible light
VWD	Variable Wavelength Detector
XPS	X-ray photoelectron spectroscopy
Xyl	Xylose
α	Alpha
β	Beta
βGal-T1	β-1,4-galactosyltransferase
ρ	Conversion

Chapter 1 Glycopolymers as Synthetic Analogues of Natural Glycosaminoglycans

1.1. Glycosaminoglycans

1.1.1. Structure

Glycosaminoglycans (GAGs) are a family of polysaccharides highly abundant in animal tissues. The GAG family is composed of five polysaccharides (Figure 1.1): chondroitin sulfate (CS), dermatan sulfate (DS), heparan sulfate (HS), keratan sulfate (KS), and hyaluronic acid (HA). These polysaccharides are linear, highly charged, with a repetitive alternating unit. This unit consists of a disaccharide made of an amino sugar, such as N-acetylgalactosamine (GalNAc) or N-acetyl glucosamine (GlcNAc), linked to a uronic acid such as glucuronic acid (GlcA) or iduronic acid (IdoA). In the case of KS, a hexose monosaccharide of galactose (Gal) is used rather than a hexuronic acid[1].
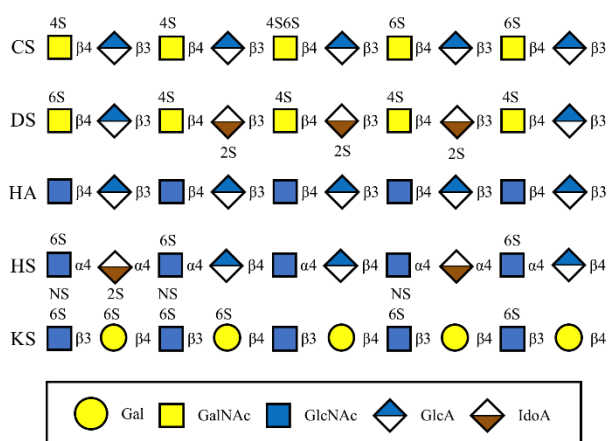
Figure 1.1 The various disaccharide structures of the GAGs repeat disaccharide.

These polysaccharides differ in their degree of sulfonation, even within the same polysaccharide. For example, HS has different degrees of sulfonation. The sulfonation position varies among each GAG as well as the heteroatom which is sulfonated. The sulfonated GAGs have the ability to bind covalently to core proteins to form proteoglycans (PGs) as listed in Table 1.1. These PGs can be found predominantly either in the extracellular matrix (ECM) or on the cell surface, representing a large group of glycoproteins found in the body[2].

Table 1.1. List of proteoglycans and their localisation in human tissues[2-3].

GAG-PG	Proteoglycan	Localization	Tissue Distribution
HS-PG	Perlecan	ECM	basement membranes, other ECM, cartilage
	Agrin	ECM	basement membranes, brain and neuromuscular junctions
	Collagen XVIII	ECM	basement membranes, longest isoform more widespread
	Syndecan 1-4	MB	most nucleated cells
	Glypican 1-6	MB	epithelial and mesenchymal cells, brain
	Betaglycan	MB	fibroblasts
	Serglycin	IG	mast cells, other leukocytes, endothelial cells
CS-PG (DS-PG)	Aggrecan	ECM	cartilage, brain
	Versican	ECM	pericellular and interstitial ECM; blood vessels; brain, leukocytes
	Neurocan	ECM	brain
	Brevican	ECM	brain-perineuronal nets
	Decorin	ECM	connective tissue cells
	Biglycan	MB/ECM	connective tissue cells, macrophages
	Phosphacan	MB	brain
	Thrombomodulin	MB	endothelial cells, but also a variety of nonvascular cells
	CD44	MB	widely distributed including lymphocytes
	NG2	MB	some stem cells, glial progenitors, vascular mural cells, melanocytes
KS-PG	Lumican	ECM	widely distributed
	Keratocan	ECM	widely distributed but sulfated only in the cornea
	Fibromodulin	ECM	widely distributed
	Mimecan	ECM	widely distributed but sulfated only in the cornea
	SV2	MB	synaptic vesicles
	Aggrecan	ECM	cartilage, brain

ECM: Extracellular Matrix; MB: Membrane-Bound; IG: Intracellular Granule.

HA is the only non-sulfonated GAG and it does not form covalent bonds with proteins to produce PGs, like sulfonated GAGs. Instead, HA interacts with various HA-binding proteins (HABPs) such as those listed in Table 1.2.

Table 1.2. Natural HA-binding proteins (HABPs) also known as hyaladherins

HABP	Localisation	Roles
TSG-6 [4]	ECM	Cell-matrix interaction regulator during inflammation and tumorigenesis
TLR4 [5]	MB	Inflammatory Response
CD38 [6]	MB	Mediation of cell binding to HA
CD44 [7]	MB	Mediation of cell binding to HA
LYVE-1 [8]	MB	Lymphatic endothelial cell marker for HA degradation
Link Protein [9-11]	ECM	G1 HA-binding domain of Aggrecan, Versican and Neurocan
HAS [12]	MB	HA synthesis
HYAL [12]	MB	HA degradation
RHAMM [13-14]	SP, MB	Cell migration and proliferation signaling and inflammation cascade

ECM; Extracellular Matrix, MB; Membrane-Bound, SP; Soluble Protien.

1.1.2. Biosynthesis and Sulfonation

1.1.2.1. Biosynthesis

CS, DS and HS are synthesised in the endoplasmic reticulum or the Golgi compartments[15-16]. They are formed sequentially on a tetrasaccharide of GlcAβ1–3Galβ1–3Galβ1–4Xylβ1–O-Ser (Scheme 1.1a) known as the GAG-protein linker. The serine residue is used to anchor the GAG-protein linker covalently to the core protein whilst the polysaccharide is systematically built up from the corresponding uridine diphosphate (UDP) saccharide donors, producing structures up to 70 kDa in weight[17]. The formation of CS is triggered by the first addition of GalNAc via GalNAc transferase I (GalNAcT-I) after which point the saccharides of CS are added sequentially by GlcA transferase II (GlcAT-II) and GalNAc transferase II (GalNAcT-II)[15].

Compared to CS, the formation of HS is triggered by the first addition of GlcNAc, rather than GalNAc onto the GAG-protein linker. Once the pentasaccharide is formed, the HS synthases of Exostosin-like (EXT) enzymes; EXT1 and EXT2 catalyse the addition of GlcA and GlcNAc respectively[18-19]. Using a C5-epimerase, the GlcA adjacent to a GlcNAc of the HS chains can be converted to IdoA. This conversion, however, does not convert all the GlcA to IdoA and therefore generates HS possessing both hexuronic acid epimers, leading to different disaccharide units within the HS.

DS and CS are epimers of one another, with the two-compounds differing in the position of the acid group. These two are formed by the use of C5 isomerisation of the

GlcA on CS to IdoA, but, again, this epimerisation is not quantitative so within DS, chain regions of the original CS chain remain[17, 20].
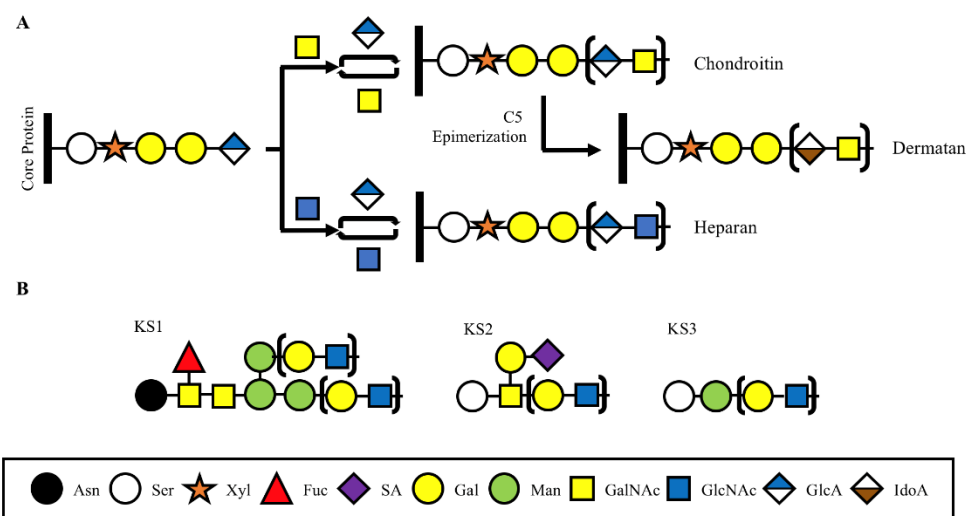
Scheme 1.1. Schematic of the GAG-protein linker (A) from which CS and HS are formed depending on the first saccharide added to the GAG-protein linker, followed by the epimerization of CS to form DS. (B) The 3 linkers from which KS can be enzymatically polymerised upon[21].

In comparison, KS is synthesised by alternative routes as well as three different KS chains dependent on the localisation of the KS. KSI was discovered in the corneal tissue, whilst KSII was found in cartilage and KSIII found recently in the brain. There is a 10-fold difference in the amount of KSI in the cornea compared to KSII in cartilage with 2 to 4 orders of magnitude more than KS in any other tissue. Whilst KS itself is a linear molecule, the linker used during the biosynthesis is not (Scheme 1.1b), with the KS chain of KSI being produced as both a monoantennary or a biantennary oligosaccharide structure[21]. KS is formed in various lengths of the disaccharide by β-1,4-galactosyltransferase (βGal-T1) and β-1,3-N-acetylglucosaminyltransferase (iGnT) enzymes responsible for the biosynthesis of KS. Once complete, the nonreducing ends of the KS chains are terminated with either a neuraminic acid, βGalNAc or αGal[22].

Whilst sulfonated GAGs are formed in the Golgi, HA is synthesised at the plasma membrane by HA synthases (HAS). These HASs are split into 3 subgroups: HAS1, HAS2 and HAS3. Whilst these share structural similarities (55-75%) they bind HA with different affinities leading to the synthesis of different size strands Large strands of 2000 kDa are formed by HAS1 and HAS2, whilst HAS3 forms smaller stands, between 100-1000 kDa using UDP saccharide donors of GlcA and GlcNAc. Upon synthesis, these strands are extruded into the extracellular space.

1.1.2.2. Sulfonation

Sulfonation of GAGs is achieved through sulfotransferases using activated sulfate 3′-phosphoadenyl-5′-phosphosulfate (PAPS) as the sulfonate donor. KS is sulfonated by GlcNAc 6-O-sulfotransferases[23] and one Gal 6-O-sulfotransferase[24] (Chst1) leading to sulfonate groups on both 6' positions. However, in the cornea, the Gal residues of KS are only partially sulfonated[21]. Compared to KS, CS is a more complex molecule to sulfonate due to the various different products possible (Figure 1.2). The majority of the CS chains ends up 4-O-sulfation at the GalNAc by chondroitin 4-O-sulfotransferase (C4ST) of which there are 3 (C4ST-1, C4ST-2 & C4ST-3)[15], these lead to the formation of CS-A and CS-B (DS), which have previously undergone C-5 epimerisation (Figure 1.2). A small set of CS has a 6-O-sulfation at the GalNAc by chondroitin 6-O-sulfotransferase (C6ST-1)[24] to form CS-C. CS-C can undergo a second sulfonation pathway by uranyl 2-O-sulfotransferase (UST)[25] to form CS-D. CS-A can also undergo a second sulfonation pathway by GalNAc 4-sulfate 6-O-sulfotransferase (GalNAc4S-6ST) to form CS-E.
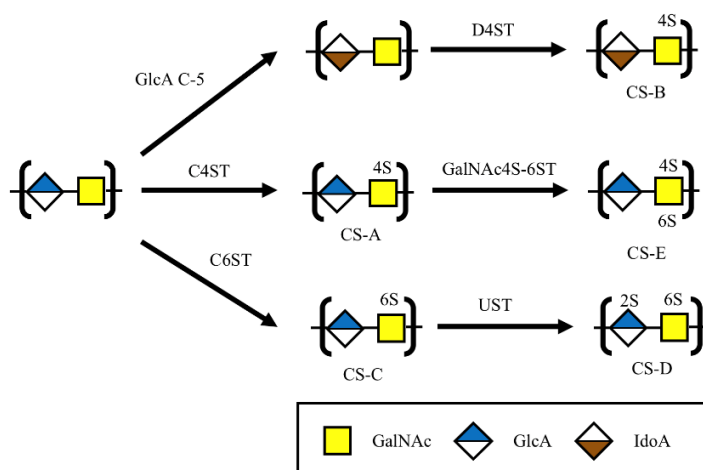
Figure 1.2. Sulfonation pathway for CS and DS. Figure adapted from Hiroshi 2013[15]

HS also has multiple potential sites for sulfonation. However, the first of these sulfonation pathways is the N-deacetylation and N-sulfonation. This N-substitution is facilitated by N-deacetylase/N-sulfotransferase-1 (NDST), but this reaction again is not quantitative leading to regions rich in N-sulfonation HS. EXT-1 and EXT-2 levels have been shown to affect this NDST ability to sulfonate at the N-acetyl group[19]. This has an impact on the remaining sulfonation pathways as N-sulfonation-rich areas have been shown to lead to further sulfonation, whilst N-acetyl-rich areas show a lack of sulfonation[26]. The C5 of HS can also undergo epimerisation, leading to the 2-O-

sulfation by a 2-O-sulfotransferase (2OST) for the majority of the IdoA units formed. The high degree of sulfonation allows HS to interact with multiple proteins such as growth factors. To this end, there are three 6-O-sulfotransferases (6OST1-3) and seven 3-O-sulfotransferases leading to a total of ten O-sulfotransferases for HS. The rich number of sulfotransferases, as well the incomplete sulfonation and selectively of some enzymes to pre-existing sulfonations, lead to a large array of HS repeats[18].

1.1.3. Biological Roles and Function

Whilst GAGs have more defined structures, compared to other biological molecules, such as the 4 base pairs that form DNA or the 20 amino acids of peptides and proteins, they play a large role in biological process including[27]: cell adhesion, proliferation and migration, through protein-carbohydrate interactions. The variations in saccharide epimers, the degree of sulfonation and the PGs bound to the GAG leads to a multitude of properties.

1.1.3.1. Extracellular Matrix

The ECM[28] is a key non-cellular component found in tissues and organs acting as a physical scaffold for cells to proliferate, migrate and differentiate as well as fill the majority of the extracellaur space. The ECM is made up of various components and compositions depending on the type of tissue, but it is primarily made of water, polysaccharides, including elements of the GAG family, and proteins such as collagen and fibronectin. Through the interactions of HA and the Link Proteins the formation of the ECM is achieved by the "link" of large aggregates of PGs, such as aggrecan in cartilage (Figure 1.3) and Perlecan with a central HA core.
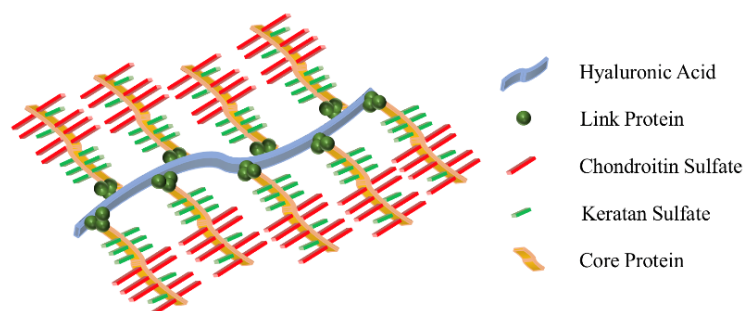
Figure 1.3. Structure of aggrecan with the CS and KS attached to the core protein connected to HA through the link protein. Adapted from Dicker 2014[12]

Through integrins, discoidin domain receptors (DDRs), cell surface PGs, and CD44, cells adhere to the ECM[1]. By varying the construct of the ECM different roles can be achieved for example a Perlecan based ECM plays a role in glomerular filtration in kidney glomerular[29]. Whereas association of PGs such as Decorin, Biglycan, Lumican with collagen fibres produces a ECM which is highly hydrated as well as mechanically stable, but collagen association with elastin in the ECM provides tissue with the ability to recoil. These matrices create an adaptive structure that can be remodelled by enzymes, physiological conditions or as part of a disease for example tumorigeneses which leads to the formation of fibrotic stroma from the ECM[30].

1.1.3.2. Inflammation and Wound Healing

Upon damage in the body, the inflammatory system works to protect the body using a cascade of reactions to activate inflammatory or immune cells. Within the wound healing process, CS/DS and CSPG/DSPGs become hydrated to swell within the wound[31] with more than 50% concentration of the GAG at the wound being DS, that activates growth factors (GF) resulting in early coagulation. Within the first two weeks, the upregulation of high molecular weight HA by fibroblasts seals the wound. The binding of HA to TNF-stimulated gene-6 (TSG-6) modulates inflammation by inhibiting neutrophil migration[32] and uses a negative feedback loop to inhibit plasmin[33]. The binding of HA to CD44 leads to the build-up of leukocytes to sites of inflammation[34]. The other GAGs within the matrix, such as CS and DS, facilitate the polymerisation of collagen and the regulation of GF. HS has been shown to bind to GFs and control their release when necessary[35], modulating the proangiogenic effects in the new tissue[36]. GAGs and other ECM components, such as fibrin, fibronectin and collagen, work together in tandem with cells to repair the injured tissue. HA and CS-A play vital antioxidant roles to inhibit the Haber–Weiss reaction and Fenton reaction caused by oxidation stress[37-38].

1.1.3.3. Coagulation

HS is a well-known anti-coagulator and is used as blood thinning supplements to treat a range of thrombotic disorders. HS binds primarily to antithrombin (AT) through a pentasaccharide (Figure 1.4). A dodecasaccharide, comprised of two pentamers linked by an IdoA and terminated at the non-reducing end by 4,5-unsaturated uronic acid,

can also be used to bind to AT. In a HS chain, approximately 0.5-10% of the sequence has the corresponding AT pentasaccharide sequence[39].
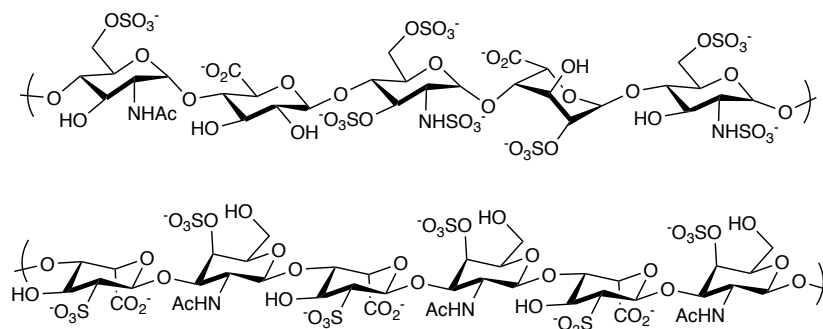
Figure 1.4. Anticoagulation oligosaccharide binding sequences of (top) HS antithrombin binding pentasaccharide and (bottom) DS HCII binding hexasaccharide.

DS has also been shown to inhibit coagulation by binding to heparin cofactor II (HCII) through a hexasaccharide (Figure 1.4), whilst only 5% of the DS sequence contains the pentasaccharide[40]. Though, compared to DS, HS binds with a 5 times higher affinity to HCII in comparison to DS. By binding to AT or HCII, thrombin and factor IXa and Xa are suppressed to prevent coagulation. These factors inhibit downstream coagulation cascade enzyme factors Xa and IXa inhibition (Figure 1.5)
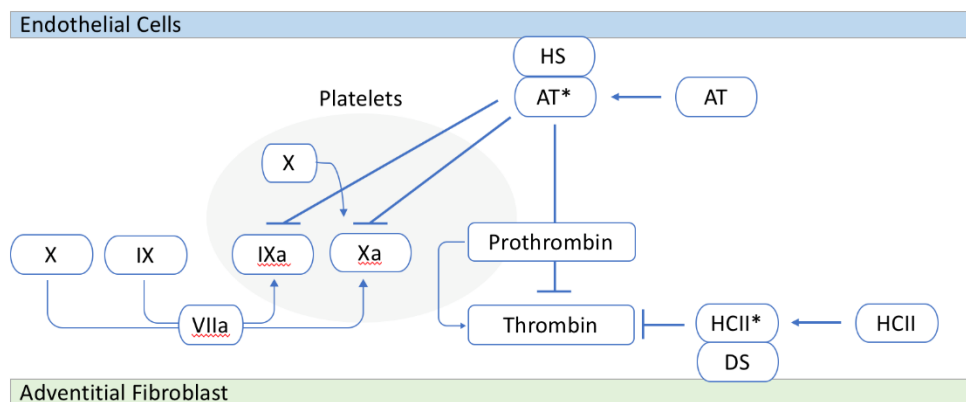
Figure 1.5. Activation pathways for anti-coagulation by HS and DS through AT and HCII binding. (*Activated). Figure adapted from Tollefsen 2010[40]

1.1.3.4. Neuronal Growth

GAGs are known to play a role in the neuronal pathway growth by directing the axon growth. Through neuronal promotion by interactions between the GAGs as well as laminin, an immunoglobin super family of cell adhesion. Whereas numerous numbers of glycoproteins, proteins and proteoglycans repel the growth of the axon. Through the use of both promoting and repelling molecules the axon through is guided towards the target[41-42]. From all the GAGS, CS and HS have been shown to be vital in axon growth, affecting the temporal and spatial distribution of the GAG around the growing axon. Downregulation and removal of CS during the development of axons leads to the uncontrolled growth of the axon into abnormal areas[43]. In a study by Schachner[44], the downregulation of various CS factors was tested against the growth of motor axons. In this instance, the downregulation of CS-C caused no change in axon growth. However, the downregulation of CS-A and CS-B reduced/increased growth inferring that the sulfonation of CS is critical to axon growth. Additionally, mice lacking the HS 2-O-sulfotransferase (Hs2st) and HS 6-O-sulfotransferase 1 showed axon defects indicating that the sulfonation of HS is also important to the direction of the axon growth[45]. Whilst KS and DS have been shown to be involved in axon growth, the higher sulfonated GAGs have shown to be vital to control the growth of axons.

GAGs have a large variety of biological roles that could be utilised to treat many diseases as well as be used as building blocks to develop new biomaterials. As described, there is a large amount of molecular machinery involved in the formation of the different GAGs. To form these GAGs through chemical synthesis would require protection and deprotection stages in order to form the even small GAG oligomers. Whilst automated synthesisers are commercially available to aid in the production of carbohydrates, they are unable to form carbohydrates with the efficiency seen in a peptide or a phosphonamidite synthesis, with a need still for the vast number of reactions to form the starting monosaccharides.

1.2. Glycosaminoglycan Mimics

Glycopolymers provide a simpler alternative method to conventional carbohydrate synthesis. Glycopolymers are synthetic polymers containing carbohydrates. The synthesis of these is a growing sub-field of polymer chemistry, due to their potential biomedical applications, such as in neuronal regeneration and anticoagulation as well as to probe the binding affinity to carbohydrate-protein binding sites in lectins to trigger downstream effects. They bring together two key components: the sugar moieties, which are biologically active through the recognition by specific proteins, and a stable polymer backbone. The polymer backbone enables rapid polymerisation avoiding the formation of glycosidic bonds. Currently, polymers can be produced with high precision over polydispersity (Đ), the degree of polymerisation[46-47] (DP) and sequence[48-53] through controlled radical polymerisation methods, such as reversible addition fragmentation chain transfer (RAFT)[54], atom-transfer radical-polymerisation (ATRP)[55] and single-electron transfer living radical polymerisation (SET-LRP)[56]. The synthesis of glycopolymers has utilised click chemistry[57] as regioselective and chemoselective reactions to link the saccharide unit to either a monomer, for pre-polymerisation modification, or orthogonally in post-polymerisation[58]. With a large array of polymerisation methods, monomers and chemoselective reactions available, more complex glycopolymers are being designed and synthesised[59-60]. This ability to produce complex glycopolymers has made it possible to produce glycopolymers based on the more challenging structures of the GAGs.

1.2.1. Chondroitin Sulfate Mimics

A glycopolymer based on the CS-E repeating unit was produced by the Hsieh-Wilson group in 2008[61]. After protection of the hydroxyls, the CS dimer was coupled to a cyclooctene monomer. After selective sulfonation of the 4' and 6' hydroxyls on the galactosamine ring, the monomer was polymerised via ring-opening metathesis polymerisation (ROMP) (Scheme 1.2). The group also showed the extension from the dimer to tetramer, which was also polymerised by ROMP. By tuning the mol% of the 3rd generation Grubbs catalyst, the polymer could be grown to large molecular weights of 119,000 Da with a narrow Đ of 1.33. The model of ROMP can be applied to other CS-based monomers. As CS is involved the control of axon growth, these CS-based glycopolymers also showed increased control over axon growth with increasing DP.

In a follow-up study, the Hsieh-Wilson group produced the norbornene equivalent of the cyclooctene[62].

The use of norbornene increases ring rigidity after the polymerisation of the double bond, whereas cyclooctene produces degrees of freedom within the bonds after polymerisation, aiming to control the orientation of the glycopolymer. By this constrained system, CS glycopolymers were obtained with a Đ range of 1.17 - 1.05 and molecular weights of 280,000 Da, approaching the molecular weights of CS in nature. The addition of biotin allowed the binding of the polymer chains on a streptavidin-coated plate. The CS-E disaccharide used was bound to CS-E selective fluorescently labelled antibody, with CS-C fluorescently labelled antibody showing no binding. The group also tested glial cell-derived neurotrophic factor (GDNF), which also showed selectivity for the areas upon the plates with the glycopolymer bound. The assays highlighted the importance of sulfonation since the non-sulfonated variant of the glycopolymer showed no binding towards any of the antibodies or proteins. These two examples from the Hsieh-Wilson group provided a synthetic route to a CS-E mimic as well as a pathway to form other CS mimics.
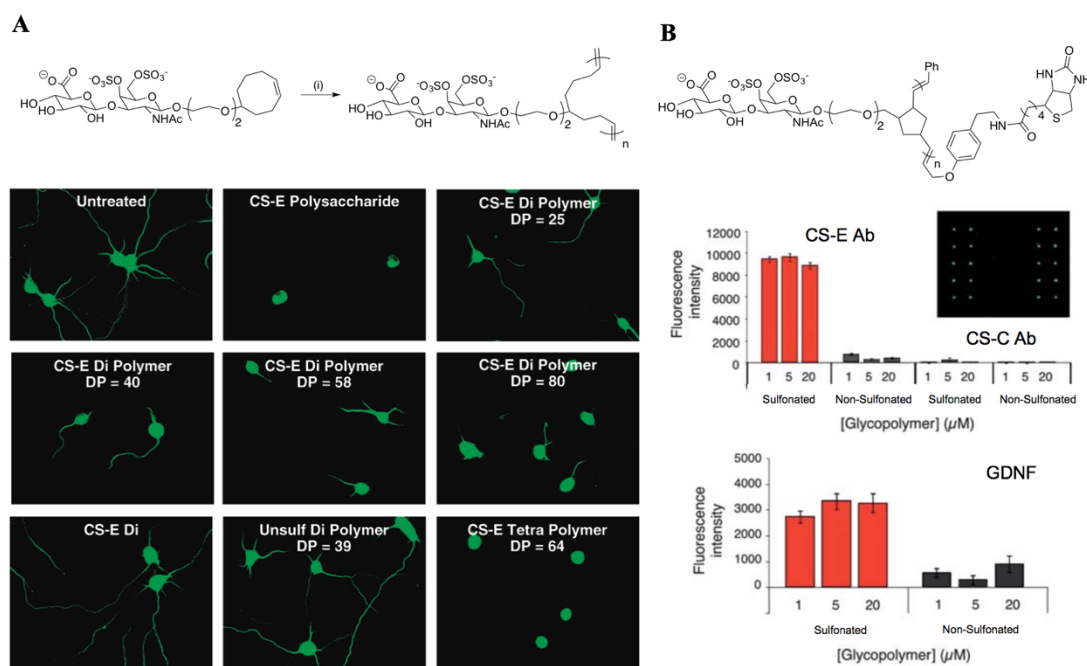
Scheme 1.2 CS glycopolymer formed by ROMP from (a) cyclooctene showing control over neurite outgrowth when increasing the degree of polymerisation and the length of the oligosaccharide. (b) Norbornene-based CS glycopolymer with biotin label attached for surface immobilization and measurement of the fluorescent output of labelled antibodies. Reagents and conditions: (i) 1:5 MeOH: ClCH$_2$CH$_2$Cl, 55 °C, 24h, Ru-Grubbs Catalyst, 1.0 % (mol %). Scheme adapted from ref. [61-62].

An alternative route devised by the Song-Gill group[63] used a peptide as the backbone, rather than an alkyne derivative. By using a proline or lysine bearing an azide group, the disaccharides alkynes synthesied could be "clicked" onto the peptide backbone. By changing the amino acid residues, the work were able to control the secondary structure to play with backbone flexibility plus the placement and number of sugars along the helix (Figure 1.6). This was determined by surface plasmon resonance (SPR) to study the change in response in the system dependent on the secondary structure.

The use of a peptide compared to a polymer monomer gives control over the localisation of saccharides, an advantage over the ROMP method to produce homopolymers and statistical polymers. The stepwise addition of a peptide-based synthesis leads to control of the sequence to make specific variations of the CS mimic. Nerve growth factor (NGF) is an important GF involved in neuron growth; using the various glycopeptides, the binding to NGF was studied[63]. The CS-peptide mimics showed increased NGF binding as a result of the secondary structure, with the linear CS peptide showing a stronger K_D than that of the alpha helix peptide ($K_D = 0.146$ mM and $K_D = 3.57$ mM, respectively).
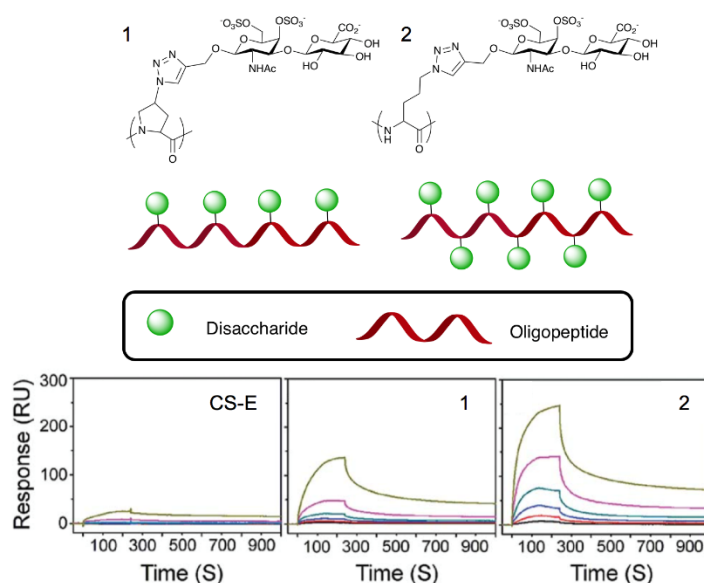
Figure 1.6. Polypeptide-based CS glycopolymer using azide proline (1) and (2) lysine with the ability to change the density of the glycopolymer leading to change in response seen in the SPR binding to NGF. Figure adapted from ref[63].

A recent example of CS glycopolymers was published by the Rojo group who reported a disaccharide based on CS-E as a glycodendrimer rather than a linear glycopolymer[64]. The glycodendrimers were used to explore the interaction with the growth factor midkine involved in neural growth processes. Increasing the disaccharide valency,

from 1 to 3, 4 6 units of the disaccharides of CS-E, showed a decreasing half maximal inhibitory concentration (IC_{50}) with increasing valency seen between 4 and 6 (Figure 1.7).
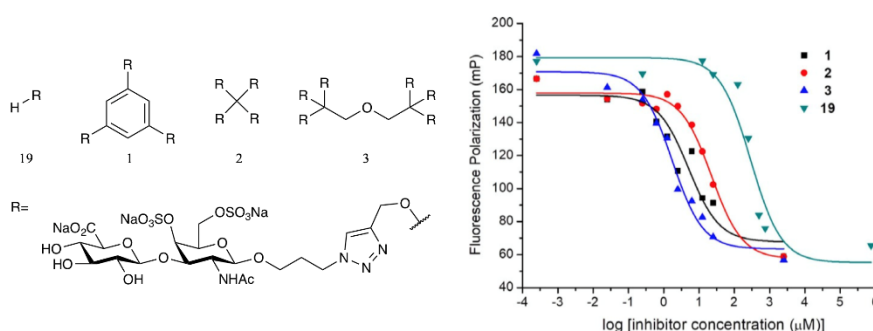
Figure 1.7. Glycodendrimers of CS (1-3) compared to dimer (19) to study the inhibition of midkine by flow cytometry. Figure adapted from ref. [64]

Due to the increase in flexibility of the alkyl core, compared with a benzene core arrangement imposed by this dendritic core, an increase in IC_{50} between 1 and 2 µM was observed, showing a higher relative inhibitory potency (RIP) of 26 compared with 5. However, when increasing the number of disaccharide units in the case of 3, the RIP increases to 42 showing that, for midkine, the arrangement of the disaccharides is important to binding as well as the multivalent effect increasing potency.

1.2.2. Heparin/Heparan Sulfate Mimics

Early examples of heparin mimics looked at simplifying the structure of the saccharide to a simple sulfonated compound such as polystyrene sulfonate and polyvinyl sulfonate[65]. However, these examples resulted in delayed clot formation and reduced complement activation. In recent years, the field has moved towards glycopolymers, rather than simple sulfonate compounds.

An early example of a glycopolymer inspired by HS came in 2004 from the Chaikof group[66]. Using fully sulfonated GlcNAc and lactose bound to an acrylate, cyanoxyl-mediated free-radical copolymerisation with acrylamide was undertaken. It was an early example of an acrylamide polymerisation based on GAGs. The polymerisation showed good control over Đ (1.13 - 1.49), which increased to 1.57 as the polymer molecular weight increased above 100 kDa. The lactose-based polymer showed a larger range of Đ (1.16 – 1.67), but this can be attributed to the greater weight average molecular weight (M_w) of lactose causing a greater difference between chains. It was

an early example of an HS mimic due to the ability to bind to fibroblast growth factor (FGF), protect FGF from tyrosine digestion and its coagulation properties.

The Grainger group[67] applied a sulfonated mannose onto a glass surface. By binding an initiator group onto the surface; ATRP could be undertaken (Scheme 1.3A). Using a mannose-based glycomonomer as the feedstock glycopolymer, brushes could be grown from the surface. After deprotection of the acetyl groups, the hydroxyls were sulfonated using 0.2 M SO_3.py solution in anhydrous pyridine, as confirmed by X-ray photoelectron spectroscopy (XPS) and elemental analysis[67]. The anticoagulation showed that post sulfonation increased the clotting time, but these times were affected by the difference in the surface energies.

The same principle of glycopolymer formation followed by sulfonation was also used to form a glycomonomer of mannose, glucose, glucosamine and lactose bearing two secondary amines, which reacted with a diisocyanate to form a step-growth polymer[68]. Again, the decision for a sulfonation pre-polymerisation led to uncontrolled sulfonation. The sulfonation was confirmed by Fourier transform infrared (FT-IR) for the S=O peaks at 1220, 999 and 931 cm^{-1}, with experimental analysis producing an average sulfonation of 3.68 – 6.88 of the hydroxides per glycomonomer/disaccharide units. These polymers were tested for their thrombin time (TT), reptilase time, prothrombin time (PT), and activated partial thromboplastin time (aPTT). Each case showed delays in coagulation time, whilst the non-sulfonated precursors showing no effect on the coagulation time. The best results were obtained for the mannose and lactose derivatives.

A follow-up study by N. Ayres[69] used the lactose based polymer with different diisocyanates units in the polymer backbone, causing an increase in the coagulation time. From here, the second generation of step-growth polymers was produced using linkers such as toluene 2,4-diisocyanate (TDI), isophorone diisocyanate (IPDI) and methylene bis (4-cyclohexyl isocyanate) (HMDI). Greater activity was observed from the second generation, due to the semi-flexibility of the polymer. It was also shown that the degree of sulfonation linearly affects the anticoagulation time. With a strong correlation on the degree of sulfonation to the coagulation time, then perhaps a controllable method of sulfonation is more suitable (Scheme 1.3B).
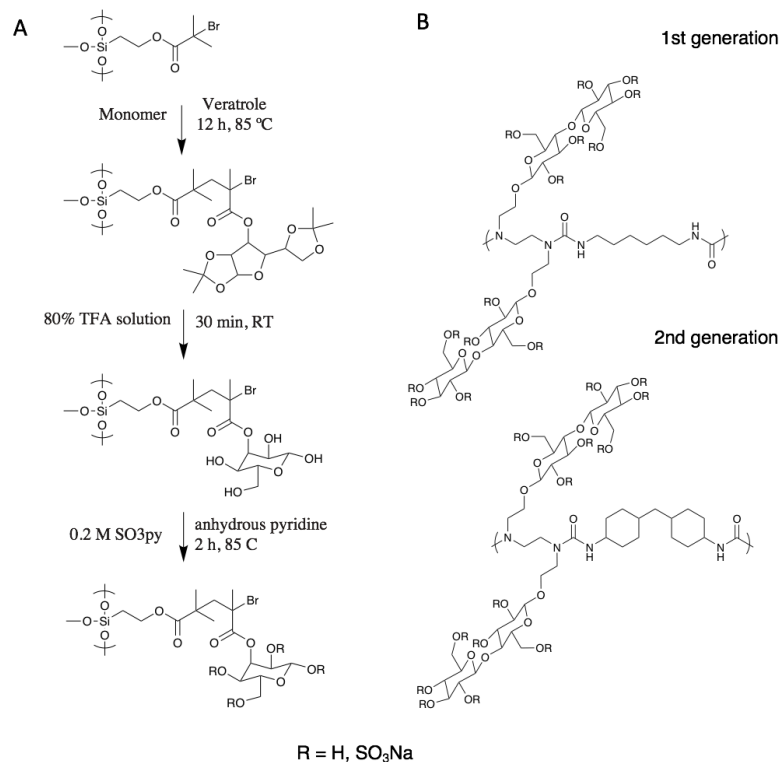
Scheme 1.3. Synthesis of heparin mimics by (a) ATRP of glycomonomer on a glass surface or by (b) step growth polymerisation using diamine glycomonomer-diisocyanates chemistry to form a polyurea backbone. Scheme adapted from ref.[67-68].

Building on the work undertaken with CS, the Hsieh-Wilson group formed heparin glycopolymers[70-71] on the same principle of ROMP to polymerise the dimer. The complex protection of the disaccharide allowed the final sulfonation to be controlled compared to previous examples of sulfonation of HS mimics (Scheme 1.4). By selective deprotection of the hydroxyl, specific locations on the disaccharide could be sulfonated. From here, different sulfonated glycopolymers could be produced and tested to probe the effects of the sulfonation.
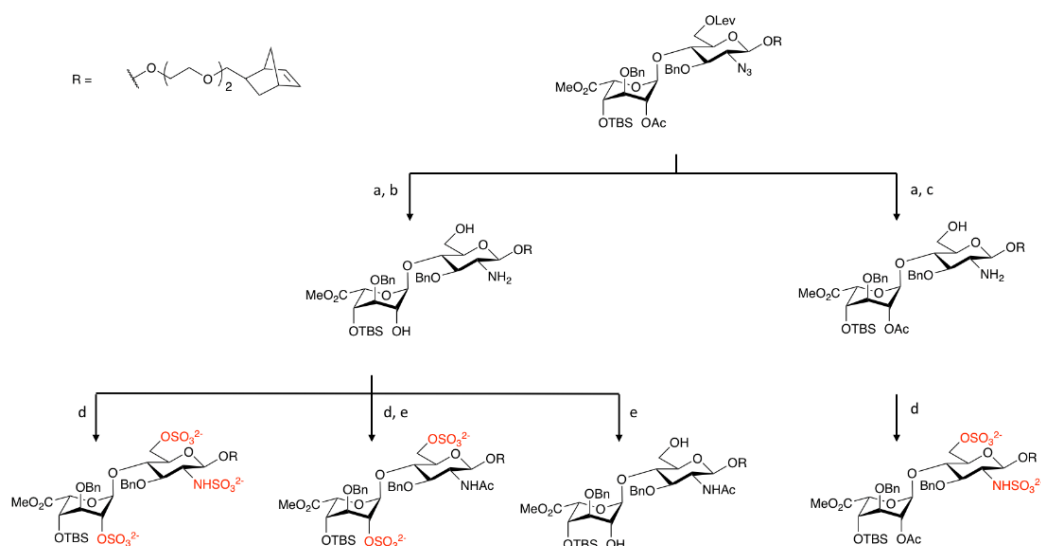
Scheme 1.4. Sulfonation pathway for heparin disaccharide[71]. Reagents and conditions: (a) 1,3-propanedithiol, DIPEA, MeOH, 87%; (b) K_2CO_3, MeOH (c) $H_2NNH_2 \cdot H_2O$, AcOH, Py (d) $SO_3 \cdot$Py, Et_3N, Py, 55 °C (e) Ac_2O, Et_3N, MeOH (f) $(H_2IMes)(Py)_2(Cl)_2Ru=CHPh$, DCE, MeOH (g) (i) TMSOK, TBAI, THF (ii) $Pd(OH)_2$/charcoal, H_2 (1 atm), phosphate buffer (pH 7.4), MeOH

This concept of controlled sulfonation of the HS mimic was taken further in the formation of a heparanase inhibitor. Heparanase cleaves GlcAβ(1,4)GlcNS bonds but also has a recognition site for the disaccharide GlcNS(6s)α(1,4)GlcA adjacent to the cleavage site. By producing a glycopolymer that contained this disaccharide moiety without the critical GlcAβ(1,4)GlcNS bond, a glycopolymer could be used as an inhibitor. The Nguyen group[72-73] took the tunability of the synthesis further by simplifying this synthesis pathway by incorporating click chemistry into the formation of the glycomonomers. In doing this, the system can be easily modified as the click reactions can tolerate the other functional groups as they are chemo and regioselective. In the example from the Nguyen group, the use of the copper azide-alkyne cycloaddition (CuAAc) was employed to create two glycomonomers based on a single carbohydrate synthesis. In general, the carbohydrate synthesis is the most labour-intensive aspect of the formation of a glycomonomer. By creating one azide bearing disaccharide, multiple glycomonomers could be produced (Scheme 1.5). In these studies, the addition of a biantennary compound was shown to be more effective than a monoantennary for a glycomonomer. The polymerisation of the biantennary by ROMP showed an increase in DP and lead to a lower IC_{50} value.
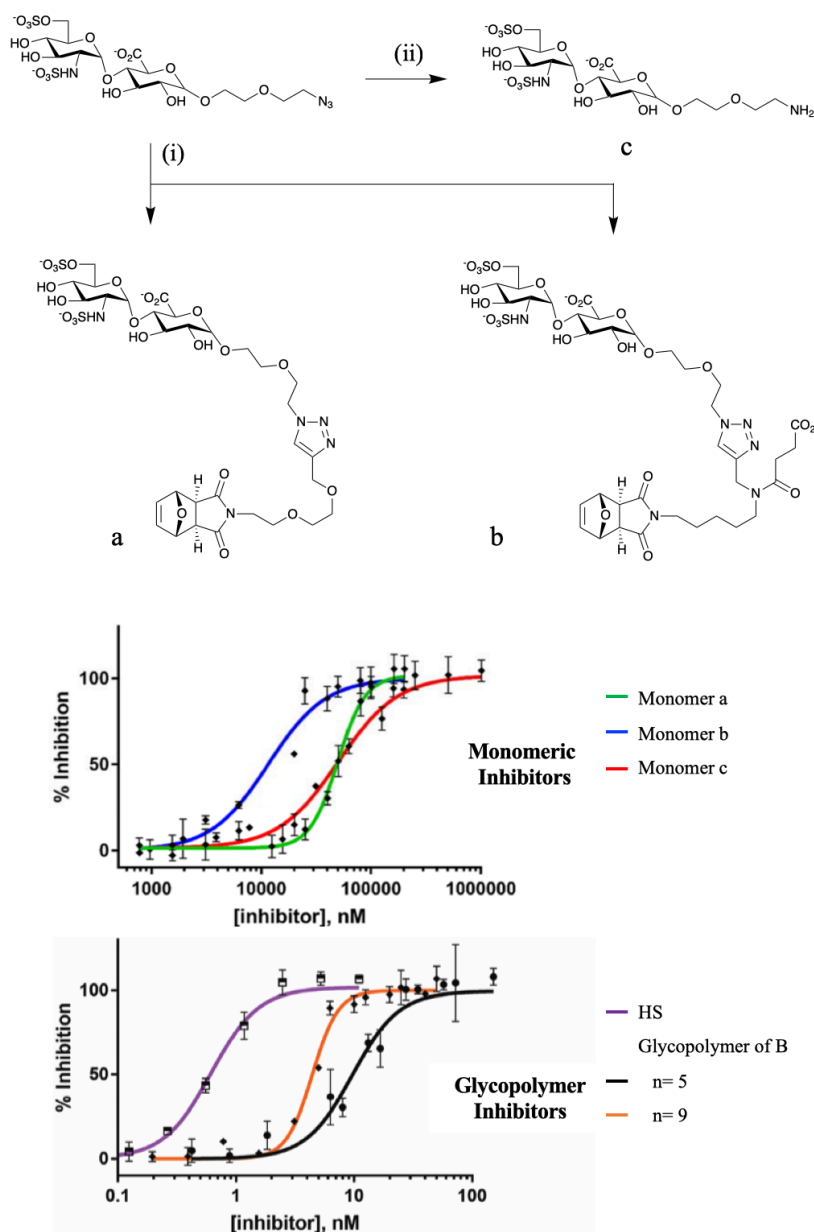
Scheme 1.5. Neoglycopolymers of HS as (a) monoantennary, (b) biantennary and (c) disaccharide monomer bottlebrush formed by CuAAC from a single azide. Reagents and conditions: (i) CuI, DBU, DMF, 50 °C (ii) PPh₃.

An alternative approach was reported by the Stupp group[74] to form an HS mimic. This was achieved by designing peptide amphiphiles (PA) with sulfonated sugars at the N-terminus of the peptide by CuAAC. These PAs were designed to self-assemble into nanofibers displaying HS sugars on their surface (Figure 1.8). Growth factors were then utilised to compare the binding of HS and the glycopeptide nanofiber as well as looking at GF signalling. This approach showed an alternative to the formation of long peptides by allowing the peptides to self-assemble into nanofibers and presenting multiple copies of HS sugars rather than producing vast oligomers.

Proteins	Experimental K_D (M)	
	Heparin	**HS PA**
BMP-2	$4.52 \pm 0.77 \times 10^{-8}$	$3.15 \pm 0.63 \times 10^{-5}$
BMP-4	$1.67 \pm 0.14 \times 10^{-8}$	$1.01 \pm 0.76 \times 10^{-4}$
FGF-1	$1.22 \pm 0.19 \times 10^{-7}$	$1.28 \pm 1.09 \times 10^{-4}$
FGF-2	$1.25 \pm 0.11 \times 10^{-9}$	$8.55 \pm 0.11 \times 10^{-5}$
VEGF	$4.75 \pm 2.47 \times 10^{-8}$	$1.39 \pm 0.35 \times 10^{-8}$
Shh	$4.49 \pm 1.23 \times 10^{-8}$	-
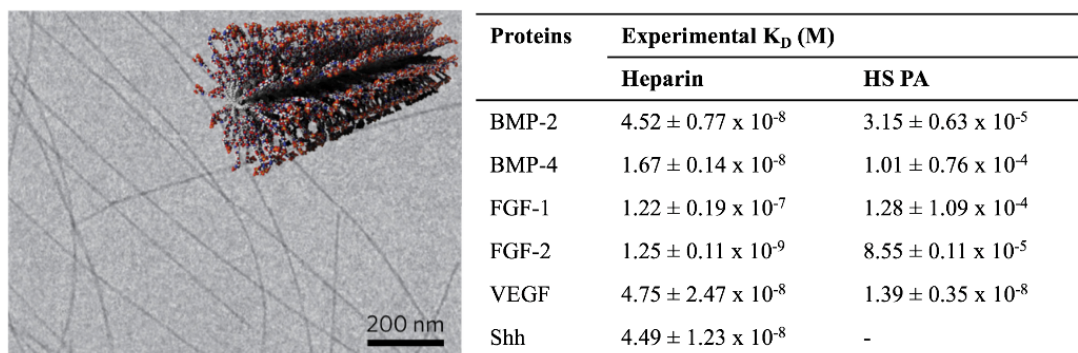
Figure 1.8. Cryo-TEM image (left) of nanofibers from the glycopeptide (HS-PA) with a structural representation of the PA; the binding comparison study (right) of HS and HS-PA with the GFs (HS-binding proteins).

Over the past 20 years, the synthesis of HS mimics has shifted from using sulfonated groups to using the more native sulfonated monosaccharides with improved results. With growing control over the sulfonation of the saccharides, further enhancing the properties of these mimics, a next generation of fully mimicking HS glycopolymers is expected in the near future.

1.2.3. Dermatan Sulfate & Keratan Sulfate

Within the scope of glycopolymers, little has been undertaken with the remaining sulfonated GAGs of KS and DS. DS has yet to be produced using a glycopolymer, but DS and HS are epimers. In contrast, carbohydrate chemistry has already produced synthetic pathways for the formation of DS[75-76] and KS[77-78] oligomers. The non-sulfonated repeat of KS, N-acetyllactosamine, has been developed as a glycopolymer[79-80] as well as fully sulfonated analogues[81]. The fully sulfonated glycopolymer showed anticoagulant properties whilst adding a sialic acid unit to N-acetyllactosamine creates inhibitors against influenza viruses. However, the selective single sulfonation of the 6'-GlcNAc of N-acetyllactosamine has yet not been produced.

1.2.4. Hyaluronic Acid

HA is produced as a mega Dalton polymer, which current glycopolymers cannot match. Although glycopolymers cannot match natural HA's size, it has been shown that HA's main receptor CD44 requires a minimum of 8 units of monosaccharide for binding[82]. The Chaikof group produced an HA dimer[83] which bore an alkene onto which a norbornene could be attached[84]. Using ROMP as described by the Kessling

group[85], the HA dimer could be polymerised to give a 9 kDa Mw polymer with a Đ of 1.17 (Scheme 1.6). Rather than forming glycopolymers of HA, in recent years the work has moved towards the production of glycoclusters. Using the same disaccharide monomer as used by Chaikof, in tandem with olefin metathesis[83], Schiff-base[86-87] and click chemistry[88-90] a variety of glycoclusters with increasing number of disaccharide units upon them have been produced.

The HA-disaccharide has been incorporated into a glycopeptide by the Lönnberg group[91] through the formation of an aldehyde from the alkene. Binding this aldehyde to a phosphonamidite building block by Schiff base chemistry produces a molecule which can be incorporated into the peptide, to add different numbers of these HA phosphonamidites. The study showed the glycoclusters are affected by the length rather than the density of HA disaccharides.
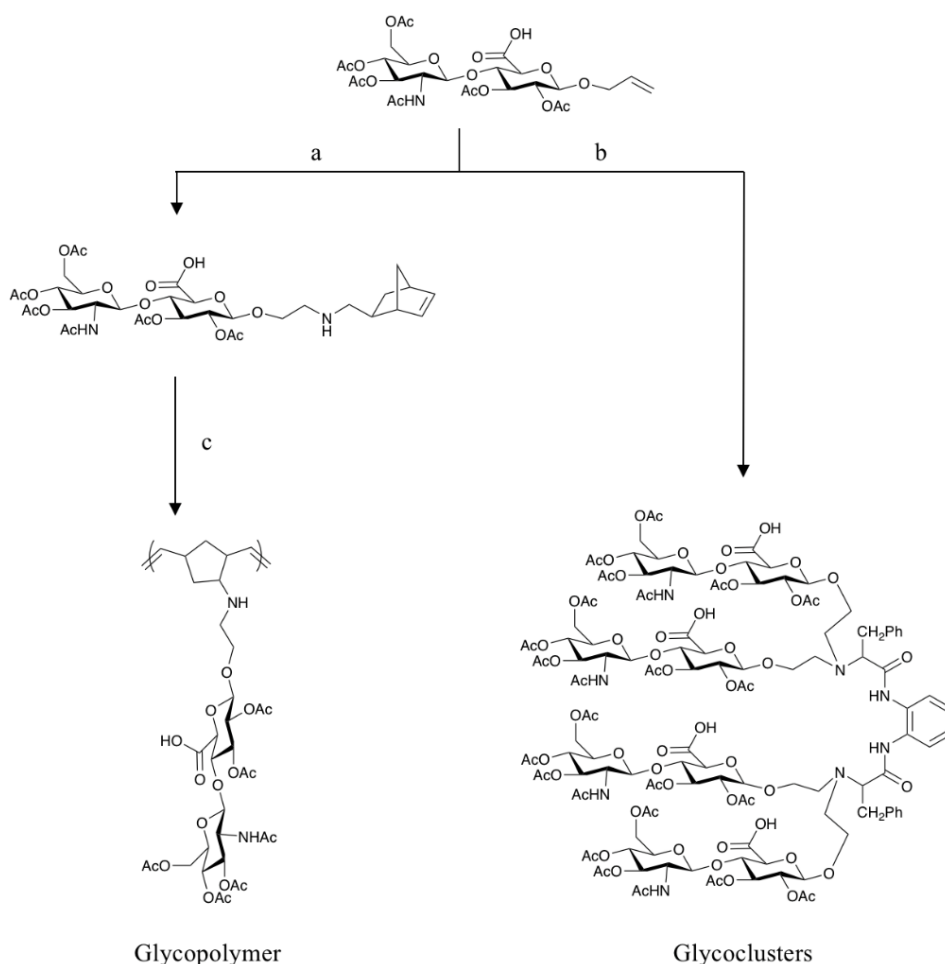
Scheme 1.6. Synthesis of HA-based glycopolymer and glycoclusters from HA-disaccharide. Reagents and conditions: (a) MeOH, 25 °C, 3 h, then add NaCNBH$_3$, 25 °C, 15 h (b) NaCNBH$_4$, MeOH (c) DTAB (1 eq.), Grubbs Catalyst (5 mol%), (CH$_2$)$_2$Cl$_2$, H$_2$O, 60 °C, 5 h.

An increase in the number of HA dimers on the sequence showed no effect on the uptake by HCE cells as observed by flow cytometry. This led to further studies to use longer tetrasaccharides of HA rather than dimers[88, 90]. A final example of the formation of an HA glycomonomer was shown by the Codée group, who produced oligomers of HA in both solutions and upon solid support[92]. The solution phase example included the formation of a trimer, pentamer and heptamer bearing an azide at the reducing end of the carbohydrate. The azide was used to "click" these oligomers onto the polymer or to a polymerisable group, similarly seen by the Nguyen group (Scheme 1.5), whereas the solid support synthesis used a designed Grubbs 2nd catalyst on a cleavable support (Scheme 1.7).
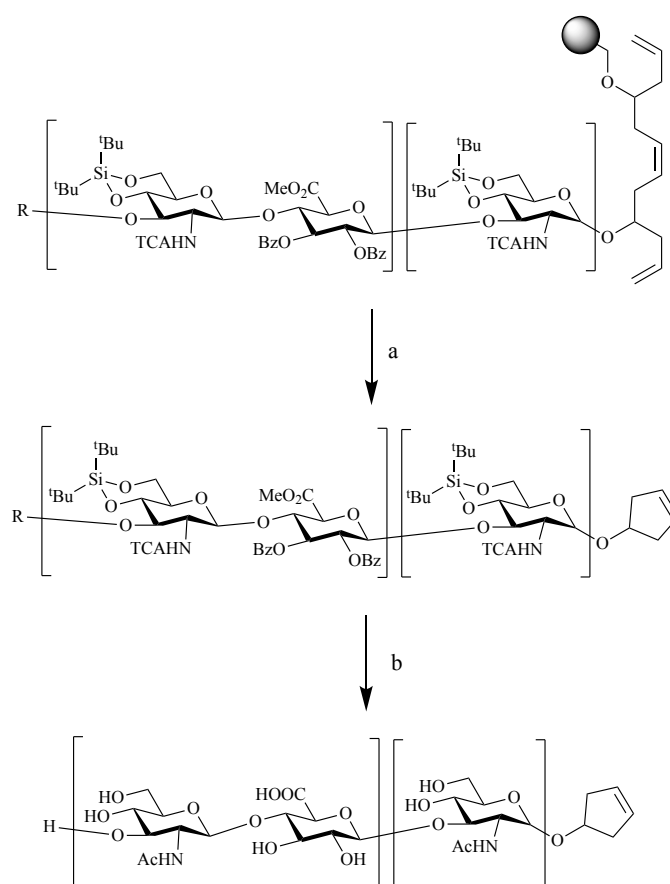
Scheme 1.7. Formation of HA oligomer on Grubbs catalyst cleavable resin. Reagents and conditions: Grubbs second-generation catalyst, trichloroacetamide, DCM, 3 h (d) i. HF/Et$_3$N, THF, 30 min; ii. 0.5 M KOH, THF, 4 days; iii. Ac$_2$O, THF/H$_2$O.

From this review on GAG-based glycopolymers, there is potential to form complex synthetic GAGs with control over the sulfonation. This control has been led to various applications being explored, such as neural growth, coagulation and enzyme inhibitors. Since CS and HS have a wider variety of applications, compared to DS and KS, research has been focused on glycopolymers of these GAGs. For the sulfonated

GAGs, a correlation between the degree of sulfonation and properties is evident like for example anti-coagulation properties. With both KS and DS only containing one sulfonate, they present a synthetic challenge to ensure mono-sulfonation of the disaccharide. Although non-sulfonated, HA owns specific biological and physical properties. However, having the largest molecular weight of all the GAGs, work has been focused more on the synthesis of glycoclusters of HA or as end group modification of polymers to add biocompatibility. The formation of an HA glycopolymers has been restricted to the ROMP as described by Chaikof[84]. However, several of the examples reported previously could easily be modified to form glycopolymers based on HA.

From the literature, the examples for CS and HS glycopolymers offer good candidates for biomimetic materials of the natural GAGs, which can be used as a platform to build new biomaterials. In several of these cases, the formation of a disaccharide, followed by the polymerisation of that disaccharide has produced comparable properties to those of natural GAGs without the requirement for extensive chemical synthesis. To date, there are examples from the literature[62, 71-72] showing glycopolymers that can be tunable and rival the properties of natural GAGs as therapeutics.

1.3. Aims and Objectives

From all the GAGs, this work is focused on HA, the structurally simplest and non-sulfonated GAG. Although not forming covalent linkages with proteins, HA is yet involved in a plethora of biological processes. Whilst few examples of HA-based glycopolymers and glycoclusters have been described in this section, many of them have not shown their biological activity with groups stating "the biological evaluation of these compounds is ongoing"[83-84, 86-87]. By contrast, the biological activity of CS (Scheme 1.2) and HS (Scheme 1.5) glycopolymers has been shown. This could be due to the fact that HA biological activity is more challenging to be assessed. In our studies, we aim to look into this gap in knowledge by using novel approaches to synthesise HA glycopolymers.

The previous examples of GAG-based glycopolymers have used the disaccharide pendants from the polymer backbone. The formation of a glycosidic bond requires multiple steps in order to achieve this producing an inefficient synthesis for the formation of glycopolymers. Compared with previous examples, the design approach used in this work is based on HA glycopolymers whereby the saccharides alternate across the polymer backbone through individual saccharides on individual monomers. We attempted both pre- and post-polymerisation modification to achieve the desired glycopolymers. Through click chemistry, various monosaccharides functionalised with a click moiety can be synthesised to produce multiple glycopolymers from a single parent polymer. This approach will provide a simple method to produce multiple glycopolymers from a single synthesis pathway. In order to achieve monosaccharide alternation across the polymer chain, we exploited alternating polymers in order to mimic the sugar pattern in HA (Scheme 1.8). By having monosaccharides rather than a disaccharide on display from the polymer, both saccharides will be involved in the binding, instead of the beta-saccharide on the disaccharide from the polymer.

Since HA only forms non-covalent interactions with peptides and proteins we studied the binding sequences of these HA binders for their self-assembly with HA. By adding structural cues to the peptides, the secondary structures and self-assembly can be controlled to design higher ordered structures such as micelles and fibres.
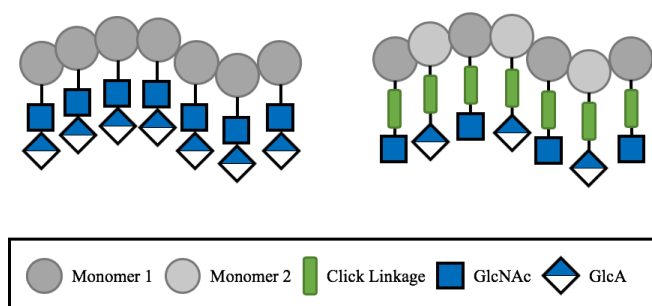
Scheme 1.8. The previous design concept for HA (left) with pendant disaccharide[84] and (right) our design concept using an alternating polymer with HA monosaccharides.

In summary, the aims of this thesis are:

- Synthesise HA-based glycopolymers using alternating polymers

- Compare the properties of the synthetic analogues with natural HA

- Use HA-binding peptides and HA glycopolymers to investigate their binding and better understand the interactions of HA with its binding partners

- Utilise the glycopolymers to investigate binding to several lectins to determine potential monosaccharide ligand binders leading to a better understanding of these receptors

- Explore HA-binding peptides for binding and self-assembly with HA to create new biomaterials for potential applications such as wound healing, drug delivery or scaffold for cellular growth.

1.4. Carbohydrate Chemistry

Polysaccharides are synthetically challenging to form in comparison to other biological molecules such as peptides or proteins. Whilst peptide synthesis pathways allow the formation of well-defined peptide structures, carbohydrates are much more complex. For a peptide, the formation of an amide bond requires the reaction between an amine and carboxylic acid, whilst the alternate carboxylic acid and amine are protected. In contrast, a saccharide is divided into two ends, the reducing and the non-reducing end (Figure 1.9). The non-reducing end consists of 4 positions around the saccharide of the 2', 3', 4' and 6' hydroxyls, whilst the reducing end is the 1' hydroxyl, also referred to as the anomeric centre.
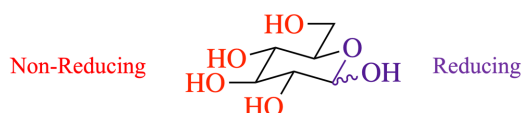
Figure 1.9. Example of a monosaccharide (glucose) highlighting the two ends of the saccharide with the reducing hydroxyl (purple) and the 4 non-reducing hydroxyls (red) along with highlighting the hemi-acetal group of the pyranose ring.

The anomeric centre of the saccharide has the ability to ring open and ring close due to its proximity to the oxygen within the ring. With the ring-opened structure, the sugar exists as a reactive aldehyde, which in the presence of an acid catalyst can be attacked at C1 with the release of water. In this ring-opened form, the aldehyde is susceptible to nucleophilic attack by hydroxides, with an acid catalyst, as well as amines. This ring-opened form is short lived as the structure is more stable as a closed ring. The 5' hydroxide is able to reclose the ring to form back the pyranose ring. However, attack by the 4' hydroxide can lead to the furanose form. Whilst the furanose ring is stable, the pyranose is more favourable due to strain in a 5-membered ring. For this reason, many saccharides appear as the 6-membered ring rather than the 5-membered ring.
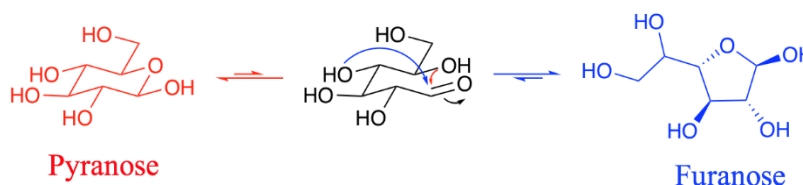
Scheme 1.9. A schematic depicting the ring-opening and closing of saccharides (glucose in this example) between the pyranose 6-membered ring form and the furanose 5-membered ring form.

1.4.1. Anomeric Effect

In the ring open form, the aldehyde has the freedom to move and therefore can invert between an axial (α) or equatorial (β) position. Due to the freedom of rotation, many reactions at the anomeric centre produce an anomeric mixture of saccharides.

There are three competing factors within the anomeric effect, those are sterics, dipole induction and orbital overlap (Scheme 1.10).

Sterics within the saccharide ring is caused by the axial position. These hydrogens are held in close proximity causing a steric repulsion. This is not seen between the equatorial positions due to the space around the functional groups. These steric effects are increased if large bulkier groups, such as hydroxide, point down axially. From a steric stand-point, the lower energy conformation is achieved if the bulkier group at the anomeric centre is in equatorial positions.
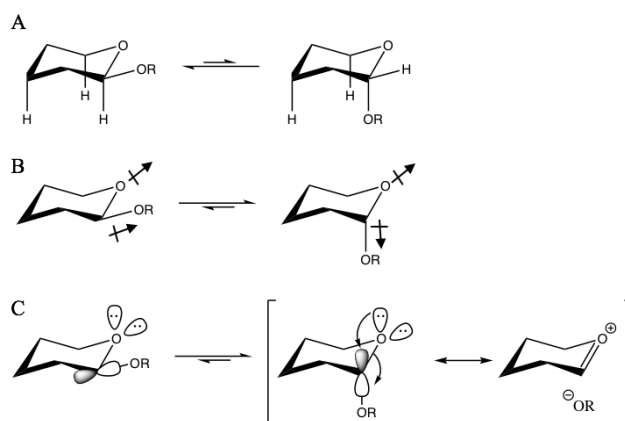
Scheme 1.10. Anomeric effect 3 factors: 1,3,5 sterics (A), dipole moments (B) and orbital overlap (C).

In comparison, the dipole induction of the monosaccharide between the ring oxygen and the 1' hydroxide is more stable in an axial position. By placing the hydroxide in an axial position, the dipoles oppose one-another making the entire molecule dipole neutral. This effect is enhanced with more electronegative substituents, such as the introduction of a chloride at the C1 position. The chloride will exist 96:4 ratio favouring the axial position, despite having a large ionic radius[93]. The dipole of a molecule can be affected by the solvent. Having an increased dipole in the solvent leads to a reduction in anomeric specificity as the solvent negates the dipole within the monosaccharide[94].

Axial position is also favourable due to the orbital of C-O* and lone pair on the ring oxygen. When in the axial position, these align and therefore make it easier for the formation of a resonance structure in which the OR group has been removed from the

saccharide to form a C=O within the ring. This is one of the most widely accepted scenarios for the anomeric effect as the leaving group or nucleophile can now attach from either face of the sp^2 centre. When forming a disaccharide, this anomeric effect has to be taken in account in order to form correct linkages. The orientations of these linkages can be critical to the function of the oligosaccharide.

1.4.2. Glycosidic Bond Formation

The glycosidic bond is the hemiacetal linkage between the reducing end and non-reducing end of two monosaccharides. The complexity of forming a glycosidic bond is caused by the ability of those four hydroxyls at the non-reducing end to form a bond with the reducing end. If left uncontrolled, dendrimer type structures would form. In nature, enzymes control the introduction of a monosaccharide to the growing polysaccharide leading to regioselectivity of the glycosidic bond, whilst in chemical synthesis, selective protection and deprotection reactions are required in order to prepare the donor and receptor monosaccharide to form the desired glycosidic bond. An additional consideration for the formation of the glycosidic bond is the low reactivity of the non-reducing hydroxyl towards the anomeric hydroxyl. To this end, monosaccharides used in biosynthesis are tagged with a UDP in order to activate the anomeric position towards substitution. Carbohydrate chemists instead use leaving groups to allow the hydroxide of the incoming monosaccharide to bond. The formation of one glycosidic bond requires a large number of synthetic steps and this methodology can be used to form simple linear carbohydrate structures such as amylose (α 1-4 linked glucose) or cellulose (β 1-4 linked glucose). However, to form more complex polysaccharides with α or β anomers, different linkages and branching, conventional carbohydrate synthesis lags behind the enzyme pathways employed by nature. Despite potential automation using phosphonamidite or amide condensation, there is still a vast amount of preparation steps before a machine is able to couple the monosaccharides.

Utilising the reducing end, functionality can be grafted to the saccharide. This functional handle allows the monosaccharide to be attached onto a polymer backbone or a monomer, that can later be polymerised. This represents two of the three methods by which a glycopolymer can be formed. The three approaches are: the formation of a glycomonomer, grafting the saccharide onto a polymer and the simultaneous grafting and polymerisation.

1.5. Polymerisation

As described previously, several polymerisation methods can be used to produce glycopolymers, including free radical polymerisation (FRP), RAFT and ROMP.

1.5.1. Ring-Opening Polymerisation

Ring-opening polymerisation (ROP) is an ionic polymerisation and utilises a cyclic molecule which has either an alkene or a breakable bond, such as lactones, cyclic carbonate derivatives or a ring strained epoxide. ROP allows very specific polymers to be formed in terms of the backbone length and composition forming biodegradable backbones using renewable sources.

1.5.1.1. Cationic/Anionic Ring-opening Polymerisation

Cationic Ring-opening Polymerisation (CROP) and Anionic Ring-opening Polymerisation (AROP) utilise charged molecules as initiators. The charge is passed onto the propagating group, with the reaction being terminated by hydroxyl-containing compounds. Schubert introduced an oxazolone based glycomonomer[95] which was used in CROP to produce the glycopolymer, with careful consideration of maintaining the temperature (Temp) below 100 °C to ensure the saccharides did not decompose.

In a second example from the Hendrick group, cyclic carbonates with attached sugar moieties were formed. These polymers have the bonus of being biodegradable due to heteroatoms present within the polymer chains. The downside, in terms of glycopolymer formation, is that, due to the termination by hydroxyl-containing compounds, the saccharide OH groups require protection.
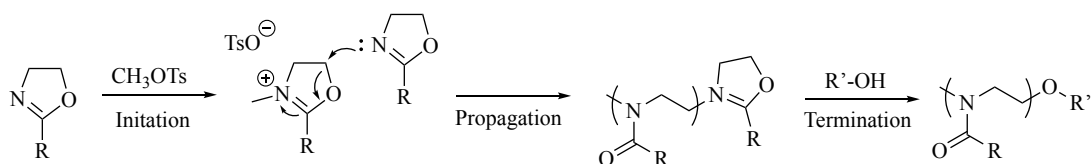
Scheme 1.11. Scheme example for ring-opening of a 2-oxazolines derivative by CROP.

1.5.1.2. Ring-opening Metathesis Polymerisation

By comparison, ROMP is a much more functional group tolerable. ROMP uses olefin derivatives along with a metal catalyst, such as Ruthenium (Ru) formed by Grubbs, with the polymerisation occurring through the metathesis of the double bond. The polymer grows out from the metal centre and is terminated by the addition of ethyl vinyl ether, which reacts with the metal-carbene species to remove the metal from the polymer.
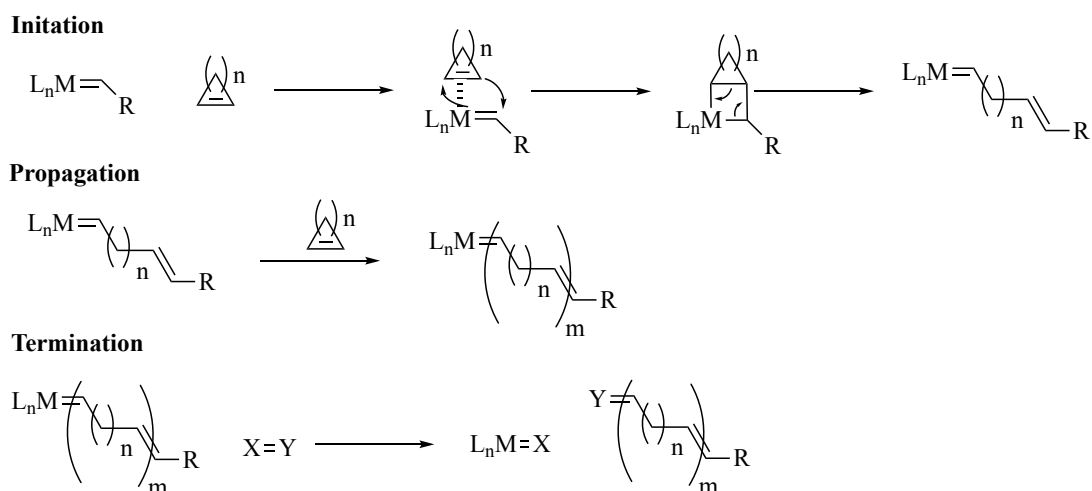
Scheme 1.12. Reaction pathway for the ROMP of an olefin.

The reaction proceeds by strained olefins driven by the release of ring strain. However, they are reversible reactions, requiring optimisation. Due to the tolerance of these reactions, several examples exist for glycopolymers[72-73, 84, 92, 96-97] as they do not require the protection of the hydroxyls, or in the case of the GAG mimics the protection of the SO_3^-, as shown by examples from the Kiessling group[85, 98].

1.5.2. Radical Polymerisation

Free radical polymerisations are one of the most common types of polymerisation, with publications dating back to 1930's[99] showing early work with vinyl compounds such as, but not limited to, styrene. "Free" radical polymerisation was the first example of a radical method, with the "free" denoting the uncontrolled nature of this reaction. The uncontrolled nature makes this technique very rapid but leads to undesirable side reactions, including branching, disproportionation and a large distribution of molecular weights contributing to a large Đ. Despite being an uncontrolled method, it enabled scientists of the time to produce compounds such as polyethylene and

polystyrene with relative ease. The process of free radical polymerisation is broken down into 3 stages: initiation, propagation (Figure 1.10) and termination (Figure 1.11).

Initation
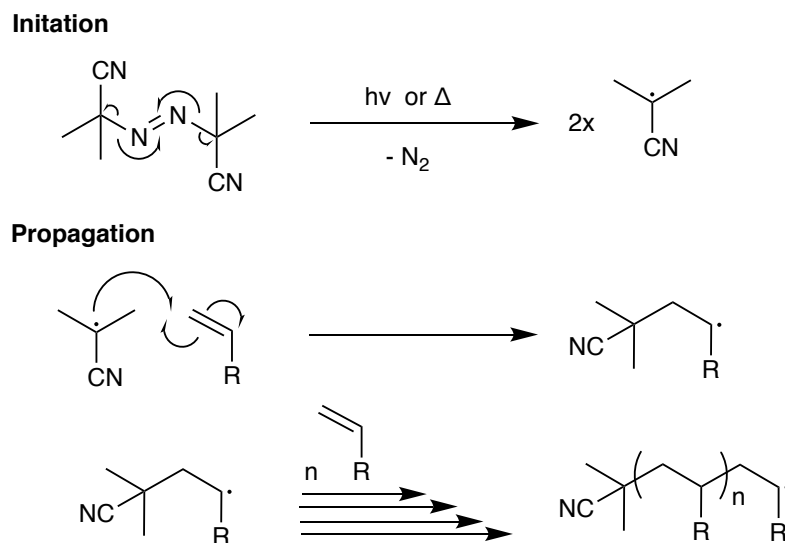
Propagation

Figure 1.10. Radical mechanism for the initiation and propagation of generic polymer initiated with AIBN.

The initial process of initiation produces the free radical, which can be used in the polymerisation. This radical can be produced in many different types of reactions, such as thermal decomposition of compounds like peroxides or azo-based compounds photolysis using compounds such as azo compounds, metal alkyls and metal iodides; and redox reactions using a metal to reduce H_2O_2 to HO^- and HO radical. In these types of reactions, alkene compounds are used as the radical produced will attack the terminus end of the alkene. Homolytic cleavage of the alkene produces a new bond and transfers the radical onto the monomer producing the propagation species. The polymerisation will move into the propagation phase of the polymerisation, where the propagating chains will continue to add monomers until either the monomer feedstock is consumed, or the reaction is terminated.

The termination of free radical polymerisation can occur by 2 major pathways (Figure 1.11). As the feedstock of monomer decreases, the probability of two polymer chains to combine from a single chain increases and this process is known as recombination. Alternatively, disportionation can occur. This is where a hydrogen is abstracted from an opposing polymer causing the polymer to terminate with a hydrogen, whilst the opposing polymer forms an alkene from the termination of the radical electron and electron from the homolyses of the hydrogen.
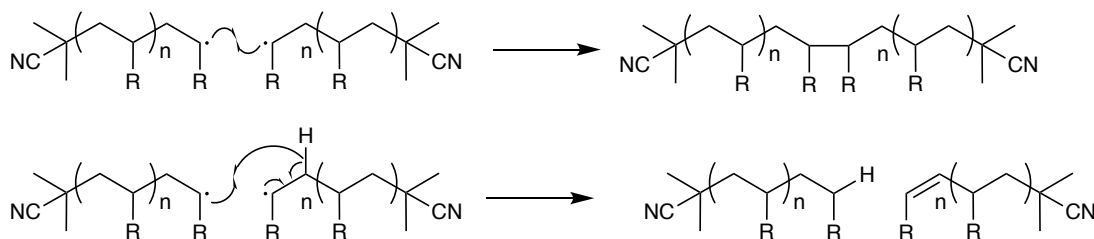
Figure 1.11. Major termination pathways of recombination (top) and disportionation (bottom).

Alternative termination pathways are available, including initiator terminated polymer. By adding additional initiator to the polymerisation towards the end of the polymerisation, recombination between the living chain and the initiator occurs to cap both ends of the polymer with the initiator. Termination of the polymer can also be achieved by exposing the polymerisation to air or a hydrogen source. The oxygen in the air forms a peroxide at the omega terminus of the polymer, which is more stable to radical species, therefore, slowing the rate of propagation. Whilst in the presence of a hydrogen source in the living polymerisation causes the polymers to be terminated with a hydrogen.

The free radical polymerisation is a very fast and efficient method to produce a polymer, but it still remains uncontrollable, leading to a large variety of polymer Number Average Molecular Weigh (Mn) being produced and thus a large Đ. Because of this, controlled polymerisation techniques have been developed in order to control the growth of these polymers and reduce the Đ of these systems to obtain polymers with a Đ closer to 1.0.

1.5.3. Controlled Radical Polymerisation

1.5.3.1. Reversible Addition-Fragmentation Chain Transfer

Reversible Addition-Fragmentation Chain Transfer or RAFT was pioneered by Graeme Moad and Ezio Rizzardo showed a method in which the growth rate of polymers could be controlled to reduce the Đ (Figure 1.12)[100]. The free radical process has no control over the propagation of the free radical after initiation. This leads to a normal distribution of molecular weights of the polymers over a prolonged reaction time. RAFT polymerisation is a controlled radical polymerisation (CRP), which utilises compounds, such as trithiocarbonates, dithiocarbamates and dithiobenzoates, to control the rate of propagation by controlling the number of propagating species in the system.
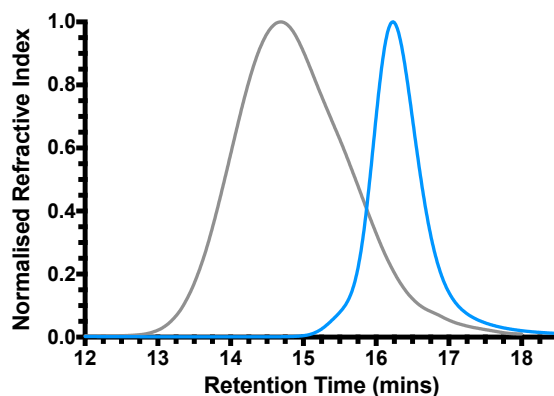
Figure 1.12. Free radical polymerisation (grey) compared to RAFT polymerisation (blue) of vinylbenzyl chloride.

Slowing the rate of propagation is achieved by trapping the radical and releasing another chain to propagate. This reversible addition to and from the chain transfer agent (CTA) ensures the polymerisation is being controlled by limiting the number of active free radical species available.

The broad range of RAFT groups now available allows the propagation rate to be tailored to suit the needs of the polymer, as well as the conditions in which the RAFT is to be used (e.g. aqueous or organic solvent systems). The RAFT group has 3 major components shown as A, X and Z in Figure 1.13.
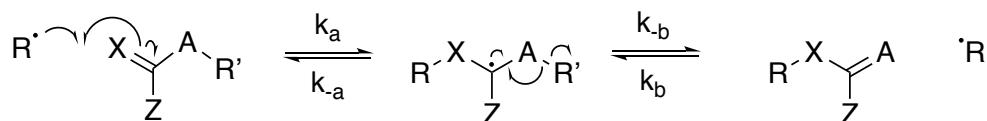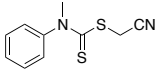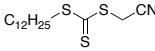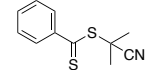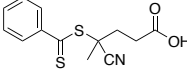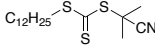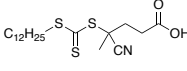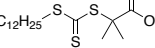
Figure 1.13. RAFT mechanism showing the association of one living radical chain R and leading to the reversible release of another living radical chain R'.

The C=X bond, where A and X are either O or S, should be reactive towards the propagating species so that R· and X form a homolytic bond leading to the formation of the intermediate, where the stability of the intermediate is governed by Z. The Z groups found on the RAFT agent stabilise the radicals and can be tuned by addition to specific radicals. This modifies the fragmentation rates, so the association and dissociation of either polymer chain are in steady state.

If Z is too electron withdrawing, this leads to stable intermediate species causing the polymerisation to terminate at the adduct (rate association >> rate dissociation). Conversely, if the Z is too electron donating, then the reaction will proceed free radically as the polymers will bind but, will almost instantaneously dissociate (rate association<< rate dissociation). The third component of the RAFT agent, A-R,' has to be weak enough so that it breaks to release R'. Initially, R' becomes the initiating species, but as the reaction proceeds, this becomes the propagating polymer species.

The reversibility of the RAFT group allows the number of propagating species to be limited. When the reaction has been terminated, the polymer will be found with the RAFT agent and the omega end of the polymer. Table 1.3 is taken from Sigma Aldrich[101], shows the various ranges of RAFT agents commercially available and their ability to regulate the polymerisations.

Table 1.3. RAFT agents performance against common classes of monomers[101].

RAFT Agent	St	A	Am	MA	MAm	VE	VA
	-	-	-	-	-	+++	+++
	+++	+++	+++	-	-	-	-
	++	+	-	+++	+++	-	-
	++	+	+	+++	+++	-	-
	+++	++	++	+++	+++	-	-
	+++	++	++	+++	+++	-	-
	+++	+++	+++	+	+	-	-

St = Styrene's, A = Acrylates, Am = Acrylamides, MA = Methacrylate, MAm = Methacrylamides, VE = Vinyl ester, VA = Vinyl amides

Whilst there are several commercially available RAFT groups, these are compounds containing trithiocarbonates, due to the wide range of monomers which can be polymerised (Scheme 1.13) using this class of RAFT agent. Trithiocarbonates can be formed with relative ease from thiol-containing reagents to produce a vast range of RAFT agents and tailored towards the polymerisation required. This approach requires controls of the Z group, as well as the initiating group (I) released by the RAFT group upon the first cycle of its use to ensure the alpha end of all the propagating polymer chain possess the same structure.
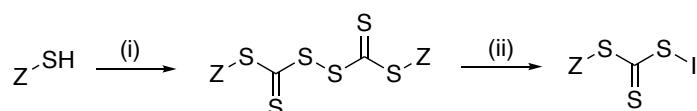
Scheme 1.13. Synthetic pathway for the synthesis of RAFT agents. (i) (a) NaOH (b) CS_2 (c) I_2 (ii) Radical Initiator

RAFT polymerisation is a popular method due to its ability to tolerate several functional groups including halides. RAFT can also be cleaved off, modified or used as a macroinitiator to extend the chain to the desired length or to include secondary blocks to add functionality to the polymer.

1.5.3.2. Atom-transfer radical-polymerization

Discovered in 1995, ATRP is another CRP technique which works on the principle of reversible-deactivation of the radical polymerisation. The principle of ATRP is the rate between the formation of the active and deactivated species. Metals such as copper, rhenium and iron are used as a catalyst together with a complexing ligand.

An ATRP polymerisation (Scheme 1.14) is initiated without the requirement of a radical initiator, such as an azido compound, which would break down under ultra-violet (UV) or thermal decomposition, but instead utilises a halide source with a weak C-X bond. This halide source allows the metal catalyst to extract the halide to initiate the reaction. The rate of initiation is dependent on the halide source, the degree of substitution and the radical stabilising group (Figure 1.14).
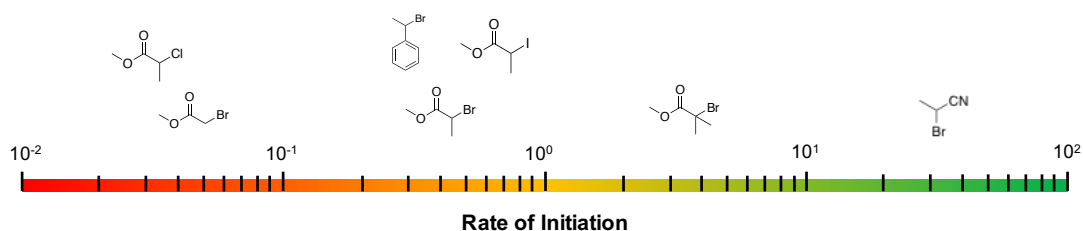
Figure 1.14. Initiation rates of ATRP effected by the R group, the substitution and the halide.

The extraction of the halide by the metal can occur as the metal complex is able to expand its coordination's to allow the Mt-X bond to form, causing a reduction in the metal's oxidation state. The now activated species is able to facilitate polymerisation. The polymerisation is controlled by the living polymers ability to extract the halide back from the metal to form the deactivated species. The reaction rate is heavily towards the deactivated species. As the monomer is consumed, the Đ improves as the rate of K_{deact} becomes larger. However, with it comes an increased probability of chain-chain termination by the combination of two living species, causing high molecular weight shoulders to appear
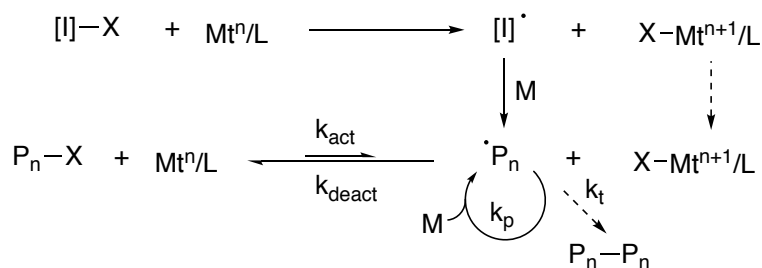
Scheme 1.14. Schematic for the polymerisation of a monomer (M) under ATRP control initiated by a halide source ([I]-X) using a metal-ligand complex (Mtn/L) to produce a halide terminated polymer (Pn-X) or to form a biopolymer terminated species (Pn-Pn).

This ability to switch between the activated and deactivated species controls the number of polymerising chains at any given time. This, like the RAFT agent, allows the reaction to produce narrow Đ's, with the rate of reaction rate of atom transfer radical polymerisation (k_{ATRP}) determined by Equation 1.1.

$$k_{ATRP} = {k_{act}}/{k_{deact}}$$

Equation 1.1

.

The use of halide sources as initiators for ATRP reactions opens up a large potential for end modification of the chains through the substitution of the halide with groups such as azides and amides, to allow for potential orthogonal reactions such as click reactions to form longer more complex chains. With the halide terminating the polymer, the polymer also becomes a macroinitiator, which with a fresh feedstock of monomer and catalyst can be chain extended to increase the molecular weight or to add different blocks of monomer to form block copolymers.

1.5.3.3. Nitroxide-mediated polymerization

Nitroxide-mediated polymerisation (NMP), like ATRP, is based on the dynamic equilibrium between an active propagating radical and a deactivated alkoxyamine (Figure 1.15A). It was first reported by the Harmer group[102] in 1993 upon the polymerisation of styrene using benzoyl peroxide and 2,2,6,6-tetramethyl-1-piperidynyl-N-oxy (TEMPO). From this first example, other NMP based radical species were produced (Figure 1.15B) with the design to prevent self-termination, initiation of new monomer and ß-hydrogen abstraction.
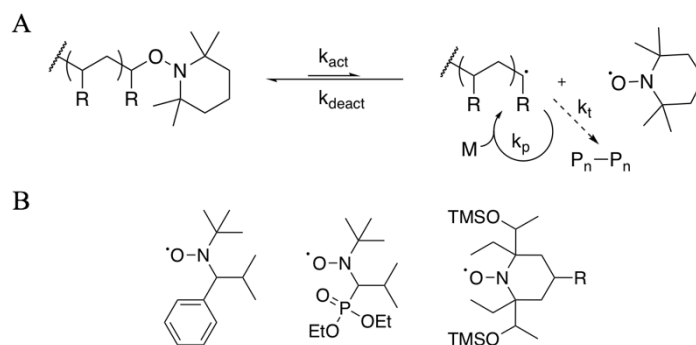
Figure 1.15. A general scheme for a dynamic equilibrium of NMP (A) as well as examples of NMP (B) based mediators

Increased steric bulk on the adjacent carbons to the nitrogen leads to a reduction in the temperature required for monomers, such as butyl acrylate, to polymerise. However, increased steric bulk also leads to a reduction in deactivation.

Advances in synthetic polymerization techniques in the past two decades allow absolute control over the polymerisation process. Currently, polymers can be produced with high precision over Đ, the degree of polymerisation[46-47] (DP) and sequence[48-53] through controlled radical polymerisation methods, such as RAFT[54], ATRP[55] and SET-LRP[56]. The synthesis of glycopolymers has utilised click chemistry[57] through regioselective and chemoselective reactions to link the saccharide unit to either monomer, for pre-polymerisation modification or onto the polymer by post-polymerisation modification.

1.6. Click Chemistry

In 2001, the concept of 'click' chemistry was born from Sharpless[103], so called because of the ease at which these molecules 'clicked' together to form more complex structures. For a reaction to be classified as 'Click', Sharpless laid out rules for which they must adhere to:

- modular and wide in scope;

- highly efficient with high yields;

- no or inoffensive by-products;

- stereospecificity;

- readily available starting materials and reagents;

- no solvent or a benign solvent;

- simple purification techniques (rather than chromatography).

These rules now govern what is known as a 'click' reaction with examples shown in Table 1.4. However, several chemistries pre-2001, which claimed to be click chemistry failed to meet the criteria set out by Sharpless, including aldol chemistry. These click reactions have been extensively used in polymer chemistry to produce or add additional functionality to glycopolymers[58, 104]. One of the most commonly used click reactions is CuAAC.

Table 1.4. Examples of metal-free "click" chemistries

Reagent A	Reagent B	Reaction Name
Alkene	Thiol	Thiol-ene
Alkyne	Thiol	Thiol-yne
Alkene	Diene	Diels Alder
Cyclooctene	Tetrazine	Hetero-Diels Alder
Triazolinedione	Diene	Hetero-Diels Alder
Dithioester	Diene	Hetero-Diels Alder
Isonitriles	Tetrazines	[4+1] cycloadditions
Alkene	O_2	Dihydroxylation
Epoxide	Nucleophile	Epoxide Ring-opening

1.6.1. Azide-Alkyne Cycloaddition

The CuAAC is one of the most widely used approaches in click reactions. Whilst azides have to be handled with care, due to their explosive nature, they can be useful in facilitating the reduction of amines and the conjugation of alkynes. Azides and

alkynes, in most instances, require a metal catalyst in order to react together, as the azide is a poor 1,3-dipolar acceptor. Scheme 1.15 depicts the catalytic cycle for the [3+2] cycloaddition of the azide and alkyne over 5 steps. The first leads to the formation of the copper(I) acetylide complex, this causes the acidification of the terminus hydrogen leading to the deprotonation and the formation of the terminus acetylide. Following the formation of the acetylide, the azide binds to the copper which can then attack the alkyne from the opposing terminus. The sterics around the copper centres causes the heterocycles to be produced as the 1,4 isomers. In comparison, non-catalysed [3+2] cycloaddition of the azide and alkyne creates both 1,4 and 1,5 isomers of the triazole[105]. The strained copper metallacycle formed is quickly converted to a Cu-triazolyl complex by the migration of nitrogen-Cu bond to the terminus carbon of the alkyne. The proton lost in the first is able to displace the copper freeing the triazole, thus allowing the catalyst to be regenerated.
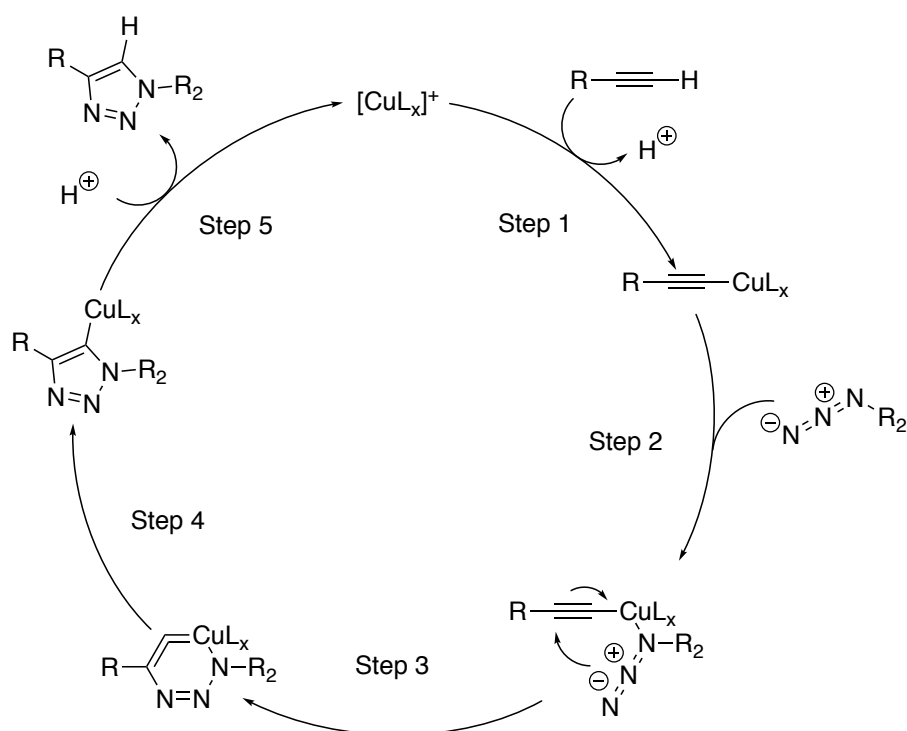
Scheme 1.15. Heterocycle of the CuAAC over 5 steps.

The CuAAC is a popular reaction due to its tolerance to functional groups, as well as the vast number of solvents, copper source and ligands available for the reaction, allowing this reaction to be tailored to suit the condition and solvent system requirements (Table 1.5). CuAAC reaction has opened the door to the formation of several different more complex molecules which by other methods would require several reactions, less efficient and lower yielding than CuAAC. However, the

primary concern with CuAAC when producing biologically active compounds is the need to remove toxic metals. This can lead to lengthy purification, which lowers the overall yield as copper exists at ppm levels after purification.

Table 1.5. Examples of CuAAC reagents

Copper Sources	Ligands	Solvents
CuBr	Na-Ascorbate	Toluene
$CuSO_4.5H_2O$	Me_6TREN	DMSO
CuI	BiPip	DMF
CuCl	$n-Bu_3N$	H_2O
$CuSO_4$	$EtNiPr_2$	t-BuOH
$Cu(II)OAc_2$	DMAP	CH_3OH
$Cu(CH_3CN)_4PF_6$	2,6-lutidine	$CHCl_3$
CuCN	DIPEA	Hexane

Recently, reactions have been developed to allow the formation of triazole without the need of Cu. Strain-promoted azide-alkyne [3+2] cycloaddition (SPAAC) reaction was developed in 2004 by Bertozzi{Baskin, 2007, Copper-free click chemistry for dynamic in vivo imaging}, which showed promise as a catalyst-free alternative to the CuAAC. The process employs cyclocetylene type compounds, due to the ring strain within the structure from the strained alkyne bond angles. The formation of the triazole is favourable as the ring strain is relieved. The rate of SPAAC reaction can be increased by making the alkyne electron deficient, thus dropping the LUMO bond of the alkyne. This is achieved by placing fluorine's on the carbon adjacent to the alkyne (Figure 1.16), leading to an increased reaction rate from 1 to 38.1 M $^{-1}s^{-1}$.
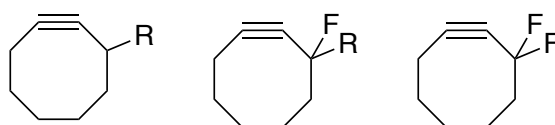
Figure 1.16. Cyclocetylene type compounds with increasing electron deficient alkyne, from left to right.

Without Cu, SPAAC has been used widely for biological applications due to the biocompatibility of the reaction. This process has been used for biologically tagging molecules through methods such as surface binding compounds. This is achieved by using carbohydrates bearing azides to click to a difluorinated cyclooctyne (DIFO) with a fluorescent label.

1.6.2. Thiol Click Reactions

Thiols are also functional groups which can be used in click reactions. Thiol-ene type reactions are very versatile, facilitating an anti-Markovnikov addition of a thiol onto an alkene. This reaction can be initiated by radical or UV induction to cleave the S-H bond. The thiol radical attacks the terminus of the alkene with the radical of the sulphur transferred onto a carbon which can then abstract a hydrogen from another thiol in order to initiate another thiol-ene reaction.
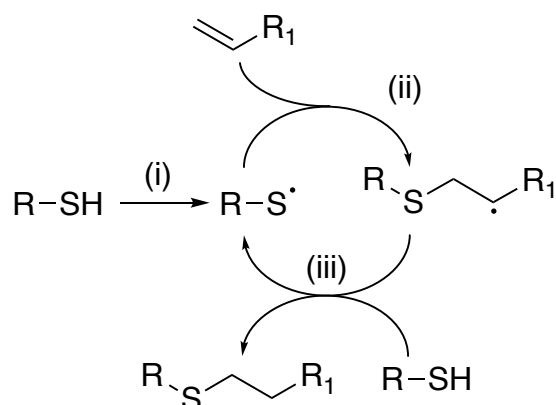
Scheme 1.16. Radically induced Thiol-ene radical reaction mechanism with the initiation (i) followed by the propagation (ii) of the alkene and the chain transfer of the radical and abstraction of the hydrogen (iii) for the next thiol-ene reaction.

Thiol-ene type reactions are used in the formation of glycopolymers to graft the sugars onto the polymers. Where an alkene is not used in the polymerisation (e.g. ROP) then it is free for the thiol-ene reaction. The Bradley group[106] produced microarrays of different glycopolymer compositions by clicking thiol monosaccharides onto pendant alkenes in order to measure the fluorescent output of labelled lectins upon binding. An example by Schubert[107] showed the challenges of polymerising an acrylamide bearing a pendant alkene by RAFT, but the remaining alkenes were able to undergo thiol-ene reactions.

RAFT groups can be reduced with sodium borohydride ($NaBH_4$) to produce a free thiol. This free thiol can be reacted with another to form a disulphide or through the thiol-ene reaction to add functionality to the omega terminus of the polymer[108-110]. The thiol-ene reaction can also work by using alkyne (Thiol-yne reaction) and this can lead to a double substitution of the alkyne by the thiol[111-112]. Thiol-ene reaction can also follow a Michael addition-type reaction if the alkyne is activated (e.g. in acrylates and maleimides). Thiol click reactions also extends to the para substitution of the pentafluorostyrene with the use of a base to form glycopolymers[113].

1.6.3. Cycloaddition Reactions

Whilst CuAAC is a [3+2] cycloaddition, other cycloaddition reactions also can be denoted as a "click' reaction. The Diels-Alder reaction, which won the Nobel prize in 1950, is considered a click reaction. The Diels-Alder works between a diene and alkene (dienophile) as a [4+2] cycloaddition similar to the CuAAc and is considered a concerted pericyclic reaction. This is a thermally activated reaction, but some reactions can undergo Diel-Alder reactions at room temperature. The reaction occurs between the highest occupied molecular orbital (HOMO) and the lowest unoccupied molecular orbital (LUMO) orbitals of the diene and dienophile. These reactions work more efficiently with the addition of electron withdrawing groups on the dienophile and electron donating groups on the diene to bring the molecular orbitals closer in energy.

The Diels-Alder reaction has been incorporated into glycopolymer synthesis through the hetero-Diels Alder (HDA) reaction. Using an HDA reaction with the RAFT end group allow conjugation to the glycopolymer with other polymer chains or add addition functionality[114-115].

Due to the versatility of click reactions and the functional group tolerance, the focus shifts toward is it more efficient to modify before or after the polymerisation. There are two main methods by which glycopolymers can be formed: either by pre-functionalisation of a monomer to form a glycomonomer, or grafting saccharides onto the pre-formed polymer. There is a third less common approach which is the simultaneous conjugation and polymerisation (Scheme 1.17). With the ability to functionalise the anomeric position with amine and oxygens readily, several examples of styrene[116-120], vinyl[121-126], acrylate[114, 127-128] and acrylamide[129-131] based glycomonomers can be synthesised. These glycomonomers are able to polymerise by both ATRP and RAFT, but examples also exist from CROP of a 2-oxazoline-based glycomonomer, as reported from Schubert[95].

Click chemistry has allowed the easier conjugation of saccharides with polymerisable groups to create new glycomonomers[46, 122, 132-133]. However, due to the high efficiency of click reactions, it has opened up the potential to post modify the polymer. There are several advantages and disadvantages (Table 1.6) of post-modification. One main advantage is the ability to form a library of glycopolymers from the same polymer by interchanging the saccharide clicked onto the backbone. This ability to graft the saccharides onto the polymer post-polymerisation has allowed synthetic pathways to form glycopolymers which do not require protection group chemistry. For example,

ROP cannot tolerate the hydroxyls of the monosaccharide. By using ROP, followed by a click reaction, the glycopolymers could be synthesised. The advantage of this is compared to the previous vinyl examples, ROP glycopolymer produced with a biodegradable backbone[134-135].
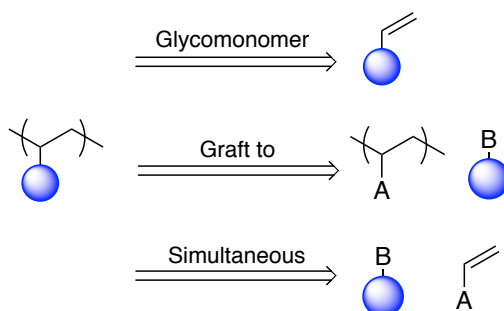
Scheme 1.17. The three strategies used to form glycopolymers either by the polymerisation of a glycomonomer or grafting onto a polymer backbone through methods such as click chemistry or by simultaneous grafting and polymerisation, where A and B are corresponding reactive groups.

The final and less used approach is the simultaneous 'one pot' approach whereby the grafting and polymerisation occur together. The major example of this is the simultaneous CuAAC and ATRP polymerisation[136] since they both require Cu^I. These reactions are less common as they require more care in order to set up to two reactions orthogonally ensuring no cross-reactions are occurring[51].

Table 1.6. List of advantages and disadvantages of the pre and post modification of the polymer.

	Pre-polymerisation functionalisation	Post polymerisation functionalisation
Advantages	Always known carbohydrate content	Polymerisation of known monomers
	Less reaction and purification steps	Facilitated characterization
	Chain extension to form block copolymers or elongated polymers	More control over molar masses and Đ values
	More suitable for large quantities of homo-glycopolymers	Suitable for preparation of libraries from the same batch of polymer
	Direct glycopolymer synthesis without deprotection	More convenient route for tailoring of properties by different monomers
Disadvantages	Cumbersome synthesis and purification of glycopolymers	Require sufficient reactivity of the backbone
	Lower control over molar masses and Đs	Limited to highly efficient reactions
	More difficult to characterize	Usage of excess of carbohydrates
	Solubility compatibility issues between carbohydrate monomers, initiators and co-monomers	Usually cumbersome synthesis of sugar derivatives
	Lower randomization and different distances between sugar and copolymers	Difficult precise determination of functionalization degree
	Usage of expensive, new monomers	

Of the two major routes, each has their advantages and disadvantages. However, it is dependent on the polymer backbone and other functional groups on the polymer as to the best synthetic pathway for the glycopolymer synthesised. With pros and cons for both methodologies, the large array of polymerisation methods, monomers and chemoselective reactions available enable the formation of more complex glycopolymers[59-60]. From these CRP and orthogonal click reactions, more complex polysaccharide analogues can be produced. Therefore, glycopolymer synthesis far surpasses nature's toolbox which is restricted by the enzymatic pathways available.

.

1.7. Peptides

Glycopeptides have shown to be a new area of carbohydrate research, due to the stepwise growth of the peptide backbone. As peptides and proteins have shown to interact with GAGs, these can be used to look at potential applications of the glycopolymers such as the fabrication of supramolecular biomaterials through non-covalent interactions.

1.7.1. Background

Peptides can be defined as polymers formed from the 20 amino acids used in natural proteins linked together by amide bonds. Each amino acid has a central carbon, which in turn is bonded to single hydrogen, a carboxylic acid, an amine, as well as a side chain group, which varies, dependent on the amino acid. Of the 20 amino acids (Figure 1.17), 19 are chiral with glycine (G) being the exception, due to the R group of G being a second hydrogen. In nature, the chiral amino acids exist in the L-form, whilst D-forms of the amino acids exist, but these are non-natural. Using the 20 naturally occurring amino acids and non-natural amino acids, countless number of peptides can be synthesized. Once a peptide chain becomes longer than 50 amino acids, these become classified as polypeptides or proteins.

The primary structure of peptides, defined by the sequence of the amino acids, leads to the formation of a secondary structure, such as alpha-helices and beta-sheet through intra/intermolecular hydrogen bonding. For larger proteins, the secondary structure can fold to form tertiary structures which through interactions with other tertiary units form quaternary structures. The folding and intra/intermolecular interactions are key to for protein function. However, small peptides are highly unlikely to form large complex structures as they do not possess a large number of amino acids required to create these tertiary structures.
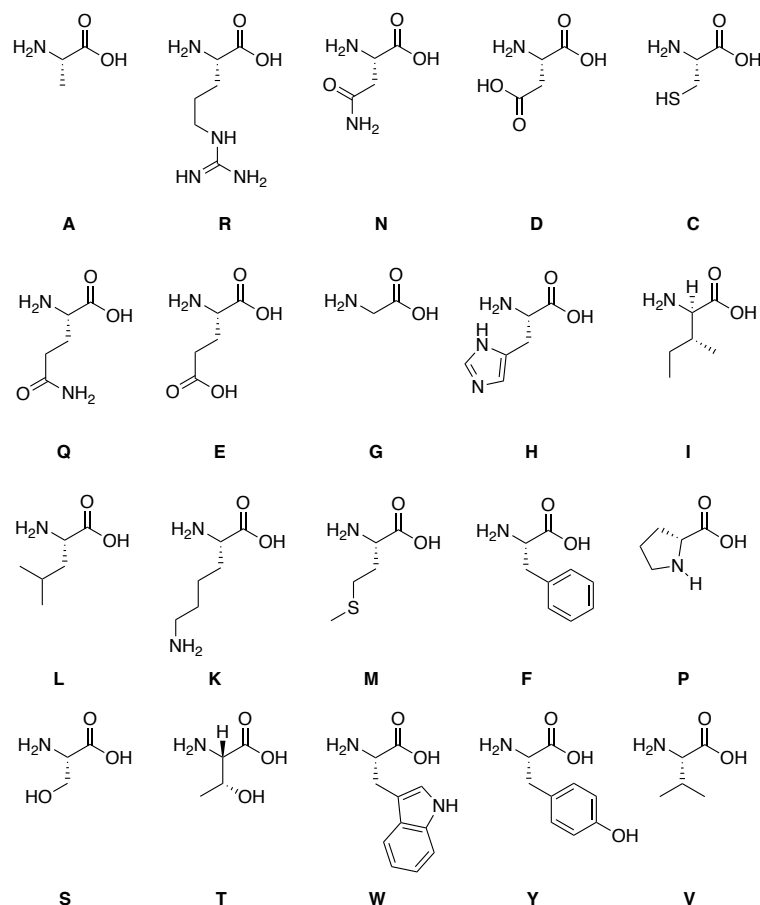
Figure 1.17. Structures of the 20 naturally occurring L-amino acids with the side chain residues.

1.7.2. Peptide Synthesis

The synthesis of a peptide appears as a simple condensation reaction between the amine and the carboxylic acid. However, the formation of this amide is no simple feat. Within peptide synthesis two sets of protecting groups are used in order to control the stepwise growth of the peptide[137]. The side groups of the amino acids are protected by a variety of groups dependent on the type of peptide synthesis and structure of the side chains, these include groups such as tert-Butyloxycarbonyl (Boc), 2,2,4,6,7-Pentamethyldihydro-benzofuran-5-sulfonyl (Pgb) and Trityl (Trt). These protecting groups inhibit the side chains from reacting causing branching or side reactions (Figure 1.17). These protecting groups are selected to be cleaved simultaneously in the final step as well as to be robust during the step-wise synthesis of the peptide.

The other protection chemistry is utilised for the terminals of the peptides, which are selectively deprotected after removal of previous coupling reaction mixture. These protection groups are typically cleaved differently to those of the amino acids, for example Fmoc, is amine protecting group that can be cleaved in the presence base

therefore the side chain groups would be base stable, whilst labile in acids. Other examples of this include the use of Boc protecting groups. These group are deprotected by TFA, so therefore the side chains are typically benzylated as these groups are acid stable and require hydrogenation for deprotection.

For the formation of the amide bond, whilst an amine can be used as a nucleophile; in the presence of an acid a simple proton exchange is typical. Therefore, there is no driving force to create an amide bond. Consequently, carboxylic acid group needs to be activated in order to be susceptible to nucleophilic attack by the amine. The activation is facilitated by reagents typically hydroxylamine such as 3-[Bis(dimethylamino)methyliumyl]-3H-benzotriazol-1-oxide hexafluoro-phosphate (HBTU), Oxyma and N-hxydroxybenzotriazole (HOBt) along with carbodiimides, for example, diisopropylcarbodiimide (DIC) and N,N'-dicyclohexylcarbodiimide (DCC). The combination of reagents produces an activated ester with the loss of a urea-based compound (Scheme 1.18). The amine can readily attack the activated ester to form the amide bond releasing hydroxylamine.
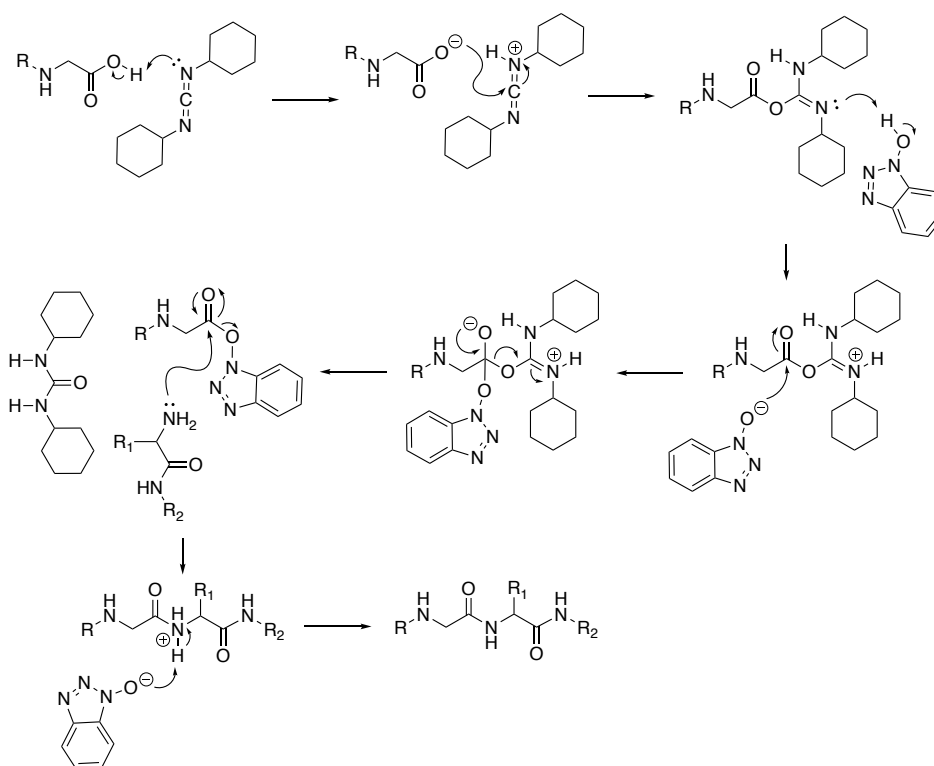
Scheme 1.18. Mechanism of amide bond formation through the use of DIC and HOBt to form an activated ester where the amine of the peptide can attack. R = protecting group e.g. Fmoc, R_1 = protected amino acid side chain, R_2 = peptide chain.

The process of forming a peptide was two main approach; solution phase synthesis and solid phase peptide synthesis (SPPS). Solution phase has been developed from the

early 20th century by Crutius[138] and Fischer[139] . They achieved the formation of the peptide bond by the use of activated carbonyl species such as acyl chlorides and acyl azides[140-141]. These methods required the use of extractions to remove the unreacted amino acids and the by-products from the reactions. By the incorporation of benxzyloxycarbonyl at the N-terminus of the peptide, this lead to directional group of the peptide, where the peptide is grown from the C-terminal of the peptide. Once the synthesis is complete, with the use of hydrogen and a palladium catalyst the benxzyloxycarbonyl is cleaved to give a free the N-terminal. Whilst solution phase peptide synthesis is still used for large scale reactions on smaller scales solid phase peptide synthesis (SPPS) was become standard practice due to the ease at which the technique is employed.

Solid supports are utilised to form peptides by a step-wise approach similar to that of solution phase but increasing the efficiency of the removal by-products and unreacted reagents by simple filtration[142]. These resins are formed of crossed linked polymers such as polystyrene with functional groups such as amines in examples such as rink amides and TantaGel, hydroxides examples such as Wang resins and chlorides such as the Merrifield Resin (Figure 1.18). By selecting the resin, the C-terminal can be selected for either a carboxylic acid or amide dependent on the use of the peptide. To note with the Wang resin several of these come preloaded with the first amino acids, this is due to the poor efficiency of the coupling to the resin.
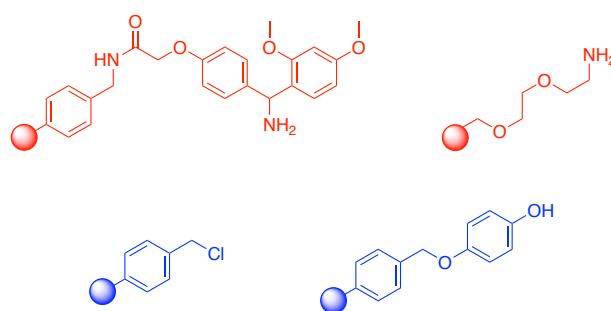
Figure 1.18. Examples of amide terminal producing resins (red) and carboxylic acid terminal producing resins (blue). Clockwise from top left: Rink Amide, TantaGel, Wang Resins and Merrifield Resin

Merrifield[143] developed in 1963 the solid phase peptide synthesis (SPPS) approach where the peptide is grown from a solid support. This support was a crosslinked polystyrene polymer copolymerised with vinylbenzyl chloride, where by the chloride could be used as an anchor to build the peptide from. The first amino acid is attached through the use of triethylammonium salt to create an ester linkage between the resin and first amino acid. In Merrifield's original work he screened the use of activated

esters and the use of dicyclohexylcarbodiimide using carbobenzoxy group protecting amine of which could be cleaved by HBr. This procedure revolutionised the synthesis of peptides as compared to solution phase synthesis as the by-products can be easily washed away with minimal purification between cycles. Since 1968 SPPS has been developed with new resins and employ more reactive chemical to refine the process (Scheme 1.19). This methodology allows the peptides to be produced through cycles of coupling and deprotection in a in a controlled step-wise approach.
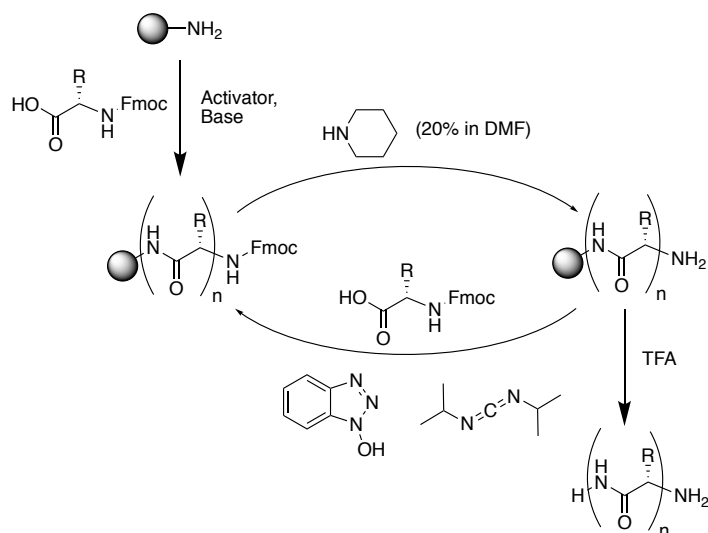
Scheme 1.19. Merrifield solid phase peptide synthesis cycle using HOBt/DIC coupling and piperidine (20% v/v in DMF) for the Fmoc deprotection with TFA cleavage to remove from the support.

However, the downfall of this approach whilst it can be used to form peptides with high purity crudes and specificity for the sequence, this comes from the use of excess reagents, therefore in terms of atom economy is very wasteful and is why solution phase at large scale is still the industry standard. Once the desired sequence has been completed, the cleavage of the peptide can take place from the resin using acids such as trifluoroacetic acid (TFA). In this step, not only is the peptide cleaved from the resin, but the side chains are also deprotected.

1.7.3. Peptide Design

Peptides can be designed using a few different techniques, including screening algorithms of computation libraries or through computer modelling of an active site. Peptides can also be derived from natural proteins which have been sequenced. Examples for HA binding sequences can be obtained in Table 1.7.

Table 1.7. HABPs and their corresponding HA-binding sequences.

Protein	Localisation	Sequence	Ref
RHAMM	SP, MB	KQKIKHVVKLK	[144]
		KLKSQLVKRK	[144]
LP	ECM	RYPISRPRKR	[10, 14, 145]
		RKSYGKYQGR	[145]
CD44	MB	KNGRYSISR	[14]
		RDGTRYVQKGEYR	[14]
		RRRCGQKKK	[14]
HAS	MB	RGTRSGSTR	[14]
		RRRKKIQGRSKR	[14]
Versican	ECM	KVGKSPPVR	[146]
		KTFGKMKPR	[146]
Aggrecan	ECM	RIKWSRVSK	[147]
		KRTMRPTRR	[147]
Human GHAP	ECM	KVGKSPPVR	[148]
TSG-6	ECM	HREARSGKYK	[4]

RHAMM = Receptor for Hyaluronan Mediated Motility, LP = Link Protein, CD44 = Cluster of Differentiation 44, HAS = Hyaluronan Synthase, Human GHAP = Glial Hyaluronate-Binding Protein, TSG-6 = Tumour necrosis factor-inducible gene 6. ECM; Extracellular Matrix, MB; Membrane-Bound, SP; Soluble Protein.

1.7.3.1. Phage Display

An alternative approach to rational peptide design is phage display, a high-throughput technique used to investigate peptide-target interactions. Phage libraries consist of bacteriophage, a virus that infects bacteria, which have been genetically modified to display a peptide as an N-terminus fusion to a viral coat protein. The first example was reported in 1985 with 24 clones[149], and today random peptide libraries are commercially available containing 10^9 unique peptide sequences[150].

In order to identify target-binding peptides rounds of biopanning are undertaken (Scheme 1.20). The target is immobilised and incubated with the phage library. Unbound phages are removed by washing and bound phages are eluted, either using a

non-specific low pH elution buffer or by incubation with a known binder of the target molecule. Binding phage can then be amplified using bacteria and further panning can be carried out. Through these rounds of panning, target-specific binders are enriched, and non-specific binders removed. Once target specific binding is confirmed by enzyme-linked immunosorbent assay (ELISA) phage DNA can be isolated and sequenced to reveal the peptide sequence responsible for binding.
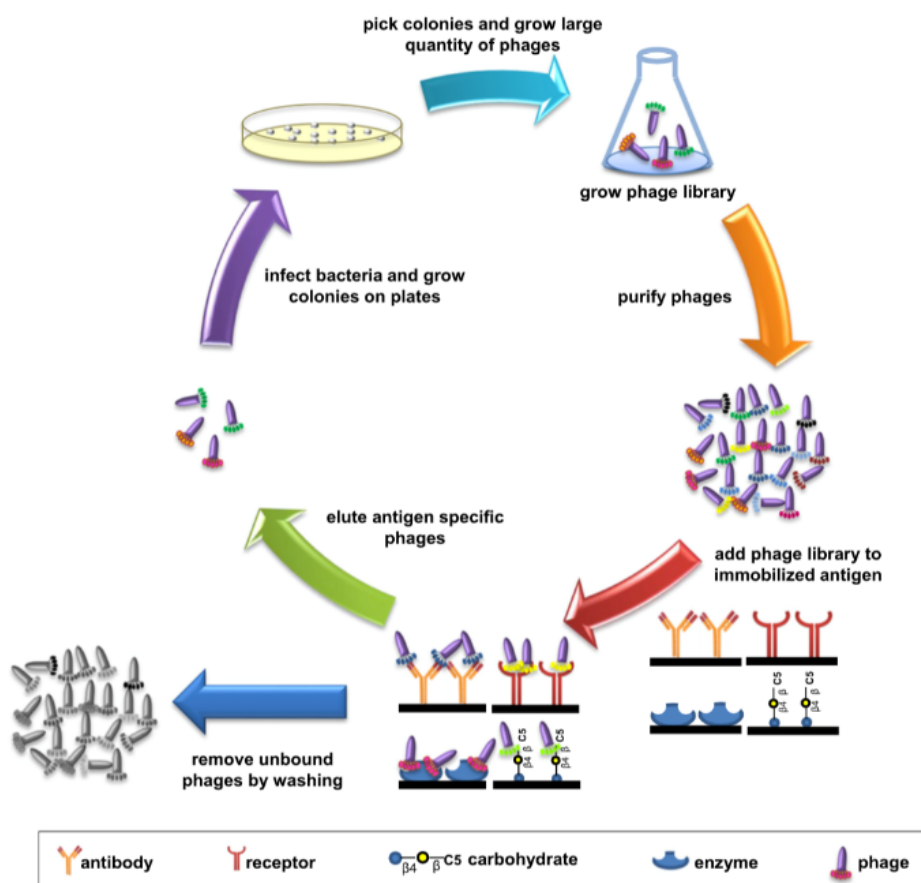
Scheme 1.20. Schematic of the phage display process with the eventual successful sequences being sequenced. Scheme taken from ref[150].

These panning experiments can be carried out both *in vivo* and *in vitro*[151]; the majority of experiments in the literature have been carried out *in vitro*, however the sequences identified do not always maintain their target-binding ability when investigated *in vivo*. Whilst *in vivo* panning is more costly the sequences isolated are more likely to retain their binding capacity in downstream applications, such as targeting specific tissues and drug delivery[152-153].

Phage display has been used to discover antibodies able to bind GAGs[154-157], as well as peptide ligands with affinity to tissues and ECM components[158]. One of these peptides is known as Pep-1[159]. Pep-1, a 12-mer peptide (GAHWNFQALTVR), was

discovered in 2000 and binds to HA. In the phage display process, Pep-1 was negatively screened against CS to ensure the selectivity for HA over CS. Pep-1 has one of the highest affinities for HA with a $K_D = 1.64$ µM and will compete with other HABPs. As a result, research has since been undertaken using Pep-1 to detect the localisation of HA in tissues[160-161], to reduce inflammatory response[162-163] and inhibition of receptor binding[164-166].

Phage display libraries are typically 7 and 12 mers in length, however, synthesis of peptides by manual or automated procedures can produce varying lengths of peptides as well as designing the peptide to contain multiple domains within them.

1.7.3.2. Peptide Amphiphile

Peptide self-assembly (SA) provides a route for the formation of complex 3D structures, which can begin to compete with the complex structures of proteins. By controlling the primary structure of the peptide, the folding of the peptide into alpha helical or beta-sheet conformations can be tailored. From the secondary structures, PAs can begin to control the stacking and interactions of those secondary structures. PAs have been designed to induce structural formation through the use of their amphiphilic nature, whereby the molecules possess a hydrophobic region, such as an alkyl "tail" chain, and a hydrophilic polar head group. This is a basic PA design that has been used to produce many different PA variations (Figure 1.19)[167-170].
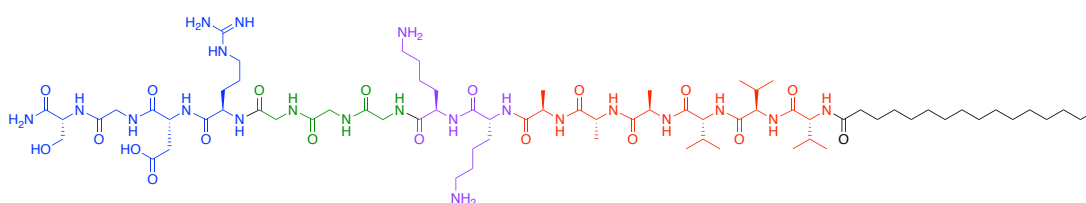
Figure 1.19. Example of a PA design with the alkyl tail (black), β-sheet forming segment (red), charged domain (purple), a spacer (green) and the bioactive sequence (blue).

This structural formulation breaks the peptide into four main sections: a hydrophobic tail, a charged domain, a spacer and a target sequence. The hydrophobic tail can be fatty acids with differing lengths of alkyl chains that can range from C_{10} to C_{16} dependent on the solubility of the peptide. Sequences such as V_3A_3 are typically coupled adjacent to the tail to promote hydrogen bonding and β-sheet formation leading to cylindrical nanofibers instead of spherical micelles. The 4 residues closest to the core hydrophobic tail has been shown[171] to be critical for the structure formation. By utilizing alanine scanning and glycine methylation experiments, it was shown that

the formation of micelles and nanofibers is affected by the order and nature of the amino acids closest to the fatty acid tail. By replacing the beta-sheet forming domain with cysteines, upon increasing of the pH or adding reducing agents intramolecular chemical crosslinking can be formed through disulphide bonds[168, 172] increasing the rigidity of the nanofibers compared to hydrogen bonding or charge-charge interactions. The charge domain ensures solubility of the peptide, whilst a spacer unit coupled before the target sequence allows the peptide to be displayed on the nanofiber surface. Through this PA design, multiple bioactive epitopes can be displayed. This approach can lead to a more stable assembly as well as response more effective binding through the multivalent presentation of bioactive signals. These two distinct sections in polarities within the structure allows for the formation of three-dimensional structures such as micelles and fibres (Scheme 1.21).
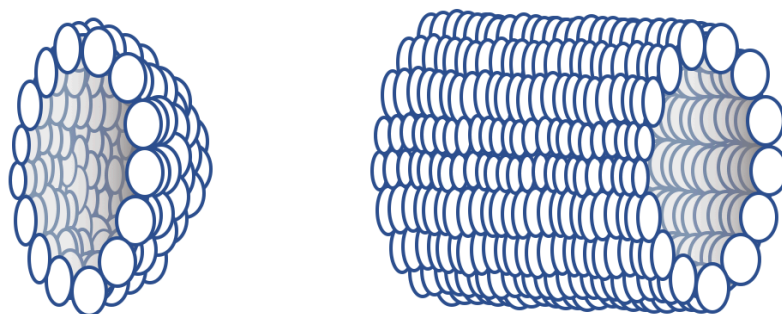
Scheme 1.21. Schematic of a cross-section representation a micelle (left) and fibres (right).

1.8. Preface

The thesis begins with an introduction to the work previously undertaken in the field of GAG-based glycopolymers, highlighting the gap on HA glycopolymers and justifying the need for the work presented in this thesis. Glycopolymer synthesis involves the use of techniques of polymer and carbohydrate chemistry, which have been covered in this part of the thesis. The synthesis of peptides is also described as peptides were used to exploit their binding to natural HA and HA glycopolymers.

The experimental work begins with the modification of HA monosaccharides at the anomeric centre to produce a click monomer, which can be grafted onto monomer or a polymer. The work then shifts towards the production of peptides known to bind to HA. Through analysis of the binding sequence, termini modifications are undertaken in order to promote their self-assembly with natural HA and create new biomaterials. The final experimental chapter compares the physical and chemical properties of the glycopolymers with native HA, as well their binding to small peptides or to carbohydrate-binding proteins (lectins). By presenting the HA sugars in a controlled manner (in homoglycopolymers or alternating glycopolymers), these glycopolymers can be used as probes to elucidate the role of each HA sugar in relevant binding processes.

In the final chapter, the results described in the preceding chapters are summarized, highlighting the main conclusions of the work and pointing out new directions for future work.

References

1. Theocharis, A.D., et al., *Extracellular matrix structure.* Advanced Drug Delivery Reviews, 2016. **97**: p. 4-27.
2. Masu, M., *Proteoglycans and axon guidance: a new relationship between old partners.* Journal of Neurochemistry, 2016. **139**: p. 58-75.
3. Lindahl, U., et al., *Proteoglycans and Sulfated Glycosaminoglycans*, in *Essentials of Glycobiology* A. Varki, R.D. Cummings, and J.D. Esko, Editors. 2017, Cold Spring Harbor Laboratory Press.
4. T. H. Lee, H. Wisniewski, and J. Vildek, *A novel secretory tumor necrosis factor-inducible protein (TSG-6) is a member of the family of hyaluronate binding proteins, closely related to the adhesion receptor CD44.* The Journal of Cell Biology, 1992. **116**(2): p. 545-557.
5. Campo, G.M., et al., *Hyaluronan differently modulates TLR-4 and the inflammatory response in mouse chondrocytes.* Biofactors, 2012. **38**(1): p. 69-76.
6. Nishina, H., et al., *Cell Surface Antigen CD38 Identified as Ecto-Enzyme of NAD Glycohydrolase Has Hyaluronate-Binding Activity.* Biochemical and Biophysical Research Communications, 1994. **203**(2): p. 1318-1323.
7. Aruffo, A., et al., *CD44 Is the Pricinple Cell-Surface Receptor for Hylauronate.* Cell, 1990. **61**(7): p. 1303-1313.
8. Jackson, D.J. *The lymphatic endothelial hyaluronan receptor LYVE-1*. 2004; Available from: http://www.glycoforum.gr.jp/science/hyaluronan/HA28/HA28E.html#III.
9. Day, A.J. and G.D. Prestwich, *Hyaluronan-Binding Proteins: Tying Up The Giant.* Journal of Biological Chemistry, 2002. **277**(7): p. 4585-8.
10. Binette, F., et al., *Link Protein is ubiquitously expressed in non-cartilaginous tissues where it enhances and stabilizes the interaction of proteoglycans with hyaluronic acid.* Journal of Biological Chemistry, 1994. **269**(29): p. 19116-19122.
11. Hasegawa, K., et al., *Versican, a major hyaluronan-binding component in the dermis, loses its hyaluronan-binding ability in solar elastosis.* Journal of Investigative Dermatology, 2007. **127**(7): p. 1657-63.
12. Dicker, K.T., et al., *Hyaluronan: A Simple Polysaccharide with Diverse Biological Functions.* Acta Biomaterialia, 2014. **10**(4): p. 1558-70.
13. Nedvetzki, S., et al., *RHAMM, a receptor for hyaluronan-mediated motility, compensates for CD44 in inflamed CD44-knockout mice: A different interpretation of redundancy.* Proceedings of the National Academy of Sciences of the United States of America, 2004. **101**(52): p. 18081-18086.
14. Yang, B., et al., *Identification of a common hyaluronan binding motif in the hyaluronan binding proteins RHAMM, CD44 and link protein.* The EMBO Journal, 1994. **13**(2): p. 286-296.
15. Mikami, T. and H. Kitagawa, *Biosynthesis and function of chondroitin sulfate.* Biochimica et Biophysica Acta, 2013. **1830**(10): p. 4719-4733.
16. Sugahara, K. and H. Kitagawa, *Recent advances in the study of the biosynthesis and functions of sulfated glycosaminoglycans.* Current Opinion in Structural Biology, 2000. **10**(5): p. 518-527.
17. Silbert, J.E. and G. Sugumaran, *Biosynthesis of Chondroitin/Dermatan Sulfate.* IUBMB Life, 2002. **54**(4): p. 177-186.
18. Kreuger, J. and L. Kjellen, *Heparan sulfate biosynthesis: regulation and variability.* Journal of Histochemistry and Cytochemistry, 2012. **60**(12): p. 898-907.
19. Presto, J., et al., *Heparan sulfate biosynthesis enzymes EXT1 and EXT2 affect NDST1 expression and heparan sulfate sulfation.* Proceedings of the National Academy of Sciences, 2008. **105**(12): p. 4751-4756.
20. Maccarana, M., et al., *Biosynthesis of dermatan sulfate: chondroitin-glucuronate C5-epimerase is identical to SART2.* Journal of Biological Chemistry, 2006. **281**(17): p. 11560-8.
21. L., F.J., *Keratan Sulfate Biosynthesis.* IUBMB Life, 2002. **54**(4): p. 187-194.

22. Tai, G.-H., T.N. Huckerby, and I.A. Nieduszynski, *Multiple Non-reducing Chain Termini Isolated from Bovine Corneal Keratan Sulfates.* Journal of Biological Chemistry, 1996. **271**(38): p. 23535-23546.

23. Habuchi, O., et al., *Enzymatic sulfation of galactose residue of keratan sulfate by chondroitin 6-sulfotransferase.* Glycobiology, 1996. **6**(1): p. 51-7.

24. Fukuta, M., et al., *Molecular Cloning and Characterization of Human Keratan Sulfate Gal-6-Sulfotransferase.* Journal of Biological Chemistry, 1997. **272**(51): p. 32321-32328.

25. Kobayashi, M., et al., *Molecular Cloning and Characterization of a Human Uronyl 2-Sulfotransferase That Sulfates Iduronyl and Glucuronyl Residues in Dermatan/Chondroitin Sulfate.* Journal of Biological Chemistry, 1999. **274**(15): p. 10474-10480.

26. Lindahl, U., M. Kusche-Gullberg, and L. Kjellén, *Regulated Diversity of Heparan Sulfate.* Journal of Biological Chemistry, 1998. **273**(39): p. 24979-24982.

27. Saied-Santiago, K. and E. Bülow Hannes, *Diverse roles for glycosaminoglycans in neural patterning.* Developmental Dynamics, 2017. **247**(1): p. 54-74.

28. Frantz, C., K.M. Stewart, and V.M. Weaver, *The extracellular matrix at a glance.* Journal of Cell Biology, 2010. **123**(Pt 24): p. 4195-200.

29. Frantz, C., K.M. Stewart, and V.M. Weaver, *The extracellular matrix at a glance.* J Cell Sci, 2010. **123**(Pt 24): p. 4195-200.

30. Rybinski, B., J. Franco-Barraza, and E. Cukierman, *The wound healing, chronic fibrosis, and cancer progression triad.* Physiological Genomics, 2014. **46**(7): p. 223-244.

31. Penc, S.F., et al., *Dermatan Sulfate Released after Injury Is a Potent Promoter of Fibroblast Growth Factor-2 Function.* Journal of Biological Chemistry, 1998. **273**(43): p. 28116-28121.

32. Jiang, D., J. Liang, and P.W. Noble, *Hyaluronan as an Immune Regulator in Human Diseases.* Physiological Reviews, 2011. **91**(1): p. 221-264.

33. Wisniewski, H.-G. and J. Vilĉek, *TSG-6: An IL-1 /TNF-inducible protein with anti-inflammatory activity.* Cytokine & Growth Factor Reviews, 1997. **8**(2): p. 143-156.

34. Taylor, K.R. and R.L. Gallo, *Glycosaminoglycans and their proteoglycans: host-associated molecular patterns for initiation and modulation of inflammation.* FASEB Journal, 2006. **20**(1): p. 9-22.

35. Handel, T.M., et al., *Regulation of protein function by glycosaminoglycans--as exemplified by chemokines.* Annual Review of Biochemistry, 2005. **74**: p. 385-410.

36. Ghatak, S., et al., *Roles of Proteoglycans and Glycosaminoglycans in Wound Healing and Fibrosis.* The International Journal of Biochemistry & Cell Biology, 2015. **2015**: p. 834893.

37. Campo, G.M., et al., *Glycosaminoglycans modulate inflammation and apoptosis in LPS-treated chondrocytes.* Journal of Biomedical Science, 2009. **106**(1): p. 83-92.

38. Campo, G.M., et al., *Glycosaminoglycans reduce oxidative damage induced by copper (Cu+2), iron (Fe+2) and hydrogen peroxide (H2O2) in human fibroblast cultures.* Glycoconjugate Journal, 2003. **20**(2): p. 133-141.

39. Shworak, N.W., et al., *Anticoagulant Heparan Sulfate.* 2010. **93**: p. 153-178.

40. Tollefsen, D.M., *Vascular Dermatan Sulfate and Heparin Cofactor II.* 2010. **93**: p. 351-372.

41. Van Battum, E.Y., S. Brignani, and R.J. Pasterkamp, *Axon guidance proteins in neurological disorders.* The Lancet Neurology, 2015. **14**(5): p. 532-546.

42. Dou, C.L. and J.M. Levine, *Differential effects of glycosaminoglycans on neurite growth on laminin and L1 substrates.* The Journal of Neuroscience, 1995. **15**(12): p. 8053.

43. Snow, D.M., et al., *A chondroitin sulfate proteoglycan may influence the direction of retinal ganglion cell outgrowth.* Development, 1991. **113**(4): p. 1473-1485.

44. Bernhardt, R.R. and M. Schachner, *Chondroitin sulfates affect the formation of the segmental motor nerves in zebrafish embryos.* Developmental Biology, 2000. **221**(1): p. 206-19.

45. Pratt, T., et al., *Heparan sulphation patterns generated by specific heparan sulfotransferase enzymes direct distinct aspects of retinal axon guidance at the optic chiasm.* The Journal of Neuroscience, 2006. **26**(26): p. 6911-23.

46. Zhang, Q., et al., *Sequence-Controlled Multi-Block Glycopolymers to Inhibit DC-SIGN-gp120 Binding.* Angewandte Chemie International Edition, 2013. **125**(16): p. 4531-4535.

47. Aksakal, R., M. Resmini, and C.R. Becer, *Pentablock star shaped polymers in less than 90 minutes via aqueous SET-LRP.* Polymer Chemistry, 2016. **7**(1): p. 171-175.

48. Gerke, C., et al., *Sequence-Controlled Glycopolymers via Step-Growth Polymerization of Precision Glycomacromolecules for Lectin Receptor Clustering.* Biomacromolecules, 2017. **18**(3): p. 787-796.

49. Lutz, J.F., et al., *Sequence-Controlled Polymers.* Science, 2013. **341**(6146): p. 628-636.

50. Williams, E.G.L., et al., *Preparation of 1:1 alternating, nucleobase-containing copolymers for use in sequence-controlled polymerization.* Polymer Chemistry, 2015. **6**(2): p. 228-232.

51. Srichan, S., H. Mutlu, and J.F. Lutz, *On the synthesis of sequence-controlled poly(vinyl benzyl amine-co-N-substituted maleimides) copolymers.* European Polymer Journal, 2015. **62**: p. 338-346.

52. Malins, E.L., C. Waterson, and C.R. Becer, *Alternating copolymers of functionalized [small alpha]-methyl styrene monomers and maleic anhydride.* Polymer Chemistry, 2015. **6**(36): p. 6543-6552.

53. Guo, Q.Q., et al., *Block versus Random Amphiphilic Glycopolymer Nanopaticles as Glucose-Responsive Vehicles.* Biomacromolecules, 2015. **16**(10): p. 3345-3356.

54. Moad, G., E. Rizzardo, and S.H. Thang, *Radical addition-fragmentation chemistry in polymer synthesis.* Polymer, 2008. **49**(5): p. 1079-1131.

55. Matyjaszewski, K. and N.V. Tsarevsky, *Nanostructured functional materials prepared by atom transfer radical polymerization.* Nature Chemistry, 2009. **1**(4): p. 276-288.

56. Percec, V., et al., *Ultrafast Synthesis of Ultrahigh Molar Mass Polymers by Metal-Catalyzed Living Radical Polymerization of Acrylates, Methacrylates, and Vinyl Chloride Mediated by SET at 25 °C.* Journal of the American Chemical Society, 2006. **128**(43): p. 14156-14165.

57. Kolb, H.C., M.G. Finn, and K.B. Sharpless, *Click chemistry: Diverse chemical function from a few good reactions.* Angewandte Chemie-International Edition, 2001. **40**(11): p. 2004-+.

58. Slavin, S., et al., *Synthesis of glycopolymers via click reactions.* European Polymer Journal, 2011. **47**(4): p. 435-446.

59. Baradel, N., et al., *Synthesis of Single-Chain Sugar Arrays.* Angewandte Chemie International Edition, 2013. **52**(8): p. 2335-2339.

60. Vinson, N., et al., *Optimised 'click' synthesis of glycopolymers with mono/di- and trisaccharides.* Polymer Chemistry, 2011. **2**(1): p. 107-113.

61. Rawat, M., et al., *Neuroactive Chondroitin Sulfate Glycomimetics.* Journal of the American Chemical Society, 2008. **130**(10): p. 2959-2961.

62. Lee, S.-G., et al., *End-functionalized glycopolymers as mimetics of chondroitin sulfate proteoglycans.* Chemical Science, 2010. **1**(3): p. 322-325.

63. Liu, P., et al., *Tailored chondroitin sulfate glycomimetics via a tunable multivalent scaffold for potentiating NGF/TrkA-induced neurogenesis.* Chemical Science, 2015. **6**(1): p. 450-456.

64. Pedro, D.-R., et al., *Glycodendrimers as Chondroitin Sulfate Mimetics: Synthesis and Binding to Growth Factor Midkine.* Chemistry: A European Journal, 2017. **23**(47): p. 11338-11345.

65. Liekens, S., et al., *Modulation of Fibroblast Growth Factor-2 Receptor Binding, Signaling, and Mitogenic Activity by Heparin-Mimicking Polysulfonated Compounds.* Molecular Pharmacology, 1999. **56**(1): p. 204.

66. Guan, R., et al., *A Glycopolymer Chaperone for Fibroblast Growth Factor-2.* Bioconjugate Chemistry, 2004. **15**(1): p. 145-151.

67. Ayres, N., et al., *Polymer brushes containing sulfonated sugar repeat units: Synthesis, characterization, and in vitro testing of blood coagulation activation.* Journal of Polymer Science Part A: Polymer Chemistry, 2008. **46**(23): p. 7713-7724.

68. Huang, Y., et al., *Synthesis and anticoagulant activity of polyureas containing sulfated carbohydrates.* Biomacromolecules, 2014. **15**(12): p. 4455-66.

69. Huang, Y., et al., *Blood compatibility of heparin-inspired, lactose containing, polyureas depends on the chemistry of the polymer backbone.* Polymer Chemistry, 2016. **7**(23): p. 3897-3905.

70. Oh, Y.I., et al., *Tailored Glycopolymers as Anticoagulant Heparin Mimetics.* Angewandte Chemie International Edition\, 2013. **52**\(45\): p. 11796\-11799\.

71. Sheng, G.J., et al., *Tunable Heparan Sulfate Mimetics for Modulating Chemokine Activity.* Journal of the American Chemical Society, 2013. **135**(30): p. 10898-10901.

72. Loka, R.S., et al., *Design, synthesis, and evaluation of heparan sulfate mimicking glycopolymers for inhibiting heparanase activity.* Chemical Communications, 2017. **53**(65): p. 9163-9166.

73. Sletten, E.T., et al., *Glycosidase Inhibition by Multivalent Presentation of Heparan Sulfate Saccharides on Bottlebrush Polymers.* Biomacromolecules, 2017. **18**(10): p. 3387-3399.

74. Lee, S.S., et al., *Sulfated glycopeptide nanostructures for multipotent protein activation.* Nature Nanotechnology, 2017. **12**(8): p. 821-829.

75. Kandasamy, J., et al., *Modular automated solid phase synthesis of dermatan sulfate oligosaccharides.* Chemical Communications, 2014. **50**(15): p. 1875-7.

76. Maza, S., et al., *Synthesis of chondroitin/dermatan sulfate-like oligosaccharides and evaluation of their protein affinity by fluorescence polarization.* Organic and Biomolecular Chemistry, 2013. **11**(21): p. 3510-25.

77. Takeda, N. and J. Tamura, *Synthesis of biotinylated keratan sulfate repeating disaccharides.* Bioscience, Biotechnology, and Biochemistry, 2014. **78**(1): p. 29-37.

78. Hahm, H.S., et al., *Automated Glycan Assembly of Oligo- N -Acetyllactosamine and Keratan Sulfate Probes to Study Virus-Glycan Interactions.* Chem, 2017. **2**(1): p. 114-124.

79. Hidari, K.I., et al., *Chemoenzymatic synthesis, characterization, and application of glycopolymers carrying lactosamine repeats as entry inhibitors against influenza virus infection.* Glycobiology, 2008. **18**(10): p. 779-88.

80. Sallas, F. and S.-I. Nishimura, *Chemo-enzymatic synthesis of glycopolymers and sequential glycopeptides bearing lactosamine and sialyl Lewisx unit pendant chains.* Journal of the Chemical Society, Perkin Transactions 1, 2000(13): p. 2091-2103.

81. Sun, X.-L., et al., *Glycosaminoglycan Mimetic Biomaterials. 4. Synthesis of Sulfated Lactose-Based Glycopolymers That Exhibit Anticoagulant Activity.* Biomacromolecules, 2002. **3**(5): p. 1065-1070.

82. Banerji, S., et al., *Structures of the Cd44-hyaluronan complex provide insight into a fundamental carbohydrate-protein interaction.* Nature Structural & Molecular Biology, 2007. **14**(3): p. 234-9.

83. Rele, S.M., S.S. Iyer, and E.L. Chaikof, *Homodimerization of hyaluronan and heparan sulfate derivatives by olefin metathesis reaction.* Tetrahedron Letters, 2003. **44**(1): p. 89-91.

84. Iyer, S., et al., *Synthesis of a hyaluronan neoglycopolymer by ring-opening metathesis polymerization.* Chemical Communications, 2003(13): p. 1518-1519.

85. Gordon, E.J., et al., *Synthesis of end-labeled multivalent ligands for exploring cell-surface-receptor–ligand interactions.* Chemistry & Biology, 2000. **7**(1): p. 9-16.

86. Iyer, S.S., et al., *Design and synthesis of hyaluronan-mimetic gemini disaccharides.* Tetrahedron, 2003. **59**(5): p. 631-638.

87. Rele, S.M., S.S. Iyer, and E.L. Chaikof, *Hyaluronan-based glycoclusters as probes for chemical glycobiology.* Tetrahedron Letters, 2007. **48**(29): p. 5055-5060.

88. Upadhyay, K.K., et al., *Biomimetic Doxorubicin Loaded Polymersomes from Hyaluronan-block-Poly(γ-benzyl glutamate) Copolymers.* Biomacromolecules, 2009. **10**(10): p. 2802-2808.

89.   Ma, Y., et al., *Construction of Hyaluronic Tetrasaccharide Clusters Modified Polyamidoamine siRNA Delivery System.* Nanomaterials, 2018. **8**(6).

90.   Sha, M., et al., *Synthesis of structure-defined branched hyaluronan tetrasaccharide glycoclusters.* Tetrahedron Letters, 2017. **58**(30): p. 2910-2914.

91.   Karskela, M., et al., *Synthesis and Cellular Uptake of Fluorescently Labeled Multivalent Hyaluronan Disaccharide Conjugates of Oligonucleotide Phosphorothioates.* Bioconjugate Chemistry, 2008. **19**(12): p. 2549-2558.

92.   de Jong, A.R., et al., *A Second-Generation Tandem Ring-Closing Metathesis Cleavable Linker for Solid-Phase Oligosaccharide Synthesis.* European Journal of Organic Chemistry, 2013. **2013**(29): p. 6644-6655.

93.   Juaristi, E. and G. Cuevas, *Recent studies of the anomeric effect.* Tetrahedron, 1992. **48**(24): p. 5019-5087.

94.   Lemieux, R.U. and A.A. Pavia, *Substitutional and solvation effects on conformational equilibria. Effects on the interaction between opposing axial oxygen atoms.* Canadian Journal of Chemistry, 1969. **47**(23): p. 4441-4446.

95.   Kempe, K., et al., *Responsive glyco-poly(2-oxazoline)s: synthesis, cloud point tuning, and lectin binding.* Biomacromolecules, 2011. **12**(7): p. 2591-600.

96.   Fan, F., et al., *Microwave-assisted synthesis of glycopolymers by ring-opening metathesis polymerization (ROMP) in an emulsion system.* Polymer Chemistry, 2017. **8**(44): p. 6709-6719.

97.   Fan, F., et al., *Synthesis of Fucoidan-Mimetic Glycopolymers with Well-Defined Sulfation Patterns via Emulsion Ring-Opening Metathesis Polymerization.* ACS Macro Letters, 2018. **7**(3): p. 330-335.

98.   Manning, D.D., et al., *Synthesis of Sulfated Neoglycopolymers: Selective P-Selectin Inhibitors.* Journal of the American Chemical Society, 1997. **119**(13): p. 3161-3162.

99.   Talyor, H.S. and A.A. Vernon, *The Photo-Polymerisation Of Styrene And Vinyl Acetate.* Journal of the American Chemical Society, 1931. **53**(7): p. 9.

100.   Chiefari, J., et al., *Living free-radical polymerization by reversible addition-fragmentation chain transfer: The RAFT process.* Macromolecules, 1998. **31**(16): p. 5559-5562.

101.   Aldrich, S. *RAFT: Choosing the Right Agent to Achieve Controlled Polymerization.* [cited 2017 17/12/2017].

102.   Georges, M.K., et al., *Narrow molecular weight resins by a free-radical polymerization process.* Macromolecules, 1993. **26**(11): p. 2987-2988.

103.   Kolb, H.C., M.G. Finn, and K.B. Sharpless, *Click Chemistry: Diverse Chemical Function from a Few Good Reactions.* Angewandte Chemie International Edition, 2001. **40**(11): p. 2004-2021.

104.   Zhang, Q. and D.M. Haddleton, *Synthetic Glycopolymers: Some Recent Developments*, in *Hierarchical Macromolecular Structures: 60 Years after the Staudinger Nobel Prize Ii*, V. Percec, Editor. 2013, Springer Int Publishing Ag: Cham. p. 39-59.

105.   Rostovtsev, V.V., et al., *A stepwise Huisgen cycloaddition process: Copper(I)-catalyzed regioselective "ligation" of azides and terminal alkynes.* Angewandte Chemie-International Edition, 2002. **41**(14): p. 2596-2599.

106.   Neumann, K., et al., *An Approach to the High-Throughput Fabrication of Glycopolymer Microarrays through Thiol–Ene Chemistry.* Macromolecules, 2017. **50**(16): p. 6026-6031.

107.   von der Ehe, C., et al., *Synthesis of Thermoresponsive Glycopolymers Combining RAFT Polymerization, Thiol-Ene Reaction, and Subsequent Immobilization onto Solid Supports.* Macromolecular Chemistry and Physics, 2014. **215**(13): p. 1306-1318.

108.   Lu, J., et al., *One-pot synthesis of glycopolymer-porphyrin conjugate as photosensitizer for targeted cancer imaging and photodynamic therapy.* Macromolecular Bioscience, 2014. **14**(3): p. 340-6.

109.   Boyer, C., et al., *Modification of RAFT-polymers via thiol-ene reactions: A general route to functional polymers and new architectures.* Journal of Polymer Science Part A: Polymer Chemistry, 2009. **47**(15): p. 3773-3794.

110. Abel, B.A. and C.L. McCormick, *"One-Pot" Aminolysis/Thiol–Maleimide End-Group Functionalization of RAFT Polymers: Identifying and Preventing Michael Addition Side Reactions.* Macromolecules, 2016. **49**(17): p. 6193-6202.

111. Semsarilar, M., V. Ladmiral, and S.b. Perrier, *Highly Branched and Hyperbranched Glycopolymers via Reversible Addition−Fragmentation Chain Transfer Polymerization and Click Chemistry.* Macromolecules, 2010. **43**(3): p. 1438-1443.

112. Kumar, J., A. Bousquet, and M.H. Stenzel, *Thiol-alkyne chemistry for the preparation of micelles with glycopolymer corona: dendritic surfaces versus linear glycopolymer in their ability to bind to lectins.* Macromolecular Rapid Communications, 2011. **32**(20): p. 1620-6.

113. Becer, C.R., et al., *Clicking Pentafluorostyrene Copolymers: Synthesis, Nanoprecipitation, and Glycosylation.* Macromolecules, 2009. **42**(7): p. 2387-2394.

114. Glassner, M., et al., *(Ultra)fast catalyst-free macromolecular conjugation in aqueous environment at ambient temperature.* Journal of the American Chemical Society, 2012. **134**(17): p. 7274-7.

115. Kaupp, M., et al., *Modular design of glyco-microspheres via mild pericyclic reactions and their quantitative analysis.* Polymer Chemistry, 2012. **3**(9): p. 2605.

116. Kobayashi, K., H. Sumitomo, and Y. Ina, *Synthesis and Functions of Polystyrene Derivatives Having Pendant Oligosaccharides.* Polymer Journal, 1985. **17**: p. 567.

117. Ohno, K., et al., *Synthesis of a Well-Defined Glycopolymer by Nitroxide-Controlled Free Radical Polymerization.* Macromolecules, 1998. **31**(4): p. 1064-1069.

118. Loykulnant, S. and A. Hirao, *Protection and Polymerization of Functional Monomers. 30. Anionic Living Polymerization of 4-Alkylstyrenes Containing Acetal-Protected Monosaccharide Residues.* Macromolecules, 2000. **33**(13): p. 4757-4764.

119. Wataoka, I., K. Kobayashi, and K. Kajiwara, *Effect of the carbohydrate side-chain on the conformation of a glycoconjugate polystyrene in aqueous solution.* Carbohydrate Research, 2005. **340**(5): p. 989-95.

120. Narumi, A., et al., *Glycoconjugated Polymer II. Synthesis of Polystyrene-block-poly(4-vinylbenzyl glucoside) and Polystyrene-block-poly(4-vinylbenzyl maltohexaoside) via 2,2,6,6-Tetramethylpiperidine-1-oxyl-Mediated Living Radical Polymerization.* Polymer Journal, 2001. **33**: p. 939.

121. Grande, D., et al., *Glycosaminoglycan-Mimetic Biomaterials. 1. Nonsulfated and Sulfated Glycopolymers by Cyanoxyl-Mediated Free-Radical Polymerization.* Macromolecules, 2000. **33**(4): p. 1123-1125.

122. Yilmaz, G., et al., *Glyconanoparticles with controlled morphologies and their interactions with a dendritic cell lectin.* Polymer Chemistry, 2016. **7**(41): p. 6293-6296.

123. Ganda, S., et al., *Biodegradable Glycopolymeric Micelles Obtained by RAFT-controlled Radical Ring-Opening Polymerization.* Macromolecules, 2016. **49**(11): p. 4136-4146.

124. Guo, W., et al., *Triple stimuli-responsive amphiphilic glycopolymer.* Journal of Polymer Science Part A: Polymer Chemistry, 2014. **52**(15): p. 2131-2138.

125. Matsuoka, K., et al., *Use of chloromethylstyrene as a supporter for convenient preparation of carbohydrate monomer and glycopolymers.* Carbohydrate Polymers, 2014. **107**: p. 209-13.

126. Sumerlin, B.S., et al., *Highly efficient "click" functionalization of poly(3-azidopropyl methacrylate) prepared by ATRP.* Macromolecules, 2005. **38**(18): p. 7540-7545.

127. Narain, R. and S.P. Armes, *Synthesis and Aqueous Solution Properties of Novel Sugar Methacrylate-Based Homopolymers and Block Copolymers.* Biomacromolecules, 2003. **4**(6): p. 1746-1758.

128. Wang, Y., et al., *Synthesis and pH/sugar/salt-sensitivity study of boronate crosslinked glycopolymer nanoparticles.* New Journal of Chemistry, 2013. **37**(3): p. 796.

129. Buckwalter, D.J., et al., *MAG versus PEG: Incorporating a Poly(MAG) Layer to Promote Colloidal Stability of Nucleic Acid/"Click Cluster" Complexes.* ACS Macro Letters, 2012. **1**(5): p. 609-613.

130.	Abdelkader, O., et al., *Generation of well-defined clickable glycopolymers from aqueous RAFT polymerization of isomaltulose-derived acrylamides.* Journal of Polymer Science Part A: Polymer Chemistry, 2011. **49**(6): p. 1309-1318.

131.	Ahmed, M. and R. Narain, *Cell line dependent uptake and transfection efficiencies of PEI-anionic glycopolymer systems.* Biomaterials, 2013. **34**(17): p. 4368-76.

132.	Hetzer, M., et al., *Neoglycopolymers Based on 4-Vinyl-1,2,3-Triazole Monomers Prepared by Click Chemistry.* Macromolecular Bioscience, 2010. **10**(2): p. 119-126.

133.	Loka, R.S., M.S. McConnell, and H.M. Nguyen, *Studies of Highly-Ordered Heterodiantennary Mannose/Glucose-Functionalized Polymers and Concanavalin A Protein Interactions Using Isothermal Titration Calorimetry.* Biomacromolecules, 2015. **16**(12): p. 4013-4021.

134.	Xu, N., et al., *Synthesis of amphiphilic biodegradable glycocopolymers based on poly(ε-caprolactone) by ring-opening polymerization and click chemistry.* Journal of Polymer Science Part A: Polymer Chemistry, 2009. **47**(14): p. 3583-3594.

135.	Lu, C., et al., *Sugars-grafted aliphatic biodegradable poly(L-lactide-co-carbonate)s by click reaction and their specific interaction with lectin molecules.* Journal of Polymer Science Part A: Polymer Chemistry, 2007. **45**(15): p. 3204-3217.

136.	Zhang, W., et al., *Precisely controlled copper(0)-catalyzed one-pot reaction: Concurrent living radical polymerization and click chemistry.* Journal of Polymer Science Part A: Polymer Chemistry, 2012. **50**(17): p. 3656-3663.

137.	Isidro-Llobet, A., M. Álvarez, and F. Albericio, *Amino Acid-Protecting Groups.* Chemical Reviews, 2009. **109**(6): p. 2455-2504.

138.	Curtius, T., *Ueber die Einwirkung von Chlorbenzoyl auf Glycocollsilber.* Journal für Praktische Chemie, 1881. **24**(1): p. 239-240.

139.	Fischer, E. and A. Speier, *Darstellung der Ester.* Berichte der deutschen chemischen Gesellschaft, 1895. **28**(3): p. 3252-3258.

140.	Carpino, L.A., et al., *Rapid, Continuous Solution-Phase Peptide Synthesis: Application to Peptides of Pharmaceutical Interest.* Organic Process Research & Development, 2003. **7**(1): p. 28-37.

141.	Yoshio, O., *Synthesis of Peptides by Solution Methods.* Current Organic Chemistry, 2001. **5**(1): p. 1-43.

142.	Jaradat, D.s.M.M., *Thirteen decades of peptide synthesis: key developments in solid phase peptide synthesis and amide bond formation utilized in peptide ligation.* Amino Acids, 2018. **50**(1): p. 39-68.

143.	Merrifield, R.B., *Solid Phase Peptide Synthesis. I. The Synthesis of a Tetrapeptide.* Journal of the American Chemical Society, 1963. **85**(14): p. 2149-2154.

144.	Hoare, K., et al., *Identification of Hyaluronan Binding Proteins Using a Biotinylated Hyaluronan Probe.* Connective Tissue Research, 1993. **30**(2): p. 117-126.

145.	Deák, F., et al., *Complete amino acid sequence of chicken cartilage link protein deduced from cDNA clones.* Proceedings of the National Academy of Sciences of the United States of America, 1986. **83**(11): p. 3766-3770.

146.	Zimmermann, D.R. and E. Ruoslahti, *Multiple domains of the large fibroblast proteoglycan, versican.* The EMBO Journal, 1989. **8**(10): p. 2975-2981.

147.	Doege, K.J., et al., *Complete coding sequence and deduced primary structure of the human cartilage large aggregating proteoglycan, aggrecan. Human-specific repeats, and additional alternatively spliced forms.* Journal of Biological Chemistry, 1991. **266**(2): p. 894-902.

148.	Perides, G., et al., *Isolation and partial characterization of a glial hyaluronate-binding protein.* Journal of Biological Chemistry, 1989. **264**(10): p. 5981-5987.

149.	Smith, G., *Filamentous fusion phage: novel expression vectors that display cloned antigens on the virion surface.* Science, 1985. **228**(4705): p. 1315-1317.

150.	Biolab, N.E. *Ph.D.™-12 Phage Display Peptide Library.* [cited 2018 16/07/2018]; Available from: https://international.neb.com/products/e8111-phd-12-phage-display-peptide-library#Product%20Information.

151.	Wu, C.H., et al., *Advancement and applications of peptide phage display technology in biomedical science.* Journal of Biomedical Science, 2016. **23**: p. 8.

152. Wu, C.-H., et al., *α-Enolase–binding peptide enhances drug delivery efficiency and therapeutic efficacy against colorectal cancer.* Science Translational Medicine, 2015. **7**(290): p. 290ra91.

153. Pi, Y., et al., *Targeted delivery of non-viral vectors to cartilage in vivo using a chondrocyte-homing peptide identified by phage display.* Biomaterials, 2011. **32**(26): p. 6324-6332.

154. Lensen, J.F.M., et al., *Selection and characterization of a unique phage display-derived antibody against dermatan sulfate.* Matrix Biology, 2006. **25**(7): p. 457-461.

155. Jenniskens, G.J., et al., *Heparan Sulfate Heterogeneity in Skeletal Muscle Basal Lamina: Demonstration by Phage Display-Derived Antibodies.* The Journal of Neuroscience, 2000. **20**(11): p. 4099-4111.

156. van Kuppevelt, T.H., et al., *Generation and Application of Type-specific Anti-Heparan Sulfate Antibodies Using Phage Display Technology: FURTHER EVIDENCE FOR HEPARAN SULFATE HETEROGENEITY IN THE KIDNEY.* Journal of Biological Chemistry, 1998. **273**(21): p. 12960-12966.

157. Lensen, J.F., et al., *Localization and functional characterization of glycosaminoglycan domains in the normal human kidney as revealed by phage display-derived single chain antibodies.* Journal of the American Society of Nephrology, 2005. **16**(5): p. 1279-88.

158. Martins, I.M., R.L. Reis, and H.S. Azevedo, *Phage Display Technology in Biomaterials Engineering: Progress and Opportunities for Applications in Regenerative Medicine.* ACS Chemical Biology, 2016. **11**(11): p. 2962-2980.

159. Mummert, M.E., et al., *Development of a peptide inhibitor of hyaluronan-mediated leukocyte trafficking.* Journal of Experimental Medicine, 2000. **192**(6): p. 769-779.

160. Zmolik, J.M. and M.E. Mummert, *Pep-1 as a novel probe for the in situ detection of hyaluronan.* Journal of Histochemistry and Cytochemistry, 2005. **53**(6): p. 745-751.

161. Rudrabhatla, S.R., C.L. Mahaffey, and M.E. Mummert, *Tumor Microenvironment Modulates Hyaluronan Expression: The Lactate Effect.* Journal of Investigative Dermatology, 2006. **126**(6): p. 1378-1387.

162. Zaleski, K.J., et al., *Hyaluronic acid binding peptides prevent experimental staphylococcal wound infection.* Antimicrobial Agents and Chemotherapy, 2006. **50**(11): p. 3856-3860.

163. Uchakina, O.N., et al., *The role of hyaluronic acid in SEB-induced acute lung inflammation.* Journal of Clinical Immunology, 2013. **146**(1): p. 56-69.

164. Campo, G.M., et al., *Combined treatment with hyaluronan inhibitor Pep-1 and a selective adenosine A2 receptor agonist reduces inflammation in experimental arthritis.* Innate Immunity, 2013. **19**(5): p. 462-478.

165. Riehl, T.E., X. Ee, and W.F. Stenson, *Hyaluronic acid regulates normal intestinal and colonic growth in mice.* American Journal of Physiology-Gastrointestinal and Liver Physiology, 2012. **303**(3): p. G377-88.

166. Riehl, T.E., et al., *CD44 and TLR4 mediate hyaluronic acid regulation of Lgr5+ stem cell proliferation, crypt fission, and intestinal growth in postnatal and adult mice.* Am J Physiol Gastrointest Liver Physiol, 2015. **309**(11): p. G874-87.

167. Hendricks, M.P., et al., *Supramolecular Assembly of Peptide Amphiphiles.* Accounts of Chemical Research, 2017.

168. Jin, H.-E., et al., *Biomimetic Self-Templated Hierarchical Structures of Collagen-Like Peptide Amphiphiles.* Nano Letters, 2015. **15**(10): p. 7138-7145.

169. Khan, S., et al., *Post-Assembly Functionalization of Supramolecular Nanostructures with Bioactive Peptides and Fluorescent Proteins by Native Chemical Ligation.* Bioconjugate Chemistry, 2014. **25**(4): p. 707-717.

170. Ferreira, D.S., et al., *Hyaluronan and self-assembling peptides as building blocks to reconstruct the extracellular environment in skin tissue.* Biomaterials Science, 2013. **1**(9): p. 952-964.

171. Paramonov, S.E., H.-W. Jun, and J.D. Hartgerink, *Self-Assembly of Peptide−Amphiphile Nanofibers: The Roles of Hydrogen Bonding and Amphiphilic Packing.* Journal of the American Chemical Society, 2006. **128**(22): p. 7291-7298.

172.   Hartgerink, J.D., E. Beniash, and S.I. Stupp, *Self-Assembly and Mineralization of Peptide-Amphiphile Nanofibers.* Science, 2001. **294**(5547): p. 1684.

Chapter 2 Synthesis and Characterisation of Hyaluronan Glycopolymers

2.1. Introduction

HA is a carbohydrate of great interest due to its biocompatibility and biological functions. As such, HA has been researched for many biomedical applications[1] in the areas of ophthalmology, orthopaedics, dermatology, drug delivery and biomaterials[2-3]. From this relatively simple molecule, a record $5.32 billion[4] was spent globally in 2012 on HA-based products in areas such as health-care and cosmetics. Forecasts estimate $9.85 billion being spent globally by 2019, with the HA raw material market reaching $7.25 billion by 2024[5]. Currently, ultrapure HA is extracted from natural sources[6] such as rooster combs and bovine vitreous humour. However, due to the risk of cross-species transmission of diseases, HA is now being manufactured on a large scale from bacteria fermentation to make the method more scalable (Figure 2.1).
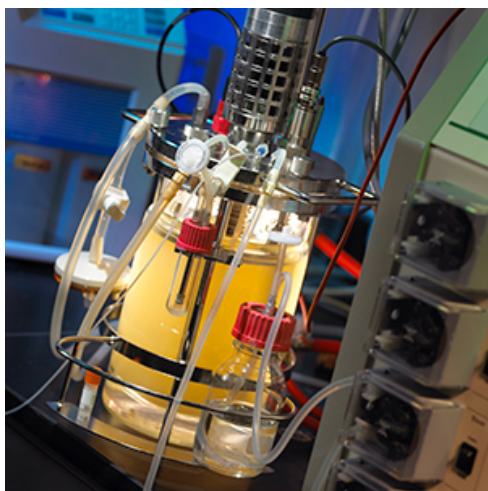
Figure 2.1. Microbial fermentation using *Streptococcus* for producing HA. Image taken from Life Core[7]

HA is readily broken down by a family of enzymes known as hyaluronidases (HYALs). These work together to break down the large mega Dalton polymer into small fragments by HYAL-2, which is then further hydrolysed by HYAL-1. The balance between the production of HA by HAS and degradation by HYALs enables HA homeostasis within the body. However, a shift towards increased degradation and/or a decrease in synthesis leads to pathological conditions such as osteoarthritis and cancer. By contrast, the inverse can also lead to diseases such as scleroderma[8]. Modern synthetic methods for the synthesis of carbohydrates to produce large

polysaccharides with precision control is challenging, time-consuming and resource demanding[9].

Glycopolymers provide a simpler alternative method to conventional carbohydrate synthesis. They bring together two key components; the biologically active sugars, which also provide water solubility, whereas the polymer backbone provides stability and control over the architecture. As previously shown, glycopolymers and glycoclusters of HA have been produced by first forming the HA repeating disaccharide (dimer) and then attaching this to a monomer, that after polymerisation yielded the HA glycopolymer[10]. The reactions to produce the disaccharide are elegant in their design, the disaccharide synthesis still requires multiple steps in order to produce them before conjugation to a monomer/polymer. Many reports in the literature suggest that the size of HA oligomers affect the interaction with receptors[11]. The architecture designed in the previously reported HA glycopolymers may not be ideal for interaction with receptors. The disaccharides on the glycopolymer will bind predominately through the terminus monosaccharide rather than the dimer. As the terminus monosaccharide is always the same, it raises the question about the availability of the internal monosaccharide for binding. This might be the reason why these publications did not report biological activities of the synthesised HA glycopolymers. Receptors such as CD44 require a minimum of 8 saccharides in order to bind [12].

In this chapter, a different approach is proposed, which eliminates excessive carbohydrate chemistry with an example shown in Scheme 2.1 for the formation of a glycosidic bond between GlcA and GlcNAc. By utilising click chemistry, various monosaccharides can be grafted onto a parent monomer/polymer to produce a variety of glycopolymers. This approach is an effective method to produce a library of glycopolymers and reduces the number of steps required[13-15]. This clicking of monosaccharides onto monomers/polymers approach can also be applied to the synthesis of more complex alternating polymers. This alternative strategy allows the easy interchange of the monosaccharides onto the polymer, as well as forming a full alternating glycopolymer based on HA compared to the formation of disaccharides.

The styrene-maleic anhydride copolymer system is well known to alternate[16-19] with examples from the Lutz group[20-23]. The group has synthesised libraries of substituted styrene monomer and the maleic anhydride derivatives to look at the effect of the side chains upon the polymerisation. As a result, a block copolymer was produced, whereby a growing styrene polymer had sequentially additions of maleimides at set

time points to form a styrene polymer with sections of alternation with a maleimide derivative. These maleimides could be orthogonally and chemoselectively deprotected and monosaccharides were clicked onto post-polymerisation.
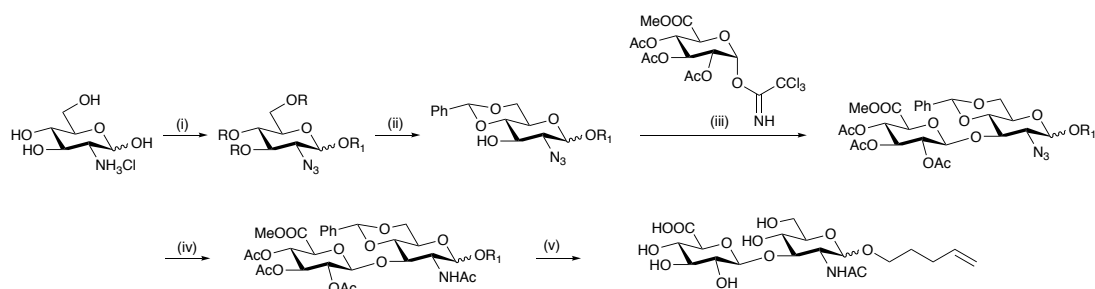
Scheme 2.1 Formation of HA dimer by a 10 step synthesis from Chaikof[10]. Reagents and Conditions: (i) (a) TfN$_3$, MeOH, DMAP, 25 °C, 18 h, (b) Ac$_2$O, pyridine, 0 °C, 10 h, R, R$_1$ = Ac; (ii) (a) H$_2$NNH$_2$·AcOH, DMF, 0–25 °C, 45 min; (b) anhydrous K$_2$CO$_3$, CCl$_3$CN, DCM, 25 °C, 48 h; (c) 4 Å mol. sieves, TMSOTf, 4-penten-1-ol, DCM, 0 °C, 1 h, R = Ac, R$_1$ = C(NH)CCl$_3$ (iii) MeONa, MeOH, 0–25 °C, 6 h; (e) CSA, THF, C$_6$H$_5$CH(OMe)$_2$, reflux, 6 h; (iv) TMSOTf, DCM, 0–25 °C, 3.5 h; (v) (a) CH$_3$COSH, 25 °C, 24 h; (b) TFA–H$_2$O (2:1), DCM, 0 °C, 1 h; (c) 3 M NaOH, 9:1 MeOH–H$_2$O, 25 °C, 2 h; (d) O$_3$ (278 °C), then add Me$_2$S, 278 °C–25 °C, 24 h.

Although this polymer is an example of an alternating glycopolymer, it is not alternating with respect to the sugar, but in regard to the backbone (Scheme 2.2). The proposed approach relies on the functionalisation of both the styrene and the maleic anhydride, whereby selective orthogonal reactions allow different monosaccharides to be grafted onto the individual monomers to produce a fully alternating glycopolymer in respect to both the backbone and the monosaccharides. In doing so, and compared to previous HA glycopolymer versions, both monosaccharides will be displayed evenly across the polymer. In this methodology, the yield of the glycopolymers will not be limited by the disaccharide synthesis. The polymerisation can be tailored in length to ensure the presence of enough monosaccharides to bind receptors in a multivalent fashion.
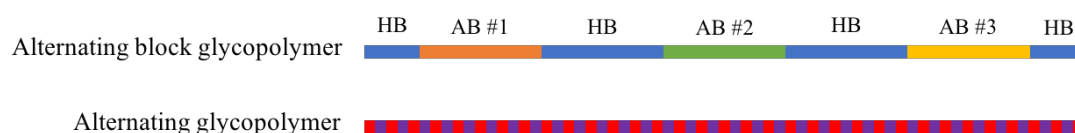
Scheme 2.2. Schematic representation of the previous work[22] into to alternating glycopolymer showing the alternation blocks (AB) in between a homopolymer block (HB, section blue) compared with the design principle of a fully alternating glycopolymer.

In this chapter, RAFT polymerisations of styrene and maleic anhydride derivatives are utilised to form a fully alternating glycopolymer. We first looked at the production of the homopolymers to provide a simple platform on which to build upon. Examples of both pre- and post-polymerisation are accessed for the formation of the glycopolymer. The homo-glycopolymers are formed from a parent polymer, which has been converted to bare a click group orthogonally to the polymerisable alkene. This orthogonal group allow the formation of multiple glycopolymer variants by supplementing different monosaccharides in the click reaction.

In the second half of the chapter, we build upon the homo-glycopolymer system to form a co-monomer system with a maleimide. With the diverse range of maleimides being discussed in the literature to polymerise with styrene[21, 24], a maleimide was selected to produce a polymer with two different orthogonal groups. The alternating behaviour of polymers was characterised by following the semi-logarithmic kinetic plots for each monomer as well as analysing the obtained polymers via matrix-assisted laser desorption ionization time of flight (MALDI-ToF) mass spectrometry. By controlling the order in which these reactions are carried out, we can control the locations of the monosaccharides and a fully alternating glycopolymer can be produced, in respect to the backbone and the monosaccharides. The synthesis of other glycopolymers based on glucose (Glc), mannose (Man) and Gal was also attempted to act as controls in binding experiments described in chapter 4.

2.2. Results and Discussion

2.2.1.1. Synthesis of Click Functionalised Monosaccharides

To synthesise a glycopolymer, we must first consider the functionality of the monosaccharides being used. GlcA and GlcNAc sugars bare potential reactive sites (carboxylic acid and N-acetyl group, respectively) for chemical modification, but these functional groups are key in the HA binding process and therefore must remain unmodified. For example, the CH_3 of 6-GlcNAc and 5-GlcA are known to be essential for the recognition by CD44 in the octasaccharide bound. Ideally, a universal method for the glycopolymer synthesis would be desirable, but several monosaccharides do not bare any functional group. However, all monosaccharides bear a common anomeric centre, which can be readily functionalised with a donor alcohol using an acid catalyst; this process is known as Fischer glycosidation. The use of H_2SO_4 immobilized on silica reported by Mukhopadhyay[25] provided an efficient methodology for Fischer glycosidation for several monosaccharides (Scheme 2.3).
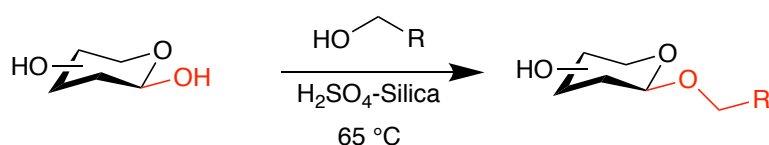
Scheme 2.3. Schematic representation of the functionalisation of monosaccharides via direct Fischer glycosidation.

Propargyl alcohol was selected as the alcohol donor since the compound possesses an alkyne. This alkyne can be used later for CuAAC click reactions. Compared with other simpler monosaccharides, such as Glc and Man, GlcNAc required an increased ratio of the catalyst and prolonged reaction time, in order to produce substantial grafting of the alkyne onto the monosaccharide. This is caused by reduced solubility of GlcNAc in neat propargyl alcohol leading to low conversions[26-27]. The ^1H nuclear magnetic resonance (NMR) of all four compounds showed the introduction of the terminus alkyne hydrogen at 3.0-2.8 ppm displaying weak triplets due to distance coupling between the terminus alkyne and the CH_2 doublet seen at 4.3-4.4 ppm (Figure 2.2). All four compounds (**1-4**) were produced as an anomeric mixture. The prolonged reaction time and the sterics of the N-acetyl group of the GlcNAc led to a decrease in the anomeric ratio for **4** comparing to **1-3**. This can be seen due to the dual peaks in the ^1H NMR of the anomeric hydrogen, as well as the CH_2 and CH of the propargyl group.
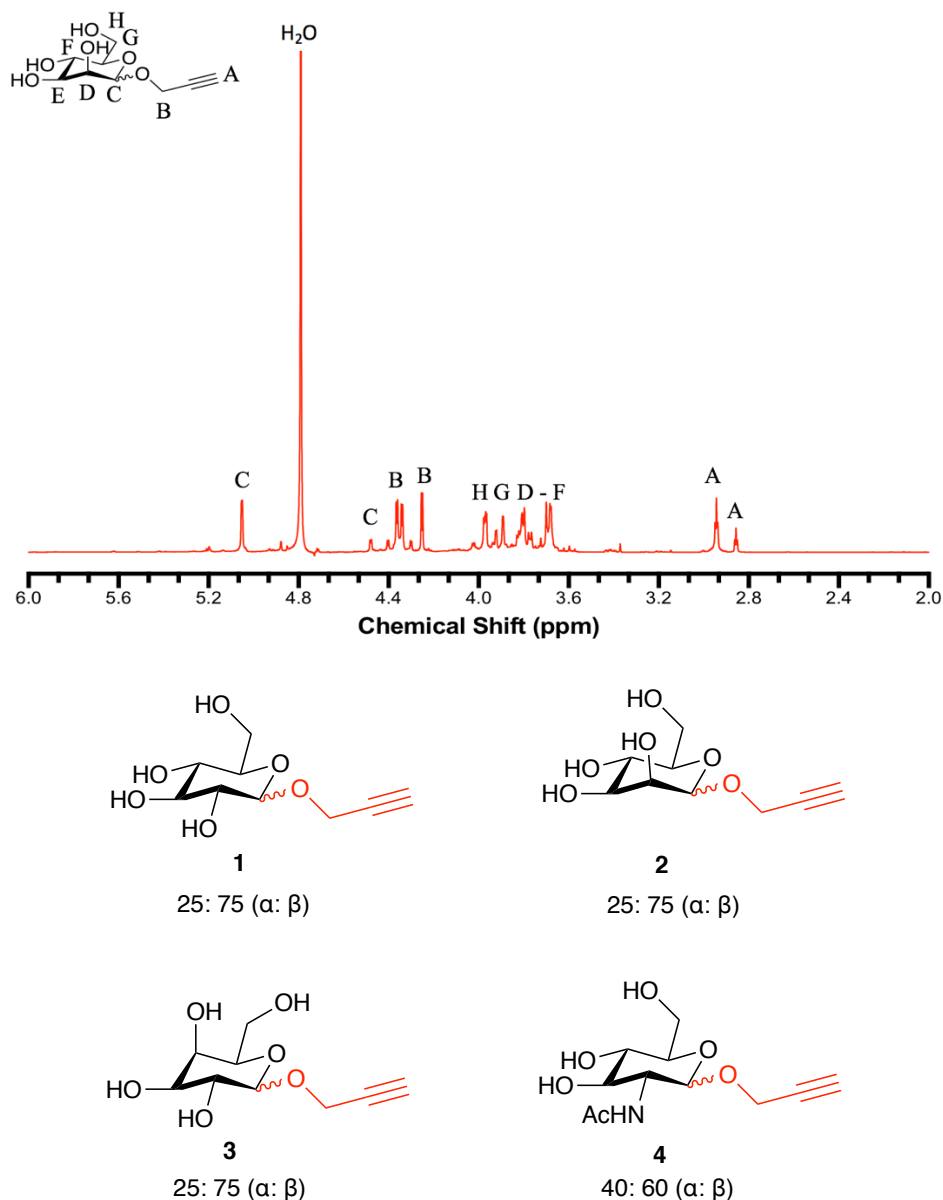
Figure 2.2. ^{1}H NMR spectrum at 400 MHz in D$_2$O (top) of compound **2**, showing the splitting of the propargyl group (A-B) and the anomeric hydrogen (C) and the anomeric ratio of products from direct Fischer glycosidation with H$_2$SO$_4$-Silica using propargyl alcohol as the donor (bottom) showing the anomer ratio of the product as determined by ^{1}H NMR.

Compared to GlcNAc, GlcA is more difficult to be functionalised at 1' position due to the carboxylic acid at the 5' position. The carboxylic acid leads to the formation of a stable bicyclic product rather than the anomeric substitution (Scheme 2.4). This is caused by the conversion of the pyranose 6-membered ring to a furanose 5-membered ring. This 5-membered ring formation is reversible but is made irreversible by the formation of a second 5-membered ring, resulted by the 3' hydroxyl reacting with the carboxylic acid to lock the very stable bicyclic structure. The formation of the bicyclic

lactone was confirmed by X-ray crystallography analysis of the crystals formed compared with those reported in literature[28].
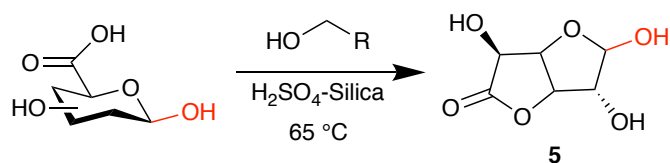
Scheme 2.4. Schematic representation of the by-product formation of Glucurono-6,3-lactone (**5**).

To inhibit the lactone ring formation, the hydroxyl groups on the sugar were protected by acetylation. Previous work by the Murphy group[29] in 2007 has shown the formation of an azide directly onto the sugar ring using $(CH_3)_3SiN_3$ as a Lewis acid and $SnCl_4$. The azide was produced as a minor product with the major product being another bicyclic lactone catalysed by the $SnCl_4$ (Scheme 2.5). The Murphy group[30] showed that in the absence of the $(CH_3)_3SiN_3$, the $SnCl_4$ catalyses the bicyclic lactone. Increasing the sugar to azide ratio, the yield of azide product was increased, but remained as the minor product behind the lactone.
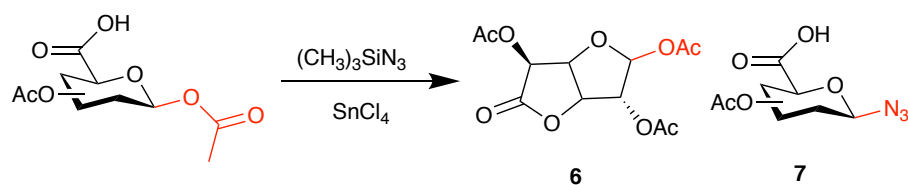
Scheme 2.5. Schematic representation of 1,2,3,4-tetra-O-acetyl-α-D-glucopyranuronate with $(CH_3)_3SiN_3$ producing the lactone by-product and the desired azide

These results infer that the azidation reaction is either unfavourable, kinetically slow, or the azide source is being destroyed during the reaction leading to a decrease in the azide source. Reports in the literature[31] showed that the protection of the carboxylic acid is required for the inhibition of the cyclisation. With the formation of methyl 1,2,3,4-tetra-O-acetyl-α-D-glucopyranuronate using the $(CH_3)_3SiN_3$ and $SnCl_4$ reaction, the azide product can be synthesised with no evidence of the lactone in the ^1H NMR. The methyl 1,2,3,4-tetra-O-acetyl-α-D-glucopyranuronate can undergo Fischer glycosidation using $BF_3.OEt_2$ as a Lewis acid catalyst to produce the alcohol-substituted at 1' position (Scheme 2.6).
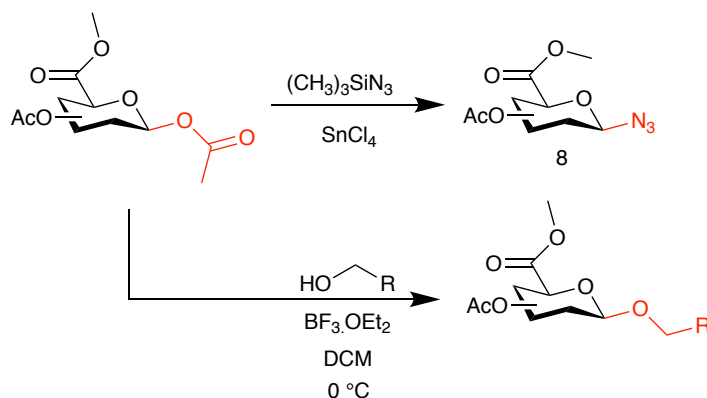
Scheme 2.6. Schematic representation of Methyl 1,2,3,4-tetra-O-acetyl-α-D-glucopyranuronate of the substitution of C1 acetyl group by $(CH_3)_3SiN_3$ catalysed by $SnCl_4$ and indirect Fischer glycosidation by alcohol donor catalysed by $BF_3.OEt_2$.

This reaction could tolerate both propargyl alcohol as well as 2-azidoethanol to yield GlcA functionalised with both an alkyne and an azide. The deprotection of the protected GlcA derivatives was achieved by Zemplen deprotection using NaOMe in MeOH to remove the acetyl and methyl protecting groups. This reaction caused the sugars to darken over time becoming brown in colour. The ^{1}H NMR showed the removal of the CH_3 of the acetyl groups, as a shift upfield of the protons within the carbohydrate ring, with no evidence of degradation of the GlcA derivatives. This cannot be directly quantified due to the use of different deuterated solvents caused by a change in solubility of the monosaccharide through the indirect Fischer glycosidation. Using this indirect route, the ß anomer product was favoured, but by using the $SnCl_4$ catalyst, compound **9** is seen exclusively as the ß anomer (Figure 2.3). With the monosaccharides bearing the click moieties being successfully synthesised, the corresponding polymer is required in order to perform the CuAAC to produce the glycopolymers.
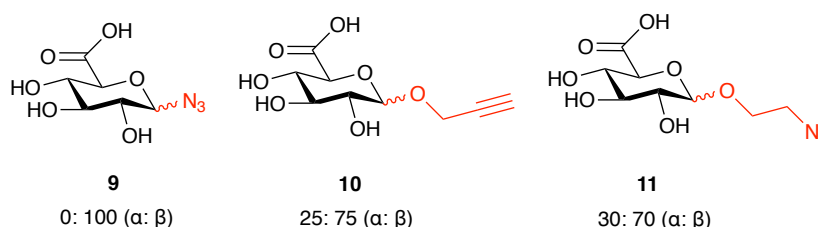
Figure 2.3. Products of functionalisation with $(CH_3)_3SiN_3$ catalysed by $SnCl_4$ and indirect Fischer glycosidation by alcohol donor catalysed by $BF_3.OEt_2$ forming both the alkyne (**10**) and azide derivative (**11**) showing the anomer ratio of the product as determined by ^{1}H NMR.

2.2.2. Glycopolymer Synthesis

2.2.2.1. Polymer Backbone Selection

Since the premise of the work is to form an alternating glycopolymer based on the styrene-maleic anhydride system, functionalised monomers of styrene were evaluated. Two commercially available styrene candidates were selected; vinyl benzyl chloride (VBC) and pentafluorostyrene (PFS) (Figure 2.4). Both monomers have been shown to be suitable for modification to bare an azide group[32-33] for CuAAC click reaction with the alkyne monosaccharides. The pendant group have also been substituted by other nucleophilic functional groups such as amines[34-35] and thiols[32, 36]. RAFT was chosen over other CRP due to the tolerance of halides during the polymerisation. In contrast, ATRP and SET-LRP were unsuitable due to the chloride of VBC interfering with the polymerisation mechanism, leading to potential crosslinking[37].
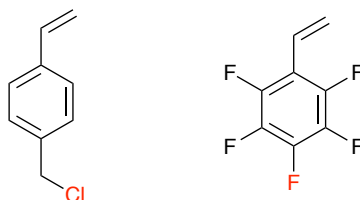
Figure 2.4. Structure of VBC (left) and PFS (right) highlighting the potential sites (red) for nucleophilic substitution.

The styrene derivatives were tested against styrene (St) as a control in both homopolymerisation and an alternating polymerisation system (Figure 2.5). Both monomers follow the trends seen by St, in which, the polymerisation under RAFT control is slow in the homopolymerisation. The high electron deficiency of the alkene in PFS leads to a conversion of 27%, which is half when compared with VBC at 54% over the same time period. However, the rate of polymerisation of both monomers increased when copolymerised with *N*-methyl maleimide.

PFS provided a much more controlled polydispersity (Đ) in both scenarios, the rate of polymerisation for the homopolymer is incredibly slow, therefore inhibiting the DP. Since HA contains thousands of disaccharide units (up to the MDa range), obtaining a very long homopolymer chain of PFS would be difficult under the current conditions. From these results, VBC was seen as a better option to that of PFS. This raises the question whether to do pre- or post-modification in order to form the glycopolymer. As shown in (Table 1.6), there are merits to both modification routes for the formation of a glycopolymer. We first investigated the synthesis of a glycomonomer as a pre-

polymerisation approach. This would ensure that the polymer produced contains 100% of monosaccharides across the polymer backbone.
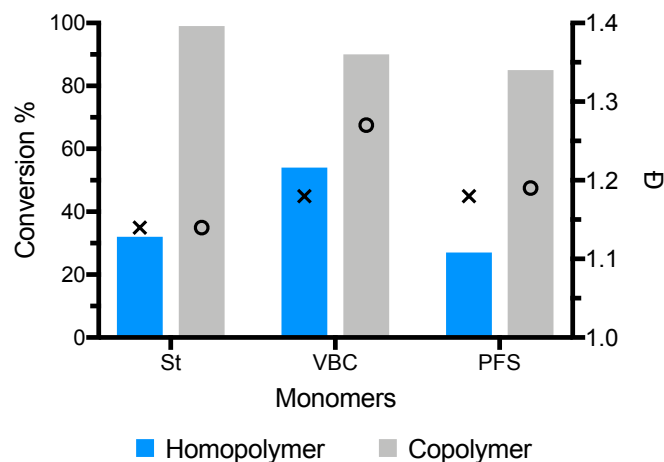
Figure 2.5. Graphical representation of the conversion (Bar) and Đ (symbols) comparing VBC and PFS against a control of St. Polymerisation under RAFT for 13 hours at 70 °C with 100: 1: 0.2 ratio between the monomer, RAFT agent and initiator respectively.

2.2.2.2. Formation of a Glycopolymer by Pre-polymerisation Modification

Using VBC, the chloride can be readily substituted for an azide, with a peak at 2098 cm^{-1} in the FT-IR indicative of an azide, on top of a shift seen from 4.61 to 4.33 ppm in the ^{1}H NMR and 46.13 to 54.70 ppm in the ^{13}C NMR for the adjacent CH$_2$. Compared with examples described in the literature[38], where the monosaccharide **4** was acetylated before clicking, these were seen as unnecessary steps. By using a solvent mixture of 2:1 methanol: water, **4** and **11** could be solvated and "clicked" together using CuSO$_4$.5H$_2$O (0.1 M) and Na-ascorbate (1 M) as the copper source and ligand, respectively. The reaction was confirmed by ^{1}H NMR which showed the addition of two triazole peaks at 8.04 and 8.00 ppm with a ratio of 60:40. The two singlets of proton K in Figure 2.6 arise due to the two isomers, which can form 1,4 or 1,5. These isomers can also be seen in the splitting of the CH$_2$ of the CH$_2$ adjacent to the triazole and CH$_3$ of the N-acetyl group of the GlcNAc.
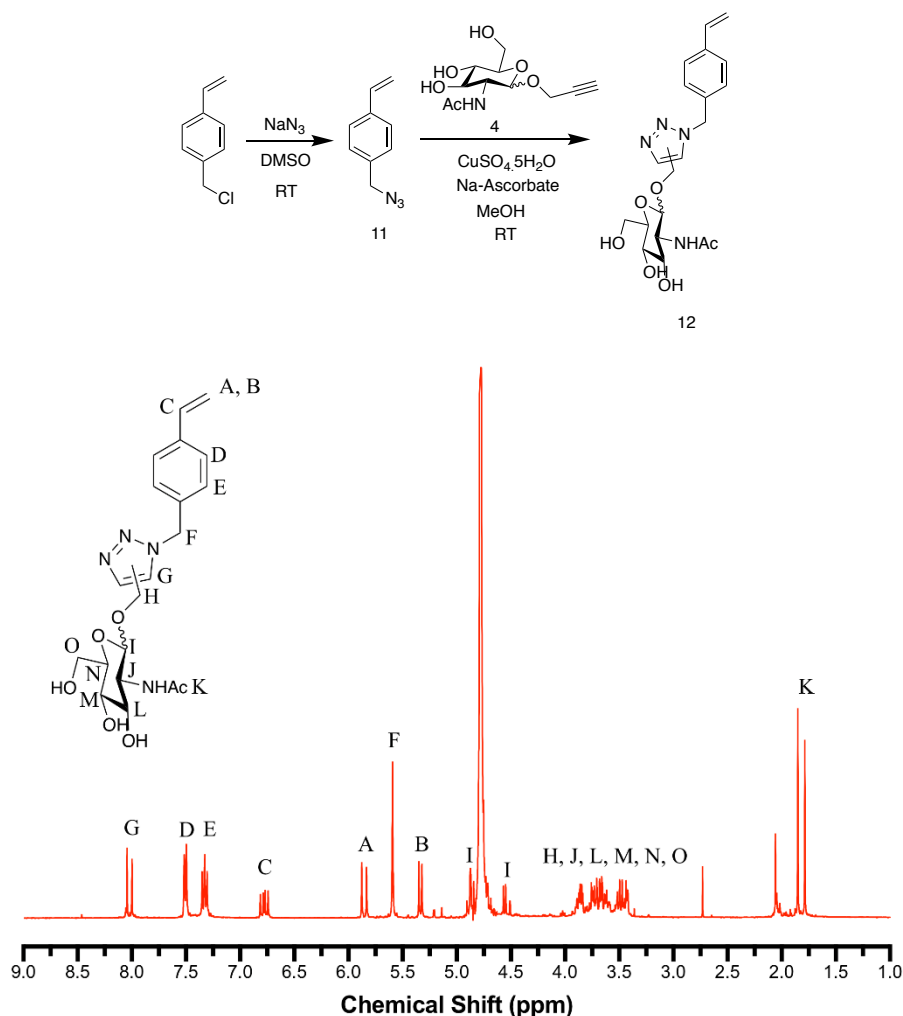
Figure 2.6. The synthetic pathway (top) for the formation of the glycomonomer (**12**) by S_n2 substitution of the chloride to azide followed by CuAAC with the corresponding ^{1}H NMR spectrum at 400 MHz in D_2O of **12** (bottom) showing the splitting of G, K and I due to anomers and triazole isomers.

Following this, the corresponding maleimide derivative synthesis was attempted. *N*-propargyl maleimide (PMI) was prepared by the ring opening and closing of the maleic anhydride with a propargylamine. The ring opening reaction was highly efficient in the formation of the corresponding acid **13**. The product crystallised out to give a white solid which by ^{1}H NMR shows the addition of the alkyne onto the maleimide through the ring opening; this ring opening can be seen due to the inequivalent hydrogen of the alkene. These hydrogens become equivalent again on the ring closing due to the symmetry of the cyclic ring (Figure 2.7). However, the reaction was highly inefficient due to the yield of 15% over the two-steps.
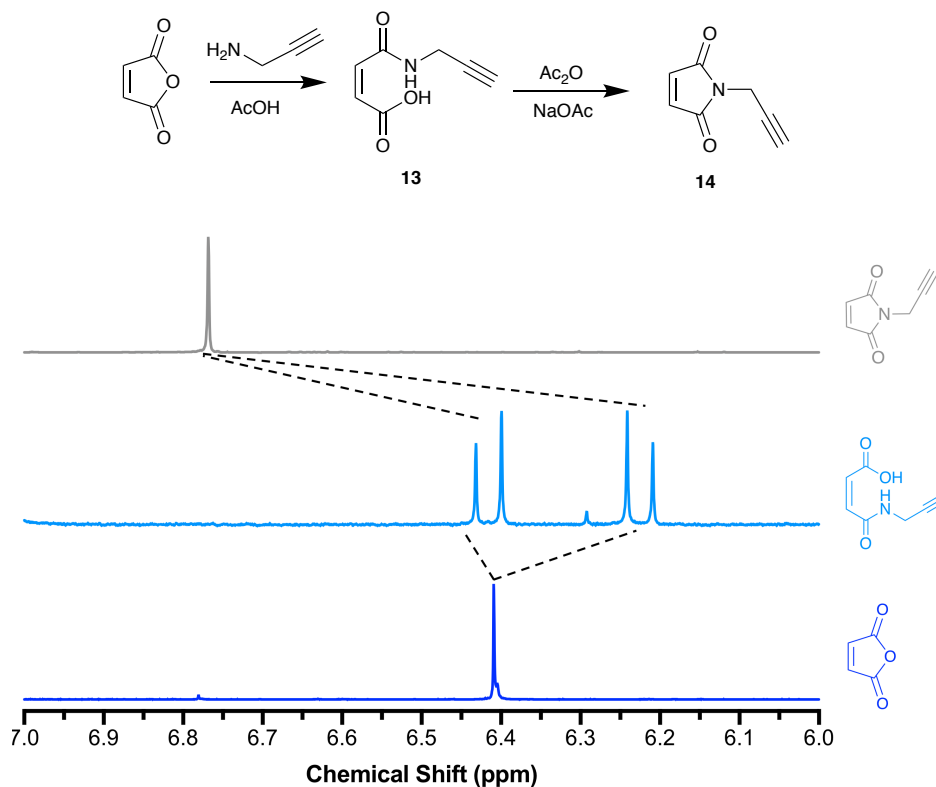
Figure 2.7. Scheme (top) for the formation of N-propargyl maleimide (**14**) through ring opened intermediate, **13** and ^{1}H NMR spectra at 400 MHz in CDCl$_3$ (bottom) of glycomonomer between 6.0 – 7.0 ppm looking at the alkene bond on through the ring opening and ring closure reaction.

The click reaction between **9** and **14** was attempted to form the glycomonomer (**15**) (Scheme 2.7). However, the reaction could never give clear evidence of the triazole peak on ^{1}H NMR; steric interference of the monosaccharide **9** could have potentially caused this issue. Other examples within literature[22, 39] use an azide extended from the carbohydrate by a small alkyl linker, so between 2-4 carbons long similar to compound **11**.
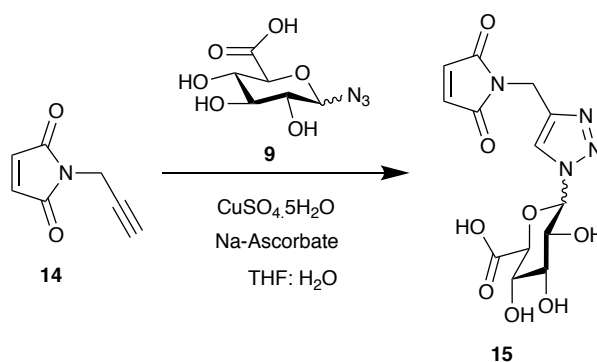
Scheme 2.7. Schematic representation of the formation of glycomonomer (**15**) through the CuAAC of **9** and **14** to produce **15** in a mixture of solvent due to solubility.

With the inability to produce **15**, **12** was tested for its ability to polymerise. The glycomonomer was tested under several different conditions (Table 2.1). The reaction was first tested with Maleic Anhydride (MAh) as a co-monomer since it was shown earlier that maleimides increase the rate of polymerisation, which was monitored by ^{1}H NMR and gel permeation chromatography (GPC). However, the reaction did not progress to polymerisation. To reduce steric hindrance, **12** was diluted in concentration with St in a mole ratio of 1:10, but the polymerisation again showed no conversion. It was also noted that during the reaction an inhibition of the polymerisation of styrene occurred when tested in different solvents, ratios, temperatures, as well as by free radical polymerisation, but the monomer failed to polymerise.

Table 2.1. Summary of polymerisation of **12** with comonomer in various conditions.

Entry	Ratio					Solvent	Temp (°C)
	12	**St**	**MAh**	**CTA**	**V601**		
1	4	-	4	1	0.1	Dioxane	70
2	4	-	4	1	0.1	Butanone	70
3	11	89	-	1	0.5	Butanone	70
4	1	9	-	1	0.5	Butanone	70
5	94	8	-	1	0.1	Butanone	70
6	80	10	-	1	0.1	DMF	100
7	98	10	-	-	1	DMF	100

With several issues seen in glycomonomer synthesis due to solvent incompatibility, sterics and lack of polymerisation, we have focused on the second alternative route in glycopolymer synthesis, which is based on the synthesis of a functional backbone and followed by post-polymerisation grafting onto the polymer. Though this leads to a better control over the polymerisation kinetics, the grafting and substitution reaction would need to be quantitative.

2.2.2.3. Formation of a Glycopolymer by Post-polymerisation Modification

The polymerisation of VBC monomer under RAFT polymerisation was solvated in 1,4-dioxane. The most common solvents in the literature[40] for this type of polymerisation are toluene, anisole or dimethyl formaldehyde (DMF), these were excluded for two reasons. First, the boiling points of these solvents are >100 °C, thus removing these solvents by evaporation to concentrate the sample before precipitation

is challenging. Secondly, these solvents have peaks within ^{1}H NMR which would resonate at the same frequency as several of the functional groups of the polymer, therefore making it more challenging to determine monomer peaks from trace solvents - e.g. the overlap of the aromatic hydrogens of toluene and styrene between 7 – 8 ppm. As seen previously (Figure 2.5) the styrene polymerisation reached a maximum of 55% conversion on average. Therefore, in order to target a polymer with a DP of approximately 50 repeats, it was necessary to work with twice the ratio of monomer to chain transfer agent (CTA) (i.e. 100: 1 rather than 50: 1) to consider the limitations of this polymerisation. The DP of 50 was selected so that the glycopolymers had an equivalent number of monosaccharides to that of a 20 kDa HA chain. The monomer was polymerised under RAFT conditions to produce a well-defined polymer with a low Đ on average below 1.2 (Table 2.2).
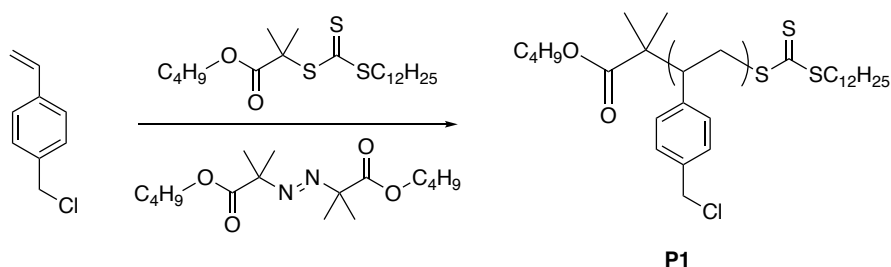
Scheme 2.8. Schematic of the synthetic route for the homopolymerization of VBC to pVBC (P1) by RAFT polymerisation with V601 initiator at 70 °C in DMF.

The poly(vinylbenzyl) chloride (pVBC) was converted to poly(vinylbenzyl) azide (pVBAz) using the same conditions as used for the VBC to Vinylbenzyl azide (VBAz) in the glycomonomer synthesis (Figure 2.6). On the addition of sodium azide to the polymer, a colour change was observed causing the solution to darken from yellow to orange. The GPC traces showed a consistent formation of a high molecular weight shoulder leading to a broadening of the Đ (Table 2.2). The peak molecular weight (M_p) was seen to be double of the high molecular weight shoulder compared to the major peak (Figure 2.8). This result inferred that coupling between two chains was occurring during this reaction facilitated by the sodium azide. To ensure quantitative conversion during azidation, the NaN$_3$ was always used in vast excess.
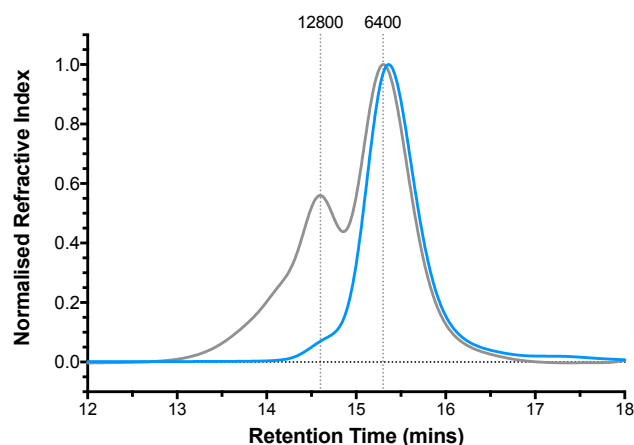
Figure 2.8. GPC comparison of pVBC produced by RAFT polymerisation (blue) to functionalised to pVBAz (grey) at 50 ºC with peaks labelled with the M_p, showing the shoulder formed during the azidation of PVBC.

However, on the reduction of the azide concentration, full conversion was still reached, with a reduction in the high molecular weight shoulder inferring a link between [NaN$_3$] and the size of the shoulder. Switching the solvent to DMF from dimethyl sulfoxide (DMSO) ensured there was no effect from the solvent, as well as a change in a drop-in temperature. By dropping the temperature to 25 ºC over the same period of time, the reaction still showed quantitative yields of the Cl to N$_3$ however, the Đ still remained broad.

Table 2.2. Conversion of pVBC to pVBAz using NaN$_3$.

Entry	Polymerisation	[Cl]:[NaN$_3$]	Temp (ºC)	Solvent	Đ [a]	
					pVBC	pVBAz
1	RAFT	5.7	50	DMSO	1.18	1.28
2	RAFT	2.2	50	DMSO	1.18	1.28
3	RAFT	4.9	50	DMF	1.09	1.34
4	RAFT	4.9	25	DMSO	1.17	1.33
5	RAFT	3.2	25	DMSO	1.17	1.30
6	Free Radical	2.8	25	DMSO	1.95	1.76
7	Free Radical	2.9	50	DMSO	1.95	1.80

[a] DMF + 5 mM NH$_4$BF$_4$ eluent, calibrated with PS standards.

The trithioester group of the RAFT agent has also been shown[41] to be susceptible to attack by nucleophiles such as NaN$_3$. Upon attack by a nucleophile, the trithioester decomposes to a free thiol. Within a basic environment, two adjacent thiols will react to form dithiol bridges. By producing the polymer free radically, followed by the azidation of the chloride, Đ is uncontrolled in these examples. However, what is evident is that on the addition of the NaN$_3$ into the system, there is no broadening

overtime with a quantitative conversion of the Cl to azide (N_3). Even at elevated temperatures (50 ºC), the GPC traces showed no distinct high molecular weight shoulder compared with the RAFT polymers (Figure 2.9). This evidence inferred the necessity to attempt the modification of the synthetic pathway to avoid this side reaction. The alternative routes were to polymerise the azide monomer *in situ*, or to cleave the RAFT end group.
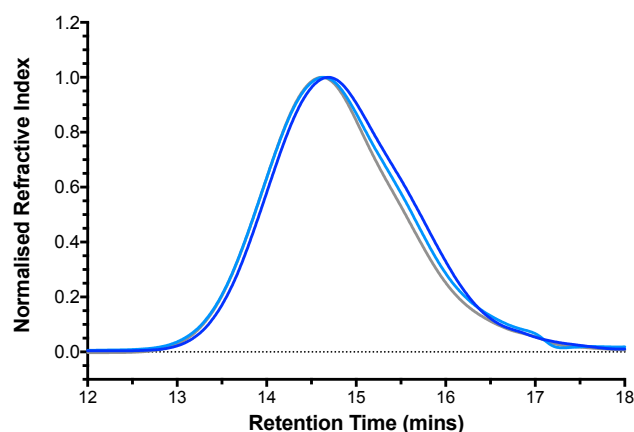
Figure 2.9. GPC traces of pVBC produced free radically (dark blue) but also converted to pVBAz at 25 ºC (light blue) and at 50 ºC (grey), with no evidence of the high molecular weight shoulder.

First looking at the polymerisation of VBAz in the literature, examples were not evident for a direct polymerisation of VBAz but rather a polymerisation of VBC and conversion to pVBAz[33]. A review[42] published in 1969 showed that at elevated temperatures an azide group can break down to form an amine, which if present within a polymerisation solution will play havoc with the polymerisation process. The amine will attack both the RAFT group and the alkenes present in the system, leading to an uncontrolled polymerisation together with crosslinking through the amine. The results of the polymerisation of VBAz (Table 2.3) showed a Đ > 2.

Table 2.3. Polymerisation conditions for pVBAz for 5 hours at 70 °C

Entry	[St]	[VBAz]	Solvent	ρ [a] (%)	M_n [b] (g mol^{-1})	Đ [b]
1	-	102	DMSO	>99	4400	2.8
2	-	50	DMF	>99	6600	2.4
3	40	10	DMF	>99	7400	2.3

[CTA]: [I] of 1: 0.2. [a] ^{1}H NMR (400 MHz, *d*-DMSO). [b] DMF + 5 mM NH_4BF_4 eluent, calibrated with PS standards.

The ^{1}H NMR results show a conversion (ρ) >99% which when comparing to previous styrene examples (Figure 2.5) infer that the alkene is being consumed by another route. When reducing the azide content to 20% of the monomer content in entry 3 of Table

2.3, the Đ & ρ remained higher than expected for a styrene polymerisation. This result showed that even a small amount of azide in solution was detrimental to the polymerisation. The GPC traces infer degradation of the azide further, due to the multimodal peak shape of the distribution with a minimum of 3 clear distinct peaks compared with GPC trace of pVBAz produced by post modification of pVBC (Figure 2.10A). The decomposition of the azide to an amine is confirmed by FT-IR. By post-modification to pVBAz, there is a clear peak at 2109 cm^{-1} for the azide (Figure 2.10B), which is present in the monomer but not after polymerisation, with the evidence of an amine between 3100-3600 cm^{-1}.
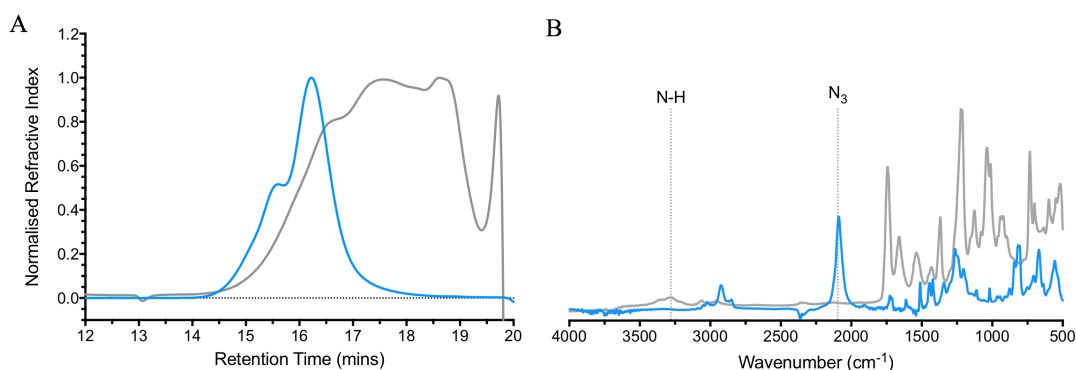
Figure 2.10. Comparison of GPC traces (A) and the FT-IR spectra (B) of the direct polymerisation of VBAz (grey) to the polymerisation of VBC followed by azidation to pVBAz (blue).

Since the polymerisation of pVBAz is an unsuitable pathway due to the decomposition of the azide, the alternative was to look at RAFT cleavage. A recent review[41] from Thang showed several functionalisation approaches to remove the RAFT end group. Of these, three were screened as a potential solution; nucleophilic, radical induced with and without H source. Radical induced RAFT cleavage[43] was attempted by the use of excess V$_{601}$ to reinitiate the polymerisation. Due to the large excess of initiator radicals within the system, this would promote termination through radical-radical recombination between the propagating chain and initiator. The polymer would, therefore, be terminated with the initiator rather than the RAFT agent as the C-C bond formation would be irreversible. The removal of the RAFT end group was monitored by UV (the RAFT trithiocarbonate absorbs between 300 – 360 nm), as seen in the yellow colour of the RAFT polymer, which is lost upon cleavage (Figure 2.11). By radical induced RAFT cleavage, a small residual amount of RAFT end group can be seen in the UV trace of the product after two cycles of cleavage.
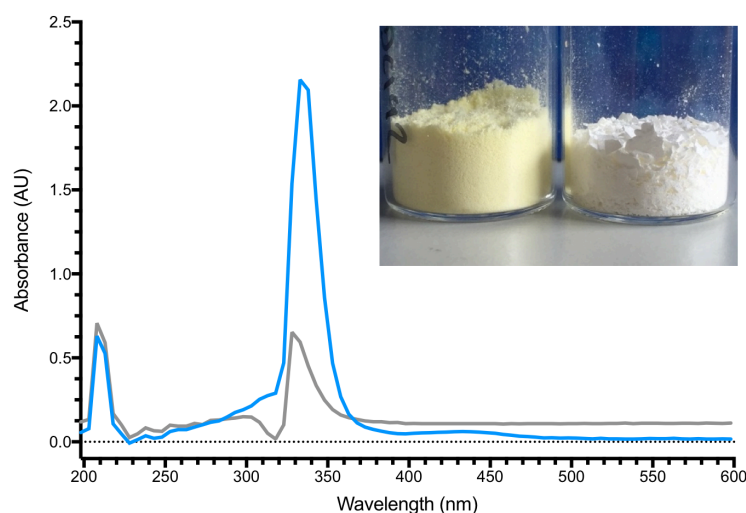
Figure 2.11. UV trace of pVBC before (blue) and after (grey) the RAFT cleavage with a colour change in the polymer seen upon partial cleavage of the RAFT agent (Insert).

Examples of RAFT cleavage of styrene-based polymers[45, 46] have been described in the literature. Many examples show incomplete cleavage due to the stability of the RAFT group on a styrenic polymer (Figure 2.12A). Supplementing the radical induced cleavage with a peroxide, such as Lauroyl Peroxide (LPO), was shown to be highly effective at RAFT removal from styrenic based polymers[47]. When carrying out the LPO supplemented RAFT cleavage it was shown by GPC UV trace at 308 nm with 95% of the RAFT end group cleaved in a single cycle. However, the RI trace showed an increase in Đ again caused by a small high molecular weight shoulder. The purpose of the RAFT cleavage was to avoid the high molecule shoulder (Figure 2.12B). The shoulder caused by the NaN_3 creating a disulphide bridge of the RAFT, rather than the unknown side reaction of the LPO. The reactions were continued as RAFT cleavage of a styrenic polymer was shown to be resource demanding for less than quantitative conversions (Table 2.4).

Table 2.4. Results of RAFT Cleavage at 80 ºC in Dioxane.

Entry	[V601]: [LPO]	Precursor		Product		Cleavage
		$M_{n, GPC}$ [a]	Đ [a]	$M_{n, GPC}$ [a]	Đ [a]	
1	20: 0	11800	1.13	12500	1.12	97 % *
2	20: 0	7200	1.18	7200	1.16	81 %
3	20: 0	11600	1.14	12500	1.15	55 %
4	20: 2	11600	1.14	12000	1.16	95 %

* Process repeated twice to achieve 97%. [a] DMF + 5 mM NH_4BF_4 eluent, calibrated with PS standards.
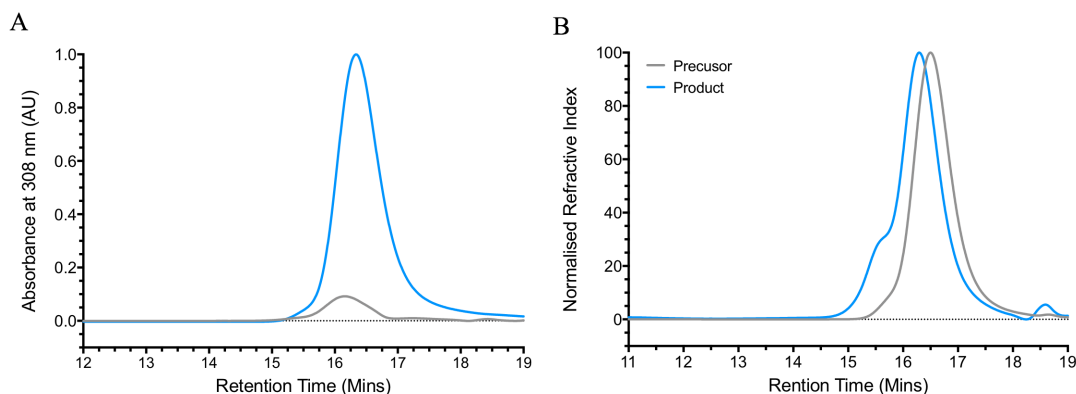
Figure 2.12. LPO assisted radical RAFT cleavage monitored by UV at 308 nm (A) showing a decrease in the absorbance at 308 nm, whilst the RI (B) shows another high molecular weight shoulder formation during the LPO assisted RAFT cleavage.

As a proof of concept, entry 1 from Table 1.4. was converted from chloride to the azide. The FT-IR spectrum showed the introduction of the azide bond at 2109 cm^{-1}, but the GPC trace showed a small peak shift between the RAFT polymer and cleaved polymer, indicating successful azidation without the formation of a high molecular weight shoulder. Although this proves the potential for the RAFT cleavage for this reaction scheme, the synthesis is not sustainable for upscaling due to the large quantities of initiator consumed. With the azidation already causing a reduction in yields, an additional step caused undesirable loss of product and thus the efficiency of the overall synthesis.
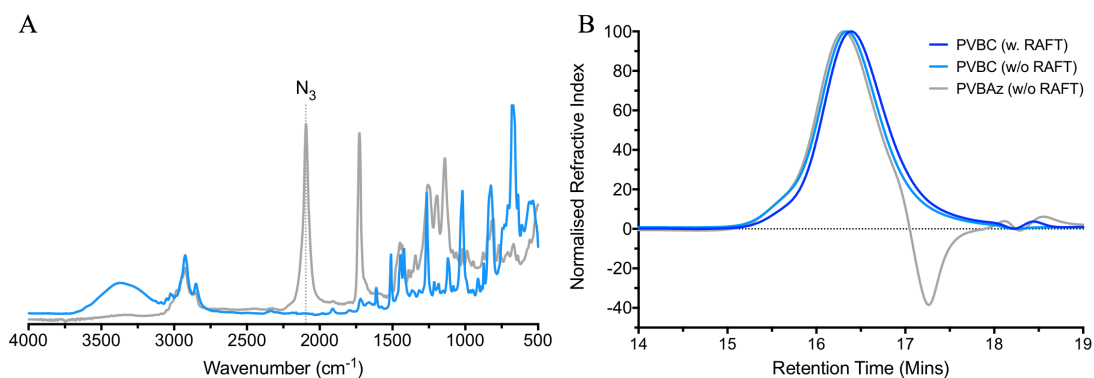
Figure 2.13. FT-IR spectra (A) showing the clear formation of the azide peak without the high molecular weight on the GPC trace (B) on conversion to pVBAz (grey) from the pVBC parent polymer after RAFT cleaved polymer (light blue) by radical induced RAFT cleavage.

With the varying success of RAFT group cleavage and the proof that the RAFT end group was degrading to a thiol causing disulphide bridges, the reactions were continued as the disulphide bridges could be reduced at a later time, if required, without the loss of the azide. Reduction of the disulphide bridge in the presence of the azide would also lead to the reduction of the azide to an amine. The final step in the

production of the glycopolymer was to 'click' the alkyne sugar onto the backbone (Scheme 2.9).
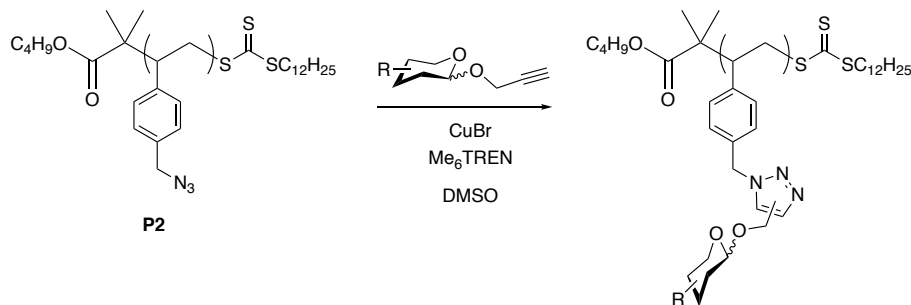
Scheme 2.9. Schematic of the synthetic route for the CuAAC reaction of P2 with a monosaccharide alkyne for 16 hours at room temperature.

The CuAAC system was changed for the post-modification compared with the pre-modification due to **11** being partially soluble in methanol, whilst P2 is not. Because of this, the reaction could not take place in $CuSO_4.5H_2O$ with Na-ascorbate. A selection of solvents was tested against all the components: Cu-catalyst, ligands as well as the monosaccharide alkynes and P2. It was found that DMSO and DMF were suitable candidates; however, DMF has a major peak at 8.0 ppm, the same resonance as the triazole of the glycopolymer, so DMF was therefore not used. Even though the monosaccharides and the polymer were soluble in DMSO, the copper (II) sulphate and Na-ascorbate were immiscible with DMSO. Therefore, a switch was made to Cu(I)Br and the ligand Me_6TREN, which are both soluble in DMSO. The switch of solvents and reagents provided the correct conditions in which to undertake the click reaction. The resulting ^{1}H NMR showed the addition of a triazole peak at 8.0 ppm for the single triazole. Referencing the triazole as 1, a ratio of 1:4:3 exists between the single hydrogen of the triazole, the four styrenic hydrogens between 6.0 – 7.2 ppm and the single hydrogen of the CH_3 from them *N*-acetyl group at 1.60 ppm. This ratio suggests full conversion of the azide to the monosaccharide **11**, this was also evident by the shift of the benzylic proton. This result is confirmed by FT-IR through the consumption of the azide peak at 2109 cm^{-1} (Figure 2.14).

With the synthetic pathway ratified using **4** as the test monosaccharide with the parent polymer, P2, the other monosaccharides were converted into other glycopolymers (Table 2.5) using the same methodology. A statistical copolymer, P8, was produced by using equal quantities of **4** and **9**. The ^{1}H NMR showed a rough 50:50 average between the two monosaccharides, with the ratio being determined by the ratio of the triazole: styrene aromatic peaks: acetyl peak of the GlcNAc at an average ratio of 1:

4: 1.5. This indicating 50% of the glycopolymer was GlcNAc compared to the styrene and triazole, therefore the remaining 50% is GlcA.
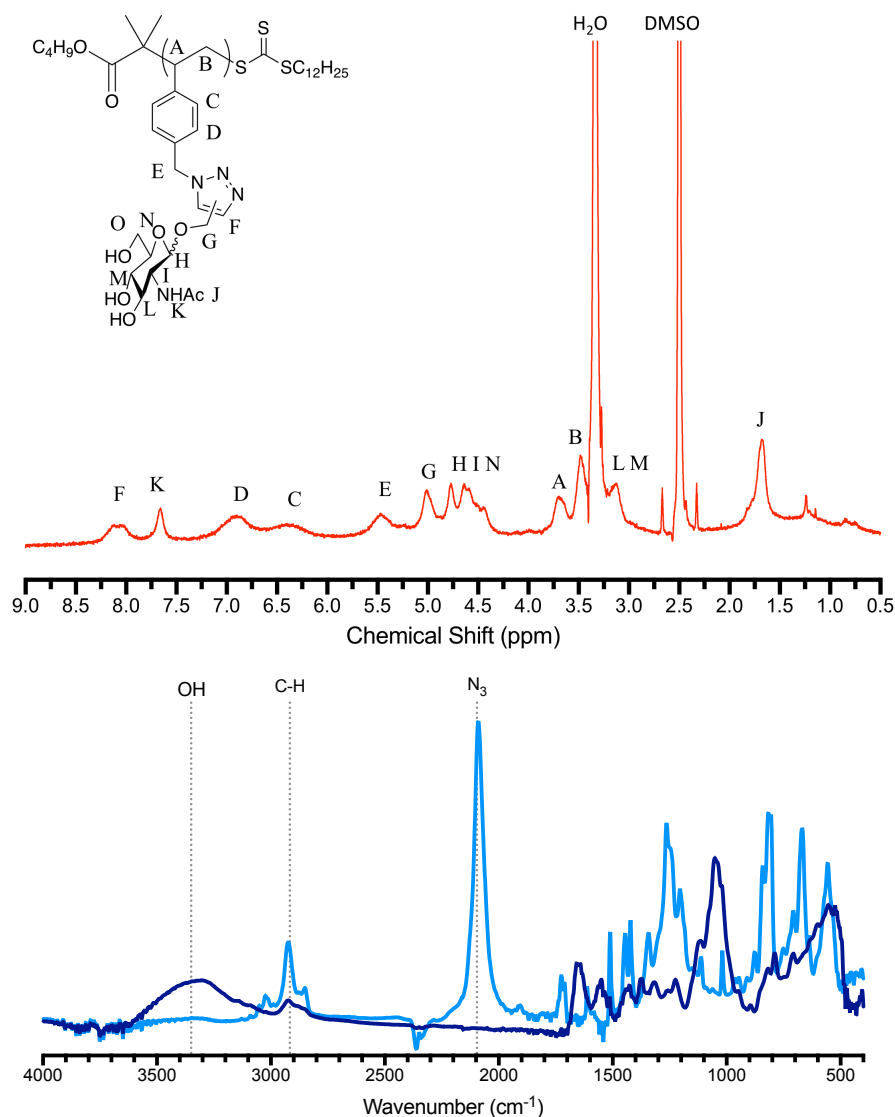
Figure 2.14. An example of glycopolymer formed by CuAAC with P2 and **4** to form P6 with structural conformation by ^{1}H NMR at 400 MHz in *d*-DMSO (top) showing the formation of the triazole and FT-IR (bottom) showing the reduction in N_3 at 2109 cm^{-1} and the increase of the OH reigon.

The clicking of protected sugars which were produced by indirect Fischer glycosidation was investigated. Although the click reaction was successful between P2 and acetylated form of compound **10**, the acetylated glycopolymer produced was highly insoluble in methanol. These solvent mixtures proved to be ineffective in deprotecting the acetylated glycopolymers, so the monosaccharides produced by the indirect Fischer glycosidation were fully deprotected before the click reaction to avoid this solvation issue.

Table 2.5. Summary of homopolymers synthesised by RAFT and click reactions.

Entry	Polymer	$M_{n,}$ (g mol^{-1})		Đ[b]
		Theo[a]	GPC[b]	
P2	pVBAz$_{56}$	13400	13400	1.20
P3	pVB-Glc$_{56}$	32000	4400	1.07
P4	pVB-Man$_{56}$	32000	4400	1.08
P5	pVB-Gal$_{56}$	32000	4300	1.04
P6	pVB-GlcNAc$_{56}$	36000	6900	1.13
P7	pVB-GlcA$_{56}$	35000	6300	1.02
P8	pVB-GlcA$_{23}$-co-VB-GlcNAc$_{23}$	35500	4100	1.04

[a] ^{1}H NMR (400 MHz, d-DMSO). [b] DMF + 5 mM NH$_4$BF$_4$ eluent, calibrated with PS standards.

2.2.3. Synthesis of Alternating Glycopolymers

2.2.3.1. Maleimide Synthesis

The incorporation of a maleimide derivative into the polymerisation will take the homopolymer version to an alternating one. With the maleimide component, the choice is to either produce a click-based monomer or to modify MAh post-polymerisation. Even though there are examples of post-modification, the MAh broke down during the polymerisation in the initial studies due to amine impurities in the solvents. The reactivity of the anhydride bond towards OH containing solvents led to ring opening of the MAh during precipitation. With the imide bond of the maleimide, whilst also susceptible, the probability is lower due to the lower reactivity of the unsaturated imide. The failure of the post-polymerisation modification of MAh comes due to the lack of a suitable point within the reaction scheme in which to form the imide (Scheme 2.10). The amine is able to break down both the chloride and the RAFT group, but the temperatures required would lead to the thermal decomposition of the azide or a monosaccharide.
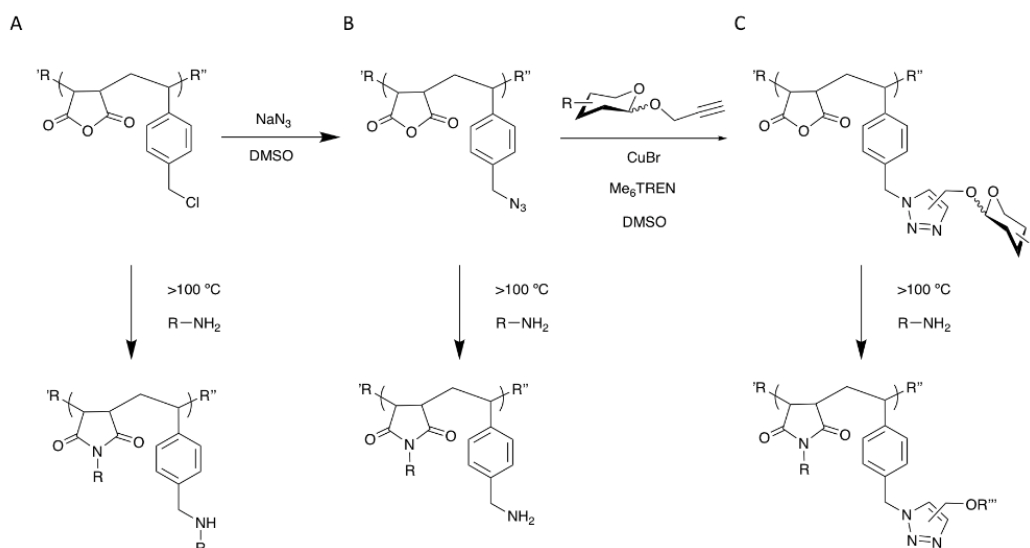
Scheme 2.10. Schematic for the post-modification of MAh to an imide with the potential side reaction; substitution of chloride (A) and the thermal decomposition of azide (B) and monosaccharide (C).

Due to the synthetic challenge of the post-modification of MAh, an *N*-substituted maleimide was used instead. Utilising the PMI, **14** (Figure 2.7) the copolymerisation with VBC was tested (Table 2.6) initially at low concentrations and at two different temperatures. This was due to the potency for a free alkyne to also undergo radical polymerisation. The Đ of entries showed fractional differences in the Đ but comparing the GPC traces at the two temperatures a cleaner peak was observed at 70 °C, as the GPC of the reaction run at 80 °C shows a much larger high molecular weight shoulder (Figure 2.15). This suggests the elevated temperatures promote the activation of the radical species on the alkyne.
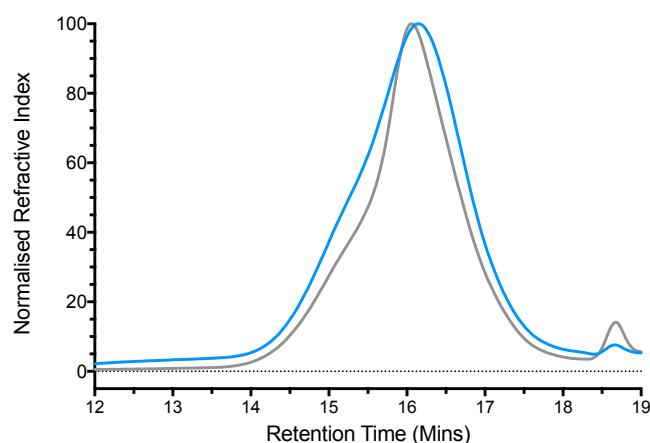
Figure 2.15. GPC traces of the copolymerisation at 70 ˚C (grey) and 80 ˚C (blue) of VBC and **14** at 70 ºC under RAFT conditions, showing increased high molecular weight shoulder with increased temperture.

The reaction was scaled up from 0.1 mmol to 1 mmol to produce a sufficient amount of polymer for further modifications, but when scaling-up crosslinking of the polymer was observed due to the formation of a gel-like substance. To try and produce the polymer at higher quantities, a batch experiment was run (Table 2.6 – Entry 4.1-10) to keep the concentration of the propargyl group at a minimum in the solution, in order to prevent crosslinking. The batch produced a wide range of Đ and M_n values for the same polymerisation and when combining the polymers followed by precipitation, the formation of a broad polymer M_n of 16,000 gmol^{-1} and a Đ of 1.74 was seen, exhibiting control over the polymerisation, but does not limit the high molecular weight shoulder of the alkyne polymerisation (Figure 2.16).
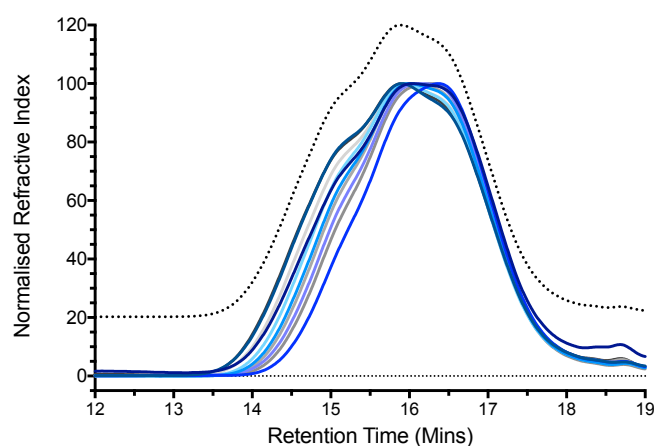
Figure 2.16 GPC traces of the individual copolymerisation of VBC with **14** at 70 ºC under RAFT conditions at 10-fold decrease in concentration, with the combined copolymersation after precipitation (offset black dotted).

Reports in the literature[24, 44-47] have previously shown that a free alkyne has the potential to be attacked by a radical in solution, but compared with the attack of the alkene by a radical, the homolytic bond breaking of pi bond of alkyne leaves one pi bond still intact. This pi bond is able to stabilise the radical. The polymer of acetylene type bond has been shown to be limited due to this stabilisation of the radical. The alkyne is a less reactive bond in PMI, it is a potential cross-linking molecule leading to broadening of the Đ. The radical on the alkyne, due to its stability, shows that as the reaction proceeds towards completion it also results to radical-radical coupling leading to coupling and termination of growing chains, which again will lead to a broadening of the Đ and irregularity of the polymers formed. Due to the peak broadening, the alkyne was protected with a trimethylsilane (TMS) group in order to inhibit the polymerisation of the alkyne, to be deprotected before the click reaction.

Table 2.6. The polymerisation of VBC and PMI under RAFT polymerisation in 1,4-Dioxane.

Entry	Scale (mmol)	Temp (°C)	[M]:[N]	Mn (g mol⁻¹)		Đ [b]
				Theo [a]	GPC [b]	
1	0.1	70	20:20	6100	16000	1.45
2	0.1	80	20:20	6100	16500	1.47
3	1	70	50:50	15000	Crosslinked	
4.1	0.1	70	17:20	2400	14700	1.68
4.2	0.1	70	17:20	2400	14800	1.89
4.3	0.1	70	17:20	2400	12100	1.57
4.4	0.1	70	17:20	2400	13700	1.68
4.5	0.1	70	17:20	2400	13100	1.63
4.6	0.1	70	17:20	2400	14200	1.72
4.7	0.1	70	17:20	2400	14300	1.83
4.8	0.1	70	17:20	2400	13500	1.65
4.9	0.1	70	17:20	2400	13200	1.58
4.10	0.1	70	17:20	2400	14800	1.88

[a] ^{1}H NMR (400 MHz, d-DMSO), [b] DMF + 5 mM NH_4BF_4 eluent, calibrated with PS standards.

Several options are available in order to produce **18**, which can be seen in Scheme 2.11. Initially, the pre-existing synthetic route for **14** (Figure 2.7) was extended to include protection of the terminus hydrogen with trimethylsilane chloride (TMS-Cl) (Route A). The reaction successfully produced **18**, but due to the low yield of the ring opening and closing producing little starting material for the formation of **18** from **14**, the reaction was reformulated so that the TMS was already present in the molecule, so the ring closing reaction was the final reaction (Route B). By forming the TMS protected propargylamine **16** and incorporating this into the ring opening and closing reactions, compound **18** could be successfully synthesised. Whilst **18** was produced with good purity, the yield over the 3-step reaction results in a costly and dangerous route, because of the use of n-BuLi and low efficiency of this approach.

An alternative strategy was to form an *N*-methoxycarbonylmaleimide **(19),** which can readily form *N*-substituted maleimides by the nucleophilic attack of methyl chloroformate by maleimide. These species can react with amines to substitute the R group of the amine. While examples of PMI formation via route C, the reaction was

less efficient when using the TMS PMI for route D with lack of evidence supporting the formation of **18** by this route.
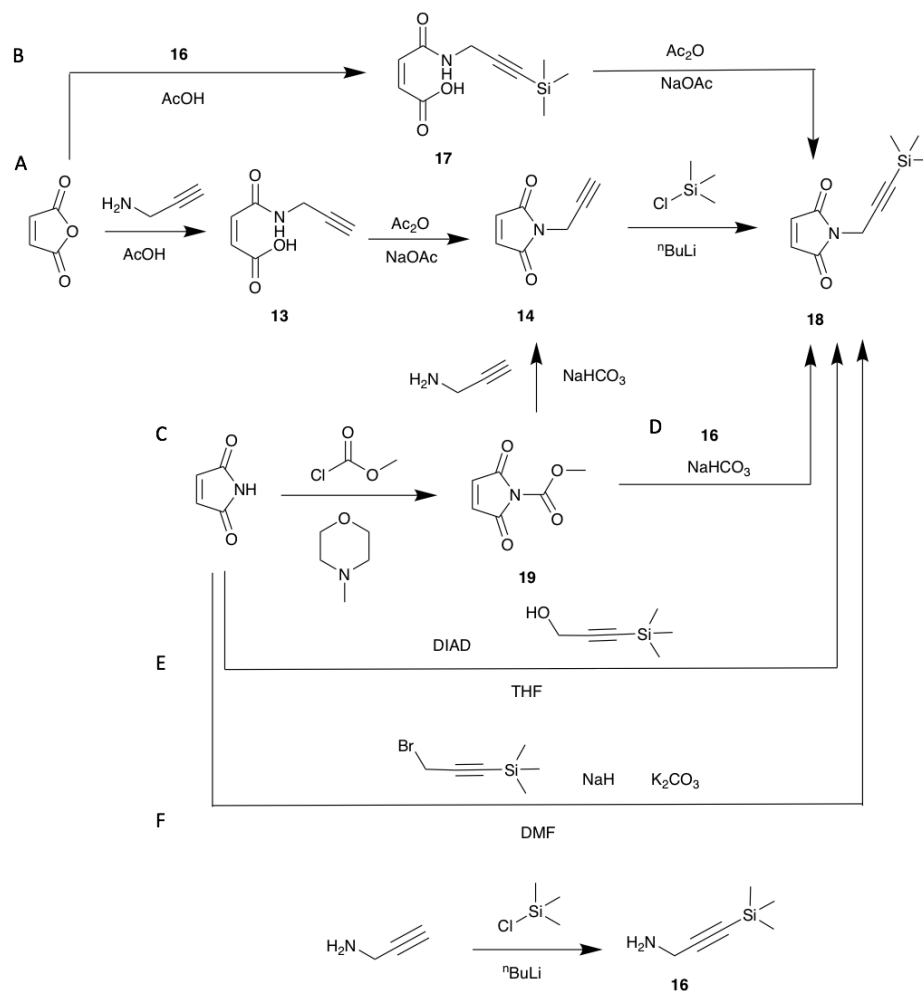
Scheme 2.11. Scheme for the synthetic pathway to TMS PMI (**15**) via multiple synthetic routes.

The Mitsunobu reaction (Route E) presented an alternative route to the synthesis of the maleimide **18** in a single step, with the use of TMS propargyl alcohol, which is commercially available, thus avoiding the use of n-butyl lithium (n-BuLi) and reducing the overall hazard in the formation **18**.

Table 2.7. Result for the formation of **18** by various different synthetic pathways.

Reaction pathway	N° Steps	Overall Yield
A	3	14 %
B	3	28 %
C	3	6 %
D	2	0 %
E	1	33%
F	1	0 %

Over a single step, it produces the highest yield for the formation of **18**, compared with the multiple step routes A-D. Finally, route F was also attempted as a single step, but this reaction produced 0% conversion as the ^{1}H NMR showed no shift in the CH$_2$ of the propargyl group, which if reacted would move downfield due to the addition of the heavily electron withdrawing maleimide group in a similar manner seen for the ^{1}H NMR of route E.

Using the synthetic route D, **18** was synthesised and after purification, by column chromatography (x 2), the product was be isolated as a mixture of isomers, which can be seen by the small secondary peaks of the alkene hydrogens and the CH$_2$ adjacent to the amine on the ^{1}H NMR (Figure 2.17A). The ^{1}H NMR shows a slight upfield of the CH$_2$ and TMS upon the addition to maleimide, whereas the maleimide CH shows only a small shift due to its distance from the centre of reaction.
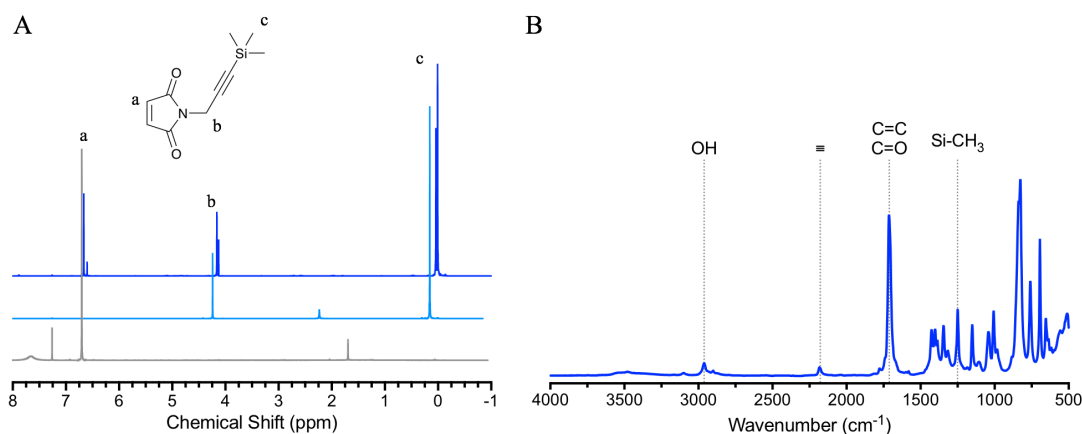
Figure 2.17. Compound **18** ^{1}H NMR spectra at 400 MHz in CDCl$_3$ (A) of maleimide (grey), TMS propargyl alcohol (light blue) and the final product (**18**) (blue) with the FT-IR (B) of **18**.

The FT-IR shows the stretch of the alkyne, which is not visible in unprotected PMI (Figure 2.17B). This is due to an increased molecular weight on the terminus alkyne of the TMS compared to a single hydrogen, which effects the reduced mass Equation 2.1 which links into FT-IR stretches.

$$\mu = \frac{m_1 m_2}{m_1 + m_2}$$

Equation 2.1

2.2.3.2. Polymerisation of an Alternating Backbone
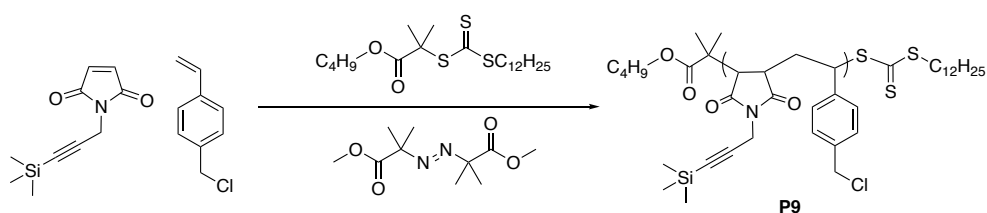
Scheme 2.12. The Polymerisation of **18** with VBC by RAFT to form P9 at 80 °C for 5 hours in a ratio 50:25:1:0.2 (18: VBC: RAFT: Initiator) in DMSO.

Using **18** as the co-monomers in a styrene-maleic anhydride-based system, with VBC utilising RAFT polymerisation (Scheme 2.12), the kinetics of the copolymerisation system showed that the reaction was proceeding under control by RAFT (as shown by the Đ and M_n) over the course of the polymerisation (Figure 2.18). The Đ shows a drop off after 2 hours, this is due to the starting material of **18** in the GPC overlapping in retention for the first few measurements. This initial high Đ is due to the TMS-PMI which elutes from the GPC at the lower end of the styrene calibration window affecting the Đ until the polymer is large enough to elute with a clear resolution from the remaining monomer.
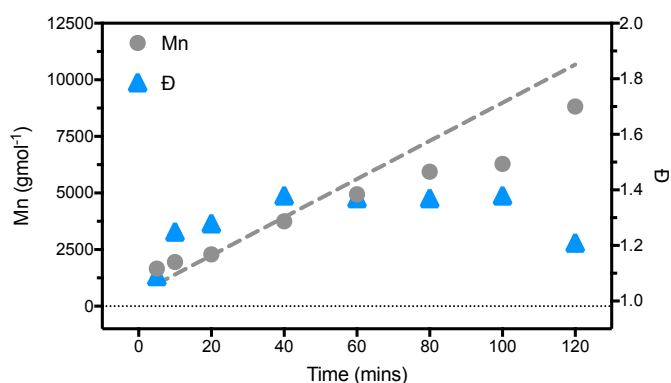
Figure 2.18. Polymerisation of **18** and VBC monitoring the parameters of Đ and M_n over the initial 2 hours of the polymerisation with the theoretical M_n (dotted line).

An alternating polymerisation can be determined by few methods including the Mayo-Lewis equations, MALDI-ToF, ^{13}C NMR and kinetics. The reactivity ratios of a co-monomer system set by Mayo-Lewis[48], Equation 2.2 to Equation 2.7 shows the potential reactions which can occur during the polymerisation with M_1 and M_2 being the two monomers; in this case VBC and TMS PMI with k denoting the reaction rate constant.

$$M_1^* + M_1 \xrightarrow{k_{11}} M_1 M_1^* \qquad \text{Equation 2.2}$$

$$M_1^* + M_2 \xrightarrow{k_{12}} M_1 M_2^* \qquad \text{Equation 2.3}$$

$$M_2^* + M_1 \xrightarrow{k_{21}} M_2 M_1^* \qquad \text{Equation 2.4}$$

$$M_2^* + M_2 \xrightarrow{k_{22}} M_2 M_2^* \qquad \text{Equation 2.5}$$
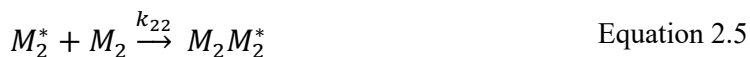
$$r_1 = \frac{k_{11}}{k_{12}} \qquad \text{Equation 2.6}$$

$$r_2 = \frac{k_{22}}{k_{21}} \qquad \text{Equation 2.7}$$

The reaction rate constant can be used to determine the reactivity ratios which determine how the polymer grows i.e.:

- $k_{11} > k_{12}$ and $k_{22} > k_{21}$ (block polymer)
- $k_{11} = k_{12}$ and $k_{22} = k_{21}$ (statistical copolymer)
- $k_{11} < k_{12}$ and $k_{22} < k_{21}$ (alternating polymer)

From these equations, it can be determined if the VBC and TMS PMI form an alternating polymer in the RAFT polymerisation condition. This is because the maleimide will not homopolymerise under RAFT conditions. However, it has been shown that maleimides will homopolymerise by other techniques, for example by nucleophilic initiated polymerisation with nucleophiles as amines[49] and thiols[50]. Maleimides have been shown to accelerate the consumption of VBC compared with the homopolymerisation of VBC (Figure 2.19). Over prolonged periods, VBC will polymerise to a small extent, as shown in the previous section (2.2.2.3.). From these results, it was shown that $k_{11} \ll k_{12}$ and $k_{22} < < k_{21}$, therefore forming a kinetic point and the polymer produced is an alternating polymer.

The rates of polymerisation (K_p^{app}) of the monomers in the copolymerisation system also show alternation in behaviour. This is shown by the two monomers that are consumed at the same rate, as denoted by the dashed trend lines with equivalent gradients of 0.47 inferring they are incorporated into the polymer at the same rate. If these two were inequivalent, then this would indicate a random or block copolymer formation. This, along with the known inability of maleimide to homopolymerise, again infers the alternation of the polymer.
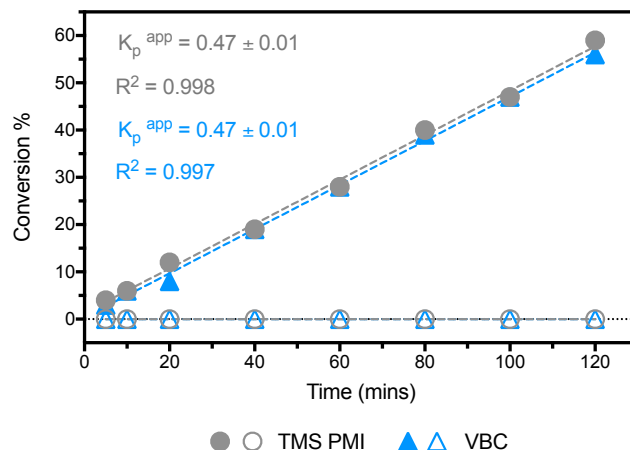
Figure 2.19. The kinetic plot of VBC (blue) and **18** (grey) in a homopolymerisation (shaded) and copolymerisation (hollow) system with corresponding trends line, where K_p^{app} is equivalent to the gradient.

MALDI-TOF was used to test the alternation of the backbone to search for the repeat unit. From the MALDI-ToF mass spectroscopy (MS) spectrum (Figure 2.20) taken between the major peaks, a difference of 360 Da is detected. This is consistent with the sum of the masses of VBC and TMS PMI. There are several smaller peaks which are summarised in Table 2.8. From the previous literature about kinetics and MALDI-ToF MS analysis, the system shows good alternation behaviour, with tolerance over the bulky side chains of the monomers. The polymerisation was precipitated in methanol, this led to ring opening of the PMI ring with the methanol to show an OMe adduct as a small impurity. The proceeding runs of this polymerisation was therefore precipitated in isopropanol as the hydroxyl is sterically hindered and therefore will reduce this ring-opening pathway.
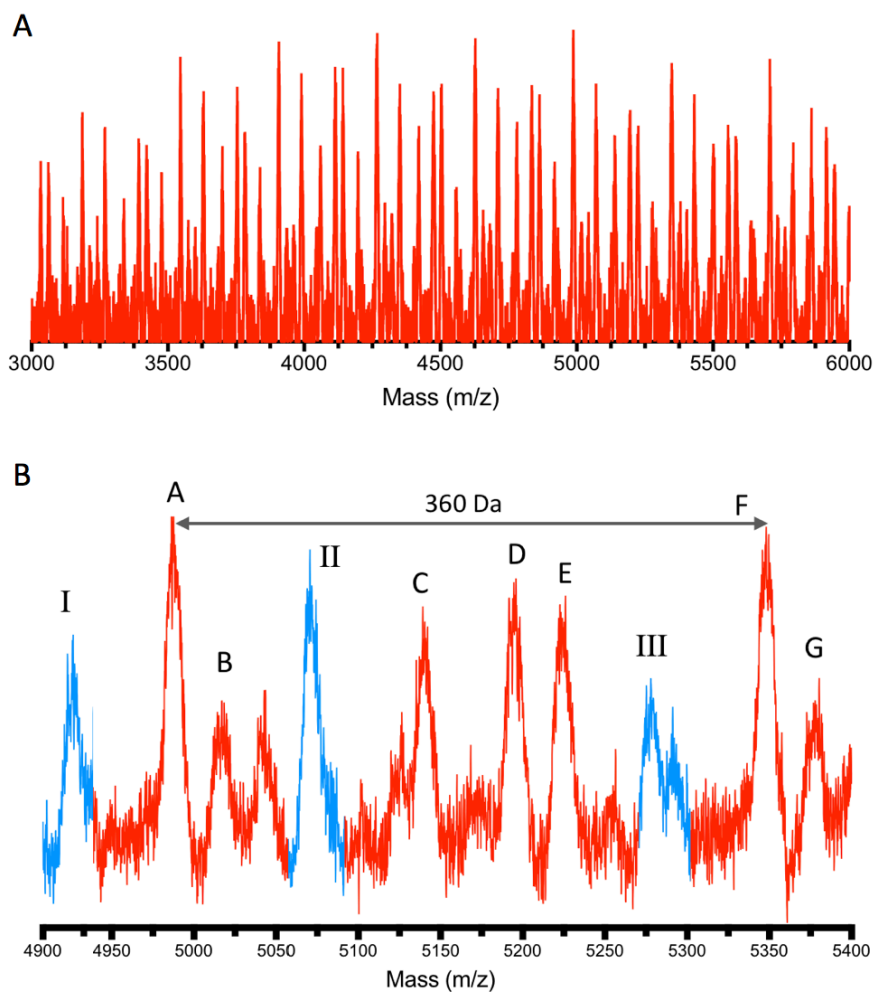
Figure 2.20. Low-resolution MALDI-ToF of P3 (a) with a labelled zoom between 4900 – 5400 Da (b) showing the minor distributions (Table 2.8) within the repeat of 360 Da for the two monomers.

Table 2.8. Peak Inference for zoom between 4900 – 5400 Da of Figure 2.20.

Peaks		Inference	Mass (m/z)	
RAFT	**Initiator**		**Theoretical[a]**	**Actual[b]**
-	I	(PVBC$_{12}$-alt-TMS PMI$_{13}$)	4918	4918
A	-		4972	4987
B	-	(PVBC$_{12}$-alt-TMS PMI$_{12}$/TMS PMA+OMe)	5003	5018
-	II	(PVBC$_{13}$-alt-TMS PMI$_{13}$)	5071	5070
C	-		5126	5139
D	-	(PVBC$_{12}$-alt-TMS PMI$_{14}$)	5182	5195
E	-	(PVBC$_{12}$-alt-TMS PMI$_{13}$/TMS PMA+OMe)	5213	5226
-	II	(PVBC$_{13}$-alt-TMS PMI$_{14}$)	5293	5278
F	-		5335	5349
G	-	(PVBC$_{13}$-alt-TMS PMI$_{13}$/TMS PMA+OMe)	5366	5380

[a]Determined by sum of the monomer mass plus either the RAFT agent or the Initiator [b]MALDI-ToF peaks.

2.2.3.3. Grafting of the Monosaccharides onto the Alternating Polymer

With the polymerisation of the monomers being shown to produce a highly alternating backbone, the synthesis began to move towards the grafting of the sugars onto the polymer. The initial polymer product has two potential orders in which to graft the sugars upon. The TMS group can be cleaved by K_2CO_3 to give a free alkyne or, alternatively, the chloride can be substituted in the same manner which produced the homopolymers to form an azide. The chloride groups in the polymer are highly reactive species that can be easily substituted, whilst the TMS group is in comparison more stable, therefore the click synthesis onto the benzylic position was run first, followed by the grafting on the maleimide alkyne (Scheme 2.13).

In a similar manner to the homopolymer system, the chloride was substituted with sodium azide. This again led to a broadening of the Đ due to the RAFT agent breaking down and forming disulphide bonds. The FT-IR showed the addition of an azide peak at 2096 cm^{-1}, whilst maintaining the TMS group of the alkyne at 2184 cm^{-1} (Figure 2.21).
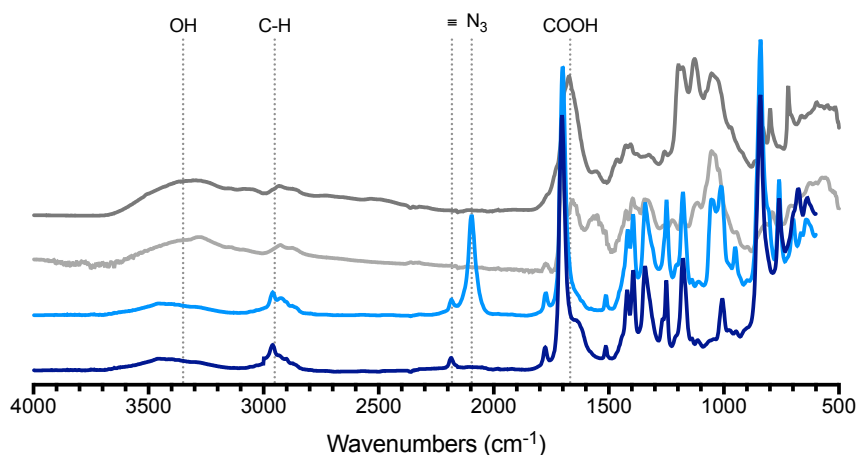
Figure 2.21. FT-IR spectra of P9 (blue), P10 (light blue), P11 (grey) followed by P12 (dark grey) highlighting the key groups of OH, alkyne, N_3 and COOH as the alternating polymer is functionalised with GlcNAc and GlcA units. Graphs offset by 0.15

The azide is then consumed during the 1,3-Huisgen cycloaddition, which was confirmed by the reduction of the peak at 2096 cm^{-1} with the survival of the TMS group seen in the IR and ^{1}H NMR at 0.12 ppm. The IR also shows the retention of the OH groups within the polymer from the hydroxyls on the sugar post lyophilisation. The ^{1}H NMR also indicates the addition of a triazole peak at 7.91 ppm, along with an introduction of sugar peaks between 4.0 – 5.0 ppm, as well as the N-acetyl group of the GlcNAc at 1.71 ppm (Figure 2.22). To quantify it further, the ^{1}H NMR shows that

the reaction has gone to full conversion due to the shift in the benzylic CH_2 and the formation of the triazole peak in the ^1H NMR.
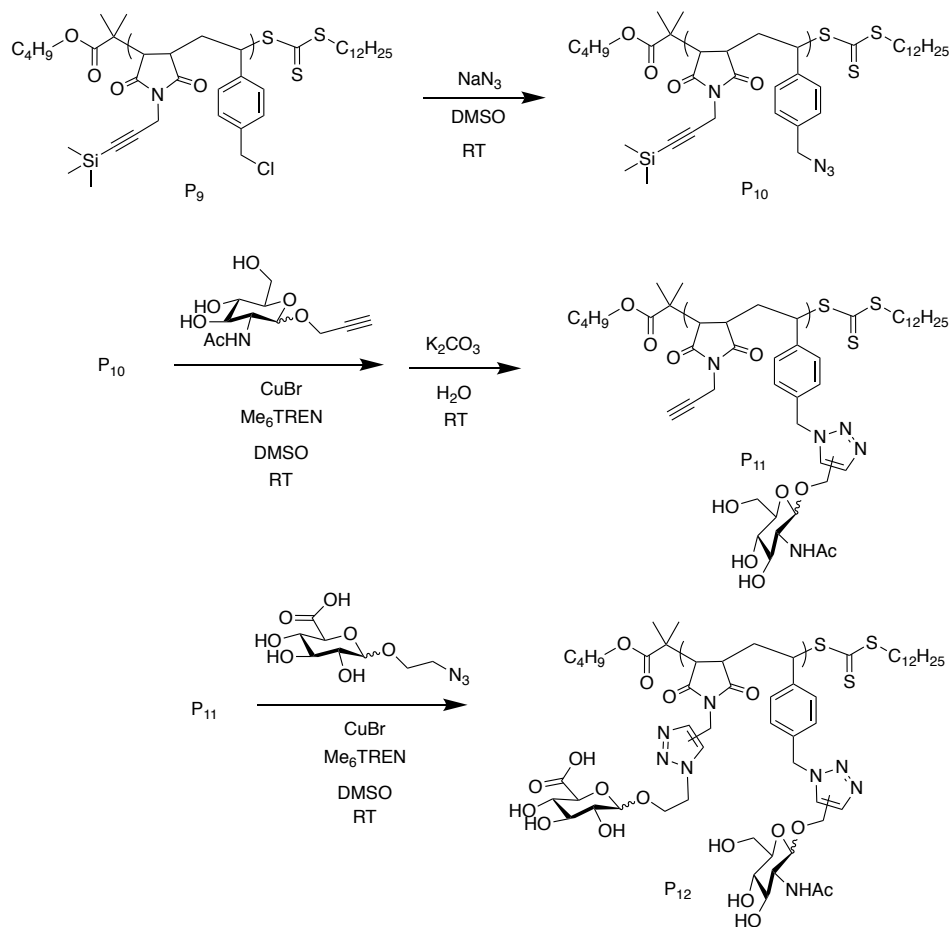
Scheme 2.13. Synthesis of alternating glycopolymer (P12) to mimic the structure of hyaluronan through controlled CuAAC, deprotection and S_n2 reactions.

With the confirmation of the first of the two monosaccharides, **4**, successfully clicked onto the polymer, the TMS group could now be removed from the polymer to expose the free alkyne. During dialysis of P11, the water was supplemented with K_2CO_3. The method of dialysis removes the excess propargylated sugar, at the same time the K_2CO_3 within the first few cycles caused the cleavage of the TMS group from the maleimide. The polymer was then dialysed against pure water to reduce the salt content, which was later freeze-dried to give the polymer as an off-white powder. The FT-IR showed a removal of the peak at 2184 cm^{-1}; this is due to the stretch of the hydrogen alkyne being unable to measure by this form of IR with the ^1H NMR showing a loss in the TMS group at 0.12 ppm.
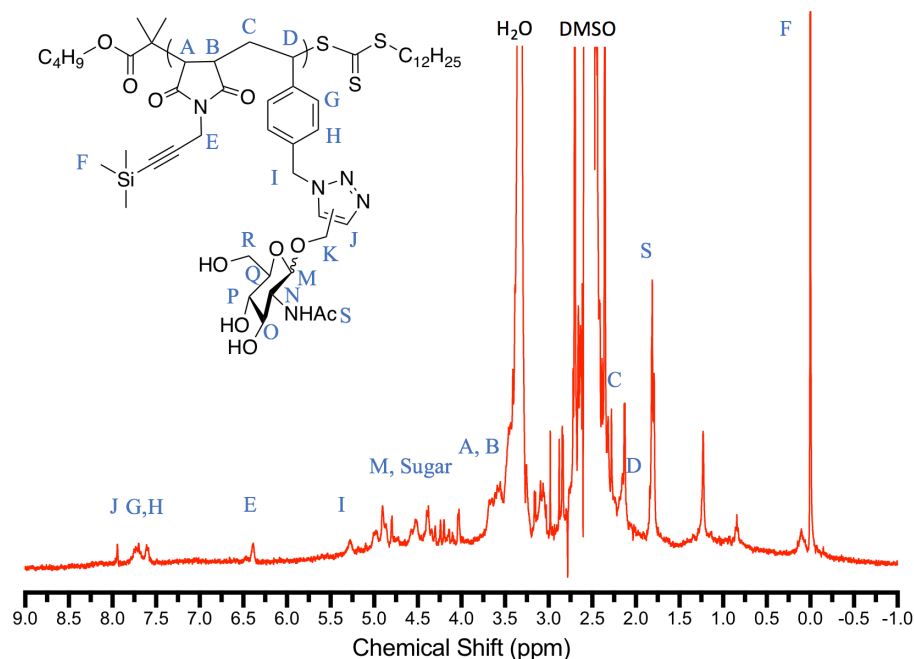
Figure 2.22. ^{1}H NMR spectra at 400 MHz in d-DMSO of P11 showing the first CuAAC success with TMS group still intact.

With the alkyne group deprotected, the second of the 1,3-Huisgen cycloadditions can be run to attach the second sugar, **11**. Using the same methodology as in the previous example, the click reaction was carried out producing in quantitative conversions an alternating glycopolymer based on HA structure. The FT-IR showed the broadening of the C=C region at 1672 cm^{-1} due to the introduction of a C=O of the carboxylic acid functional group on **11** (Figure 2.21). Since these two groups vibrate within the same region, this is seen by a widening of the band.

Table 2.9. Summary of homopolymers synthesised by RAFT and click reactions.

Entry	Polymer	M_n (g mol^{-1})		$Đ^b$
		Theo^a	GPC^b	
P9	pVBC$_{24}$-alt-TMS PMI$_{24}$	12800	19500	1.57
P10	pVBAz$_{24}$-alt-TMS PMI$_{24}$	19900	18300	2.40
P11	pVB-GlcNAc$_{24}$-alt-PMI$_{24}$	27000	4800	1.02
P12	pVB-GlcNAc$_{24}$-alt-PMI-GlcA$_{24}$	40000	5700	1.06

^{a} ^{1}H NMR (400 MHz, d-DMSO). ^{b}DMF + 5 mM NH$_4$BF$_4$ eluent, calibrated with PS standards.

The FT-IR reveals a qualitative increase in the OH peaks, whilst the ^{1}H NMR shows more of a quantitative change (Figure 2.23). The ratio of 1: 4: 3 between the triazole: styrene: acetyl increases to 2: 4: 3 after the second click reaction. An increase is also

seen in the number of hydrogens associated with the region in the ^{1}H NMR with the protons of the ring of the monosaccharide between 3.0 - 4.5 ppm.
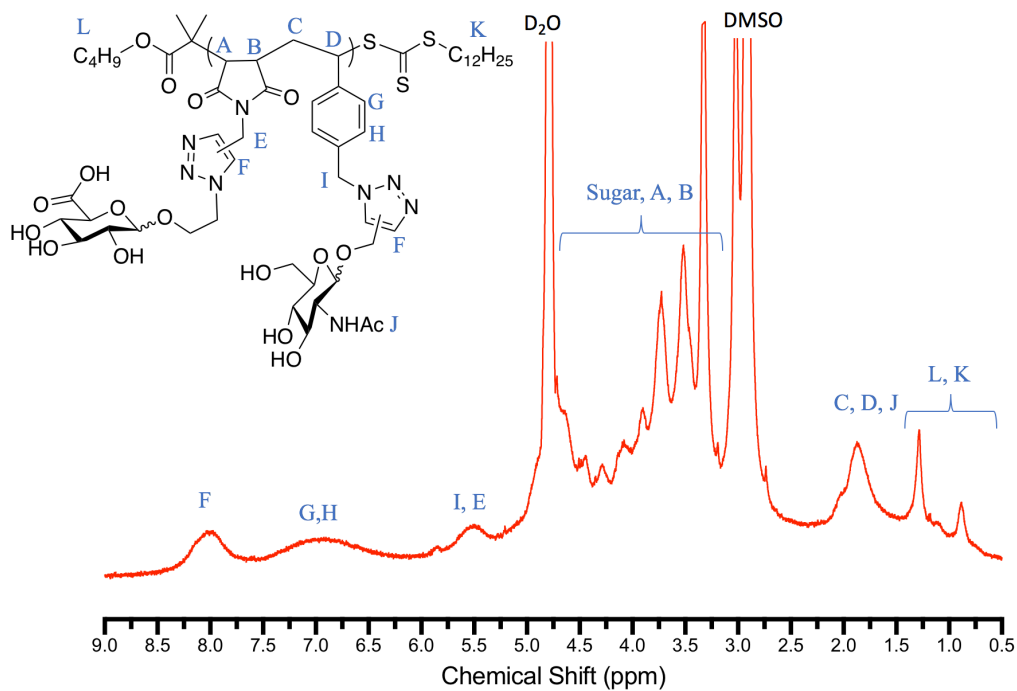
Figure 2.23. ^{1}H NMR spectra at 400 MHz in D_2O of P12 showing the second CuAAC success.

The results from the FT-IR and the ^{1}H NMR show the successful synthesis of the alternating glycopolymer. The GPC shows a change in hydrodynamic volume in DMF as on the addition of the sugar, a drop-in value output by the GPC decrease in both M_n and Đ on the addition of the sugars onto the polymer.

2.3. Conclusion

To conclude, we have successfully produced a range of glycopolymers (homo and alternating) and characterised them by various methods, including ^{1}H NMR, FT-IR and MALDI. We first looked into the production of glycomonomers, which in the styrene-based monomer was possible. However, these monomers were unable to polymerise under the several conditions tested. This led to the synthetic pathway to become a post-polymerisation modification rather than a pre-polymerisation modification. This post-modification provided a much better control of the polymers being produced, especially in the later alternating system, as the steric bulk of the sugars had the potential to disturb the polymerisation. Using post-polymerisation techniques, we were able to show the conversion of a homopolymer of VBC, P1 to a full glycopolymer, by the conversion to an azide based polymer P2 followed by CuAAC to produce a range of glycopolymers with various monosaccharide pendant groups.

We selected the homopolymerisation synthetic pathway and incorporated a propargyl functionalised maleimide within the system, causing broadening of the Đ. This was improved by the addition of a TMS protecting group to inhibit the alkyne polymerisation. The incorporation of the TMS propargyl group was tested in many different reaction pathways in order to find the most suitable one. We showed the increase in steric upon the styrene-maleic anhydride based alternating system of VBC and **18** indicated no detrimental effects on the alternation of the polymer backbone when producing P9. Through the careful arrangement of the post-polymerisation modifications of the backbone, we could produce a fully alternating glycopolymer as shown by ^{1}H NMR, MALDI and GPC.

2.4. Experimental

2.4.1. Materials

Vinylbenzyl chloride (VBC, ≥90% (GC), 0.05% 4-tert-butylcatechol and 0.05% nitroparaffin as stabilizer), *N*-acetyl-D-glucosamine (GlcNAc, >99%), D-Glucuronic Acid (GlcA, >98 %), sodium azide (NaN$_3$, ≥99.5%), propargyl alcohol (99%), propargyl acrylate (98%), D-(+)-mannose (Man, ≥99%), D-(+)-galactose (Gal, ≥99%), D-(+)-glucose (≥99%), sodium methoxide (CH$_3$ONa, 25 wt.% in methanol), maleimide (99%), dichloromethane (DCM, >99%), methanol (CH$_3$OH, >99.9%), acetic acid (AcOH, >99.9%), iodine (I$_2$, >99.9%), sulphuric acid (H$_2$SO$_4$, 95-98%), ethyl acetate (EtOAc, 95%), sodium acetate (NaOAc, >99%), boron trifluoride-diethyl etherate (BF$_3$OEt$_2$, synthesis grade), dimethyl formaldehyde (DMF, >99.9%), iodomethane (MeI, copper stabilised, 99.5%) 2-bromoethanol (95%), Tetrabutylammonium bromide (NBu$_4$Br, 98%), diethyl ether (Et$_2$O, 1ppm BHT inhibitor, >99.7%, dimethyl sulfoxide (DMSO, anhydrous, >99.9%), Triphenylphosphine (PPh$_3$, >95%), Tetrahydrofuran (THF, anhydrous, 99.9%), diisopropyl azodicarboxylate (DIAD, 98%) (6.1 mL, 30.9 mmol), 3-(Trimethylsilyl)propargyl alcohol (99%), hexane (>95%), maleic anhydride (MAh, >95%), propargylamine (98%) and copper bromide (CuBr$_2$, 99.9%) were purchased from Sigma Aldrich. Sodium thiosulfate (Na$_2$S$_2$O$_3$), magnesium sulfate (MgSO$_4$), sodium chloride (NaCl), sodium bicarbonate (NaHCO$_3$), silica, potassium carbonate (K$_2$CO$_3$) and aluminium oxide (Al$_2$O$_3$) were purchased from VWR. All monomers were passed through basic Al$_2$O$_3$ before use in polymerisations. 1 kDa dialysis tubes was purchased from Spectrum Laboratories (California, USA).

2.4.2. Instruments and Analysis

2.4.2.1. Gel Permeation Chromatography (GPC).

Size-exclusion chromatography measurements were conducted on an Agilent 1260 infinity system operating in DMF with 5 mM NH$_4$BF$_4$ and equipped with 2 PLgel 5 μm mixed-C columns (300 × 7.5 mm), a PLgel 5 mm guard column (50 × 7.5 mm), a differential refractive index (DRI) and a variable wavelength detector (VWD). The system was eluted with DMF at a flow rate of 1 mL min^{-1} and the DRI was calibrated with linear narrow polystyrene standards.

2.4.2.2. Nuclear Magnetic Resonance (NMR) Spectroscopy

Spectra of the molecules were collected on a Bruker AV-III spectrometer at 400 MHz for ^{1}H NMRs and at 101 MHz for ^{13}C NMRs. CDCl$_3$ was used as a solvent and the resonance signal at 7.26 ppm (^{1}H) and 77.16 ppm (^{13}C) served as a reference for the chemical shift δ of the spectra.

2.4.2.3. Matrix Assisted Laser Deposition Ionisation Time of Flight (MALDI-ToF).

The polymers were analysed on a Bruker Daltonics AuToFlex MALDI-ToF mass spectrometer equipped with a nitrogen laser at 337 nm and positive ion ToF detection. The samples were prepared in a 9:1:1 mixture from a solution of the matrix (30 mg/mL), potassium trifluoroacetate (10 mg/mL) with the sample (10 mg/mL) dissolved in THF and 2 μL being deposited onto the stainless-steel target plate. Spectra were recorded in reflectron mode with the laser set at 20-30% power and the mass spectrometer was calibrated against polymers at mixture up to 6000 Da.

2.4.3. Methods

2.4.3.1. Monosaccharide functionalization

2.4.3.1.1. General procedure of the synthesis of Prop-2-ynyl monosaccharides (1 - 4).

The synthesis has been modified from a previously reported method[51]. The example given for **4.** Briefly, GlcNAc (10.01 g, 45.3 mmol) was suspended in propargyl alcohol (25 mL, excess) which was heated to 65 ºC. H$_2$SO$_4$.Silica (1.30 g, 30 mg per mmol) was added and the reaction was stirred for 16 hours. The reaction mixture was added to a silica column with the propargyl alcohol eluted with DCM and then the product was eluted out with methanol (100 %). The product was reduced under reduced pressure with the resulting oil being suspended in water and lyophilized to produce a yellow powder.

2.4.3.1.2. Prop-2-ynl-D-glucopyranoside (1)
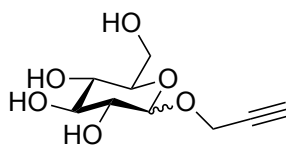
^{1}H NMR (CDCl$_3$, 400 MHz)	δ: 5.11 (d, 0.4H, J = 3.8 Hz H-1), 4.67 (d, 0.6 H, J = 12 Hz, 1H, H-1), 4.50 (t, J = 3.0 Hz, H-2), 4.36 (1H, q, J = 2.3 Hz C<u>H</u>≡CH), 4.25 (d, 0.6H, J = 2.4 Hz) 3.96–3.69 (3H, m, H-6, H-5) 3.55-3.29 (2H, m H-4, H-3), 2.93 (1H, dt, 11 Hz, J = 2.4 Hz, CH≡C<u>H</u>).

2.4.3.1.3. Prop-2-ynl-D-mannopyranoside (2)
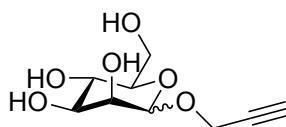
^{1}H NMR (CDCl$_3$, 400 MHz)	δ: 5.05 (d, 0.4H, J = 1.6 Hz H-1), 4.67 (d, 0.6 H, J = 12 Hz, 1H, H-1), 4.50 (t, J = 3.0 Hz, H-2), 4.32 (1.4H, dd, J = 6.1 Hz, 2.4 Hz C<u>H</u>≡CH), 4.25 (d, 0.6H, J = 2.4 Hz, C<u>H</u>≡CH) 3.96–3.68 (5H, m, H-6, H-5, H-4, H-3), 2.94 (0.75 H, t, J = 2.4 Hz, CH≡C<u>H</u>) and 2.86 (0.75 H, t, J = 2.4 Hz, CH≡C<u>H</u>).

2.4.3.1.4. Prop-2-ynl-D-galactucopyranoside (3)
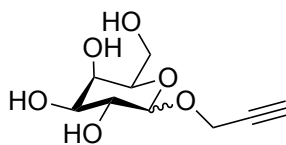
^{1}H NMR (CDCl$_3$, 400 MHz)	δ: 5.17 (dd, 0.75H, J = 15.6 Hz, 2.8 Hz H-1), 4.59 (d, 0.25 H, J =12 Hz, 1H, H-1), 4.36 (1.4H, dd, J = 2.4 Hz C<u>H</u>$_2$≡CH), 4.25 (d, 0.6H, J = 2.4 Hz, C<u>H</u>≡CH) 4.12–3.67 (5H, m, H-6, H-5, H-4, H-3), 2.93 (0.75 H, t, J = 2.4 Hz, CH≡C<u>H</u>) and 2.85 (0.75 H, t, J = 2.4 Hz, C$_2$≡C<u>H</u>).

2.4.3.1.5. Prop-2-ynl 2-acetamido-2-deoxy-D-glucopyranoside (4)
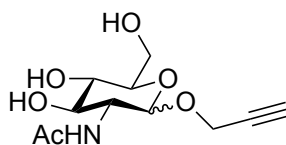
^{1}H NMR (CDCl$_3$, 400 MHz)	δ: 5.10 (d, 0.4H, J = 4 Hz H-1), 4.77 (d, 0.6 H, J = 12 Hz, 1H, H-1), 4.36 (1H, q, J = 14.0 Hz, 2 Hz C<u>H</u>≡CH), 3.98 (1H, t, H-2), 3.74 – 3.84 (3H, m, H-6, H-5), 3.50-3.63 (2H, m, H-4, H-3), 2.96 (1H, dt, J = 11 Hz, 2.4 Hz, CH≡C<u>H</u>), 2.09 (3H, s, NH(O)C<u>H</u>$_3$).
FT-IR (ATR):	3274 (br, OH), 2931 (w, C-H), 2118 (w, C≡C), 1650 (s, C=O).14, 1556, 1438,1417,1387, 1316, 1254 (w, C-O), 1099, 1079, 1026, 950, 890, 662, 525

2.4.3.1.6. 2-Acetamido-1,3,4,6-tetra-O-acetyl-2-deoxy-glucopyranose
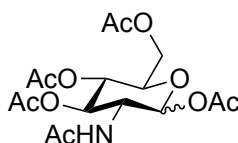
GlcNAc (4.01 g, 18.13 mmol) was suspended in acetic anhydride (20 mL) followed by I$_2$ (1.98 g) and stirred for 48 hours. DCM (50 mL) was added to the suspension and the solution was then added to ice, washed with Na$_2$S$_2$O$_3$ (1 M, 100 mL) and the phases separated. The aqueous layer was washed with DCM (2 x 50 mL). The organic layers were combined, washed with NaHCO$_3$. sat (50 mL) and then dried over MgSO$_4$, filtered and reduced under reduced pressure. The oil produced was placed under high vac to give a white powder (6) (5.61g, 14.40 mmol, 80%).

^{1}H NMR (CDCl$_3$, 400 MHz)	5.70 (d, J = 8.7 Hz, 1H H-1), 5.60 (d, J = 9.3 Hz, 1H, NH), 5.17 - 5.11 (m, 2H, H-2, H-5), 4.34 - 4.25 (m, 2H, H-4) 4.13 (dd, 2.1 Hz, J = 10.4 Hz, CH$_2$), 2.12 (s, 3H CH$_3$), 2.10 (s, 3H CH$_3$) 2.12 (s, 3H CH$_3$), 2.05 (s, 3H CH$_3$), 2.04 (s, 3H CH$_3$), 1.94 (s, 3H NCH$_3$)
FT-IR (ATR):	3434 (w, C-H), 1715 (s, C=O), 1672 (s, C=O), 1510, 1361, 1216 (s, C-O), 1126, 1016, 937, 605, 497

2.4.3.1.7. 2-Acetamido-3,4,6-tri-O-acetyl-1,2-deoxy-1-O-propragyl-glucopyranose
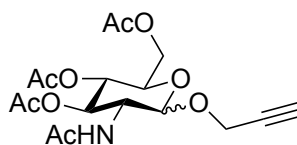
2-Acetamido-1,3,4,6-tetra-O-acetyl-2-deoxy-glucopyranose (500 mg, 1.28 mmol) was suspended in anhydrous DCM (20 mL) and cooled to 0 ºC. BF_3OEt_2 (0.68 mL, 5.27 mmol) was added dropwise and then stirred at 0 ºC for 30 minutes after which point propargyl alcohol (0.38 mL, 6.6 mmol) was added and heated to reflux. After 5 hours, the solution was quenched with DCM (100 mL), washed with $NaHCO_3$. sat (2 x 100 mL), H_2O (100 mL) followed by NaCl. sat (100 mL). The organic layer was dried over $MgSO_4$ and reduced under vacuum to produce an oil. The oil was placed under high vacuum to form a white solid (231.8 mg, 0.6 mmol, 47%).

^{1}H NMR (CDCl$_3$, 400 MHz)	5.92 (s, 1H, NH), 5.33 - 5.20 (m, 2H, H-3, H-5) 5.04 (t, 1H, J = 8.3Hz, H-2), 4.85 (d, 1H, J = 8.3 Hz, H-1), 4.40 (t, 2H, J = 1.9 Hz, CH$_2$≡CH) 2.48 (t, 1H, J = 2.4Hz, CH$_2$≡CH) 2.07, 2.03 (s, 9H, Ac), 1.94 (s, 3H NCH$_3$)
FT-IR (ATR):	2950 (w, C-H), 1743 (s, C=O), 1664 (s, C=O), 1510, 1371, 1216 (s, C-O), 1168, 1043, 981, 929, 844, 597, 491

2.4.3.1.8. 1,2,3,4-tetra-O-acetyl-α-D-glucopyranuronate
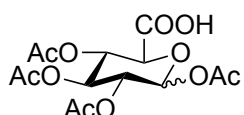
The synthesis has been modified from a previously reported method[29]. Briefly, GlcA (5.14 g) was added to a stirring solution of Ac_2O (25 mL, 264 mmol) followed by the addition H_2SO_4 (conc. 5 drops) which was then heated to 65 ºC. Once the sugar was dissolved, more GlcA (5.09 g) was added (Total GlcA; 10.23 g, 52.7 mmol). The solution was stirred for an hour and then cooled to 25 ºC. H_2O (75 mL) was added and then the product was extracted into DCM (3 x 50 mL). The organic layers were combined, dried over $MgSO_4$ and reduced under reduced pressure and azeotroped against toluene. The product was used without further purification.

^{1}H NMR (CDCl$_3$, 400 MHz)	6.43 (bs, 1H COOH), 5.78 (d, J = 7.5 Hz, 1H, H-1), 5.29 (m, 2H, H-2, H-5), 5.12 (m, 1H, H-3), 4.24 (m, 2H, H-4), 2.10, 2.03, 2.02, 2.01 (4s, 12H, OAc)
FT-IR (ATR):	3303 (br, O-H), 2950 (w, C-H), 1756 (s, C=O), 1726 (s, C=O) 1392, 1369, 1510, 1361, 1205 (C-O), 1122, 1045, 1005, 892, 657, 597, 565, 495

2.4.3.1.9. Methyl 1,2,3,4-tetra-O-acetyl-α-D-glucopyranuronate
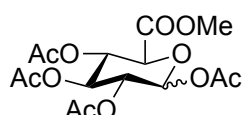
The crude 1,2,3,4-tetra-O-acetyl-α-D-glucopyranuronate was dissolved in DMF (25 mL) and reacted with NaHCO$_3$ (8.9 g, 106 mmol) followed by the addition of MeI (8.2 mL, 132 mmol). The reaction was stirred for 16 hours at 25 ºC. and then quenched with H$_2$O (200 mL). The product was extracted into EtOAc (3 x 200 mL). The organic layers were combined, dried over MgSO$_4$ and concentrated under reduced pressure. The resulting oil was taken up in acetone and precipitated in water. The precipitate was filtered and dried under vacuum to give a white powder (12.74 g, 33.9 mmol, 64 %).

^{1}H NMR (CDCl$_3$, 400 MHz)	5.76 (d, 1H, J = 7.7 Hz, H-1), 5.31 (t, 1H, J = 10.0 Hz, H-3), 5.25 (t, J = 9.4 Hz, H-4), 5.14 (t, 1H, J = 8.9 Hz, H-2), 4.18 (d, 1H, J = 9.5 Hz, H-5), 3.74 (s, 3H, OCH$_3$), 2.11 (s, 3H, CH$_3$), 2.03 (s, 6H, 2 x CH$_3$), 2.02 (s, 3H, CH$_3$).
FT-IR (ATR):	2948 (w, C-H), 1749 (s, C=O), 1436, 1369, 1209 (s, C-O), 1051, 1037, 889, 597, 505

2.4.3.1.10. 2-Azidoethanol
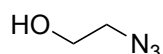
The synthesis method has previously been reported[52]. Briefly, 2-bromoethanol (10 g, 80 mmol) was suspended in H$_2$O (20 mL) followed by the addition of NaN$_3$ (9.53 g, 144 mmol) and NBu$_4$Br (590 mg). The reaction was stirred for 16 hours at 80 ºC. The reaction was cooled and extracted into Et$_2$O (10 x 50 mL). The organic layers were combined and reduced to give the product as a clear oil.

^{1}H NMR (CDCl$_3$, 400 MHz)	3.73 (t, 2H, J = 4.5 Hz, CH$_2$OH), 3.38 (t, 2H, J = 4.5 Hz, CH$_2$N$_3$).
FT-IR (ATR):	3373 (br, O-H), 2935 (w, C-H), 2098 (s, N$_3$), 1441, 1347 1283 (w, C-O), 1060, 977, 877, 828, 631, 554, 503

2.4.3.1.11. General procedure for the glycosidation by Lewis acid

Methyl 1,2,3,4-tetra-O-acetyl-α-D-glucopyranuronate (1 equiv) and propargyl alcohol (4 equiv) was suspended in anhydrous DCM (25 mL). The reaction was cooled to 0 ºC at which point BF$_3$.OEt$_2$ (2 equiv) was added. The reaction was stirred at 0 ºC for 15 minutes and then allowed to warm to 25 ºC and stirred for 16 hours. The reaction was diluted with DCM and then washed with water (2 x 50 mL) and brine (50 mL). The organic layers were combined, dried over MgSO$_4$ and reduced under reduced pressure. The oil was purified by flash chromatography, EtOAc: hexane (1:1).

2.4.3.1.12. Methyl 2,3,4-tri-O-acetyl-1-propargyl-α-D-glucuronate (9)
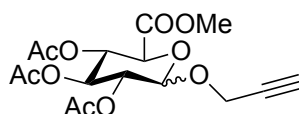
Methyl 1,2,3,4-tetra-O-acetyl-α-D-glucopyranuronate (5.06 g, 13.4 mmol) and propargyl alcohol (3.2 mL, 54.8 mmol) was suspended in anhydrous DCM (25 mL). The reaction was cooled to 0 ºC at which point BF$_3$.OEt$_2$ (3.3 mL, 25.3 mmol) was added producing an off-white solid (2.94 g, 7.90 mmol, 59%)

^{1}H NMR (CDCl$_3$, 400 MHz)	5.76 (d, 1H, J = 7.7 Hz, H-1), 5.49 (t, 1H, J = 10.0 Hz, H-3), 5.28-5.10 (m, 3H, H-4, H-2), 4.82 (d, 1H, CH$_2$C≡CH), 4.18 (d, 1H, J = 9.5 Hz, H-5), 3.73 (s, 3H, OCH$_3$), 2.63 (t, 2H, C≡CH) 2.11 (s, 3H, CH$_3$), 2.03 (s, 6H, 2 x CH$_3$), 2.02 (s, 3H, CH$_3$).
FT-IR (ATR):	3278 (w, C-H), 1743 (s, C=O), 1437, 1369, 1212, 938, 897, 651, 599, 529

2.4.3.1.13. Methyl (2-azidoethyl 2,3,4-tri-O-acetyl-β-D-glucopyranosid)uronate (10)
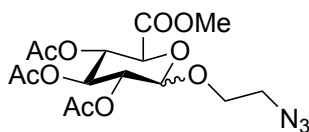
Methyl 1,2,3,4-tetra-O-acetyl-α-D-glucopyranuronate (5.03 g, 13.4 mmol) and 2-azidoethanol (2.6 mL, 52.6 mmol) was suspended in anhydrous DCM (25 mL). The reaction was cooled to 0 °C at which point $BF_3.OEt_2$ (3.3 mL, 25.3 mmol) was added.

^{1}H NMR (CDCl$_3$, 400 MHz)	δ 5.49 (t, 1H, J = 10.1 Hz, H-2), 5.21 (q, 2H, J = 9.4 Hz, H-3, H-4), 5.09 (dd, 1H, J = 8.4 Hz, 3.7 Hz, H-5), 4.63 (d, 0.4 Hz, J = 7.7 Hz, H-1), 4.38 (d, 0.4 Hz, J =10.2 Hz, H-1), 4.21 (t, 2H, J = 5.1 Hz, CH$_2$N$_3$), 3.73 (s, 3H, OCH$_3$), 3.45 (t, 2H, J = 5.2 Hz, OCH$_2$), 2.48 (m, 1H, CH) 2.02 (s, 3H, CH$_3$), 2.01 (s, 3H, CH$_3$), 1.98 (s, 3H, CH$_3$).
FT-IR (ATR):	2957 (w, C-H), 2106 (s, N$_3$), 1743 (s, C=O), 1438, 1370, 1209, 1038, 936, 893, 599, 508

2.4.3.1.14. Vinylbenzyl azide (11)
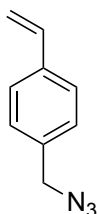
VBC (9.8 mL, 65 mmol) was added dropwise to a solution of NaN$_3$ (8.58 g, 130 mmol) in DMSO (100 mL) at 80 °C and left to stir for 16 hours. The solution was cooled and diluted with ether (100 mL) and washed with H$_2$O (3 x100 mL). The aqueous layers where collected and washed with ether (3 x 100 mL). All the organic layers where combined and dried over MgSO$_4$, filtered then reduced under vacuum to give a yellow oil (8.84 g, 56 mmol, 86%)

^{1}H NMR (CDCl$_3$, 400 MHz)	δ: 7.43 (d, 2H, J = 8.1 Hz, Ortho-CH), 7.28 (d, 2H, J = 8.1 Hz, Meta-CH), 6.73 (dd, 2H, J = 16.8, 10.0 Hz, CH=CH$_2$), 5.77 (d, 1H, J = 16.8 Hz, trans-CH=CH$_2$), 5.28 (d, 1H, J = 10.0Hz, cis-CH=CH$_2$), 4.33 (s, 2H, J = 16.8 Hz, trans CH$_2$N$_3$)

^{13}C NMR (CDCl$_3$, 133 MHz)	137.82 (Para-CH), 136.38 (1C, C̲H=CH$_2$), 134.95 (1C, C) 128.59 (2C, Ortho-C), 126.78 (2C, Meta-C), 114.59 (1C, CH=C̲H$_2$), 54.70 (1C, C̲H$_2$N$_3$)
FT-IR (ATR)	3004 (CH), 2977 (CH), 2098 (N$_3$), 1710 (C=C), 1678 (C=C), 1359, 1220, 1092, 529

2.4.3.1.15. [1-(4-Vinylphenylmethyl)-1H-1,2,3-triazol-4-yl]methyl2-acetamido-3,4,6-tri-O-acetyl-2-deoxy-d-glucopyranoside (12)
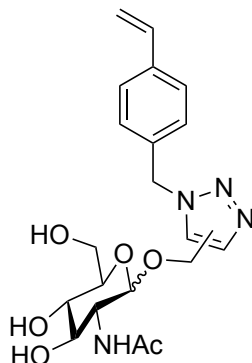
Vinylbenzyl azide (2.76 g, 17.74 mmol) and 1.4.3.5 - Prop-2-ynl 2-acetamido-2-deoxy-D-glucopyranoside (3.00 g, 13.59 mmol) in methanol (10 mL) was purged in N$_2$ for 30 minutes. The CuSO$_4$.5H$_2$O (0.15 g, 0.07 mmol) in H$_2$O (2 mL) was added followed by Na-Ascorbate (0.23 g, 1.11 mmol) in H$_2$O (3 mL); the reaction was sealed and stirred for 16 hours at 25 ºC. The reaction crude was reduced in reduced pressure and diluted in water (100 mL). The aqueous layer was washed with DCM (3 x 100 mL) and the aqueous layer passed through Al$_2$O$_3$ (neutral). The solution was lyophilised forming an off-white powder (3.61 g, 8.79 mmol, 64 %).

^{1}H NMR (CDCl$_3$, 400 MHz)	δ: 8.04 (s, 0.4 H, Triazole-CH), 8.00 (s, 0.6H, Triazole-CH), 7.51 (d, 2H, J = 8.1 Hz, ortho-CH), 7.33 (t, 2H, J = 8.2 Hz, meta-CH), 6.78 (dd, 1H, J = 17.7 Hz, 11.0 Hz, C̲H=CH$_2$), 5.85 (d, 1H, J = 17.7 Hz, C̲H=CH$_2$-trans), 5.59 (s, 2H, CH$_2$), 5.33 (d, 1H J = 11.0 Hz, C̲H=CH$_2$-cis), 4.85 (m, 1H, H-1), 4.56 (d, 1H, J = 8.4 Hz, H-1), 3.42 – 3.86 (m, 6H, H-2, H-3, H-4, H-5, H-6), 1.85 (s, 1.7 H, CH$_3$), 1.79 (s, 1.3H, CH$_3$)
FT-IR (ATR)	3291 (br, OH), 3086 (w, CH), 2928 (w, CH), 1615 (C=C), 1546 (C=C), 1514, 1430, 1408, 1374, 1314, 1254, 1221,

1110, 1034, 947, 916, 827, 792, 715, 661, 610, 550, 526, 518, 511

2.4.3.1.16. (E)-4-oxo-4-(prop-2-yn-1-yl amino)but-2-enoic acid (13)
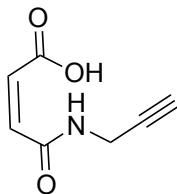
MAh (10.0 g, 105 mmol) and propargylamine (6.5 mL, 103 mmol) were suspended in AcOH (50 mL) and stirred for 16 hours in the dark. The orange suspension was dried under reduced pressure to produce the intermediate yellow.

^{1}H NMR (CDCl$_3$, 400 MHz)	6.42 (d, 1H, J = 12.9 Hz, CH), 6.23 (d, 1H, J = 12.9 Hz, CH), 4.20 (dd, 2H, J = 2.6 Hz, 4.6 Hz, NHCH$_2$), 2.35 (t, 1H, J = 2.6 Hz, C≡CH)
FT-IR (ATR)	3261 (s, O-H), 3050 (w, C-H), 1697 (s, C=O), 1592 (s, C=O), 1538, 1492, 1245, 1056,1018, 852, 715, 676, 624, 590, 530

2.4.3.1.17. N-Propargyl maleimide (14)
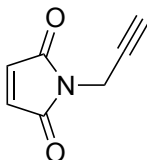
13 was suspended in Ac$_2$O (20 mL) and AcONa (1.5070 g) which was stirred for 2 hours at 65 °C. The red solution was poured into ice water and extracted in ether (3 x 50 mL). The organic layer was combined, dried over MgSO$_4$ and reduced under vacuum. The product was columned on DCM: EtOAc to give a black oil, which was left to crystallise (6.60 g, 48.8 mmol, 47% across two steps).

^{1}H NMR (CDCl$_3$, 400 MHz)	6.76 (s, 2H, CH=CH), 4.30 (d, 2H, J = 2.5 Hz, CH$_2$) 2.22 (t, 1H, J = 2.5 Hz, C≡CH)
FT-IR (ATR):	3238 (w, C-H), 3102 (w, C-H), 2127 (w, C≡C), 1730 (s, C=O), 1428, 1406, 1346, 1316, 1225, 1175, 1099, 938, 760, 693, 643, 517

2.4.3.1.18. 1-(3-(triisopropylsilyl)prop-2-ynyl)-1H-pyrrole-2,5-dione (18)
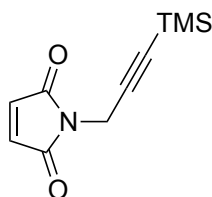
The synthesis has been modified from the previously reported method[53]. Briefly, triphenylphosphine (8.1 g, 30.9 mmol) was dissolved in THF (80 mL) and cooled to - 78 °C under an inert atmosphere. DIAD (6.1 mL, 30.9 mmol) was added dropwise over 5 minutes followed by 3- (trimethylsilyl)prop-2-yn-1-ol (4.1 mL, 28.1 mmol) dropwise over 5 minutes. The maleimide (3 g, 31.6 mmol) was suspended in THF (100 mL) and added dropwise. The resulting foam was stirred for 10 minutes at the – 78 °C and then 24 for hours at 25 °C. The solvent was removed in vacuo and the residue purified by column chromatography first hexane: EtOAc (1:1) with a second column using hexane: EtOAc (2:1) followed by the reduction under vacuum to give 1-(3-(trimethylsilyl)prop-2-ynyl)-1H-pyrrole-2,5-dione as a yellow oil.

^{1}H NMR (CDCl$_3$, 400 MHz)	δ: 6.74 (s, 2H, HC=CH), 4.28 (s, 2H, CH$_2$), 0.12 (s, 9H, Si(CH$_3$)$_3$
FT-IR (ATR):	2961 (w, C-H), 2182 (w, C≡C), 1713 (s, C=O), 1425, 1401, 1344, 1249, 1151, 1041, 1007, 826, 759, 694, 654, 509

2.4.3.1.19. Polymerisation

2.4.3.1.20. General procedure for polymerisation

The polymerisation worked in both homopolymerisation and copolymerisation systems. The synthesis has been modified from the previously reported method[54]. The polymers were synthesised by RAFT polymerisation using BDTMP as the RAFT agent and V601 as the initiator, modified from the previously reported method. Briefly, all the components were combined and purged in a Schlenk tube under nitrogen flow for 30 minutes, after which point the reaction was put into an oil bath at 70 ºC to initiate the reaction. Once complete, the reaction was quenched in an ice bath followed by exposure to the atmosphere. The solution was precipitated into cold methanol or isopropanol and the product collected by filtration.

2.4.3.1.21. pVBC (P1)
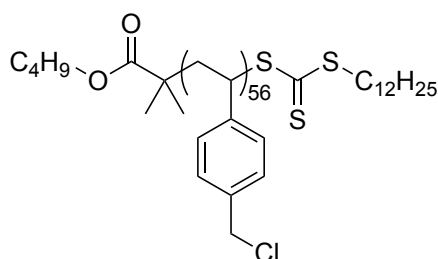
^{1}H NMR ((CD$_3$)$_2$CO, 400 MHz)	δ: 7.18 (br, 2H, ortho-CH), 6.68 (br, 2H, meta-CH), 4.64 (br, 2H, CH$_2$), 1.89 (br, CH backbone), 1.64 (br, CH$_2$ backbone), 1.39 (br, RAFT-CH$_2$), 0.86 (br, RAFT-CH$_3$)
FT-IR (ATR):	2925 (w, C-H), 1723 (w, C=C), 1612, 1510, 1443, 1421, 1264, 1187, 1133, 1019, 824, 671, 638, 534

2.4.3.1.22. pVBC-alt-TMS PMI (P9)
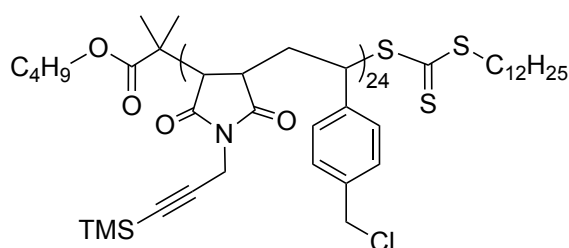
^{1}H NMR ((CD$_3$)$_2$CO, 400 MHz)	δ: 7.17 (br, 2H, ortho-CH), 6.74 (br, 2H, meta-CH), 4.52 (br, 2H, CH$_2$), 4.10 (br, 2H, CH$_2$), 3.22 (br, CH backbone), 2.55(br, CH backbone), 2.08 (br, CH$_2$ backbone), 1.39 (br, RAFT-CH$_2$), 0.87 (br, RAFT-CH$_3$), 0.13 (s, 9H, TMS)
FT-IR (ATR):	2925 (w, C-H), 1723 (w, C=C), 1612, 1510, 1443, 1421, 1264, 1187, 1133, 1019, 824, 671, 638, 534

2.4.3.1.23. General procedure for polymer azidation.

The synthesis has been modified from previously reported method[33]. Briefly, the polymer was suspended in DMSO (300 % v/v) followed by the addition of NaN$_3$ (1.5 equiv per chloride) and stirred 16 hours at 25 ºC. The resulting solution is diluted into water and extracted in EtOAc (3 x 50 mL). The organic layers were combined, dried over MgSO$_4$, filtered and reduced under reduced pressure to give the polymer.

2.4.3.1.24. pVBAz (P2)
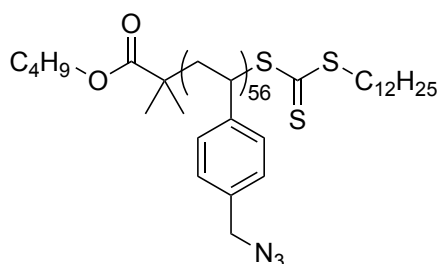
^{1}H NMR ((CD$_3$)$_2$CO, 400 MHz)	δ: 7.12 (br, 2H, ortho-CH), 6.70 (br, 2H, meta-CH), 4.38 (br, 2H, CH$_2$), 1.85 (br, CH backbone), 1.65 (br, CH$_2$ backbone), 1.41 (br, RAFT-CH$_2$), 0.88 (br, RAFT-CH$_3$)
FT-IR (ATR):	2924 (w, C-H), 2091 (s, N$_3$), 1758 (w, C=C), 1721, 1676, 1611, 1510, 1446, 1421, 1341, 1245, 1205, 1112, 1019, 877, 843, 805, 753, 703, 666, 556

2.4.3.1.25. pVBAz-alt-TMS PMI (P9)

^{1}H NMR ((CD$_3$)$_2$CO, 400 MHz)	7.29 (br, 2H, ortho-CH), 6.74 (br, 2H, meta-CH), 4.66 (br, 2H, CH$_2$), 4.07 (br, 2H, CH$_2$), 2.70 (br, CH backbone), 2.07 (br, CH backbone), 1.65 (br, CH$_2$ backbone), 1.42 (br, RAFT-CH$_2$), 1.04 (br, RAFT-CH$_3$).
FT-IR (ATR):	2960 (w, C-H), 2183 (w, C≡C), 2091 (s, N$_3$), 1773 (w, C=C), 1700 (s, C=O), 1512, 1417, 1394, 1341, 1248, 1177, 1110, 1011, 950, 840, 759, 698, 642

2.4.3.1.26. General procedure for CuAAc click reaction on polymers

The polymer (1 equiv with respect to azide), alkyne sugar (1.5 equiv), Me$_6$TREN (2 equiv) were suspended in DMSO (2 ml/g of solid) and degassed by gentle bubbling of Ar gas for 30 minutes. CuBr was charged into a Schlenk tube and degassed by gentle bubbling of Ar gas for 30 minutes. The degassed solution was cannulated into the Schlenk tube, with the solution and catalyst being stirred. The reaction was stirred at

25 ºC for 2 days. The resulting solution was diluted by water (v/v) and passed through Al_2O_3 (neutral). The resulting solution was dialyzed in the presence of Cuprisorb© and then lyophilized to give the pure product.

2.4.3.1.27. Poly(vinylbenzyl) – graft – Glc (P3)

^{1}H NMR	8.18 (br, 1H, triazole-H), 6.97 (br, 4H, ortho-CH, meta-CH), 5.33
$((CD_3)_2CO$, 400 MHz)	(br, 2H, CH$_2$), 4.99 (br, 2H, OCH$_2$), 3.55 (br, 5H Sugar-H), 1.30
	(br, RAFT-CH$_2$), 0.89 (br, RAFT-CH$_3$).
FT-IR (ATR):	3332, (br, O-H), 2917 (w, C-H), 1222, 1018, 787, 557, 459

2.4.3.1.28. Poly(vinylbenzyl) – graft – Man (P4)

^{1}H NMR	8.18 (br, 1H, triazole-H), 7.08 (br, 4H, ortho-CH, meta-CH), 5.56
$((CD_3)_2CO$, 400 MHz)	(br, 2H, CH$_2$), 4.92 (br, 2H, OCH$_2$), 3.70 (br, 5H Sugar-H), 1.30
	(br, RAFT-CH$_2$), 0.90 (br, RAFT-CH$_3$).
FT-IR (ATR):	3332, (br, O-H), 2946 (w, C-H), 1639, 1326, 1022, 788, 537

2.4.3.1.29. Poly(vinylbenzyl) – graft – Gal (P5)
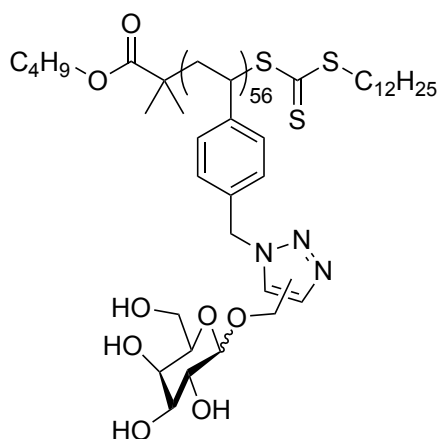
^{1}H NMR ((CD$_3$)$_2$CO, 400 MHz)	8.11 (br, 1H, triazole-H), 6.96 (br, 4H, ortho-CH, meta-CH), 5.53 (br, 2H, CH$_2$), 4.50 (br, 2H, OCH$_2$), 3.70 (br, 5H Sugar-H), 1.22 (br, RAFT-CH$_2$), 0.81 (br, RAFT-CH$_3$)
FT-IR (ATR):	3348, (br, O-H), 2928 (w, C-H), 1611, 1512, 1425, 1345, 1223, 1041, 789, 540

2.4.3.1.30. Poly(vinylbenzyl) – graft – GlcNAc (P6)

^{1}H NMR ((CD$_3$)$_2$CO, 400 MHz)	8.12 (br, 1H, triazole-H), 7.66 (br, 1H, NH), 6.90 (br, 2H, ortho-CH), 6.40 (br, 2H, meta-CH), 5.47 (br, 2H, CH$_2$), 5.01 (br, 2H, OCH$_2$), 4.77 (br, 1H, CH Sugar-H), 4.64 (br, 2H, Sugar-H), 3.69 (br, 1H, CH), 3.48 (br, 2H, CH$_2$), 3.12 (br, 2H, Sugar-H), 1.67 (br, 3H, CH$_3$), 1.24 (br, RAFT-CH$_2$), 0.85 (br, RAFT-CH$_3$).
FT-IR (ATR):	3348, (br, O-H), 2928 (w, C-H), 1611, 1512, 1425, 1345, 1223, 1041, 789, 540

2.4.3.1.31. Poly(vinylbenzyl) – graft – GlcA (P7)
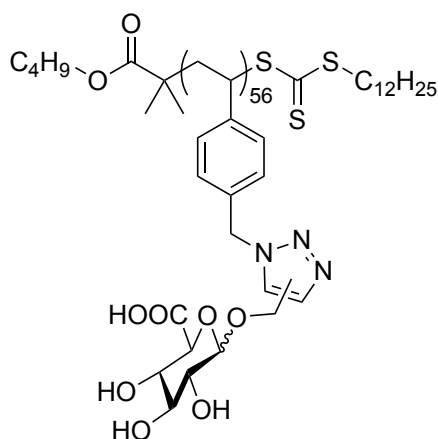
¹H NMR ((CD₃)₂CO, 400 MHz)	8.13 (br, 1H, triazole-H), 6.90 (br, 2H, ortho-CH), 6.37 (br, 2H, meta-CH), 5.39 (br, 2H, **CH₂**), 5.04 (br, 2H, OC**H₂**), 4.80 (br, 1H, CH Sugar-**H**), 4.66 (br, 2H, Sugar-**H**), 3.69 (br, 1H, C**H**), 3.48 (br, 2H, C**H₂**), 3.12 (br, 2H, Sugar-**H**), 1.24 (br, RAFT-C**H₂**), 0.85 (br, RAFT-C**H₃**).
FT-IR (ATR):	3356, (br, O-H), 2919 (w, C-H), 1740, 1605, 1512, 1423, 1289, 1221, 1043, 789, 544.

2.4.3.1.32. Poly(vinylbenzyl) – graft – GlcNAc-co-(vinylbenzyl)-graft-GlcA (P8)
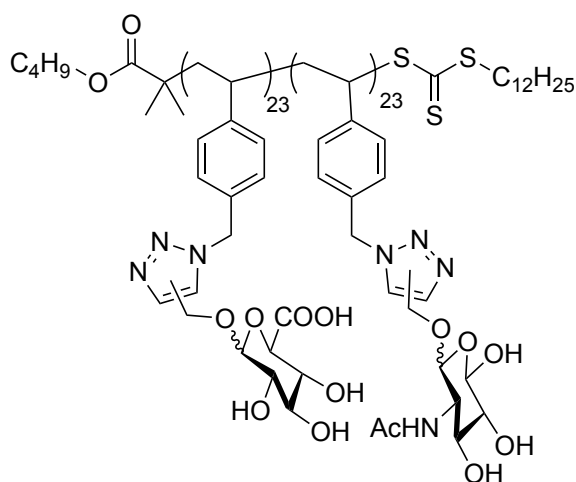
¹H NMR ((CD₃)₂CO, 400 MHz)	8.18 (br, 1H, triazole-H), 7.05 (br, 4H, ortho-CH, meta-CH), 5.33 (br, 2H, CH₂), 3.74-3.55 (br, 4H, Sugar-H), 1.67 (br, 1.5H, CH₃)1.28 (br, RAFT-CH₂), 0.90 (br, RAFT-CH₃)
FT-IR (ATR):	3268, (br, O-H), 2875 (w, C-H), 1608, 1546, 1419, 1345, 1214, 1037, 777, 532

2.4.3.1.33. General procedure for TMS deprotection of polymer

The polymer was suspended in DMSO (10% v/v) in water and put in a dialysis membrane (MWCO 1 kDa). The glycopolymer was dialyzed against K_2CO_3 solution followed by H_2O. The deprotected glycopolymer was lyophilized to give the deprotected glycopolymer as a lyophilized powder.

2.4.3.1.34. Poly(vinylbenzyl) – graft – GlcNAc-alt-(vinylbenzyl)-graft-GlcA (P12)
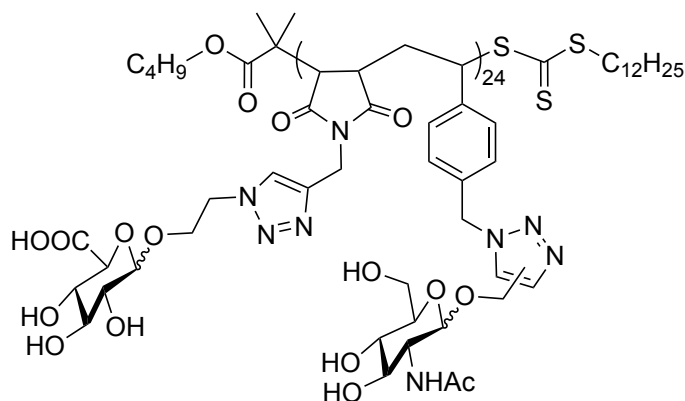
^{1}H NMR	7.97 (br, 1H, triazole-H), 6.92 (br, 4H, ortho-CH, meta-CH), 5.50
$((CD_3)_2CO$, 400 MHz)	(br, 2H, CH_2), 4.29-3.33 (br, 14H, backbone, Sugar-H), 1.87 (br, 3H, CH_3)1.28 (br, RAFT-CH_2), 0.92 (br, RAFT-CH_3)
FT-IR (ATR):	3293, (br, O-H), 2934 (w, C-H), 1672 (C=O), 1462, 1405, 1324, 1257, 1196, 1127, 1052, 831, 798, 720, 596, 515

References

1. Liao, Y.H., et al., *Hyaluronan: pharmaceutical characterization and drug delivery.* Drug Delivery, 2005. **12**(6): p. 327-42.
2. Burdick, J.A. and G.D. Prestwich, *Hyaluronic acid hydrogels for biomedical applications.* Advanced Materials, 2011. **23**(12): p. H41-56.
3. Rodell, C.B., A.L. Kaminski, and J.A. Burdick, *Rational design of network properties in guest-host assembled and shear-thinning hyaluronic acid hydrogels.* Biomacromolecules, 2013. **14**(11): p. 4125-34.
4. S., S. *Global Hyaluronic Acid Products Market Driven by High Demand for Anti-ageing Products, to Reach US$9.85 bn by 2019.* 2016 [cited 2018 29/03/2018].
5. *Hyaluronic Acid (HA) Raw Material Market Worth $7.25 Billion By 2024.* 2017 [cited 2018 29/03/2018].
6. A, B.E., *Ultrapure Hyaluronic Acid And The Use Thereof,* U.P. Office, Editor. 1979, Balazs Endre A: US.
7. Core, L. *Sodium Hyaluronate.* 2017 [cited 2018 10/04/2018].
8. Jiang, D., J. Liang, and P.W. Noble, *Hyaluronan as an Immune Regulator in Human Diseases.* Physiological Reviews, 2011. **91**(1): p. 221-264.
9. Mende, M., et al., *Chemical Synthesis of Glycosaminoglycans.* Chemical Reviews, 2016. **116**(14): p. 8193-255.
10. Iyer, S., et al., *Synthesis of a hyaluronan neoglycopolymer by ring-opening metathesis polymerization.* Chemical Communications, 2003(13): p. 1518-9.
11. Karskela, M., et al., *Synthesis and cellular uptake of fluorescently labeled multivalent hyaluronan disaccharide conjugates of oligonucleotide phosphorothioates.* Bioconjugate Chemistry, 2008. **19**(12): p. 2549-58.
12. Banerji, S., et al., *Structures of the Cd44-hyaluronan complex provide insight into a fundamental carbohydrate-protein interaction.* Nature Structural & Molecular Biology, 2007. **14**(3): p. 234-9.
13. Aksakal, R., M. Resmini, and C.R. Becer, *Pentablock star shaped polymers in less than 90 minutes via aqueous SET-LRP.* Polymer Chemistry, 2016. **7**(1): p. 171-175.
14. Sletten, E.T., et al., *Glycosidase Inhibition by Multivalent Presentation of Heparan Sulfate Saccharides on Bottlebrush Polymers.* Biomacromolecules, 2017. **18**(10): p. 3387-3399.
15. Zhao, Y., et al., *Role of Protecting Groups in Synthesis and Self-Assembly of Glycopolymers.* Biomacromolecules, 2017. **18**(2): p. 568-575.
16. Malins, E.L., C. Waterson, and C.R. Becer, *Alternating copolymers of functionalized α-methyl styrene monomers and maleic anhydride.* Polymer Chemistry, 2015. **6**(36): p. 6543-6552.
17. Williams, E.G.L., et al., *Preparation of 1 : 1 alternating, nucleobase-containing copolymers for use in sequence-controlled polymerization.* Polymer Chemistry, 2015. **6**(2): p. 228-232.
18. Davies, M.C., J.V. Dawkins, and D.J. Hourston, *Radical copolymerization of maleic anhydride and substituted styrenes by reversible addition-fragmentation chain transfer (RAFT) polymerization.* Polymer, 2005. **46**(6): p. 1739-1753.
19. Zhu, M.-Q., et al., *A unique synthesis of a well-defined block copolymer having alternating segments constituted by maleic anhydride and styrene and the self-assembly aggregating behavior thereof.* Chemical Communications, 2001(4): p. 365-366.
20. Pfeifer, S. and J.F. Lutz, *A facile procedure for controlling monomer sequence distribution in radical chain polymerizations.* Journal of the American Chemical Society, 2007. **129**(31): p. 9542-3.
21. Lutz, J.F., B.V. Schmidt, and S. Pfeifer, *Tailored polymer microstructures prepared by atom transfer radical copolymerization of styrene and N-substituted maleimides.* Macromolecular Rapid Communications, 2011. **32**(2): p. 127-35.
22. Baradel, N., et al., *Synthesis of Single-Chain Sugar Arrays.* Angewandte Chemie International Edition\, 2013. **52**(8): p. 2335-2339.

23. Srichan, S., H. Mutlu, and J.-F. Lutz, *On the synthesis of sequence-controlled poly(vinyl benzyl amine-co-N-substituted maleimides) copolymers.* European Polymer Journal, 2015. **62**: p. 338-346.

24. Pfeifer, S. and J.F. Lutz, *Development of a library of N-substituted maleimides for the local functionalization of linear polymer chains.* Chemistry, 2008. **14**(35): p. 10949-57.

25. Mukhopadhyay, B., S. Mandal, and N. Sharma, *H2SO4-Silica Promoted Direct Formation of β-Glycosides of N-Acetyl Glycosylamines under Microwave Conditions.* Synlett, 2009. **2009**(19): p. 3111-3114.

26. Vauzeilles, B., et al., *A one-step β-selective glycosylation of N-acetyl glucosamine and recombinant chitooligosaccharides.* Tetrahedron Letters, 2001. **42**(43): p. 7567-7570.

27. Rowan, A.S., et al., *Nucleoside triphosphate mimicry: a sugar triazolyl nucleoside as an ATP-competitive inhibitor of B. anthracis pantothenate kinase.* Organic & Biomolecular Chemistry, 2009. **7**(19): p. 4029.

28. Kim, S.H., et al., *The crystal structure of beta-D-glucurono-gamma-lactone.* Acta Crystallographica, 1967. **22**(5): p. 733-43.

29. Loukou, C., et al., *Synthesis of sugar-lactams from azides of glucuronic acid.* Carbohydrate Research, 2007. **342**(12-13): p. 1953-9.

30. Tosin, M. and P.V. Murphy, *Synthesis of alpha-glucuronic acid and amide derivatives in the presence of a participating 2-acyl protecting group.* Organic Letters, 2002. **4**(21): p. 3675-8.

31. McDonagh, A.W. and P.V. Murphy, *Synthesis of α-galactosyl ceramide analogues with an α-triazole at the anomeric carbon.* Tetrahedron, 2014. **70**(19): p. 3191-3196.

32. O'Shea, J.-P., et al., *Sequence-controlled copolymers of 2,3,4,5-pentafluorostyrene: mechanistic insight and application to organocatalysis.* Polymer Chemistry, 2014. **5**(3): p. 698-701.

33. Ting, W.-H., et al., *Facile synthetic route toward poly(vinyl benzyl amine) and its versatile intermediates.* Polymer, 2008. **49**(6): p. 1497-1505.

34. Ott, C., R. Hoogenboom, and U.S. Schubert, *Post-modification of poly(pentafluorostyrene): a versatile "click" method to create well-defined multifunctional graft copolymers.* Chemical Communications, 2008(30): p. 3516-8.

35. ten Brummelhuis, N. and M. Weck, *Orthogonal Multifunctionalization of Random and Alternating Copolymers.* ACS Macro Letters, 2012. **1**(10): p. 1216-1218.

36. Becer, C.R., et al., *Clicking Pentafluorostyrene Copolymers: Synthesis, Nanoprecipitation, and Glycosylation.* Macromolecules, 2009. **42**(7): p. 2387-2394.

37. Cheng, Z., et al., *Polymer Microspheres with Permanent Antibacterial Surface from Surface-Initiated Atom Transfer Radical Polymerization.* Industrial & Engineering Chemistry Research, 2005. **44**(18): p. 7098-7104.

38. Matsuoka, K., et al., *Use of chloromethylstyrene as a supporter for convenient preparation of carbohydrate monomer and glycopolymers.* Carbohydrate Polymers, 2014. **107**: p. 209-13.

39. Slavin, S., et al., *Synthesis of glycopolymers via click reactions.* European Polymer Journal, 2011. **47**(4): p. 435-446.

40. Henry, S.M., et al., *pH-responsive poly(styrene-alt-maleic anhydride) alkylamide copolymers for intracellular drug delivery.* Biomacromolecules, 2006. **7**(8): p. 2407-14.

41. Moad, G., E. Rizzardo, and S.H. Thang, *End-functional polymers, thiocarbonylthio group removal/transformation and reversible addition-fragmentation-chain transfer (RAFT) polymerization.* Polymer International, 2011. **60**(1): p. 9-25.

42. L'Abbe, G., *1969* Chemical Reviews, 1969. **69**(3): p. 345-363.

43. Perrier, S., P. Takolpuckdee, and C.A. Mars, *Reversible Addition−Fragmentation Chain Transfer Polymerization: End Group Modification for Functionalized Polymers and Chain Transfer Agent Recovery.* Macromolecules, 2005. **38**(6): p. 2033-2036.

44. Gordon, D.A., V.A. Volodina, and A.I. Mikhailov, *Characteristics of the radical polymerization of acetylene monomers.* Russian Journal of Physical Chemistry A, 2014. **88**(12): p. 2129-2136.

45. Doak, K.W., *Copolymerization. XV.1Copolymerization of Acetylene Derivatives with Olefins. Retardation by Radicals from Acetylenes.* Journal of the American Chemical Society, 1950. **72**(10): p. 4681-4686.

46. Higashiura, K. and M. Oiwa, *Retardation of radical polymerization by phenylacetylene and its p-substituted derivatives.* Journal of Polymer Science Part A: Polymer Chemistry, 1968. **6**(7): p. 1857-1869.

47. Schmidt, B.V.K.J., et al., *Controlled folding of synthetic polymer chains through the formation of positionable covalent bridges.* Nat Chem, 2011. **3**(3): p. 234-238.

48. Mayo, F.R. and F.M. Lewis, *Copolymerization. I. A Basis for Comparing the Behavior of Monomers in Copolymerization; The Copolymerization of Styrene and Methyl Methacrylate.* Journal of the American Chemical Society, 1944. **66**(9): p. 1594-1601.

49. Abel, B.A. and C.L. McCormick, *"One-Pot" Aminolysis/Thiol–Maleimide End-Group Functionalization of RAFT Polymers: Identifying and Preventing Michael Addition Side Reactions.* Macromolecules, 2016. **49**(17): p. 6193-6202.

50. Takeishi, M., et al., *Polymerization of N-Substituted Maleimides Initiated by Thiophenol.* Polymer Journal, 1992. **24**(4): p. 365-373.

51. Roy, B. and B. Mukhopadhyay, *Sulfuric acid immobilized on silica: an excellent catalyst for Fischer type glycosylation.* Tetrahedron Letters, 2007. **48**(22): p. 3783-3787.

52. Pfaendler, H.R. and V. Weimar, *Synthesis of Racemic Ethanolamine Plasmalogen.* Synthesis, 1996. **1996**(11): p. 1345-1349.

53. Schmidt, B.V., et al., *Controlled folding of synthetic polymer chains through the formation of positionable covalent bridges.* Nature Chemistry, 2011. **3**(3): p. 234-38.

54. Moraes, J., et al., *The synthesis of well-defined poly(vinylbenzyl chloride)-grafted nanoparticles via RAFT polymerization.* Beilstein Journal of Organic Chemistry, 2013. **9**: p. 1226-34.

Chapter 3 Engineering hyaluronan (HA)-binding peptides for self-assembly with natural HA

3.1. Introduction

Hyaluronan (HA) is the largest polysaccharide found in the human body, being the only pure polyanion in the extracellular space. While not forming covalent bonds, HA has many natural binders (Table 1.2) which enable its ability to interact with other ECM components, such as proteoglycans or collagen, and cells.

Due to HA biocompatibility and rheological properties, it has been used in the formulation of many biomaterials. To form stable HA-based biomaterials, work has been undertaken by several groups, most notably by Burdick's lab[1-3], the Ramamurthi group[4-6] and the Prestwich group[7-9], where they have introduced chemical and physical crosslinks in the polysaccharide. The physical and chemical crosslinking has been achieved through chemical modification of the primary hydroxyls, the carboxylate and the N-acetyl when deacetylated to form a primary amine (Figure 3.1). These modifications can allow for a range of reactions to be undertaken, such as alkene polymerisation, thiol-ene click reaction[10] or the use of divalent molecules such as dihalides, diamines and dihydrazides.
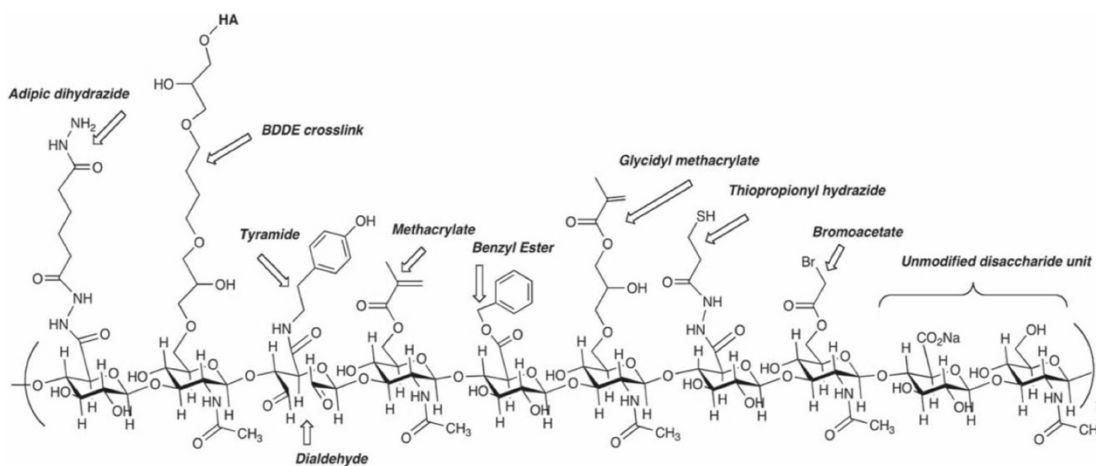
Figure 3.1. The potential chemical modifications on HA, through the carboxylate, primary alcohol and breaking of the saccharide ring. Taken from Burdick and Prestwich 2011[11]

These modifications are aimed at producing permanent crosslinks between HA chains and generating more stable biomaterials. HA chemical modification can lead to detrimental effects, such as lack of control over the modifications, polymer degradation, as well as changing the HA repeat unit which serves as a recognition unit by HA-binders.

In recent years, researchers have looked at more dynamic/reversible crosslinking systems, as they have the ability to re-assemble over time and reform after breaking of the intermolecular forces, conferring self-healing properties. The most famous example of a dynamic system is the use of cyclodextrin (Cd) and adamantane (Ada) for host-guest interactions. Cd and Ada have been conjugated to HA to form self-assembling hydrogels [12-13] that can be used for 3D printing[14] as well as a drug delivery vehicles[15]. Whilst these systems are dynamic, they still require the modification of HA.

An alternative approach consists in producing supramolecular HA biomaterials using peptides and pure intermolecular forces without covalent crosslinking. This ensures HA is in its native form with its intrinsic physical and biochemical properties retained. This approach also does not require the use of harsh or toxic reagents used for the chemical modifications. Within the HABPs, the sequences of the binding domain have been determined (Table 1.2). A pattern is evident in the natural HA-binding sequences, following the $B(X_7)B$ design, where B is a basic residue and X is a non-acidic residue, with at least one of the X amino acids being basic. Fundamentally, these peptides work through charge-charge interactions between the positive charge of the basic residues and the negative carboxylates of HA at physiological pH. An early example of the use of a polysaccharide and peptide can be seen from the interaction of heparin and with a positively charged heparin-binding peptide (LRKKLGKA) included into a s structure[16-17]. Examples of HA-peptide systems can be taken from the Stevens[18] and Bryant[19] groups who have used sequences taken from the binding site of HABPs in order to build biomaterials which can interact through intermolecular forces with HA. As an alternative to the use of sequences derived from natural proteins, phage display offers the possibility to identify new sequences through panning on the target of interest (Scheme 1.20). Pep-1[20] is a 12-mer peptide (GAHWNFQALTVR) discovered by phage display in 2000 with binding affinity to HA. Whilst Pep-1 does not conform to the $B(X_7)B$ design, it has one of the highest affinities for HA with a $K_D = 1.64$ µM and will compete with other HABPs. Since its discovery and demonstrated binding, work has been undertaken to utilise Pep-1 to monitor the localisation of HA[21-22], to reduce inflammatory responses caused by HA[23-24] and inhibit the HA binding to its receptors[25-27] such as CD44 and toll-like receptor (TLR). By inhibiting HA binding to receptors, the role of HA on cell signalling can be studied. Diseases have been shown to utilise HA, as patients with conditions such as lung fibrosis, asthma and osteoarthritis have abnormal levels of HA[28]. HA based biomaterials, therefore, could

lead to a potential use as probes or therapeutics to combat these diseases. By understanding the role of HA in these diseases we can begin to treat them. For this reason HA is being used to form hydrogels and drug delivery vehicles[29].

In this chapter, we have looked into the formation of new supramolecular biomaterials based on HA and different HABPep, such as Pep-1 and others taken from the link protein and CD44. These peptides were synthesised and characterised using their native sequences before testing their SAs with HA of varying sizes. In the second half of the chapter, the work discusses how the peptides were modified to form PAs a self-assembling design pioneered by the Stupp group[30-32] (Figure 1.19).

3.2. Results and Discussion

3.2.1. Unmodified HA-Binding Peptides

3.2.1.1. Synthesis and Characterisation

The HABPeps were synthesised by SPPS and purified by High-Performance Liquid Chromatography (HPLC) coupled to Electrospray Ionisation Mass Spectroscopy (ESI-MS). The peptide sequences taken from natural proteins, i.e. the Link Protein (HABPep-1) and CD44 (HABPep-2) were acetylated at the N-terminus, whilst Pep-1 (HABPep-3) was synthesised to bear a free amine at the N-terminus (Figure 3.2). This was due to the N-terminus on the phage being displayed to HA during the panning experiments, whilst the sequences taken from the natural sources are within a protein sequence and the N-terminus is capped by the neighbouring amino acid, therefore not available to bind.
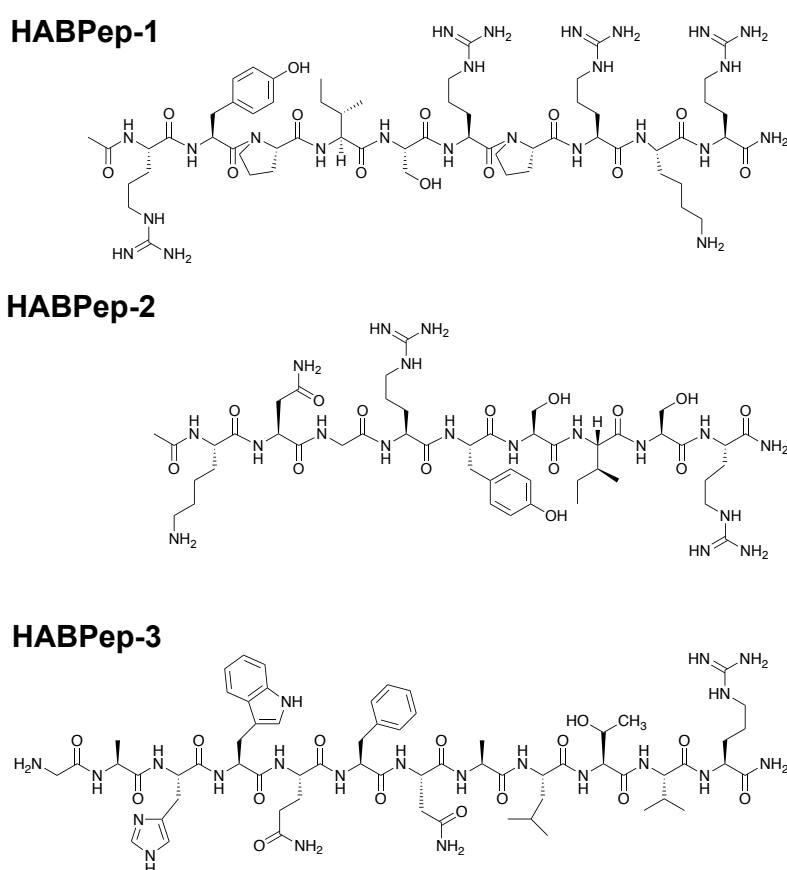
Figure 3.2. Chemical structures of the native HABPeps derived from natural HABPs (HABPep-1, HABPep-2) and from phage display (HABPep-3).

The secondary structure of the peptides can be deduced by circular dichroism (CD). CD uses circular polarised light through the sample and measures the change in angle of the outputted polarised light given by the ellipticity parameter. Proteins and peptides can display different secondary structures, such as a random coil, β-sheets and α-helices. The peptides were analysed at 0.01 mM and at different pHs to see the effect of charge on the peptide's conformation (Figure 3.3). These peptides possess several residues which can be charged (e.g. lysine, histidine and arginine).
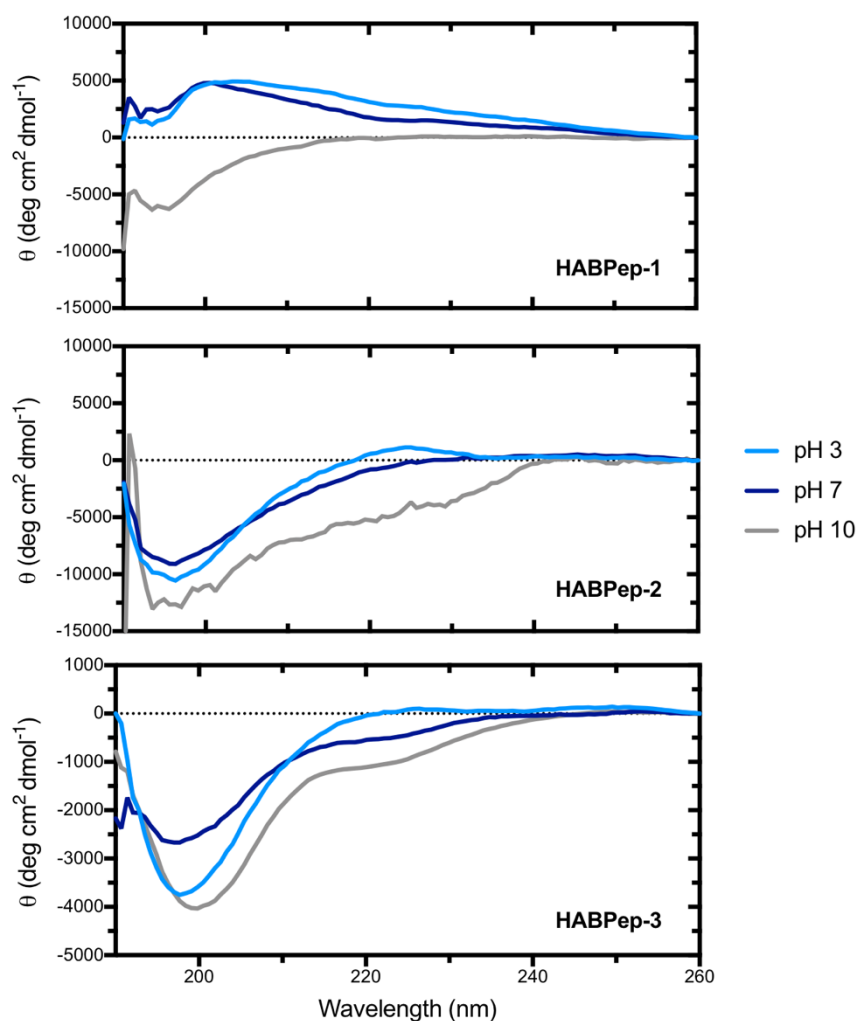
Figure 3.3. CD spectra of HABPep-1, 2 & 3 at pH 3 (light blue), 7 (blue) and 10 (grey) at 110 μM

The CD spectra of HABPep-2 and HABPep-3 show random coil behaviour at all pHs, due to the minima seen at between 205 – 195 nm. HABPep-1 spectra display random coil at pH<10 which is a transition to a β-sheets at pH>10. This is due to the minimum coming at 195 nm but a peak appearing at 201 nm. HABPep-1 is a highly charged peptide, with 50% of the residues being basic residues (4 arginines and 1 lysine). Using zeta-potential (ζ-potential) to measure the molecular charge in solution (Figure 3.4), it becomes apparent that at the lower pHs the molecules have a higher positive ζ-

potential. This increase in charge will affect the secondary structure of the peptide due to charge-charge repulsion.
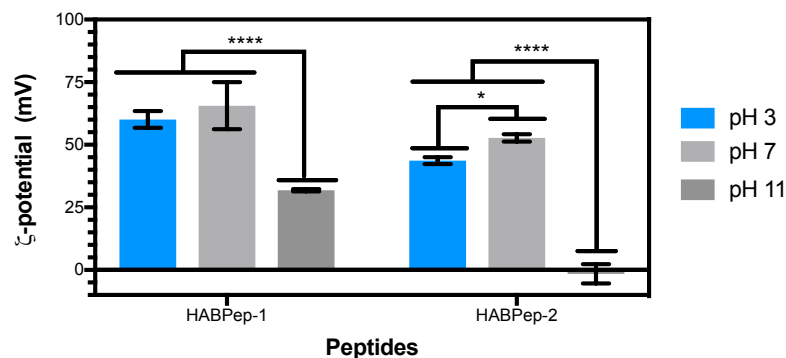
Figure 3.4. ζ-potential of native HABPep-1 and HABPep-2 at various pHs. Analysed by two-way ANOVA analysis, where * significant at $P < 0.0332$, ** significant at $P < 0.0021$, *** significant at $P < 0.0002$ and **** significant at $P < 0.0001$.

The ζ-potential also shows that HABPep-2 has significant charge between neutral pH and pH 3 and increasing the pH to 10 results in a substantial drop in charge. HABPep-2 has an estimated isoelectric point (pI) of 12.5, indicating that at pH closer to the pI the amine groups will become unprotonated (neutral).

3.2.1.2. Self-assembly with HA

The peptides were screened against a variety of HA molecular sizes to test their ability to form self-assembled structures. When mixing HABPep-1 and HABPep-2 with HA no structures was observed, whereas HABPep-3 lead to the formation of a membrane with HA (Figure 3.5).

The membranes formed were imaged by scanning electron microscopy (SEM) to give details on the microstructure formed. From the SEM images, it is possible to observe that the surface topology of these membranes can be tuned depending on the HA to HABPep-3 weight percentage ratio (Figure 3.6). The SEM images show that whilst maintaining a constant weight percentage, there is an increase in density of the fibres on increasing the HA molecular weight; this might be a result of the long HA strands being linked together by HABPep-3. The topology caused by tuning the percentage and size of HA gave membranes with different physical characteristic. These differing physical characteristics will influence cell attachment and spreading.
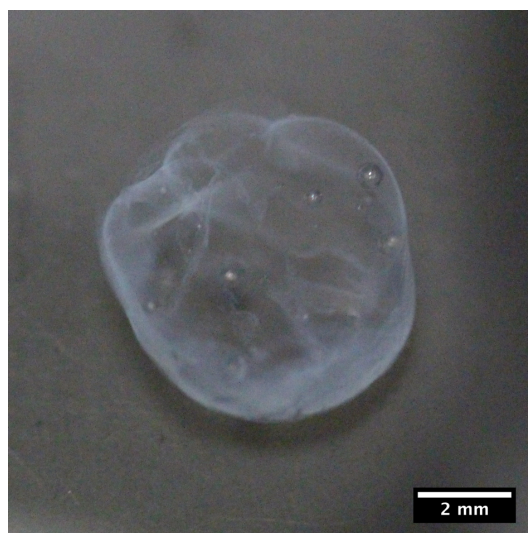
Figure 3.5 Photography of the membrane formed when combining 700 kDa HA 1% with 20 mM HABPep-3.
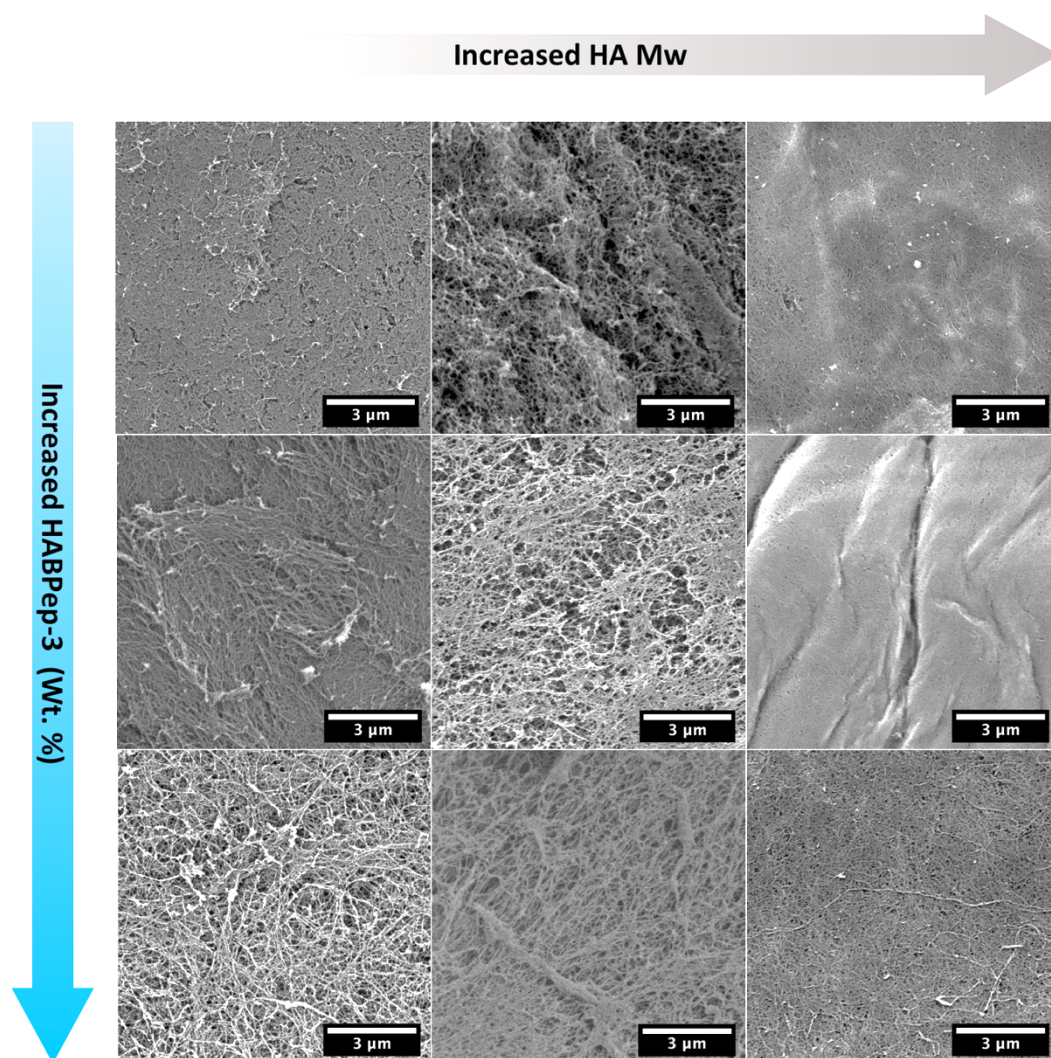
Figure 3.6. SEM images of the surface of complexes obtained by combining different concentrations of HABPep-3 (wt%), 1% (top), 2% (middle) and 3% (bottom) with HA of various MWs: 60, 200 & 700 kDa at 1% (.wt%) (left to right).

The inverse is seen as the wt% of HABPep-3 is increased. By increasing the HABPep-3 concentration, the peptide provides more interaction sites for HA, because of the change in the surface. Changing the concentration of HABPep-3 leads to the formation of aggregates in solution. This aggregation can be measured using Nile Red as a probe dye. In aqueous environments, Nile Red exhibits low fluorescence. However, upon incorporation into a hydrophobic pocket, Nile Red blue shifts to a lower wavelength and the fluorescence intensity increases linearly with increasing concentration. The concentration at which the peptide aggregates in solution is known as the critical aggregation concentration (CAC). Using the Nile Red assay to probe the HABPep-3, there is a clear aggregation at 6.7×10^{-5} M (Figure 3.7).
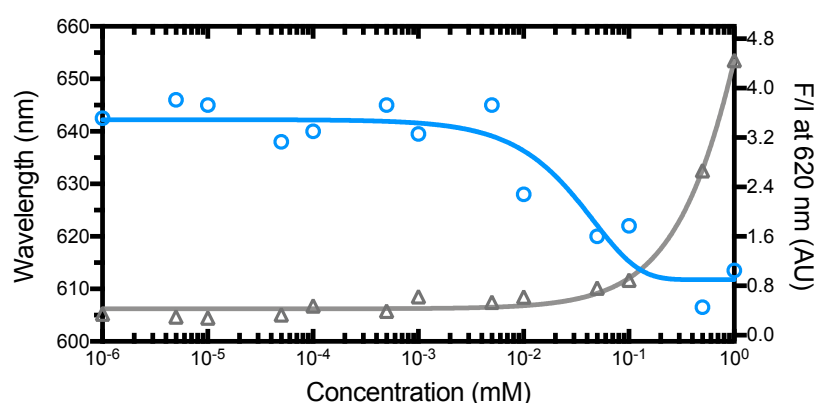
Figure 3.7. Nile Red assay of HABPep-3 with fluorescence maxima (blue) and fluorescence intensity (grey) at 620 nm at pH 7.

The aggregation of HABPep-3, as demonstrated by the CAC, produces a scaffold that HA can bind upon to creating more intricate network leading to formation of a stable membrane (Figure 3.5). By comparison, HABPep-1 and HABPep-2 show no CAC point, this can be attributed to the high solubility of these peptides. HABPep-3 also bears a ζ-potential of 55.1 ± 4.1 mV, a higher charge than that of the other two peptides, whilst bearing less basic amino acid residues. Using transmission electron microscope (TEM) on HABPep-3 (Figure 3.8), the images show the formation of nanofibrous structures with an average cross-section of 47.9 ± 12.9 nm.

These short fibres show no morphological change upon the screening of charge by increasing the pH to 10. The HABPep-3 bares 2 residues with amine-containing side chains, arginine at the C-terminus and histidine at position 10, and an amine group at the N-terminus, giving a total charge of +3. The other residues in the sequence are highly hydrophobic. Within the hydrophobic core, the aromatic residues lead to the formation of pi-pi stacking. The CAC and hydrophobicity of the peptide, along with the TEM result, explain the high ζ-potential of the peptides. The TEM and

arrangement of the hydrophobic residues in peptide lead to arginine of HABPep-3 to be displayed on the exterior of the nanofibers. A surface of predominately arginine's will cause the high ζ-potential observed.

The nanofibrous structure and high positive charge seen in the HABPep-3, explains the formation of a stable membrane with the negatively charged HA. The SA of HABPep-1 and HABPep-2 with HA was also attempted. However, these did not form any stable structures. This is not due to a lack of binding of the peptides to HA, but due to the lack of stable SA structures formed by the HABPep-1 and HABPep-2 alone. Whilst the addition of the peptide to HA caused increased turbidity of the solutions, this faded over time, as the peptides diluted into the HA solutions.
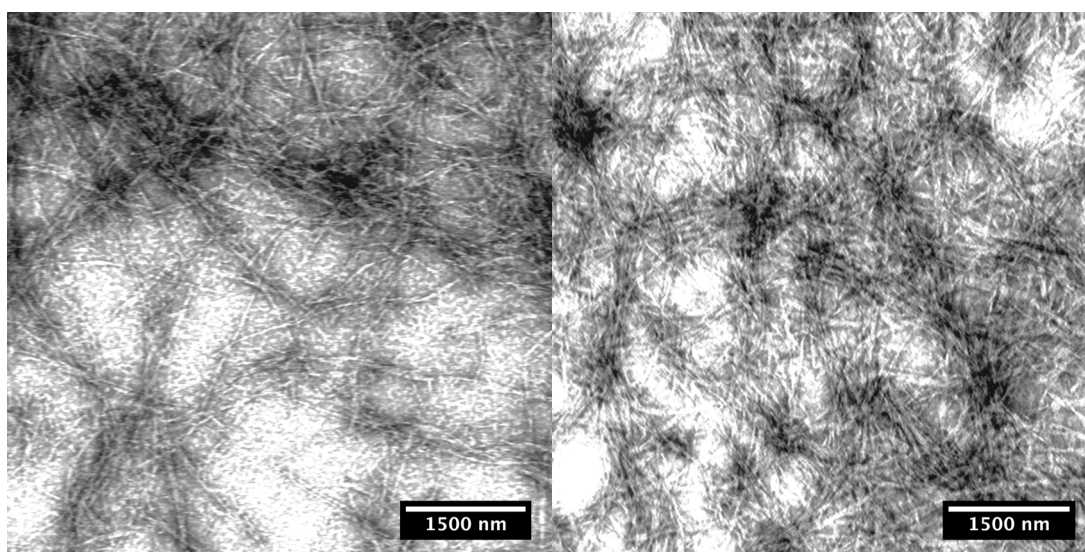
Figure 3.8. TEM images of HABPep-3 at 0.1 mM showing fibrous structures at pH 7 (left) and pH 10 (right)

The lack of stable HA complexes formed by HABPep-1 and HABPep-2 sequences, compared with HABPep-3, can be explained by the mode by each sequence was derived. HABPep-3 was discovered through phage display (12-mer attached to the phage surface) whilst HABPep-1 and HABPep-2 are sequences taken from a binding site in a much larger and more complex protein structure. By taking the sequence from the binding cavity of HABPs, the 3D environment is lost. A way to circumvent the lack of optimal presentation of these sequences for binding HA would be to incorporate these sequences into a self-assembling molecular platform for the multivalent display of the peptide. To form stable structures from HABPep-1 and HABPep-2, an amphiphilic design was implemented.

3.2.2. N-terminus Modifications of HA-Binding Peptides for Amphiphilic Design

3.2.2.1. Synthesis and Characterisation of Amphiphiles

With the lack of self-assembly with HA of both the HABPep-1 and HABPep-2 sequences, the N-terminus was modified to possess additional domains able to drive their controlled SA. This amphiphilic design was incorporated to try and give these peptides a 3D structure. By displaying the binding epitopes of HABPep-1 and HABPep-2 across the surface of a micelle or a fibre, the HA binding sequence can interact multiple time with HA to create stable a self-assembly. The PA design approach was utilised, but, due to the high solubility of HABPep-1 and HABPep-2, the charged domain was deemed unnecessary. Therefore, this portion of the PA design was not included in the design whilst the C_{16} and the β-sheet domain was included to create HABPA-1 & HABPA-2 based on HABPep-1 & HABPep-2, respectively (Figure 3.9).
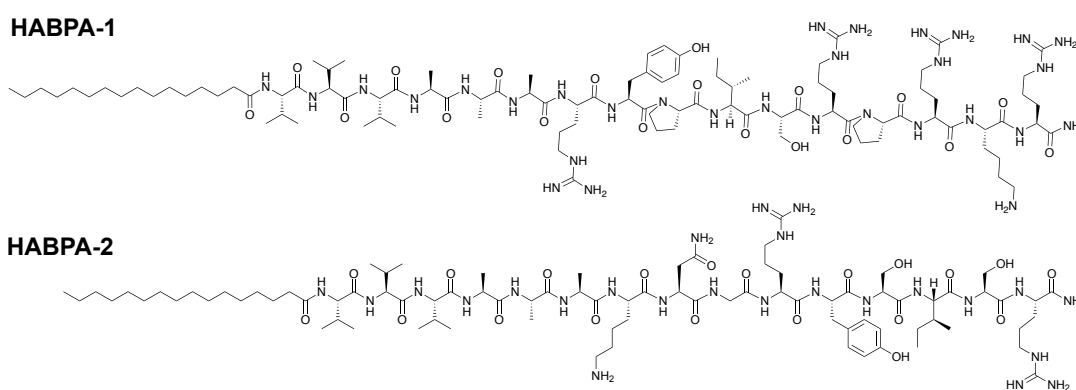
HABPA-1

HABPA-2

Figure 3.9. The PA structures of HABPA-1 and HABPA-2 based on HABPep-1 and HABPep-2 respectively.

Once synthesised and purified by HPLC, with conformation by ESI-MS, the PAs were analysed for their secondary structure by CD (Figure 3.10). HABPA-1 showed a random coil at all pHs; at lower pHs, this can be explained by the charge on the HA-binding sequence which has 5 basic residues, including 4 at the head of the peptide. At higher pHs, the charge of these residues will become neutral, but HABPA-1 still presents random coil conformation suggesting sterics between the amino acid residues are playing a role in preventing the formation of a defined secondary structure.

Whilst the peptide contains the V_3A_3 sequence, known to form β-sheets, the sequence contains two prolines and one serine which have a high propensity for β-turn, disturbing the formation of stable β-sheets. Compared to the sequence of HABPep-1, HABPep-2 has only 3 charged residues, but these are evenly spread throughout the 9 mer of the binding sequence. This reduction in charge and size of the overall peptide,

leads to hydrophobic residues within the β-sheet domain to be the dominating factor on the secondary structure. The CD spectra for HABPA-2 display β-sheet at all pHs.
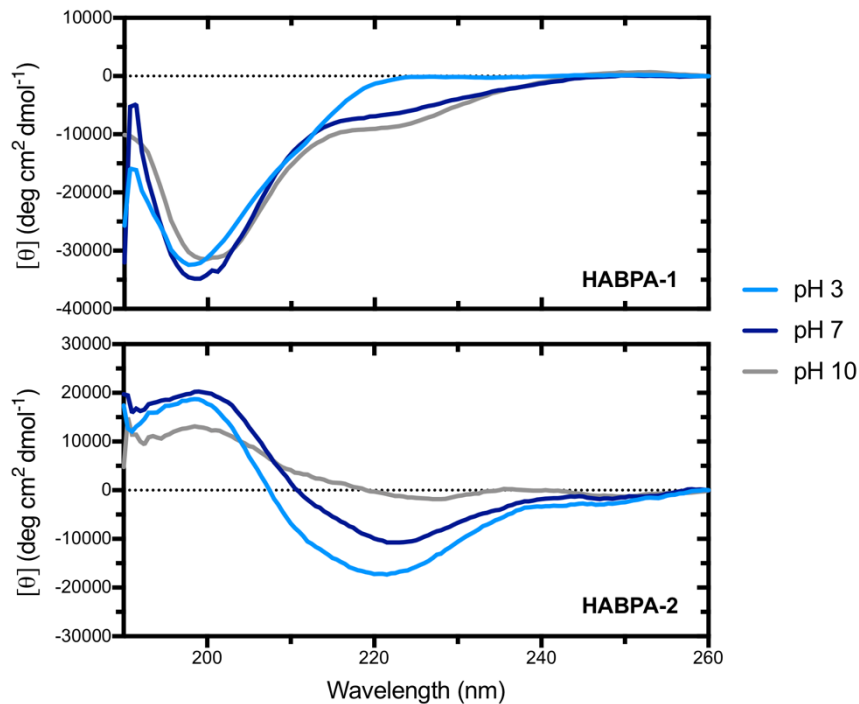
Figure 3.10. CD spectra of HABPA-1 & 2 at pH 3 (light blue), 7 (blue) and 10 (grey) at 110 μM

Using Nile Red, the CAC of HABPA-1 (Figure 3.11) was determined to be 5.4×10^{-2} mM. HABPA-1 displayed a dramatic increase in fluorescence after 5×10^{-3} mM, with a blue shift from 646 to 618 nm indicative of the formation of an aggregate. By contrast, HABPA-2 showed no blue shift with a consistent peak maximum at 620 nm through all pH ranges, inferring any self-assembly was occurring below 1 nM. The comparisons in structures and charge location within the two PAs showed that electrostatic repulsion caused an increase of the CAC for HABPA-1 compared to HABPA-2.

ζ-potential can be measured to estimate the surface charge of the aggregates (Figure 3.12). HABPA-1 and HABPA-2, as well as their parent peptide sequences of HABPep-1 and HABPep-2, all show a positive ζ-potential, due to the number of arginine and lysine residues within the sequence.
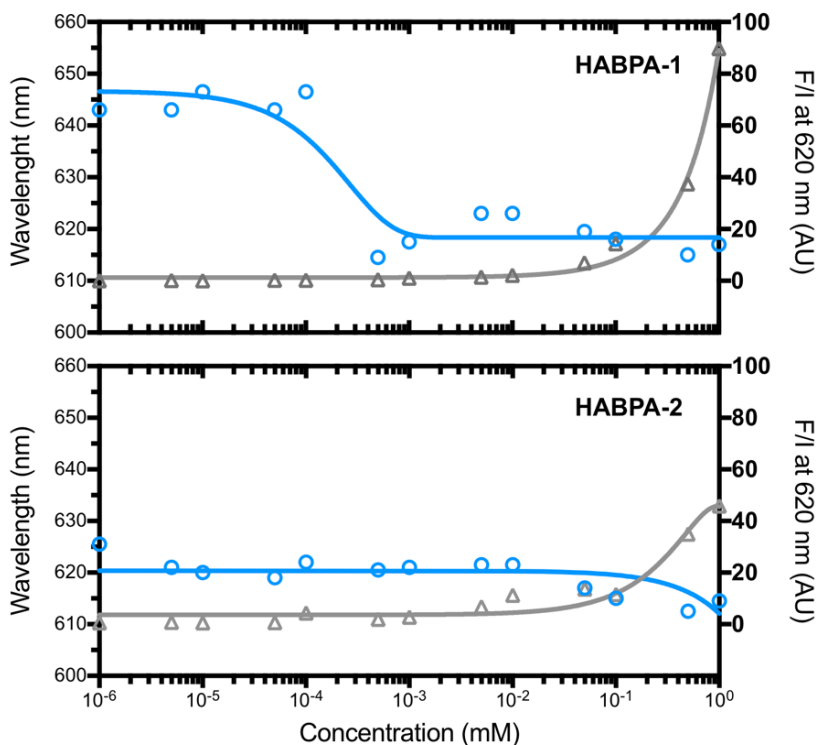
Figure 3.11. Nile Red assay of HABPA-1 & 2 with fluorescence maxima (blue) and fluorescence intensity (grey) at 620 nm at pH 7.

What is evident from the ζ-potential is that due to the amphiphilic design, there is a significant increase in surface charge. This increase in ζ-potential ($> +30$ mV) infers that stable aggregates have been formed. The data also shows a significance ($P < 0.0001$) between the charge on the surface of the two PAs. Again, this is due to the higher number of charged residues on the binding sequences of HABPep-1 compared to HABPep-2 on the PAs.
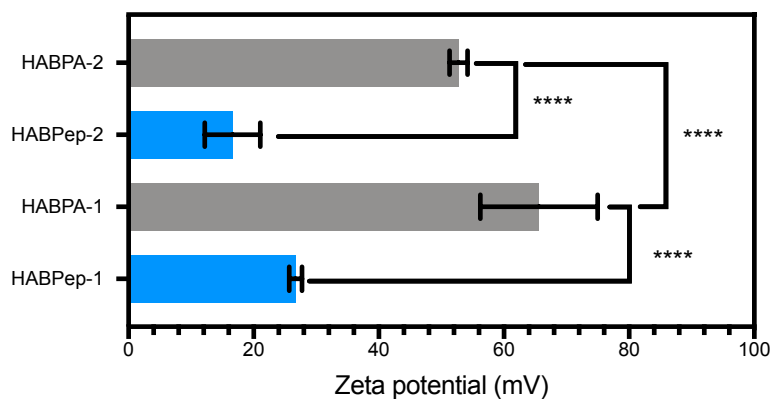
Figure 3.12. ξ-potential for HABPA-1 and HABPA-2 and comparison to the unmodified/native sequences (HABPep-1 and HABPep-2). Analysed by two-way ANOVA analysis, where * significant at $P < 0.0332$, ** significant at $P < 0.0021$, *** significant at $P < 0.0002$ and **** significant at $P < 0.0001$.

Using the information obtained from the Nile Red assay and ζ-potential, TEM images could be captured at concentrations above the CAC and by varying the pH to adjust the charge. At neutral pH, HABPA-1 sequence showed predominantly micelle structures as well as some short fibrous structures. Whilst the incorporation of C_{16} and V_3A_3 favour the formation of fibres over micelles, the charge-charge repulsion on the head of the PA will negate this effect[33-35]. Increasing the pH from 7 to 10, the charge-charge repulsion is cancelled due to charge screening on the basic residues of arginine (pKa = 12.5) and lysine (pKa = 10.5)[36], leading to the formation of long fibres as the predominant structure.
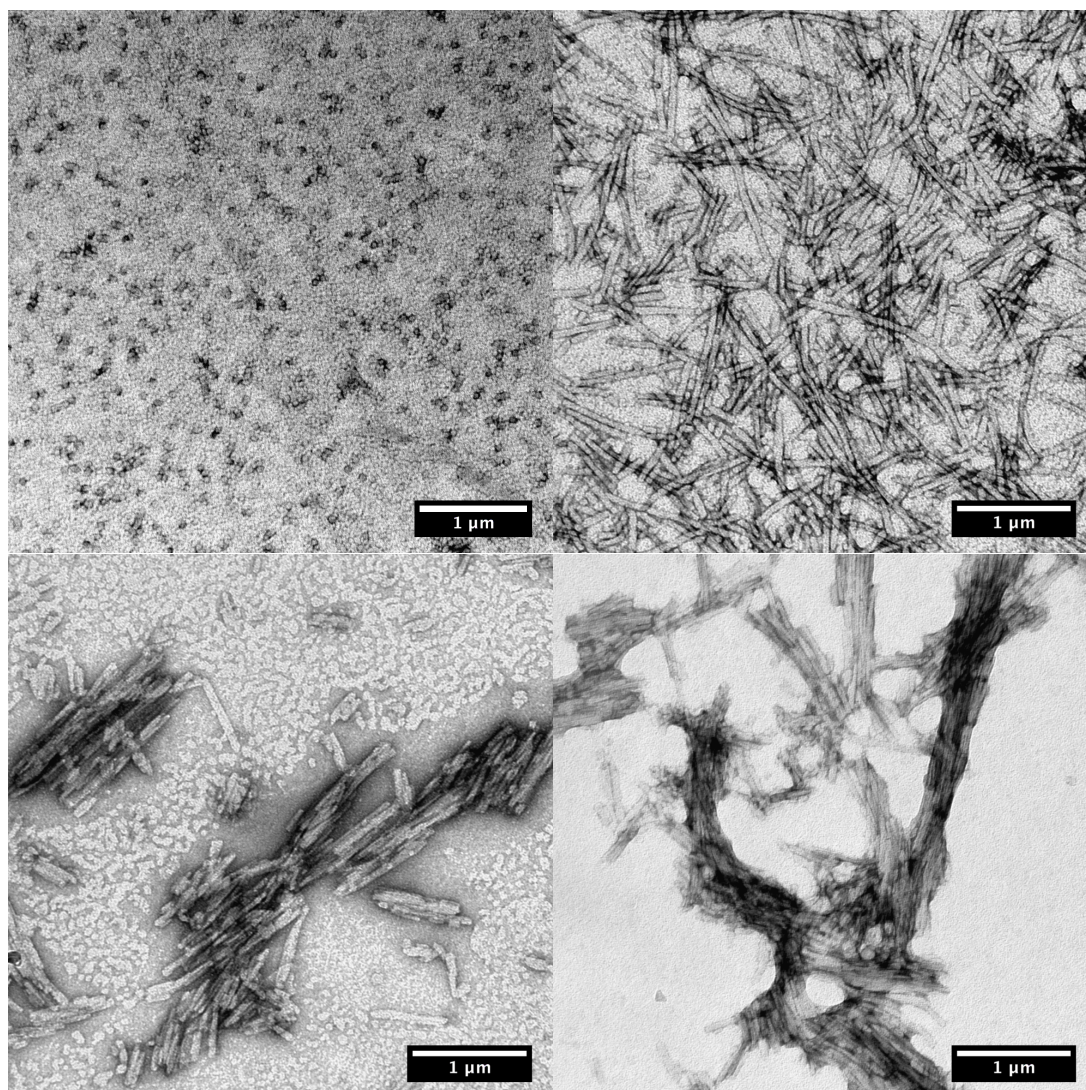
Figure 3.13. TEM images of the nanostructures formed by HABPA-1 (top) and HABPA-2 (bottom) at 0.1 mM and pH 7 (left) and pH 10 (right)

In comparison, HABPA-2 showed small fibres and micelles at pH 7, following the trends seen in the literature when using the C_{16} and V_3A_3 domains. However, when increasing the pH to 10, large bundles of fibres are formed potentially driven by

hydrogen bonding between the serine's, arginine's, lysine and the tyrosine, once the charge has been screened, these residues can interact through hydrogen bonding. At pH 7 the side chains of the basic residues are positively charged causing repulsion between adjacent PAs inhibiting long fibre self-assembly.

From this data, it can be seen that charge plays a large role in the SA of these two PAs as the difference seen between the two in both secondary structures and the nanostructures formed by the PAs (Table 3.1).

Table 3.1. Characterisation of HABPAs from CD, TEM and ζ-potential

PA	CD	pH	Morphology	Width [a] (nm)	Length [a] (nm)	ζ-Potential (mV)
HABPA-1	RC at all pHs	7	Micelle	58 ± 8	-	65.6 ± 9.4
		10	Fibre	69 ± 7	1240 ± 160	-
HABPA-2	β at all pHs	7	Short Fibres	70 ± 11	570 ± 180	52.7 ± 1.4
		10	Short Fibres	24 ± 4	197 ± 54	-

RC = Random Coil, β = Beta Sheet. [a] average measurement acquired using ImageJ analysis.

N-terminus modifications was also undertaken on HABPep-3. Whilst HABPep-3 was able to form complexes with HA, this was not controllable due to the random interaction of the peptide rather than through its controlled presentation. In the initial publication reporting the discovery of Pep-1 in 2000, alanine scanning studies were performed which showed that the hydrophobic residues W, F, A, L, T and V, as well as G and Q, were essential for binding, whilst the charged residues H and R, as well as N, where non-essential for binding (Figure 3.14). Since the core of HABPep-3 is highly hydrophobic, upon aggregation, these residues which are essential to interact with HA will be trapped in the core of the aggregates.
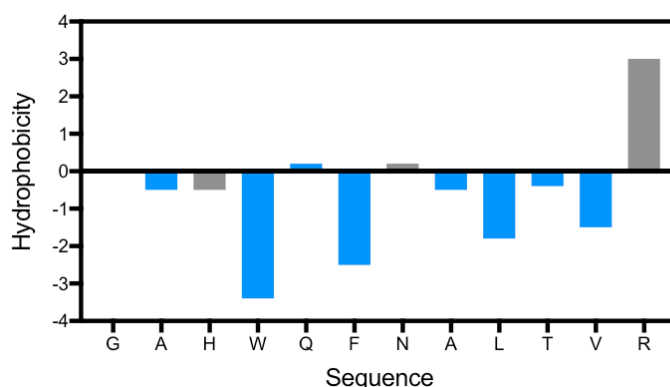
Figure 3.14. Hydrophobicity of individual amino acids in HABPep-3 according to the Hoop & Wood hydrophobicity, highlighting the essential (blue) and the non-essential (grey) residues for HA binding.

By designing a PA version of HABPep-3, the binding residues would be freed up to bind to HA in a more controlled manner. Due to the hydrophobicity of the Pep-1, the initial designs moved away from the use of V_3A_3 for the β-sheet segment, using $(VQ)_2$ instead. Glutamine (Q) has been shown to be β-sheet promotor, compared with alanine[37], as well as has lower hydrophobicity: -0.5 (A) and 0.2 (Q). For this reason, V_3A_3 was replaced with $(VQ)_2$ (Figure 3.15). Whilst SPPS was able to form HABPA-3, as shown by ESI (data not shown). The hydrophobicity of this HABPA-3 led to insolubility in water and therefore an inability to purify by HPLC.
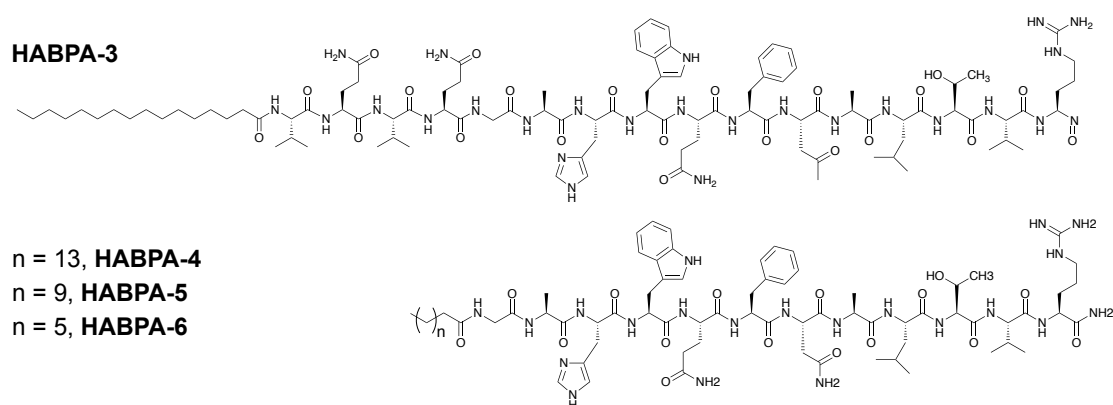
Figure 3.15. Amphiphilic design of HABPep-3 based PAs with use of a β-sheet forming domain (HABPA-3) and reduction in hydrophobicity by removal of the β-sheet forming domain (HABPA-4) and reduction the alkyl tail (HABPA-5, HABPA-6).

The minimum requirement for several PA designs is a hydrophobic alkyl tail and bioactive domains. To improve solubility, the β-sheet domain was removed, leaving the alkyl tail which was systematically shortened in an attempt to increase the solubility. Again, the SPPS showed no problem in the synthesis of these peptides (confirmed by ESI for the crude materials), but solubility still remained a challenge.

By looking at the manner in which the HABPep-3 is displayed by the phage, we can look at exploiting similar designs to replicate the mode the phage displays the peptide. On the phage (Figure 3.16), the peptide is displayed from the C-terminus rather than the N-terminus, so in fact, adding the modification to the N-terminus would cause the peptide to be displayed in the reverse orientation as to the phage. Furthermore, the peptide is anchored on the phage surface through a linker, known as the fusion linker, which is made up of 3 glycine residues, which spaces the peptide out from the phage to allow the 12-mer freedom to bind without sterics. With these two features in mind, the peptide modification moved from the N-terminus to the C-terminus.
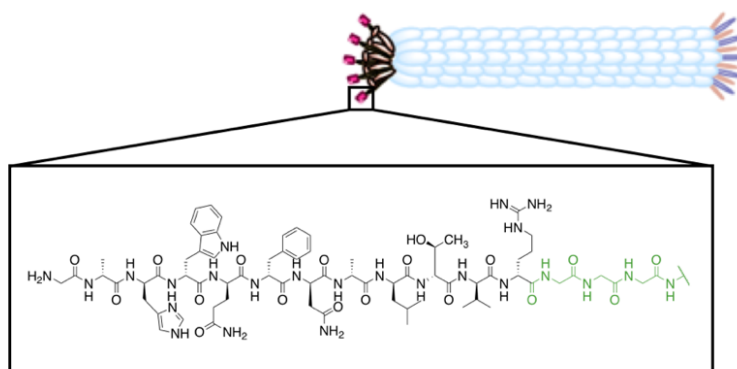
Figure 3.16. Cartoon of a phage showing the pendant peptide attached to the phage through the C-terminus by a fusion linker (green).

3.2.2.2. Self-assembly with HA

HA was added onto HABPA-1 leading to the formation of a membrane (Figure 3.17). Varying the HA size from 60 kDa to 700 kDa, a change in the morphology is observed under SEM (Figure 3.18). With low molecular weight HA, two distinct sides of the membrane are observed. One is highly fibrous, and the other is more uniform. In comparison, the longer HA produces two sides which show no distinct differences, both forming a fibrous network on the membrane's surface. The high viscosity of the large Mw HA solution allows it to sink into the PA solution, forming sac compared to the lighter, low Mw HA which forms a facial interaction with the PA. This facial interaction leads to two distinct sides in the SEM images of the 60 kDa HA and HABPA-1 example.
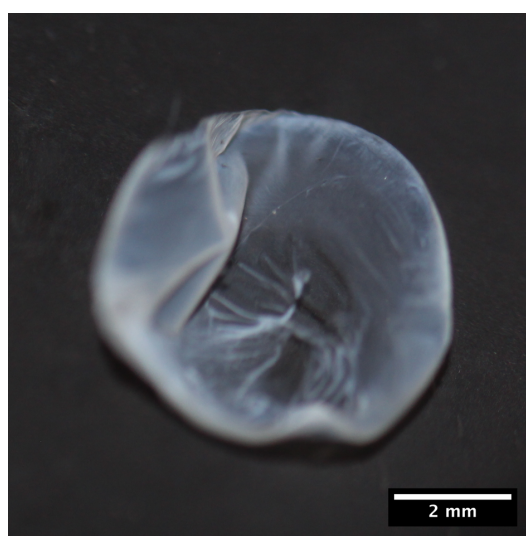
Figure 3.17. Photography of the membrane formed when combining 700 kDa HA 1% with HABPA-1 1% (wt.%).

Comparing the cross-sections of the membranes, the lower molecular weight produces a disorganised array of fibres. Using higher molecular weights, the fibres within the interior begin to align. Collagen is the primary structural element in connective tissues [38-39]. Collagen type 1 packs in fibrillar elements through SA, which produces fibres with directionality [40]. This alignment of the collagen fibres has been shown to determine the morphology and function of several cell types [41]. Alignment with a matrix has been shown to guide migration cells in morphogenesis, wound healing, and tissue regeneration [42-43]. The fibres seen in the membrane cross-section (Figure 3.18) resemble the bundles of collagen fibres. The formation of aligned fibres with HA, produces a biomimetic environment in which cells could grow and proliferate.

Compared to HABPA-1, HABPA-2 failed to form any assemblies with HA at any weight percentage or various HA molecular weights, whilst in the TEM HABPA-2 showed the ability to form defined nanofibers. These are short and carry less charge. These peptides follow the $B(X)_7B$ design of HABPs, with one of the X residues requiring to be another basic residue (B). However, on displaying the peptide as a PA, sterics will begin to be a factor. The residues closest to the alkyl tail will be difficult for a longer macromolecule such as HA to intercalate into the SA structure.

Figure 3.18. SEM images of the membranes formed with HABPA-1 1% (wt.%) comparing the effect of high and low molecular weight HA.

Two of HABPep-2's basic residues are buried into the structure of the PA, reducing the ability for HA to interact to those charged residues. Therefore, HABPA-1 and HABPA-2 are likely to bind through electrostatic interactions through the residues located at the surface of the PA. If we only consider that only the first 3 amino acids are presented to HA, due to steric of the remaining sequence, HABPep-1 has 3 basic residues at the surface whilst HABPep-3 only has 1. HABPep-2 sequence does not possess another basic residue until the 6th amino acid in the sequence. The ζ-potential shows both PAs with a high positive surface, HABPA-1 shows an increase in the ζ of +12.9 mV. This, coupled with the placement of the charged residues, allow HABPA-1 to form stable assemblies with HA but not HABPA-2.

3.2.3. PA design by C-terminus modifications

3.2.3.1. Synthesis and Characterisation of C-terminus modifications

HABPep-3 was modified at the C-terminus to include 4 domains[30]. This design includes the fusion protein linker of the triple glycine, a charged domain of two lysine's, the HA-binding sequence (HABPep-3) and the C_{16} alkyl tail (Figure 3.19). Whilst previous examples of PAs use the V_3A_3 sequence to provide the β-sheet forming domain[34], the N-terminus work highlighted HABPep-3 extremely low solubility. This block was removed following the example from the Chun Group[44].

Figure 3.19. Amphiphilic design of HABPA-7 with the incorporation of HABPep-3.

Compared with coupling onto the N-terminus, the C terminus presents additional synthetic challenges in conventional SPPS. The use of lysine protected with a 4–methyltrityl (Mtt) group can be inserted as the first amino acid. The side chain can be selectively deprotected with 4% TFA and 2.5% TIS in DCM followed by 5% DIEA in DCM to neutralise the remaining TFA. These mild conditions provide the removal of the Mtt group with minimal loss of lysine from the resin surface. The exposed epsilon amine can be easily confirmed qualitatively by the Kaiser test. This amine can be capped by a palmitic acid in order to attach the C_{16} at the C-terminus. Some examples in the literature produce the complete peptide sequence first and then cap

the Lys-(Mtt) with the alkyl tail at the end. However, because of the steric bulky and hydrophobic groups loaded on the resin, this was low yielding. Whilst "preloading" the C_{16} onto the resin before building the remainder of the peptide allows the C_{16} tail to be attached from which the peptide can be grown stepwise. The crude result of HABPA-7 synthesised by this approach showed dual peaks on the HPLC (Figure 3.20). Mass analysis of each peak showed the peptide with and without the lysine functionalisation. It was necessary to perform double deprotection and coupling of the Lys (Mtt).
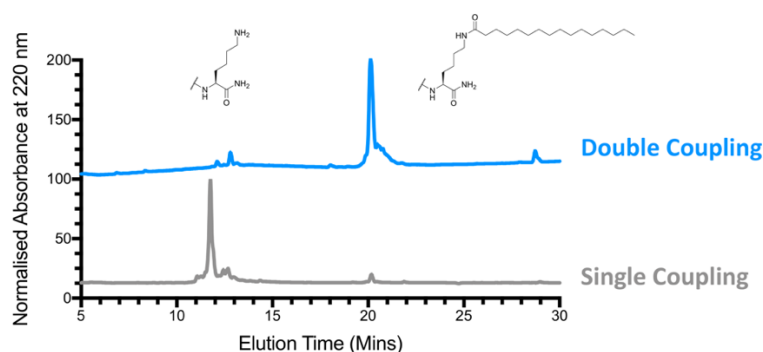
Figure 3.20. HPLC traces of crude of HABPA-7 showing the difference in conversion of the Lys (Mtt) by single or double coupling (offset by 100).

Despite the Kaiser test gives a qualitative analysis of the resin, the Mtt group is also heat sensitive, so it can give a false positive as the Kaiser test run at 120 °C; when double coupling of the C_{16} group was performed, the predominant peak is now the C_{16} coupled. Once purified by HPLC, the PA secondary structure was characterised by CD (Figure 3.21). The CD spectrum of HABPA-7 showed that at pH 3 the peptide behaved as a random coil, whilst at pH 7 and 10 it indicated β-sheet propensities.
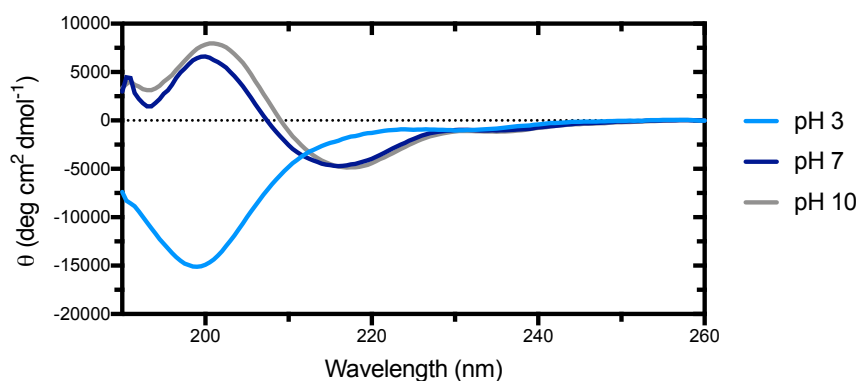
Figure 3.21. CD spectra of HABPep-7 at pH 3 (light blue), 7 (blue) and 10 (grey) at 110 µM

This result is expected as at acidic pH basic amino acids can be charged, including the histidine (pKa = 6.4). This would lead to mutual repulsion among PA molecules leading to a random coil conformation. In contrast, at basic pH, these charges are screened. The Nile Red assay (Figure 3.22) showed a CAC of 4.3×10^{-1} mM, which compared to HABPA-1 is two orders of magnitude higher, but within a similar magnitude to that of HABPep-3.
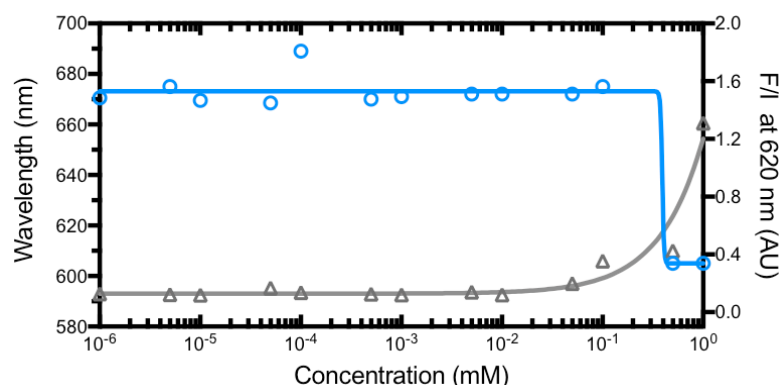
Figure 3.22. Nile Red assay of HABPA-7 with fluorescence maxima (blue) and fluorescence intensity (grey) at 620 nm at pH 7.

The TEM of the HABPA-7 (Figure 3.23) showed worm-like fibres, which was consistent at both pH 7 and 10. These fibres are significantly shorter than those of HABPep-3 (Figure 3.8); this might be caused by the amphiphilic design of HABPA-7 breaking up the aggregation of the HABPep-3 sequence. The addition of the V_3A_3 to the HABPA-7 sequence would increase the β-sheet propensity leading to the increased probability of elongated fibres, if soluble.
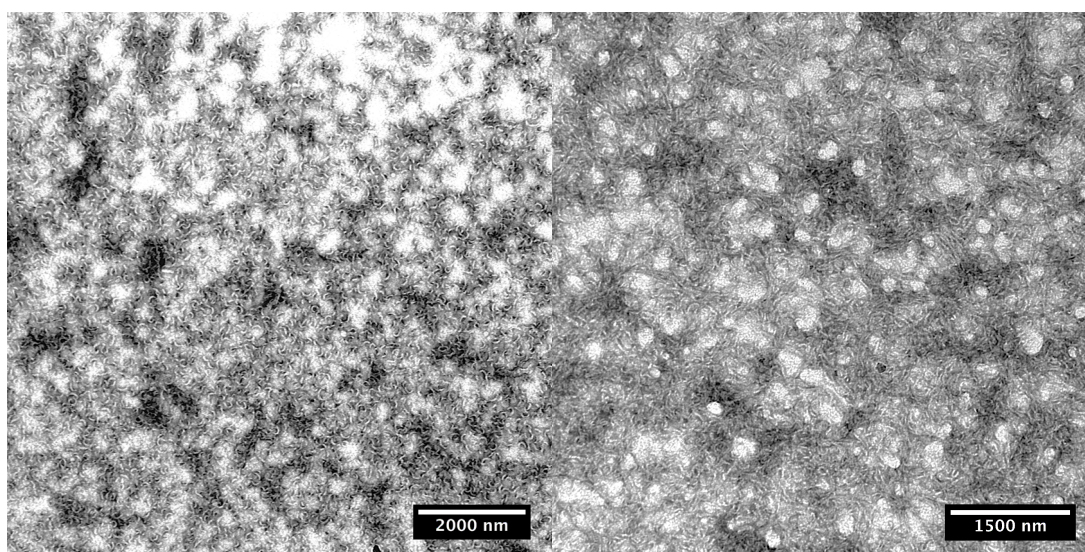
Figure 3.23. TEM image of HABPA-7 at 1 mM, pH 7 (left) and pH 11 (right).

3.2.3.2. Self-assembly of C-terminus PA with HA

When combining HABPA-7 with HA, on average thicker fibres are observed in the SEM of the membranes formed (Figure 3.24) compared with those of HABPep-3 at 125 nm ± 25 nm compared to 78 nm ± 12 nm (Figure 3.6), this might be due the difference in the self-assemblies seen in TEM. HABPA-7 forms shorter fibres with HABPep-3 being displayed on the exterior of the short nanofibers. These nanofibers therefore become more fibrous as there are more points on the HABPA-7 for the HA to interact with compared to HABPep-3. By displaying the HABPep-3 on the PA of HABPA-7 more of the essential amino acids in the HABPep-3 sequence are exposed to interact with HA.
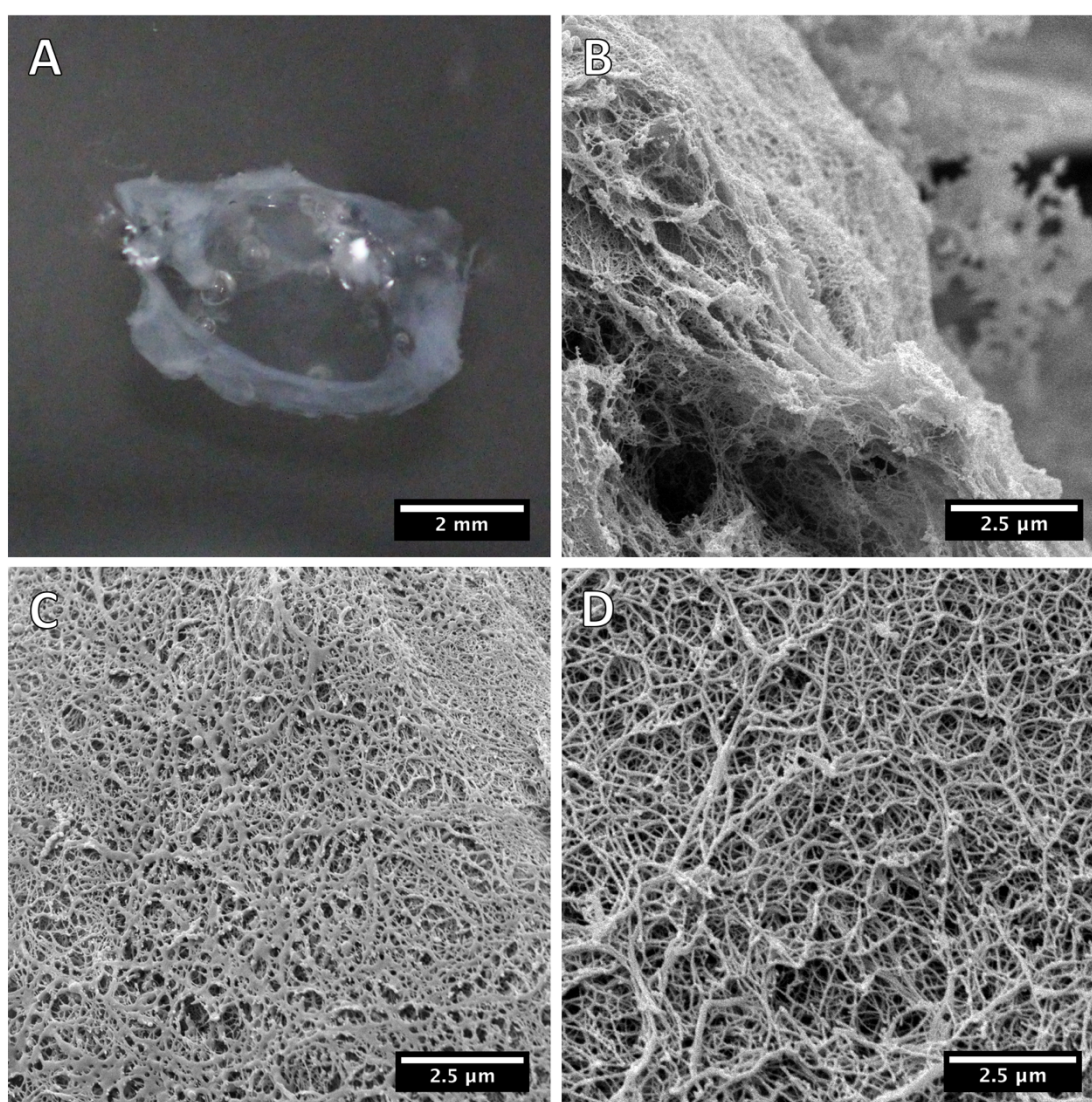
Figure 3.24. Photography of the membrane formed when combining 700 kDa HA 2% with 20 mM HABPA-7 (A) and SEM images of the membrane showing: cross-section (B), surface (C) and the opposing surface (D).

Whilst HABPA-7 with HA lead to a more fibrous material shown by the SEM images, HABPA-7 has a ζ-Potential of +58 mV similar to that of HABPep-3. This suggests that HABPep-3 sequences are aggregating on the surface of the aggregates formed (Scheme 3.1). The free N-terminus will be displayed on the surface of the nanofibers, but the histidine and arginine are buried in the aggregate within the self-assembly. Changing the pH showed no dramatic nanostructure variation in TEM when compared to HABPA-1 and HABPA-2 (Figure 3.13). This is caused by the difference in sequences with HABPA-1 and HABPA-2 possessing several basic residues towards the surface of the PA structure. To utilise the full HABPep-3 sequence in a similar manner to the phage, the intramolecular interactions between the HABPep-3 sequence in the HABPA-7 require separation.
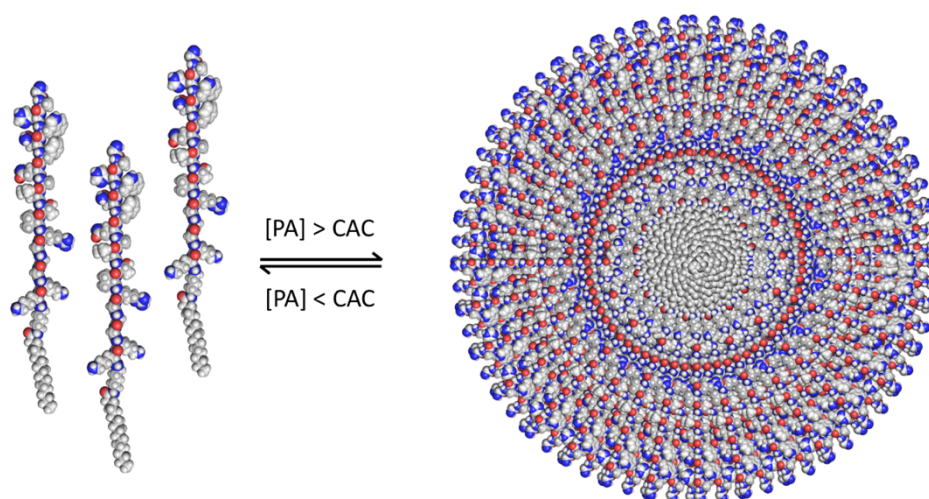
Scheme 3.1. Schematic representation of HABPA-7 as isolated PA monomers below the CAC and a cross-section of the self-assembly formed above the CAC.[45]

3.2.4. Peptide Amphiphile Co-assembly

To space out the HABPep-3 sequence, to allow for improved interactions with HA, a complementary PA was designed. This PA can interact with HABPA-7 through non-covalent interactions, such as electrostatics[35, 46-47] and opposing charge[48], as well as through the formation of chemical bonds such disulphide bridges[44] to allow their co-assembly. Studies have also used this dual system to look into the dynamics of self-assembly[49]; these dual co-assembly systems also allow control over theircytotoxicity[50]. This idea of a complementary peptide as a '*diluent PA*' or '*control*

PA' has been previously shown to control the percentage of a bioactive epitope on the surface of a PA[51-53].

3.2.4.1. Synthesis and Characterisation of Diluent Peptide Amphiphile

The aim of using a diluent peptide (Dil-PA) was to reduce the aggregation on the surface of HABPA-7 caused by hydrophobic residues in HABPep-3 (Scheme 3.2). The Dil-PA was designed to incorporate an opposing charge domain of glutamic acids to interact with the lysines of HABPA-7. The Dil-PA was synthesised through standard SPPS but reversed the sequence in comparison to HABPA-7. This is due to the simplicity at which the peptide can be synthesised compared to the Lys (Mtt) approach. However, by reversing the sequence, the PA will still align with the complementary domains of the HABPA-7.
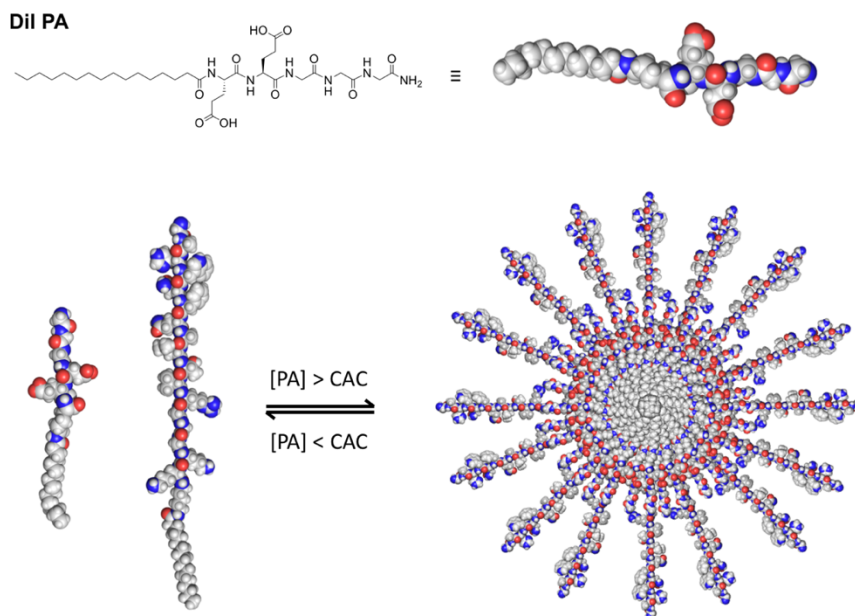
Scheme 3.2. Amphiphilic design of Dil-PA (top) and the co-assembly of HABPA-7 with Dil-PA monomers below the CAC and a cross-section of the self-assembly formed above the CAC.

The Dil-PA peptide was purified by HPLC and mass confirmed by ESI-MS. The Dil-PA showed random coil at pH 7 and 10, however, at pH 3 the CD showed weak β-sheet propensity (Figure 3.25A). At neutral pH, the Dil-PA has a ξ-potential of -38 mV, whereas at pH 3 the two glutamic acids (pKa = 4.3) of the PA are protonated causing screening of charge repulsion, leading to the conformation change. The Dil-PA had a much lower CAC (Figure 3.25B) in comparison to that of HABPA-7, with a CAC of 2.2×10^{-3} mM, two orders of magnitude lower. However, above 0.1 mM,

whilst the fluorescence increased rapidly, the peptide started to crash out of solution causing the fluorescence output to become inconsistent. At this high concentration, aggregation led to precipitation and therefore data had to be discarded.
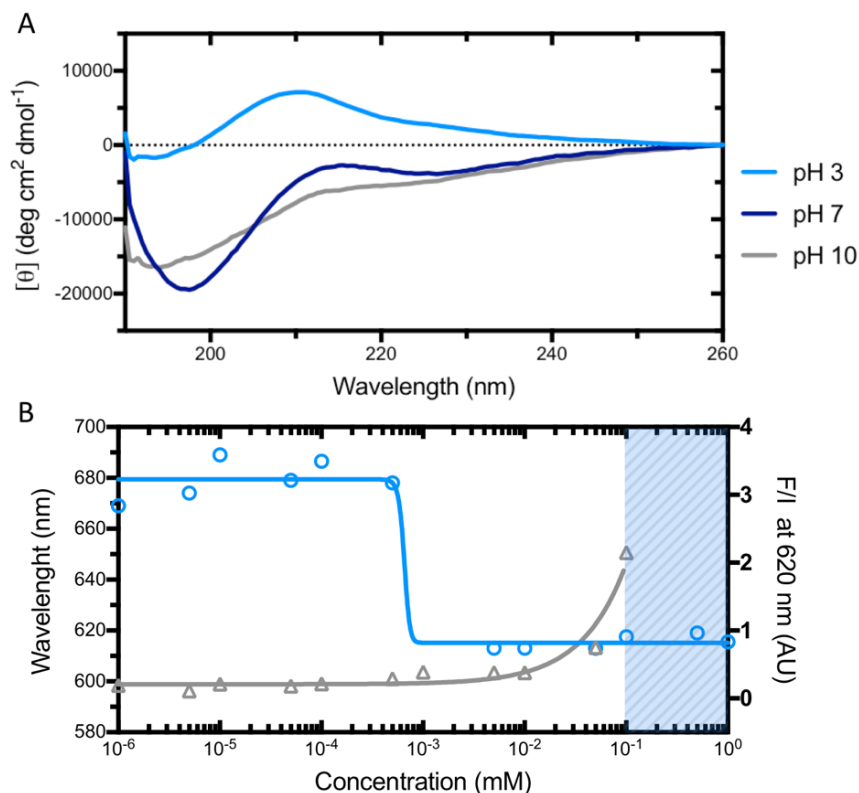
Figure 3.25. CD spectra (A) of Dil-PA at pH 3 (light blue), 7 (blue) and 10 (grey) at 110 μM and Nile Red assay (B) with fluorescence maxima (blue) and fluorescence intensity (grey) at 620 nm at pH 7.

Looking at the peptide under TEM (Figure 3.26) at 0.1 mM, aggregation of fibres are seen by the darker areas on the TEM as the fibres bundled together. The Dil-PA showed very elongated nanostructures with an average width of 136 nm ± 22 nm. These nanostructures closely resemble assemblies observed by the Stupp[54-55] group using $C_{16}(VE)_2$ PA which formed nanobelt structures, which had a monodisperse width of 150 nm.
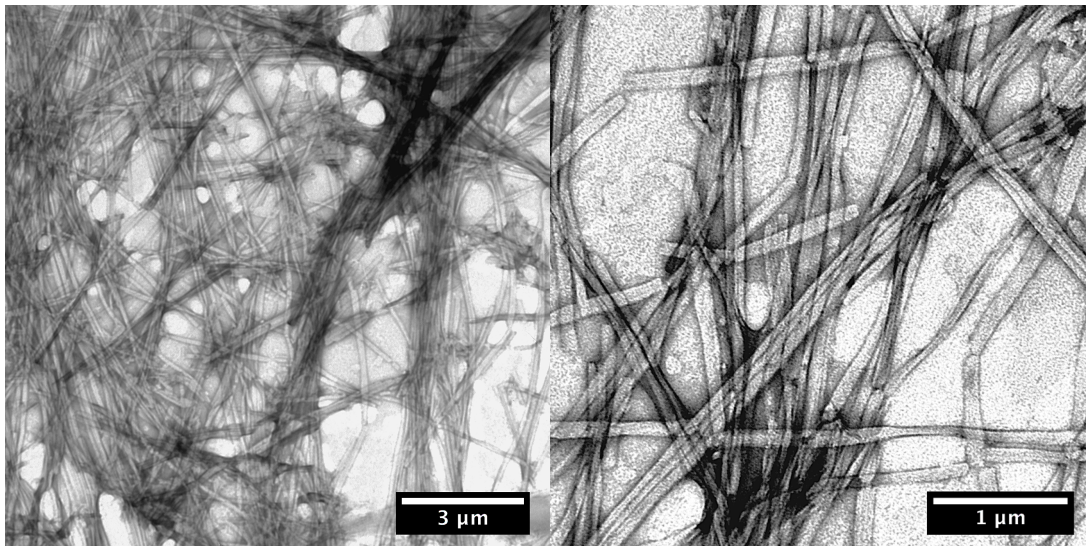
Figure 3.26. TEM images of the nanostructures formed by Dil-PA at 0.1 mM and pH 7 showing a high density of elongated structures.

3.2.4.2. Co-assembly Study

The co-assembly of the two PAs was monitored by combining different methods. The two PAs were mixed in a 50:50 molar ratio. If the co-assembled system would show two distinct blue shifts, then it could be inferred that the two PAs were assembling separately. Also, due to the solution having a 50:50 ratio of both PAs, if the PAs were self-assembling individually, then the CAC of HABPA-7 would be unmeasurable on the concentration scale, whilst the Dil PA would show a shift in 10^{-1} to 10^{-2} mM range. The mixture has a single CAC of 3.6×10^{-4} mM. The single blue shift at 7.5×10^{-4} mM infers co-assembly of the PAs (Figure 3.27).
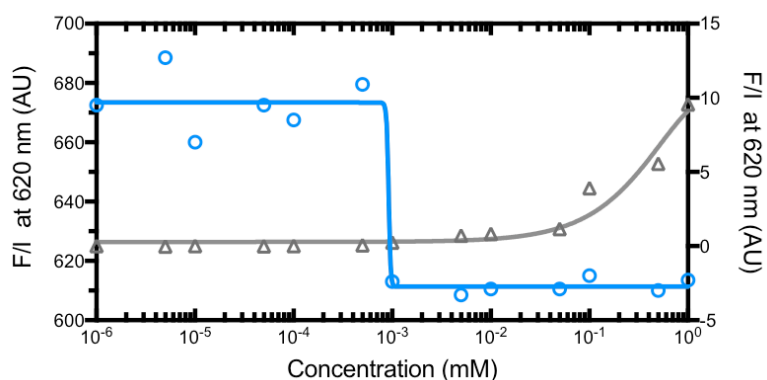
Figure 3.27. Nile Red assay of the mixed PA system at a 50:50 ratio with fluorescence maxima (blue) and fluorescence intensity (grey) at 620 nm at pH 7.

The mixture of PAs at 50:50 ratio acts synergistically to help solubilise each other, due to the absence of precipitation at higher concentrations of the Dil-PA. This is due to the positively charged domain of the lysine residues on HABPA-7, interacting with the negative charge of the carboxylates of the glutamic acid residues on Dil-PA. Therefore, the CAC analysis suggests the successful co-assembly of HABPA-7 with Dil-PA.

CD analysis of individual PAs at lower concentrations showed β-sheet for Dil PA whilst HABPA-7 showed a random coil. When changing the ratio of the two PAs in the co-assembling system, the CD showed a shift in the propensity from random coil to β-sheet, as the percentage of the Dil-PA was increased (Figure 3.28). The dotted lines represent the simulated CD spectra by summing the individual PA's CD signal at the mixture percentages. If the CD of the co-assembled systems was simply the sum of the two individual CD spectra at the various ratios, then CD trace would overlay with those of the simulated. The fact that the observed CD signal does not coincide, we can infer their co-assembly rather than individual assemblies. The CD also shows the highest β-sheet maxima for HABPA-7 and Dil PA at a ratio of 20:80, almost double that of 40:60; this indicates the co-assembly system is more ordered at this ratio. The peak then decays back down in intensity when scanning the 0:100 ratio.
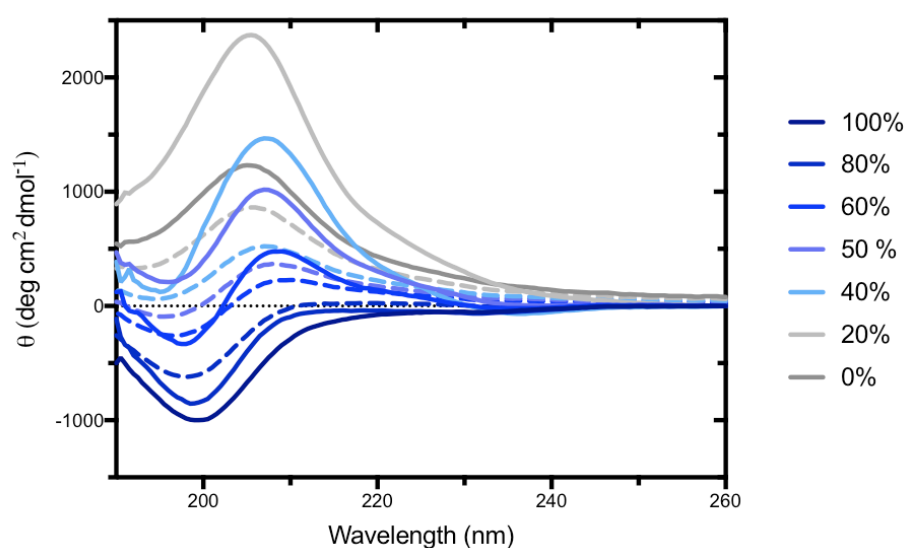
Figure 3.28. CD analysis of the co-assembled system of HABPA-7 and the Dil-PA at varying compositions with the actual data at pH 7 (solid) overlaid on the simulated data (dotted).

When varying the composition of the PAs in the co-assembly system, an effect was seen in the CD. To further confirm the co-assembly, the ζ-potential was measured (Figure 3.29). At 100% of each individual PA, the observed charge was as expected.

HABPA-7 shows a positive ζ-potential due to the charge domain of HABPep-3 as well as the additional positive charge arising from the free amine at the N-terminus.

Upon addition of the Dil-PA, an initial decrease in the ζ-potential is observed as the inner positively charged lysine domain of HABPA-7 is quenched by the glutamic acid domain of the Dil-PA. However, through the aggregation of the HABPep-3 sequence, the N-terminus amine creates a positive surface of the co-assembly, which is remains constant until the 40% of HABPA-7, where the charge drops off dramatically from 40.1 mV (40% HABPA-7) to 4.5 mV (20% HABPA-7). The N-terminus and the arginine in the HABPep-3 sequence remain positive, hence a net positive ζ is observed until 0% HABPA-7. However, the drop-off in the magnitude of the charge at 20% HABPA-7 infer small localisations of charge rather than large clusters of positive charge. The simulated ζ-potential shows a linear growth with increasing % of HABPA-7.

In a similar manner, the simulated data for the co-assembly system is giving larger values of ζ-potential eluding the co-assembly of the two PAs as the negative charge of Dil-PA is suppressed by the positive charge domain of HABPA-7 leaving the HABPep-3 of HABPA-7 to dictate the charge of the self-assembly.
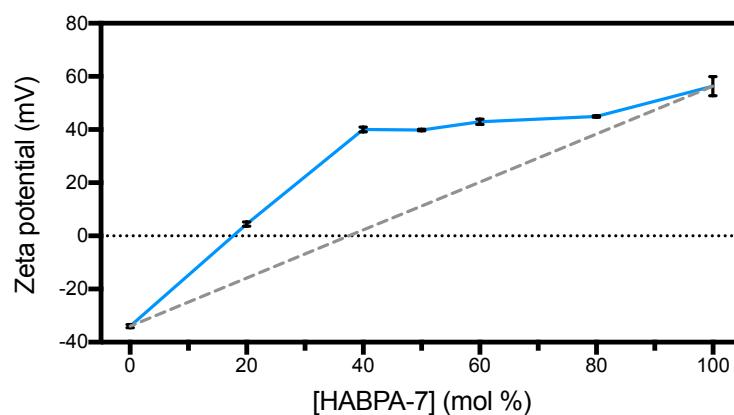
Figure 3.29. ζ-potential of the co-assembled system of HABPA-7 and the Dil-PA at varying compositions of the PAs with the actual data (solid) overlaid on the simulated data (dotted).

Analysis by Nuclear Overhauser effect (NOE) NMR provided more conclusive proofs of the co-assembly of the two PA into a single assembly. By taking background NOE and correlation spectroscopy (COSY) NMRs, background couplings between intra and intermolecular bonds between each PA in a single assembly can be determined. From here, a 50:50 solution of HABPA-7 and Dil-PA can be measured to seek out any cross peaks. The NOE spectra of the 50:50 solution (Figure 3.30) showed a new additional cross peak between 1.37 ppm and 2.58 ppm. The two major differences

between the two PAs is the HA-binding sequence in HABPA-7 and the charged domain. Of these, the peak corresponds to the CH_2 of the lysine (1.37 ppm) and the CH_2 of the glutamic acid (2.58 ppm). For a cross peak to exist in the NOE NMR, these hydrogens need to be in close proximity as the NOE with a maximum distance of 6 Å as the NOE rapidly decays by $1/r^6$, where r is distance.
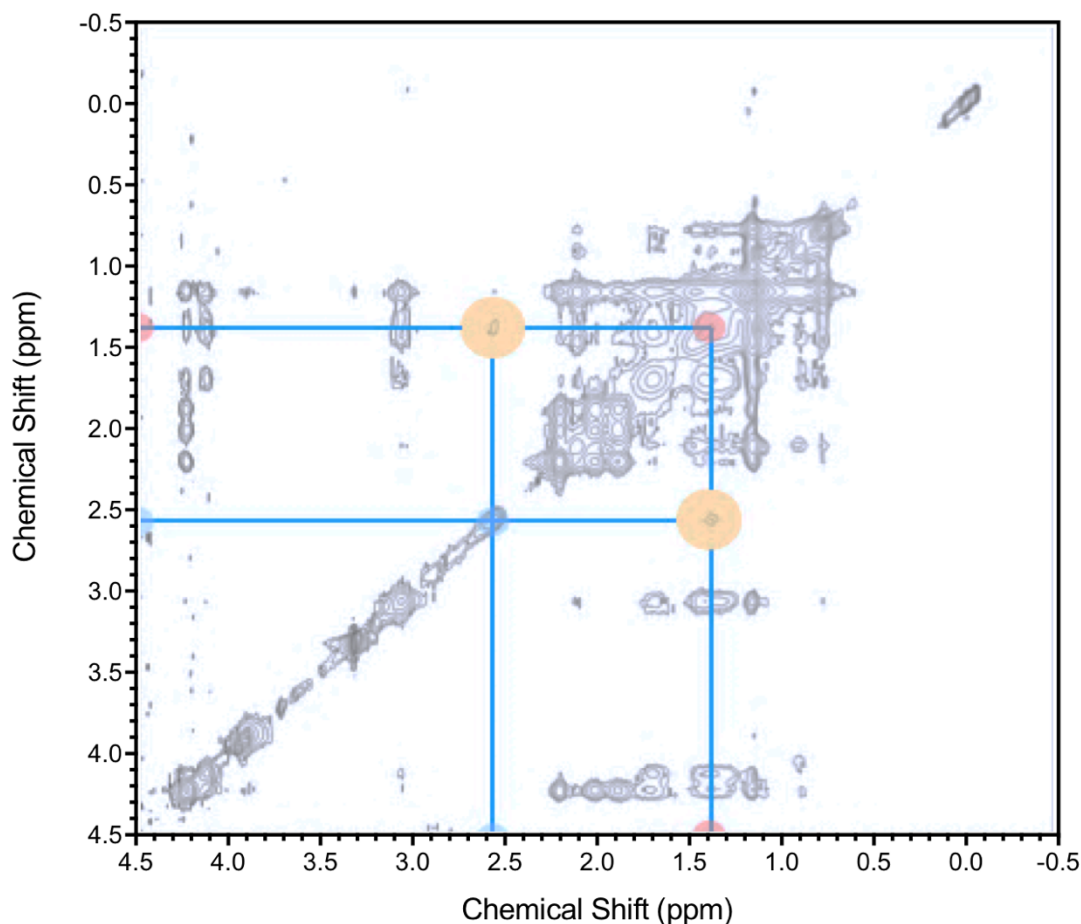
Figure 3.30. NOE NMR spectra at 400 MHz in D_2O of the PA mixture 50:50 ratio with the cross peak (yellow), lysine CH_2 at 2.58 ppm (red) and the glutamic acid CH_2 at 1.37 ppm (blue).

The NOE analysis, along with the results from CD, CAC and ζ-potential, provides evidences that points towards the co-assembly of HABPA-7 with Dil-PA. Using TEM, the nanostructures formed can be visualized. Morphological differences are observed between HABPep-3 and HABPA-7 assemblies due to the PA design. In the lowest percentage of Dil-PA, HABPA-7 dominates in the aggregate with little differences seen between 20% - 40% (Figure 3.31A-B). At 50%, a morphology switch, with long fibrous aggregates is seen in the TEM, as the hydrophobicity of the HABPep-3 epitopes on the surface are reduced in number (Figure 3.31C). Upon increasing the amount of Dil-PA further, larger aggregates are seen. The likely cause of this is the

reduction of surface aggregation upon the fibres from the HABPep-3 epitopes, but with adjacent fibres through inter-fibre interactions of the HABPep-3 sequence.

The hydrophobicity of the HABPep-3 sequence causes a strong tendency to aggregate caused by hydrophobic residues in an aqueous environment. This aggregation drops as the percentage of the Dil-PA increases towards the formation of nanobelt-like structures of 60% Dil-PA (Figure 3.31D-F) which complies with the ζ-potential of the co-assembly (Figure 3.29).
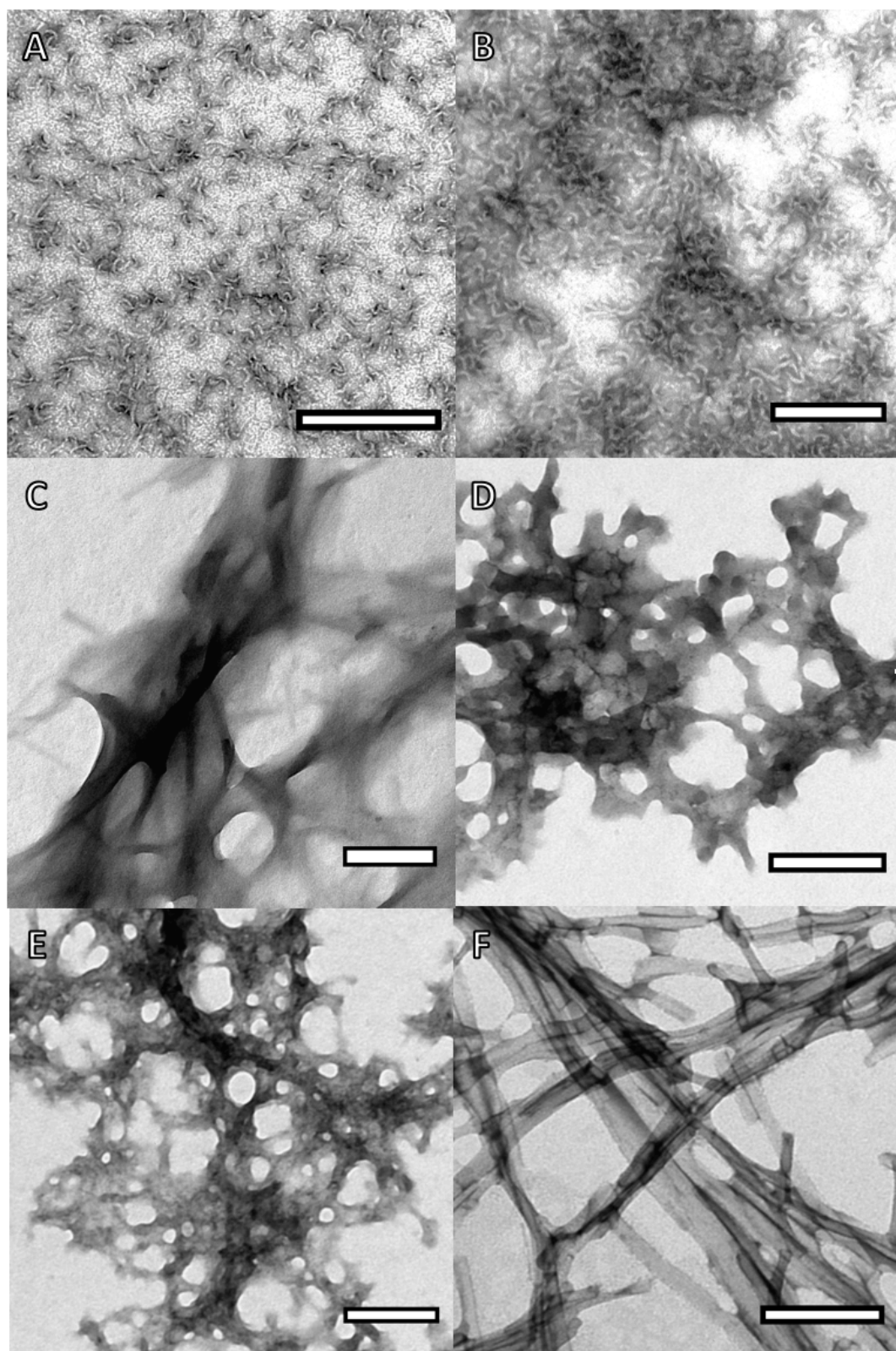
Figure 3.31. TEM comparison Co-assembly of HABPA-7 and Dil-PA, with increasing Dil PA: 20% (A), 40% (B), 50% (C), 60% (D), 80% (E) and 100% (F) showing the morphology change of the co-assembly system. 1 nm for all scale bars.

3.2.4.3. Self-assembly with HA

To form macroscopic assemblies, higher peptide concentrations are necessary. When trying the co-assembly of two PAs, solubility difficulties were found, caused by Dil-PA, which becomes insoluble at higher concentrations as seen during the CAC measurements (Figure 3.25). The Dil-PA was insoluble at 1 % (% .wt) in H_2O, however, the solubility increased on the addition of HABPA-7 inferring a synergistic effect between the HABPA-7 and Dil-PA. Though, the solution remained turbid with small insoluble particles. The key to forming a homogenous co-assembly solution was to raise the pH to 10, by doing this the Dil-PA solubilises (Scheme 3.3). By dissolving HABPA-7 in pH 10 solution and then adding this onto dry powder of Dil-PA ensure the solubility of Dil-PA through both effects of the pH and the synergy with HABPA-7. The solution can then be adjusted to pH 7 to produce a stable solution. It was noted that by reducing the pH below pH 7 the Dil-PA precipitated from the solution.
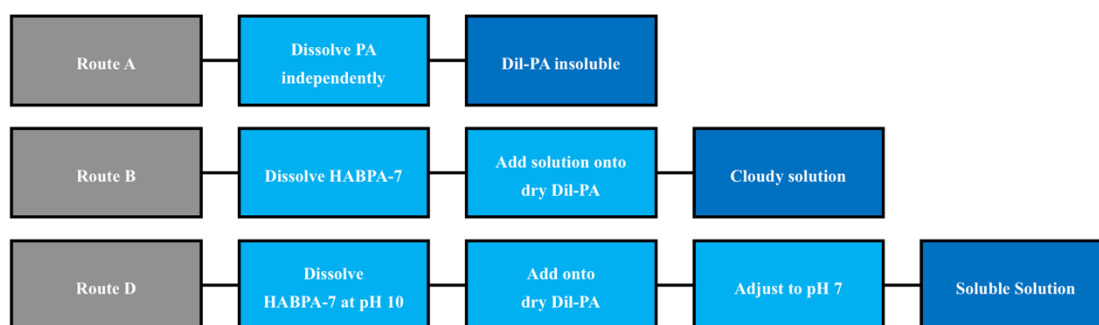
Scheme 3.3. A flow chart depicting the solubilisation routes tested (grey) with the steps (blue) and the outcome (dark blue).

The co-assembly solution was mixed with HA (700 kDa, 2%) to compare the assemblies formed with and without the Dil-PA. Upon addition of the Dil-PA at a 50:50 molar ratio, the membranes formed were opaquer (Figure 3.32a) as opposed to the formation of membranes with HABPA-7 alone.

A change in the surface topology is seen for the membranes formed dependent on the order of HA addition (Figure 3.32b). By adding the HA first, two distinct sides can be seen in the membrane, with one side showing rough irregular layers, whilst the opposing side shows a smooth surface covered by globular aggregates (Figure 3.33A). By adding HA onto the co-assembled PA solution, both surfaces become littered with these small globular structures, which are consistent upon repetition of the membrane preparation and imaging.
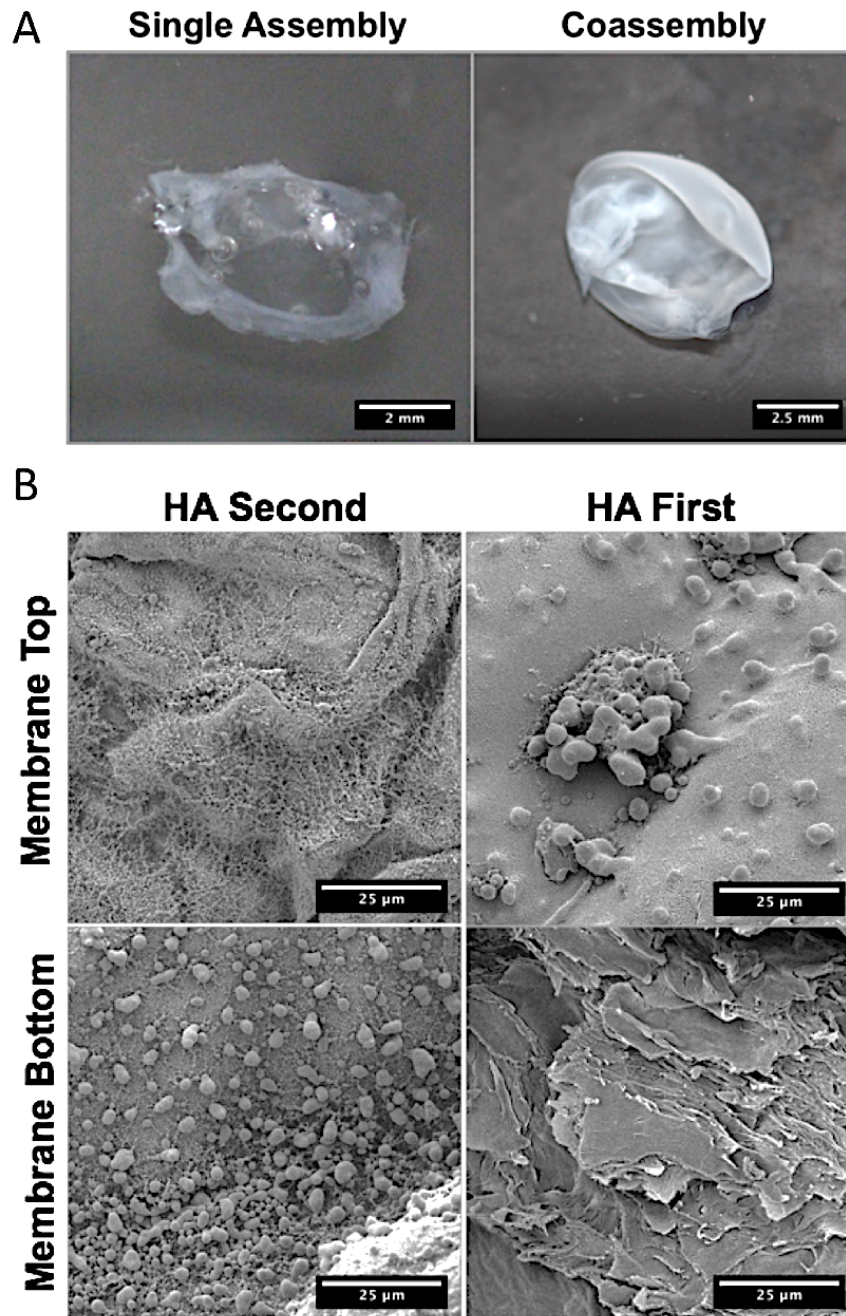
Figure 3.32. Co-assembly of HABPA-7 and Dil-PA (10 mM, 50:50) mixed with HA 700 kDa (2%) showing the change in transparency of the membranes formed (A) and the change in surface dependent on the order of mixing with HA (B).

Being denser and more viscous, the HA solution gets enveloped into the PA solution, similar to examples from the Stupp group[56]. When focusing on the topology, regardless of these globular structures, the surface still remains very fibrous similar to that of HABPA-7 alone (Figure 3.24). The differences in structure also becomes apparent in the cross-section examination. By adding the Dil-PA, we observe the alignment of the fibres (Figure 3.33B), similar to those of the HABPA-4 (Figure 3.18)
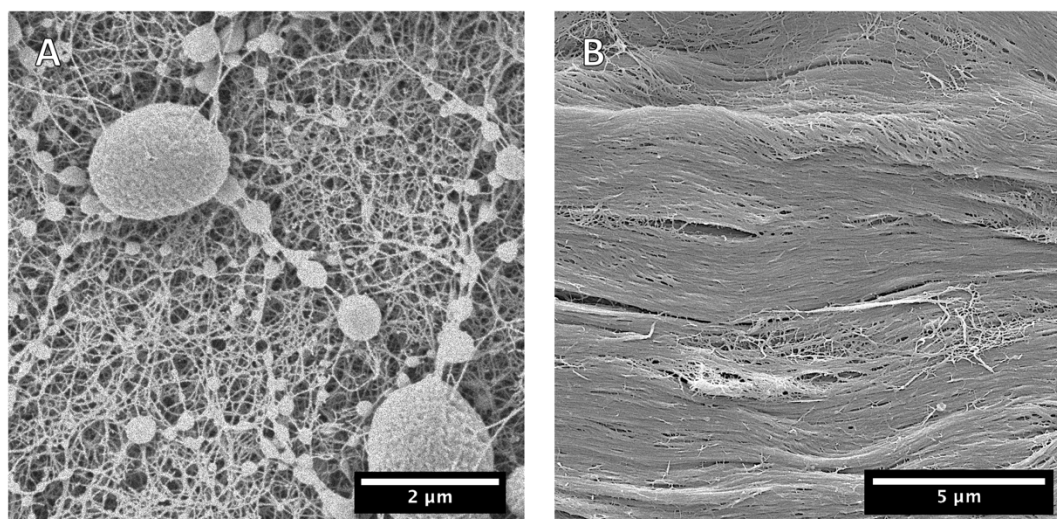
Figure 3.33. SEM images of 50:50 PA co-assembly (10 mM) mixed with HA 700 kDa (2%) showing the surface (A) and cross-section (B).

This phenomenon is only witnessed by the inclusion of the DiI-PA, as HABPA-7 on its own with HA shows an irregular cross-section, consistent to the two sides of the HABP-7 membrane (Figure 3.24). To gain insights on the nature of the globular aggregates formed on the surface of the membranes using the co-assembled PA system, energy-dispersive X-ray spectroscopy (EDX) was performed (Figure 3.34).
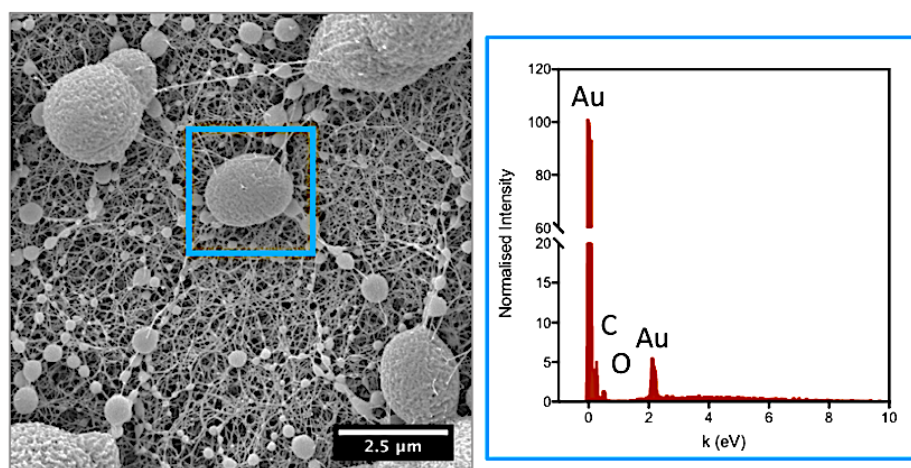
Element	Weight (%)	Atomic (%)
C	25.89	70.07
O	9.48	19.26
Au	64.64	10.67
Totals	100.00	100.00

Figure 3.34. Globular structures shown in the SEM image (top-left) with the EDX analysis (top-right) and detailed elemental composition percentages (bottom)

No signals of salts were detected. Only peaks of the gold coating used for sample preparation for SEM was observed, plus peaks of oxygen and carbon, the main elements present in the two PAs and HA. These globular structures were consistent when repeating these experiments, as well increasing the two PA concentrations from 10 mM to 20 mM. To determine if these globular spheres were HABPA-7 with the Dil-PA, HA or a combination of both, the membranes were reproduced with 10% of HA 700 kDa within the solution supplement with HA 1.5 MDa which had been fluorescently tagged with Texas red. The Z-stacks collected from confocal microscopy show evidence of the HA being spread throughout the membrane (Figure 3.35).
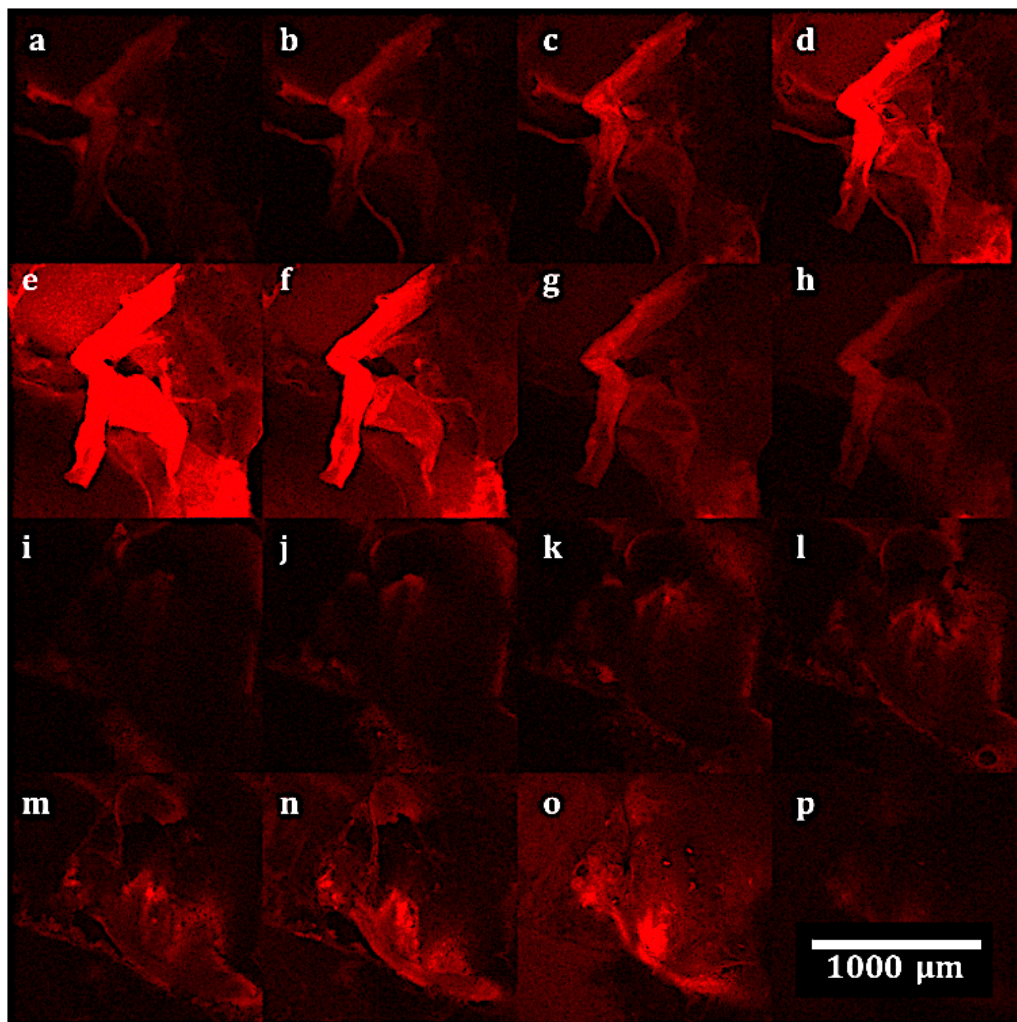
Figure 3.35. Z-stacks of the membrane formed with 2% HA (700 kDa 90% and 10% of Texas Red-labelled 1.5MDa) and HABPA-7: Dil-PA (50:50 ratio). Stacks taken from (a) bottom to (p) top of the membrane.

All the images show small red regions, with a build-up of HA localised towards the lower end of the membrane. This is expected as on addition the HA would sink towards the bottom of the solution due to the density difference between 700 kDa HA and 2.1 kDa of HABPA-7. The envelopment of HA by PAs of opposite charge has been previously shown by the Stupp group with the formation of sacs[56]. The lack of hot spots at the edges of the membrane infers that these globular structures are caused by the addition of the Dil-PA with the HABPA-7; the globular aggregates are not present in the absence of the Dil-PA nor does the Texas red labelled of HA suggest it is caused by the HA. Comparing the TEM images of HABPA-7 (Figure 3.23) and the 50:50 mixture (Figure 3.31E) the large aggregated fibres on the TEM of the mixture give rise to the ball-like structures on the SEM. HABPA-7 and Dil-PA are first allowed to co-assemble before self-assembly with HA. The aggregates seen in the TEM when mixed with HA appear to cause these globular structures. Whilst the true compositions of these globular structures are as yet unknown they are repeatable. What is important is the cross-section of the membranes showing again alignment similarly to HABPA-1 with HA, producing an environment where cells have the potential to bind and grow.

3.3. Conclusion

In conclusion, it has been demonstrated that we can engineer the self-assembly of HABPeps by controlling their secondary structure through the design of the peptide sequence. For example, HABPA-1 shows promise to be used in drug delivery applications due to its pH-sensitive behaviour, whilst the HABPA-2 showed no stable assemblies. CD44 possesses two other HA binding sequences that could tested as PA (Table 1.7). Alternatively, a co-assembly between two or three of these HA binding sequences taken from CD44 as in a PA design as a co-assembly could lead to stable SA structures with HA such as membranes or gels. Of all the peptides, HABPep-3 shows the most promise, as it successfully assembled with HA as both a native peptide and as PA. Hydrophobicity is the clear driving force for the assembly, but tests would need to be carried out to confirm this, using for example a $X_{11}R$ sequence, where X is hydrophobic residue such as alanine. By running this test, it can be determined if the if HABPep-3 is interacting through the entire peptide or simply the arginine. HABPA-7 with Dil-PA shows promising results with the increased solubility seen from HABPA-7 compared to HABPep-3. The addition of a β-sheet domain within the two PAs could form longer fibres in the TEM, to produce gels for cell encapsulation studies.

3.4. Methods and Materials

3.4.1. Materials

Fmoc-amino acids and 4-methylbenzhydrylamine (MBHA) rink amide resin were purchased from Novabiochem. 1-hydroxybenzotriazole hydrate (HOBt), N,N′-diisopropyl carbodiimide (DIC), piperidine, dimethylformamide (DMF), dichloromethane (DCM), trifluoroacetic acid (TFA), anisole, thioanisole, 1,2-ethanedithiol (EDT) triisopropyl silane (TIS), diethyl ether, acetonitrile (ACN), acetic anhydride (Ac$_2$O) and the Kaiser Test Kit were purchased from Sigma-Aldrich and used without further purification.

3.4.2. Instruments and Analysis

3.4.2.1. Electrospray Ionization Mass Spectrometry (ESI-MS)

The peptide's mass was determined using an LC-MS, comprising a 1100 Series LC and SL Ion Trap MSD (Agilent, USA).

3.4.2.2. Analytical High-Performance Liquid Chromatography (HPLC)

The crude and purified peptides were analysed on analytical HPLC (Alliance HPLC System, Waters, UK) using a RP X-bridge column (C18, 3.5 μm, 4.6 × 150 mm) with a gradient running from 98:2 to 0:100 of water/acetonitrile over a 30-minute period at 1 mL/min flow rate at 25 ℃. The peptide elution was monitored by UV at 220 nm (2489 UV/Vis Detector, Waters, UK) controlled by Alliance software.

3.4.2.3. Preparative High-Performance Liquid Chromatography (prep-HPLC)

The peptides were purified on a Waters Auto Purification System using a preparative reverse-phase C18 column (XBridge, 130 Å, 5 μm, 30×150 mm, Waters, USA) with a gradient (Waters 2545 Binary Gradient HPLC system, Waters, USA) running from 98:2 to 0:100 of water/acetonitrile over a 30-minute period at 20 mL/min flow rate at 25 ℃. The peptide elution was monitored by UV at 220 nm (2489 UV/Visible (UV/Vis) Detector for Purification and Modular LC Systems, Waters, USA) and ESI-MS (SQ Detector 2, Waters, USA) with mass directed fraction collection (2747 Sample Manager-Injector, Waters, USA) controlled by Mass Lynx software.

3.4.2.4. Circular Dichroism (CD)

The peptides were dissolved in Milli-Q water to obtain 11 μM solutions with the pH adjusted to 3, 7 and 10 using NH_4OH (0.1 M) and HCl (0.1 M). The CD measurements were taken on a Chirascan CD spectrometer (Applied Photophysics, UK) in the far-UV, from 190 to 300 nm, at 25 °C under a constant flow of N_2 using a quartz cuvette with 3-mm in path length. The spectra displayed are an average of 3 spectra with molar ellipticity [θ] calculated form the measured ellipticity θ taken from the CD and converted using Equation 3.1.

$$[\theta] = \frac{\theta}{cl}$$

<div align="right">Equation 3.1</div>

Where *c* is concentration in dmol L^{-1} and *l* is path length in cm.

3.4.2.5. Nuclear Magnetic Resonance (NMR) Spectroscopy

Spectra of the peptides were collected on a Bruker AV-III spectrometer at 400 MHz for ^1H NMRs and at 101 MHz for ^{13}C NMRs. $CDCl_3$ was used as a solvent and the resonance signal at 7.26 ppm (^1H) and 77.16 ppm (^{13}C) served as a reference for the chemical shift δ of the spectra. NOE experiments where run at 8 scans with the corresponding COSY also ran beforehand.

3.4.2.6. Transmission Electron Microscopy (TEM)

The peptide solutions were prepared at 0.01 wt% in ultrapure water and their pH was adjusted with 0.1 M HCl or 0.1 M NH_4OH. After being aged for 48 hours, the peptide solutions were loaded onto the carbon film coated copper grids (400 mesh, Agar Scientific, UK) and negatively stained by 2 wt% uranyl acetate (Agar Scientific, UK). The excess staining solution on the grids was removed with filter paper and the grids were allowed to dry at room temperature for at least 3 hours. Bright field TEM imaging was performed on a JEOL 1230 TEM operated at an acceleration voltage of 100 kV and the TEM images were recorded by an SIS Megaview III wide-angle CCD camera.

3.4.2.7. ζ-Potential Measurement

ζ-potential of the peptide solutions was measured on a Nano-ZS Zetasizer (Malvern Instruments) at 100 μM with the pH adjusted to 7.4, 3 and 11 using 0.1 M HCl or 0.1 M NH_4OH.

3.4.2.8. Critical Aggregation Concentration (CAC)

The CAC for the peptides was determined by producing a serial dilution of peptide solutions from 1 mM to 1 nM. These solutions were added to Eppendorf's containing Nile Red, with the samples being left 16 hours to allow the incorporation of the Nile Red into any aggregates formed by the peptides. The fluorescence emission spectrum was measured on an LS55 fluorescence spectrometer (PerkinElmer) ranging from 580 to 720 nm with an excitation wavelength at 550 nm.

3.4.2.9. Scanning Electron Microscopy (SEM)

The micro/nanostructure of HA-peptide assemblies was examined by SEM. The membranes or gels were first fixed in 2% glutaraldehyde in PBS for 1 hour at 4 °C followed by washing with PBS. Sequential dehydration in increasing percentages of ethanol (from 20 to 100%) was performed and ethanol removed by a critical point dryer (EMS 850 Electron Microscopy Science, USA). The samples were stored in a desiccator until coated with a gold layer (5 – 30 nm) using an Emitech SC7620 sputter coater (Quorum Technologies, UK). The samples were imaged in a scanning electron microscope equipped with a field emission gun (FEG SEM, Inspect F50, FEI, Netherlands)

3.4.2.10. Confocal Microscopy

Membranes with components possessing fluorophores were imaged under a confocal microscopy (Leica TCS SP2) fitted with fluorescent filters. With Z-stacks taken to build a 3D image of the membranes.

3.4.3. Methods

3.4.3.1. Peptide Synthesis

3.4.3.1.35. Peptide Synthesis

The peptides were synthesised using standard 9-fluorenyl methoxycarbonyl (Fmoc) and solid phase peptide synthesis (SPPS) on Rink amide 4-methylbenzhydrylamine resin assisted by a Liberty Blue automated microwave peptide synthesizer (CEM). The Fmoc-amino acids, HOBt and DIC in a 4 times excess were dissolved in DMF. The Fmoc group was deprotected with 20% piperidine in DMF (v/v). After each cycle, the resin was subsequently washed with DMF followed by DCM.

3.4.3.1.36. Acetyl Capping

The peptide on the resin was N-capped with acetyl groups by shaking the resin-bound peptide with acetic anhydride in DMF (10% w/v) for 10 minutes twice. After the capping cycle, the resin was subsequently washed with DMF followed by DCM with Kaiser test confirming the coupling.

3.4.3.1.37. C-Terminus Modification

PAs were synthesized in the same manner, but Fmoc-Lys(4-methyltrityl) was loaded onto the resin, followed by the cleavage of the 4-methyltrityl (Mtt) by 5% TFA in DCM for 10 minutes followed by 10% DIPEA in DCM for further 10 minutes. This cycle was repeated twice to ensure full cleavage of the side chain Mtt. The deprotected ε-amine of the lysine was coupled with palmitic acid (4 equivalents) using the same coupling reagents and repeated twice to ensure high conversion.

3.4.3.1.38. Cleavage

Once the desired peptide sequence was achieved, the peptide and acid-labile side groups were cleaved by TFA/TIS/H_2O (95:2.5:2.5) for 3 hours. The solution was collected, concentrated by reduced pressure and precipitated in cold ether. The resulting suspension was collected by centrifugation and decanting the supernatant, followed by lyophilisation of the resulting white solid.

3.4.3.1.39. Purification

The crude peptides were passed through a 0.2 μm filter and then injected on a preparative reverse-phase C18 column (XBridge, 130 Å, 5 μm, 30×150 mm, Waters, USA) in an Auto Purification System (Waters, USA) using a gradient from H_2O to ACN supplemented with 0.1% TFA for positively charge peptides and 0.1% NH_4OH for negatively charged peptides. The fractions were detected by the SQ Mass Detector (Waters, USA). These fractions were combined, reduced under reduced pressure and then lyophilised to produce a white powder.

3.4.3.2. Peptide-HA Membrane Preparation

Peptide-HA membranes were prepared in a vial by solvating the peptide first followed by the addition of 2% HA solution. Upon addition of HA, an interface was observed instantaneously, but allowed to form fully at 37 ºC for 16 hours at which point the membrane was removed from the vial, washed with ultrapure water to remove any unreacted HA or peptide and left for 16 hours to test the stability in water.

3.4.3.3. Co-assembled PAs-HA Membrane Preparation

For a mixture of PAs, the PAs were combined as a dry powder in a vial and dissolved in ultrapure water. The sample was vortexed to aid solubilisation of the two PAs and incubated at 37 ºC for 16 hours to allow the SA of the two peptides. 2% HA solution was cast on top of the PAs solution and incubated again for 16 hours at 37 ºC. The membrane which was formed was removed from the vial, washed with ultrapure water to remove any unreacted HA or peptide and left for 16 hours to test the stability in water.

References

1.   Dorsey, S.M., et al., *Visualization of Injectable Hydrogels Using Chemical Exchange Saturation Transfer MRI.* ACS Biomaterials Science & Engineering, 2015. **1**(4): p. 227-237.
2.   Rodell, C.B., et al., *Selective Proteolytic Degradation of Guest–Host Assembled, Injectable Hyaluronic Acid Hydrogels.* ACS Biomaterials Science & Engineering, 2015. **1**(4): p. 277-286.
3.   Burdick, J.A. and G.D. Prestwich, *Hyaluronic acid hydrogels for biomedical applications.* Advanced Materials, 2011. **23**(12): p. H41-56.
4.   Ramamurthi, A. and I. Vesely, *Ultraviolet light-induced modification of crosslinked hyaluronan gels.* Journal of Biomedical Materials Research Part A, 2003. **66A**(2): p. 317-329.
5.   Ramamurthi, A. and I. Vesely, *Evaluation of the matrix-synthesis potential of crosslinked hyaluronan gels for tissue engineering of aortic heart valves.* Biomaterials, 2005. **26**(9): p. 999-1010.
6.   Ibrahim, S., et al., *Characterization of glycidyl methacrylate - crosslinked hyaluronan hydrogel scaffolds incorporating elastogenic hyaluronan oligomers.* Acta Biomaterialia, 2011. **7**(2): p. 653-65.
7.   Skardal, A., J. Zhang, and G.D. Prestwich, *Bioprinting vessel-like constructs using hyaluronan hydrogels crosslinked with tetrahedral polyethylene glycol tetracrylates.* Biomaterials, 2010. **31**(24): p. 6173-81.
8.   Pouyani, T. and G.D. Prestwich, *Functionalized Derivatives of Hyaluronic Acid Oligosaccharides: Drug Carriers and Novel Biomaterials.* Bioconjugate Chemistry, 1994. **5**(4): p. 339-347.
9.   Luo, Y., K.R. Kirker, and G.D. Prestwich, *Cross-linked hyaluronic acid hydrogel films: new biomaterials for drug delivery.* Journal of Controlled Release, 2000. **69**(1): p. 169-184.
10.   Vanderhooft, J.L., B.K. Mann, and G.D. Prestwich, *Synthesis and Characterization of Novel Thiol-Reactive Poly(ethylene glycol) Cross-Linkers for Extracellular-Matrix-Mimetic Biomaterials.* Biomacromolecules, 2007. **8**(9): p. 2883-2889.
11.   Burdick, J.A. and G.D. Prestwich, *Hyaluronic Acid Hydrogels for Biomedical Applications.* Advanced Materials, 2011. **23**(12): p. H41-H56.
12.   Charlot, A. and R. Auzély-Velty, *Synthesis of Novel Supramolecular Assemblies Based on Hyaluronic Acid Derivatives Bearing Bivalent β-Cyclodextrin and Adamantane Moieties.* Macromolecules, 2007. **40**(4): p. 1147-1158.
13.   Charlot, A., et al., *Controlled Synthesis and Inclusion Ability of a Hyaluronic Acid Derivative Bearing β-Cyclodextrin Molecules.* Biomacromolecules, 2006. **7**(3): p. 907-913.
14.   Ouyang, L., et al., *3D Printing of Shear-Thinning Hyaluronic Acid Hydrogels with Secondary Cross-Linking.* ACS Biomaterials Science & Engineering, 2016. **2**(10): p. 1743-1751.
15.   Elamin, K.M., et al., *Supramolecular Complex of Methyl-β-cyclodextrin with Adamantane-Grafted Hyaluronic Acid as a Novel Antitumor Agent.* Chemical and Pharmaceutical Bulletin, 2018. **66**(3): p. 277-285.
16.   Rajangam, K., et al., *Heparin Binding Nanostructures to Promote Growth of Blood Vessels.* Nano Letters, 2006. **6**(9): p. 2086-2090.
17.   Chow, L.W., et al., *Self-assembling nanostructures to deliver angiogenic factors to pancreatic islets.* Biomaterials, 2010. **31**(24): p. 6154-61.
18.   Chow, L.W., et al., *Peptide-directed spatial organization of biomolecules in dynamic gradient scaffolds.* Advanced Healthcare Materials, 2014. **3**(9): p. 1381-6.
19.   Roberts, J.J., et al., *Interaction of Hyaluronan Binding Peptides with Glycosaminoglycans in Poly(ethylene glycol) Hydrogels.* Biomacromolecules, 2014. **15**(4): p. 1132-1141.
20.   Mummert, M.E., et al., *Development of a peptide inhibitor of hyaluronan-mediated leukocyte trafficking.* Journal of Experimental Medicine, 2000. **192**(6): p. 769-779.

21. Zmolik, J.M. and M.E. Mummert, *Pep-1 as a novel probe for the in situ detection of hyaluronan.* Journal of Histochemistry and Cytochemistry, 2005. **53**(6): p. 745-751.

22. Rudrabhatla, S.R., C.L. Mahaffey, and M.E. Mummert, *Tumor Microenvironment Modulates Hyaluronan Expression: The Lactate Effect.* Journal of Investigative Dermatology, 2006. **126**(6): p. 1378-1387.

23. Zaleski, K.J., et al., *Hyaluronic acid binding peptides prevent experimental staphylococcal wound infection.* Antimicrobial Agents and Chemotherapy, 2006. **50**(11): p. 3856-3860.

24. Uchakina, O.N., et al., *The role of hyaluronic acid in SEB-induced acute lung inflammation.* Journal of Clinical Immunology, 2013. **146**(1): p. 56-69.

25. Campo, G.M., et al., *Combined treatment with hyaluronan inhibitor Pep-1 and a selective adenosine A2 receptor agonist reduces inflammation in experimental arthritis.* Innate Immunity, 2013. **19**(5): p. 462-478.

26. Riehl, T.E., X. Ee, and W.F. Stenson, *Hyaluronic acid regulates normal intestinal and colonic growth in mice.* American Journal of Physiology-Gastrointestinal and Liver Physiology, 2012. **303**(3): p. G377-88.

27. Riehl, T.E., et al., *CD44 and TLR4 mediate hyaluronic acid regulation of Lgr5+ stem cell proliferation, crypt fission, and intestinal growth in postnatal and adult mice.* Am J Physiol Gastrointest Liver Physiol, 2015. **309**(11): p. G874-87.

28. Liang, J., D. Jiang, and P.W. Noble, *Hyaluronan as a therapeutic target in human diseases.* Advanced Drug Delivery Reviews, 2016. **97**: p. 186-203.

29. Al-Qadi, S., et al., *The role of hyaluronic acid inclusion on the energetics of encapsulation and release of a protein molecule from chitosan-based nanoparticles.* Colloids and Surfaces B: Biointerfaces, 2016. **141**: p. 223-232.

30. Cui, H., M.J. Webber, and S.I. Stupp, *Self-assembly of peptide amphiphiles: From molecules to nanostructures to biomaterials.* Peptide Science, 2010. **94**(1): p. 1-18.

31. Hartgerink, J.D., E. Beniash, and S.I. Stupp, *Self-Assembly and Mineralization of Peptide-Amphiphile Nanofibers.* Science, 2001. **294**(5547): p. 1684.

32. Hartgerink, J.D., E. Beniash, and S.I. Stupp, *Peptide-amphiphile nanofibers: a versatile scaffold for the preparation of self-assembling materials.* Proceedings of the National Academy of Sciences of the United States of America, 2002. **99**(8): p. 5133-8.

33. Ferreira, D.S., et al., *Hyaluronan and self-assembling peptides as building blocks to reconstruct the extracellular environment in skin tissue.* Biomaterials Science, 2013. **1**(9): p. 952-964.

34. Pashuck, E.T., H. Cui, and S.I. Stupp, *Tuning Supramolecular Rigidity of Peptide Fibers through Molecular Structure.* Journal of the American Chemical Society, 2010. **132**(17): p. 6041-6046.

35. Niece, K.L., et al., *Self-Assembly Combining Two Bioactive Peptide-Amphiphile Molecules into Nanofibers by Electrostatic Attraction.* Journal of the American Chemical Society, 2003. **125**(24): p. 7146-7147.

36. Lide, D.R., *Handbook of Chemistry and Physics.* 88 ed. Vol. 130. 2007.

37. Costantini, S., G. Colonna, and A.M. Facchiano, *Amino acid propensities for secondary structures are influenced by the protein structural class.* Biochemical and Biophysical Research Communications, 2006. **342**(2): p. 441-51.

38. Pins, G.D., et al., *Self-assembly of collagen fibers. Influence of fibrillar alignment and decorin on mechanical properties.* Biophysical Journal, 1997. **73**(4): p. 2164-2172.

39. Lee, K.Y. and D.J. Mooney, *Hydrogels for Tissue Engineering.* Chemical Reviews, 2001. **101**(7): p. 1869-1880.

40. Mouw, J.K., G. Ou, and V.M. Weaver, *Extracellular matrix assembly: a multiscale deconstruction.* Nature reviews. Molecular cell biology, 2014. **15**(12): p. 771-785.

41. Nam, E., W.C. Lee, and S. Takeuchi, *Formation of Highly Aligned Collagen Nanofibers by Continuous Cyclic Stretch of a Collagen Hydrogel Sheet.* Macromol Biosci, 2016. **16**(7): p. 995-1000.

42. Lowe, C.J., et al., *Production of Highly Aligned Collagen Scaffolds by Freeze-drying of Self-assembled, Fibrillar Collagen Gels.* ACS Biomater Sci Eng, 2016. **2**(4): p. 643-651.

43.   Nikkhah, M., et al., *Directed endothelial cell morphogenesis in micropatterned gelatin methacrylate hydrogels.* Biomaterials, 2012. **33**(35): p. 9009-18.

44.   Jin, H.-E., et al., *Biomimetic Self-Templated Hierarchical Structures of Collagen-Like Peptide Amphiphiles.* Nano Letters, 2015. **15**(10): p. 7138-7145.

45.   Webber, M.J., et al., *Development of bioactive peptide amphiphiles for therapeutic cell delivery.* Acta Biomaterialia, 2010. **6**(1): p. 3-11.

46.   Yu, Z., et al., *Co-assembly of Peptide Amphiphiles and Lipids into Supramolecular Nanostructures Driven by Anion−π Interactions.* Journal of the American Chemical Society, 2017. **139**(23): p. 7823-7830.

47.   Hamley, I.W., A. Dehsorkhi, and V. Castelletto, *Coassembly in binary mixtures of peptide amphiphiles containing oppositely charged residues.* Langmuir, 2013. **29**(16): p. 5050-9.

48.   Behanna, H.A., et al., *Coassembly of Amphiphiles with Opposite Peptide Polarities into Nanofibers.* Journal of the American Chemical Society, 2005. **127**(4): p. 1193-1200.

49.   Ortony, J.H., et al., *Internal dynamics of a supramolecular nanofibre.* Nature Materials, 2014. **13**(8): p. 812-6.

50.   Toft, D.J., et al., *Coassembled Cytotoxic and Pegylated Peptide Amphiphiles Form Filamentous Nanostructures with Potent Antitumor Activity in Models of Breast Cancer.* ACS Nano, 2012. **6**(9): p. 7956-7965.

51.   Castelletto, V., et al., *New RGD-peptide amphiphile mixtures containing a negatively charged diluent.* Faraday Discussions, 2013. **166**: p. 381.

52.   Matson, J.B., et al., *Nanostructure-templated control of drug release from peptide amphiphile nanofiber gels.* Soft Matter, 2012. **8**(13): p. 3586-3595.

53.   Lee, S.S., et al., *Gel scaffolds of BMP-2-binding peptide amphiphile nanofibers for spinal arthrodesis.* Advanced Healthcare Materials, 2015. **4**(1): p. 131-141.

54.   Cui, H., et al., *Self-Assembly of Giant Peptide Nanonbelts.* Nano Letters, 2009. **9**(3): p. 945-951.

55.   Moyer, T.J., H. Cui, and S.I. Stupp, *Tuning nanostructure dimensions with supramolecular twisting.* Journal of Physical Chemistry B, 2013. **117**(16): p. 4604-10.

56.   Capito, R.M., et al., *Self-assembly of large and small molecules into hierarchically ordered sacs and membranes.* Science, 2008. **319**(5871): p. 1812-6.

3.5. Appendix

3.5.1. Peptide Characterisation

3.5.1.1. Ac-RYPISRPRKR-CONH$_2$ (HABPep-1)
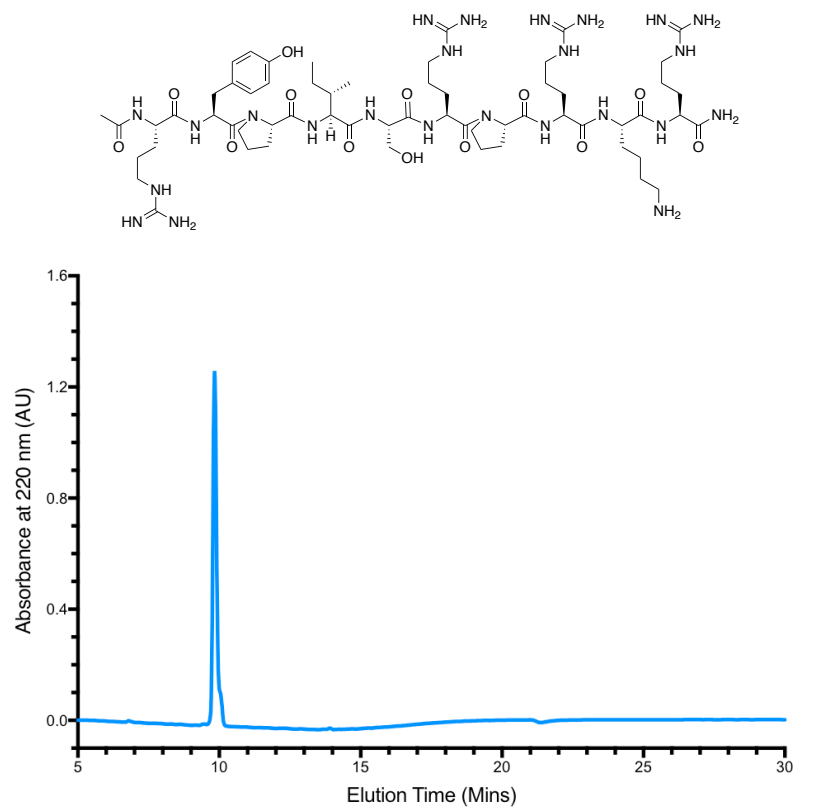
Figure A 3.1. HPLC trace of purified HABPep-1 running a gradient of 98: 2 to 0: 100 (H$_2$O + 0.1 % TFA: ACN + 0.1 % TFA) over a 30-minute period at a flow rate of 1 ml/min
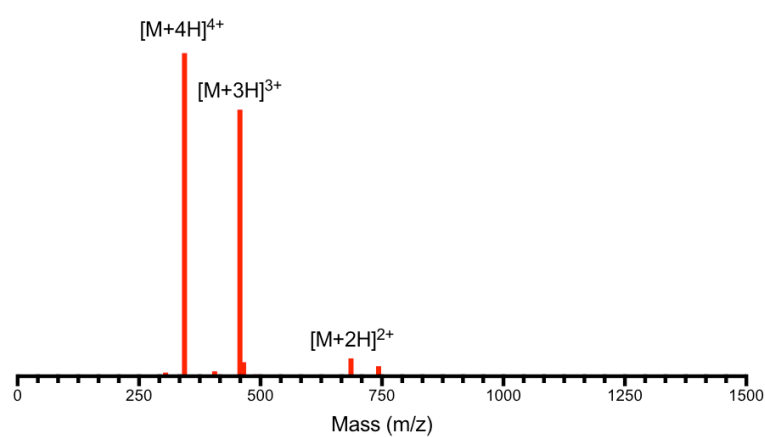
Figure A 3.2. ESI Mass spectrum of HABPep-1 measured in the positive ion channel

RP-HPLC (mins)	9.85
Purity (%)	> 99
ESI-MS (m/z)	1369 [Expected], 686 [M+2H]2+, 458 [M+3H]3+, 343 [M+4H]4+

3.5.1.2. Ac-KNGRYSISR-CONH₂ (HABPep-2)
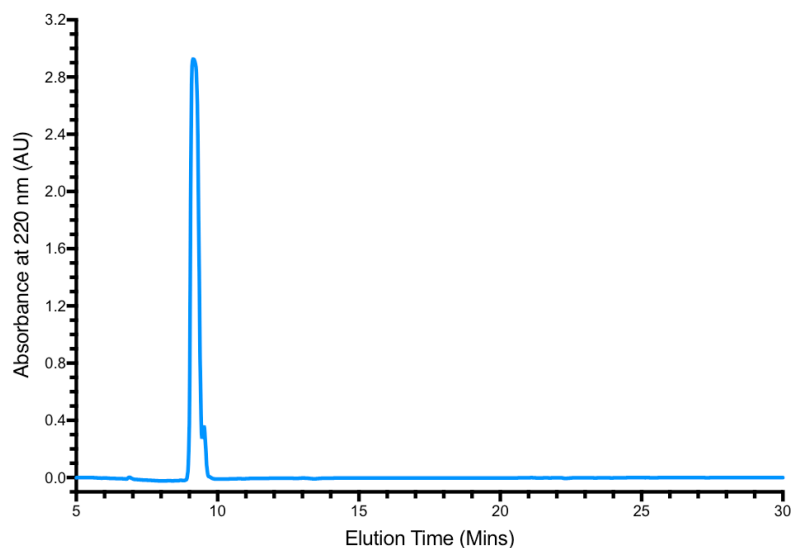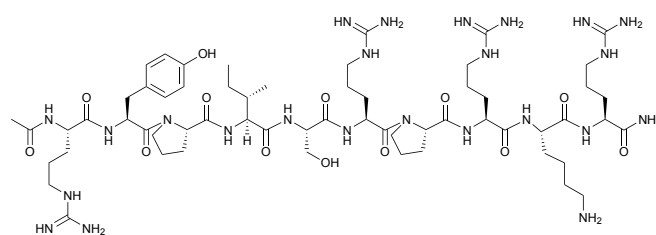
Figure A 3.3. HPLC trace of purified HABPep-2 running a gradient of 98: 2 to 0: 100 (H_2O + 0.1 % TFA: ACN + 0.1 % TFA) over a 30-minute period at a flow rate of 1 ml/min
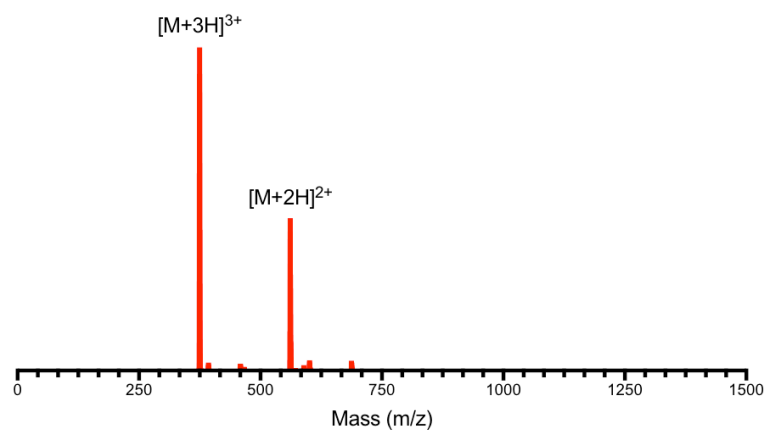
Figure A 3.4. ESI Mass spectrum of HABPep-2 measured in the positive ion channel

RP-HPLC (mins)	9.23
Purity (%)	> 99
ESI-MS (m/z)	1121 [Expected], 561 [M+2H]²⁺, 374 [M+3H]³⁺

3.5.1.3. H₂N-GAHWNFQALTVR-CONH₂ (HABPep-3)
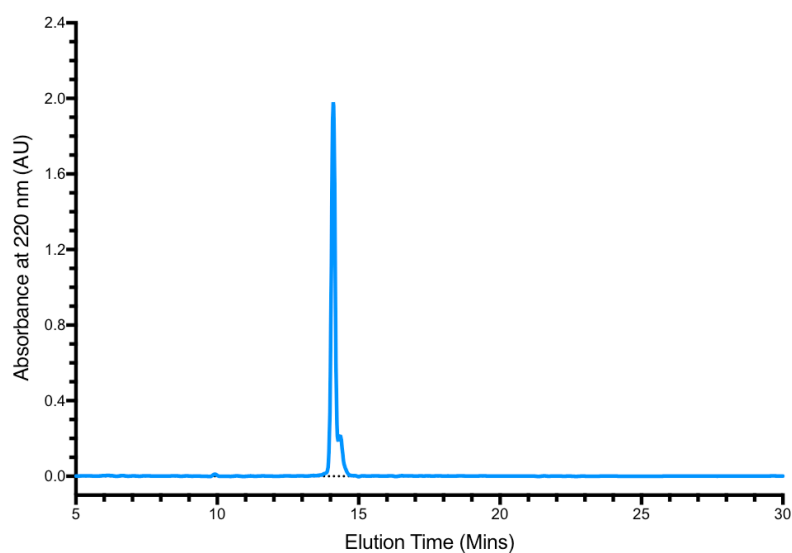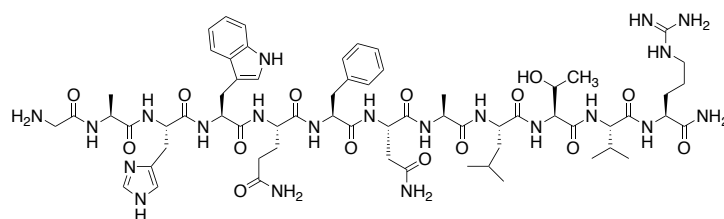
Figure A 3.5. HPLC trace of purified HABPep-3 running a gradient of 98: 2 to 0: 100 (H₂O + 0.1 % TFA: ACN + 0.1 % TFA) over a 30-minute period at a flow rate of 1 ml/min
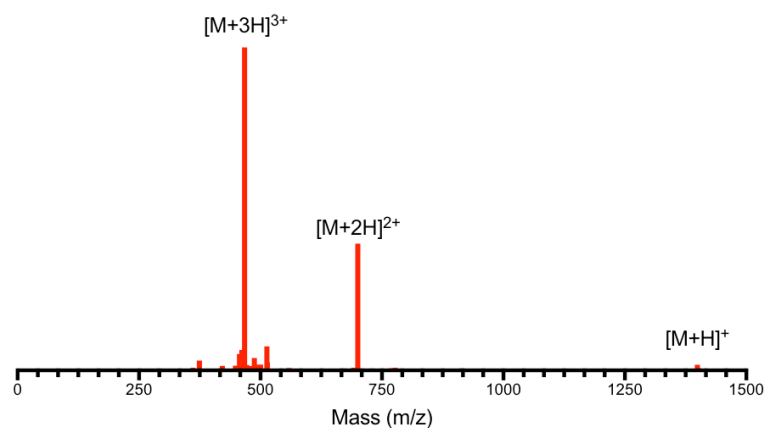
Figure A 3.6. ESI Mass spectrum of HABPep-3 measured in the positive ion channel

RP-HPLC (mins)	14.11
Purity (%)	> 99
ESI-MS (m/z)	1398 [Expected], 1399 [M+H]⁺, 700 [M+2H]²⁺, 467 [M+3H]³⁺

3.5.1.4. C_{16}-VVVAAARYPISRPRKR-CONH$_2$ (HABPA-1)
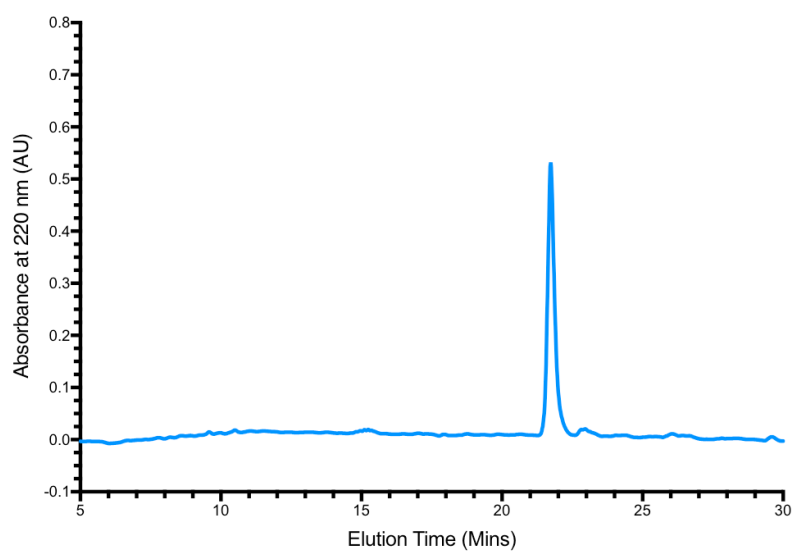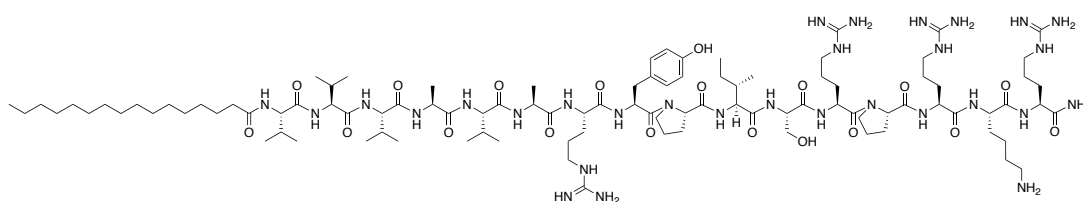
Figure A 3.7. HPLC trace of purified HABPA-1 running a gradient of 98: 2 to 0: 100 (H_2O + 0.1 % TFA: ACN + 0.1 % TFA) over a 30-minute period at a flow rate of 1 ml/min
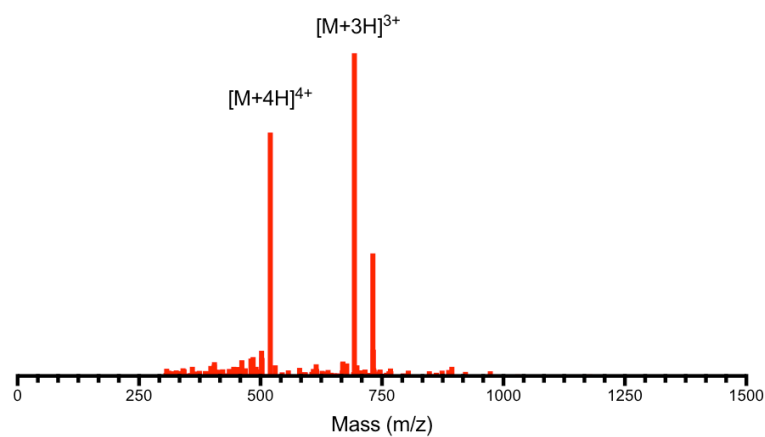
Figure A 3.8. ESI Mass spectrum of HABPA-1 measured in the positive ion channel

RP-HPLC (mins)	21.75
Purity (%)	> 97
ESI-MS (m/z)	2076 [Expected], 693 [M+3H]$^{3+}$, 520 [M+4H]$^{4+}$

3.5.1.5. C_{16}-VVVAAAKNGRYSISR-CONH$_2$ (HABPA-2)
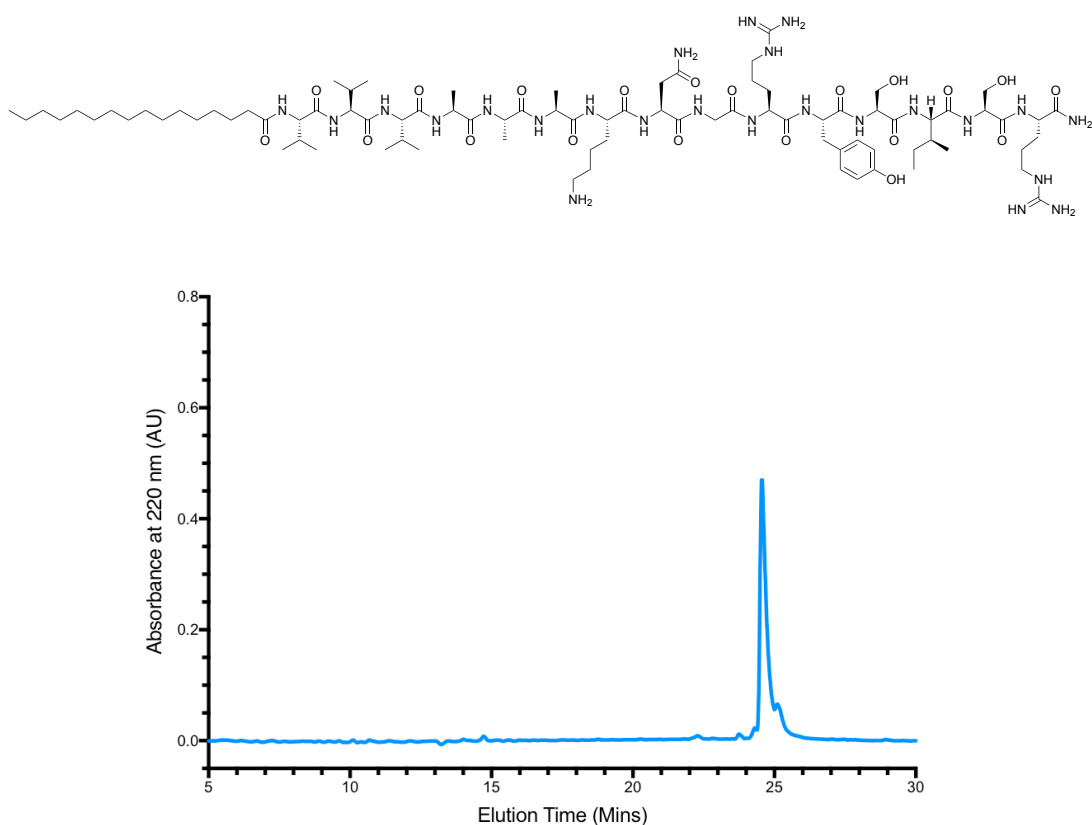
Figure A 3.9. HPLC trace of purified HABPA-2 running a gradient of 98: 2 to 0: 100 (H_2O + 0.1 % TFA: ACN + 0.1 % TFA) over a 30-minute period at a flow rate of 1 ml/min
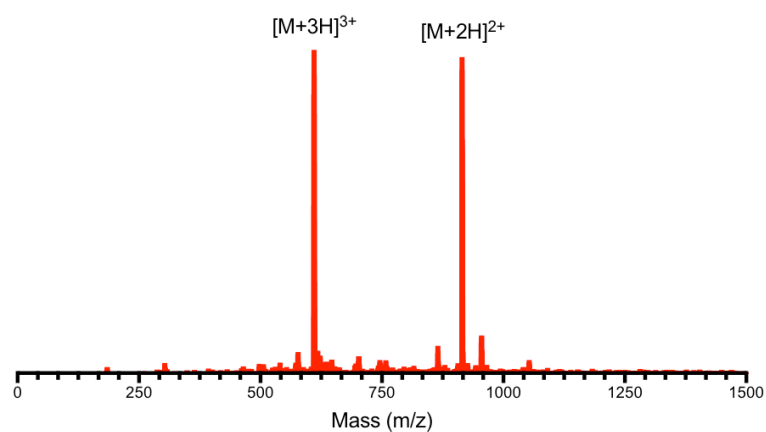
Figure A 3.10. ESI Mass spectrum of HABPA-2 measured in the positive ion channel

RP-HPLC (mins)	24.57
Purity (%)	97
ESI-MS (m/z)	1828 [Expected], 915 [M+2H]$^{2+}$, 610 [M+3H]$^{3+}$

3.5.1.6. H₂N-GAHWNFQALTVRGGGKK[K](C16)-CONH₂ (HABPA-7)
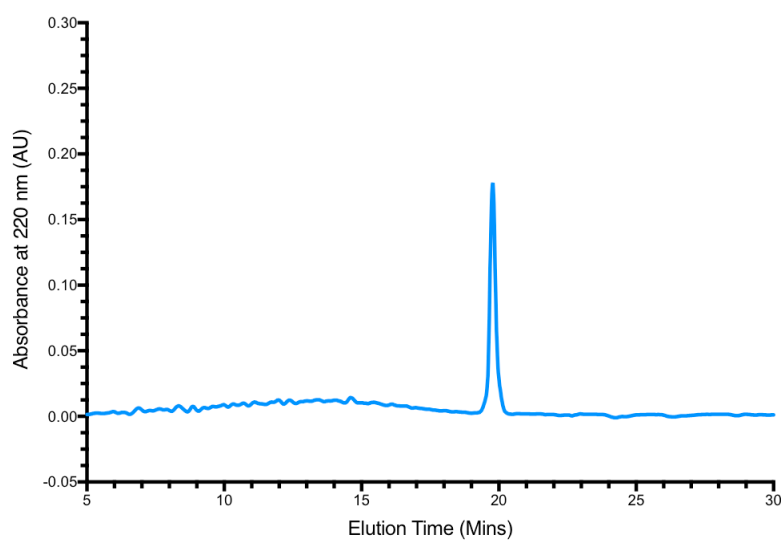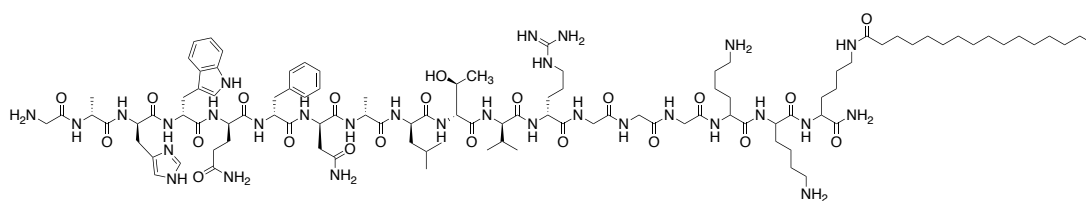
Figure A 3.11. HPLC trace of purified HABPA-7 running a gradient of 98: 2 to 0: 100 (H_2O + 0.1 % TFA: ACN + 0.1 % TFA) over a 30-minute period at a flow rate of 1 ml/min
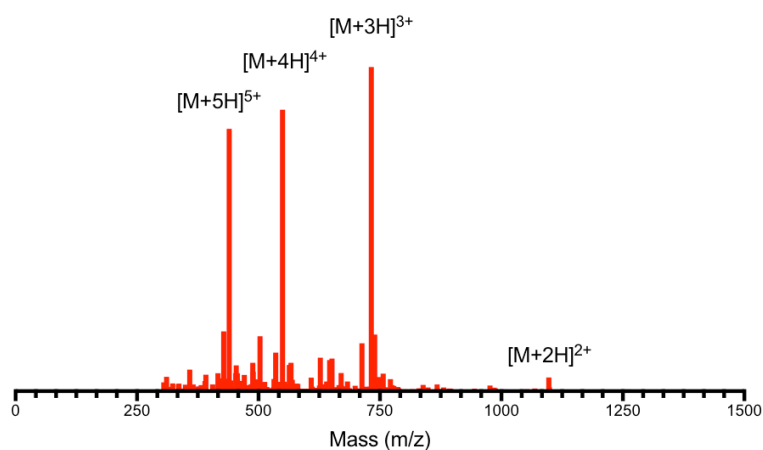
Figure A 3.12. ESI Mass spectrum of HABPA-7 measured in the positive ion channel

RP-HPLC (mins)	19.8
Purity (%)	> 99
ESI-MS (m/z)	2192 [Expected], 1097 [M+2H]$^{2+}$, 732 [M+3H]$^{3+}$, 549 [M+4H]$^{4+}$, 439 [M+5H]$^{5+}$

3.5.1.7. C₁₆-EEGGG-CONH₂ (Dil-PA)
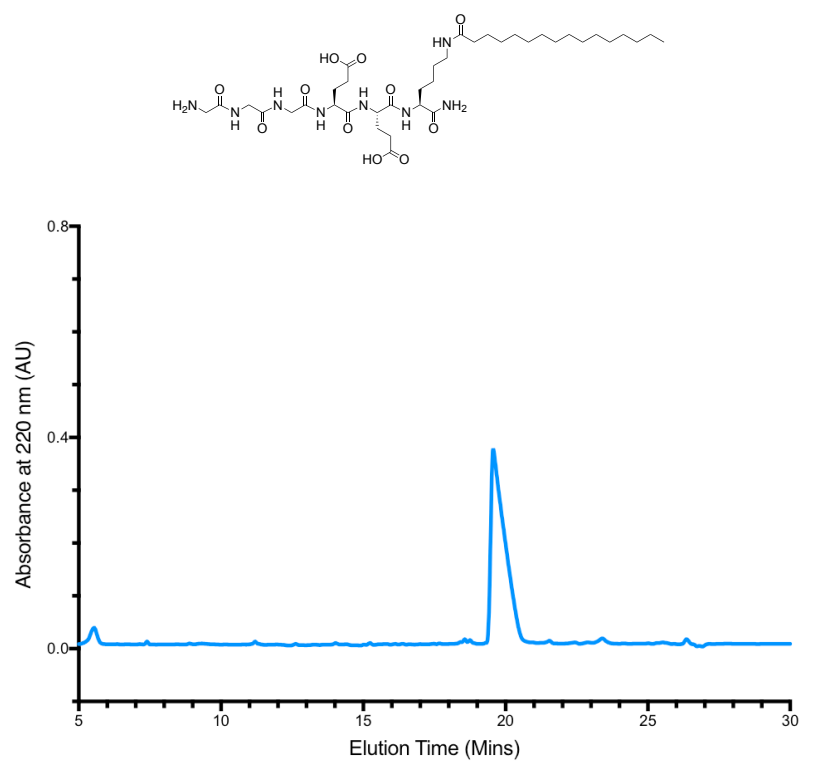
Figure A 3.13. HPLC trace of purified Dil-PA running a gradient of 98: 2 to 0: 100 (H_2O + 0.1 % NH_4OH: ACN + 0.1 % NH_4OH) over a 30-minute period at a flow rate of 1 ml/min
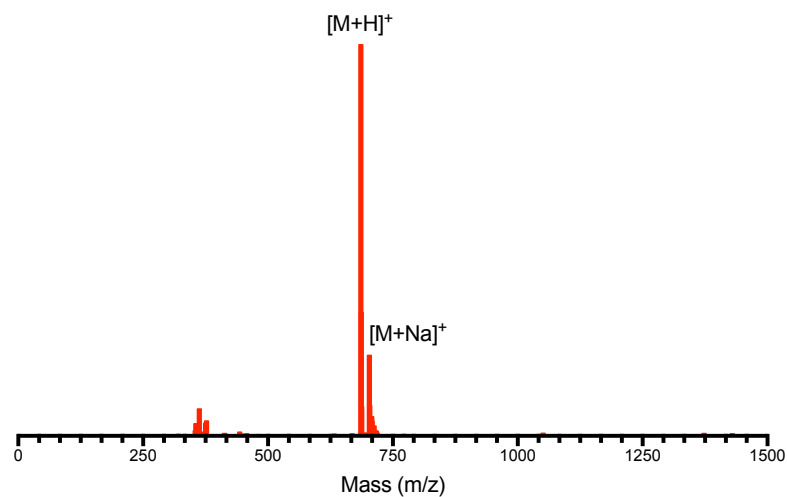
Figure A 3.14. ESI Mass spectrum of Dil-PA measured in the positive ion channel

RP-HPLC (mins)	19.6
Purity (%)	> 99
ESI-MS (m/z)	684 [Expected], 685 [M+H]⁺, 702 [M+Na]⁺

3.5.2. Additional Spectra

3.5.2.1. Nile Red Fluorescence
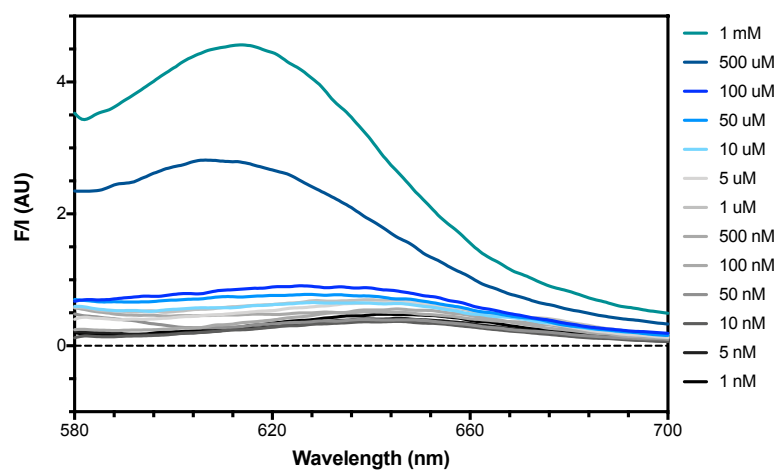
Figure A 3.15. Nile Red emission when excited at 550 nm at increasing concentrations of HABPep-3 in H_2O
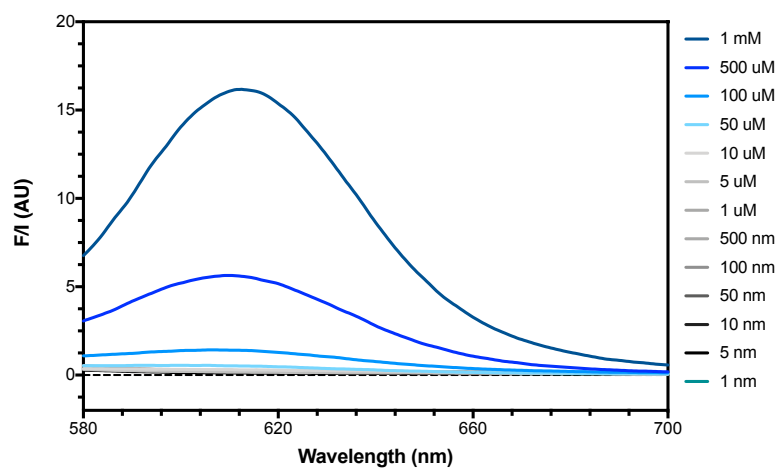
Figure A 3.16. Nile Red emission when excited at 550 nm at increasing concentrations of HABPA-1 in H_2O
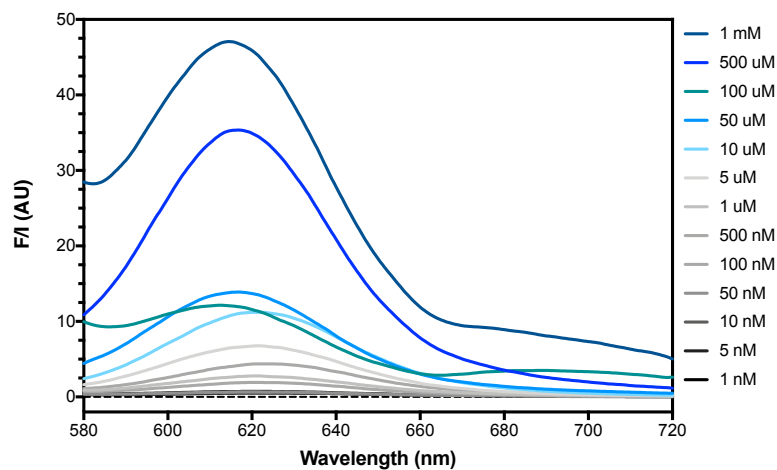
Figure A 3.17. Nile Red emission when excited at 550 nm at increasing concentrations of HABPA-2 in H_2O
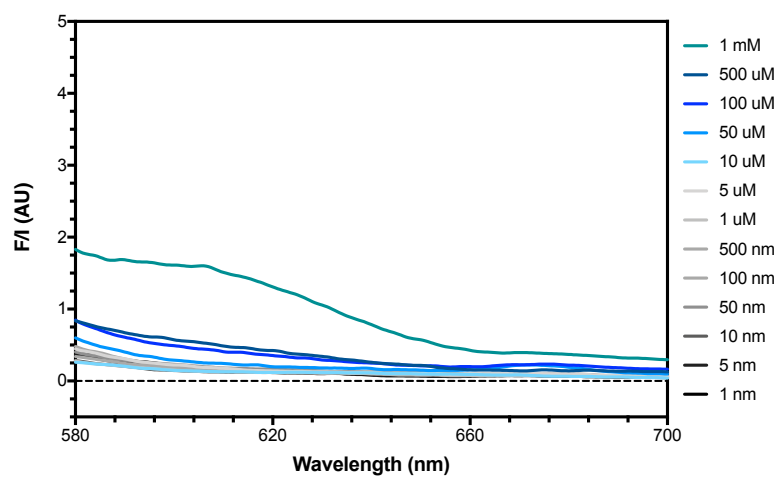
Figure A 3.18. Nile Red emission when excited at 550 nm at increasing concentrations of HABPA-7 in H_2O
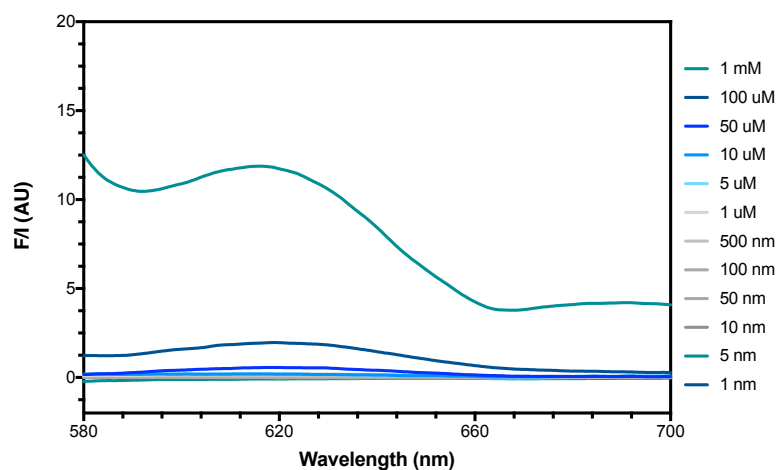
Figure A 3.19. Nile Red emission when excited at 550 nm at increasing concentrations of DiI-PA in H_2O
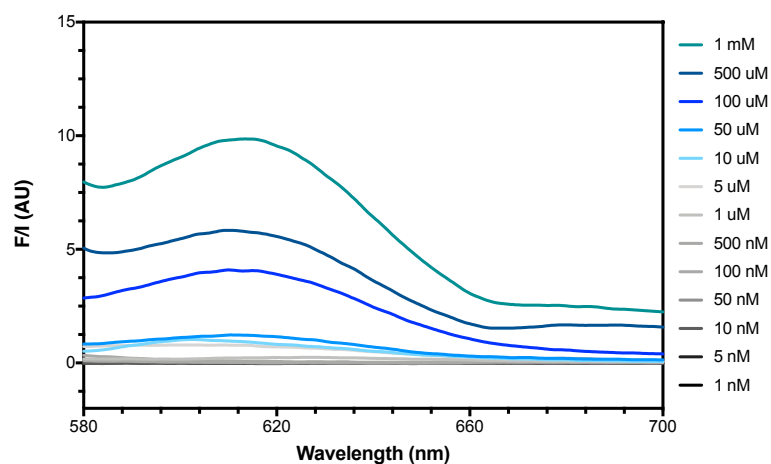
Figure A 3.20. Nile Red emission when excited at 550 nm at increasing concentrations of 50:50 ratio of HABPA-7 and Dil-PA in H_2O

3.5.2.2. Nuclear Overhauser Effect (NOE) NMR
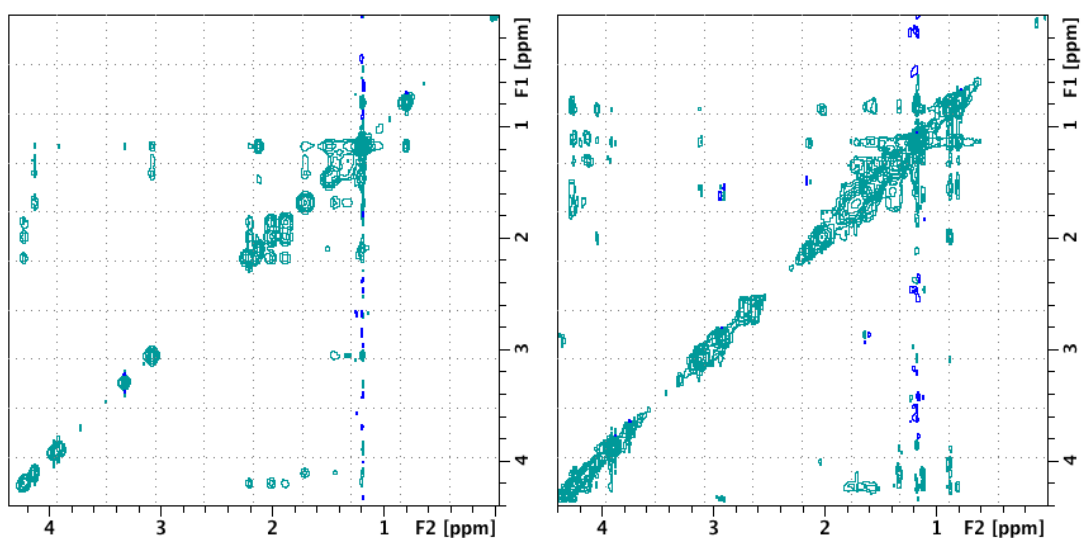
Figure A3.21. NOE NMR analysis of Dil-PA (left) and HABPA-7 (right) in D_2O at 400 MHz. The negative peptide was supplemented with a drop of NaOH to aid solubility

Chapter 4 Physical, Chemical, Biological and Binding Properties of Hyaluronan Glycopolymers

4.1. Introduction

As previously mentioned, HA has many important functions in the human body. It is believed that some of these functions are derived from its physico-chemical properties, including high viscosity and polyelectrolyte behaviour. At physiological pH, the carboxylic groups of GlcA are unprotonated and HA displays a negative charge which is 1 nm apart[1]. In the first half of this chapter, the HA-based glycopolymers are compared to natural HA in terms of physical properties, such as viscoelasticity, charge and conformation. A second group of HA glycopolymers were also synthesised from an acrylate backbone. These were compared to styrenic glycopolymers and HA to determine the effect of the polymer backbone upon their physical properties.

The alternating structure of HA might be important for the binding to specific HA-binding proteins such as CD44, LYVE-1 and TSG-6, but the role of each HA sugar in the binding process is not completely clear. For example, are both sugars essential for the binding and is the order necessary? Using the diverse HA glycopolymers described in chapter 2, their binding to a group of selected molecules was probed using SPR. In order to do this, HABPeps[2-3] described in chapter 3 were functionalized with a thiol terminus group to allow their immobilisation onto the surface of a gold (Au) chip.

Carbohydrates in the body are known to be recognised by cell surface receptors, such as lectins. The interaction between lectins and carbohydrates are responsible for a plethora of biological processes such as pathogen invasion, immune system activation and cell proliferation. Predominantly found on the cell surface, lectins elicit a weak cellular response when binding to a carbohydrate. These multivalent interactions cause the lectin to initiate a larger cellular response, thus triggering downstream effects from the system, which in most cases leads to an immune response. Upon the binding of a single monosaccharide, a weak response is produced by the lectin. However, many of these carbohydrate-binding proteins exist as dimers, trimers and higher orders of oligomers, therefore they have sites to bind as multiple carbohydrates. By increasing the local concentration of the carbohydrate on a glycopolymer, the lectins on the cell surface can bind multiple carbohydrates, known as the multivalent effect[4]. When binding multiple lectin domains simultaneously a large response is elicited leading to a response from the system such as cytokine release leading to downstream effect through cell signalling (Scheme 4.1). This multivalency leading to a larger system

response is known as produces a "cluster-glycoside effect". C-type lectins predominantly bind through the C4 and 3 hydroxides in the equatorial position mediated by a metal ion such as calcium[5].
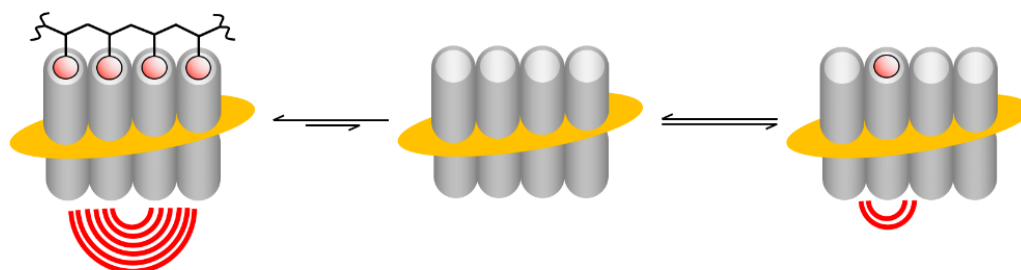
Scheme 4.1. Schematic representation of the cellular response from the lectin upon reversible binding of a single saccharide compared to the binding of a glycopolymer with multiple saccharides. Adapted from Ref[4]

Glycopolymers offer the possibility to present multiple monosaccharides to lectins in order to cause a larger response, since the glycosidic bond does not exist in these synthetic alternatives. In the last section of the chapter, the glycopolymers are used as probes to test the binding to lectins, to obtain an improved understanding of the binding. With hits for HA from to 2 of the 5 lectins tested the glycopolymers can give an improved assessment of the binding of lectins. The glycopolymers allow for a vast array of monosaccharides to be tested against multiple lections to give a better picture of the binding process to lectins as potential therapeutics.

4.2. Results and Discussion

4.2.1. Physical Properties of Glycopolymers

The properties of the synthetic HA glycopolymers (Table 4.1) were compared to those of natural HA with 20 kDa, as the glycopolymers possess a similar molecular weight. HA is water soluble and in order to be soluble in organic solvents, such as DMF or DMSO, HA requires chemical modification or ion exchange of the carboxylate counter (commonly sodium) to a larger counter-ion such as tetrabutylammonium ion (TBA). After the grafting of the sugars, the solubility of the glycopolymers switched from organic based to aqueous-based solvents, due to the large number of free hydroxides along the backbone of the polymer.

Table 4.1. Summary of polymers from Chapter 2.

Polymer		Type	M_n (g mol^{-1})		Đ[b]
			Theo[a]	GPC[b]	
P1	pVBC$_{56}$	Homopolymer	12800	13100	1.13
P2	pVBAz$_{56}$	Homopolymer	13400	13400	1.20
P3	pVB-Glc$_{56}$	Glycohomopolymer	32000	4400	1.07
P4	pVB-Man$_{56}$	Glycohomopolymer	32000	4400	1.08
P5	pVB-Gal$_{56}$	Glycohomopolymer	32000	4300	1.04
P6	pVB-GlcNAc$_{56}$	Glycohomopolymer	36000	6900	1.13
P7	pVB-GlcA$_{56}$	Glycohomopolymer	35000	6300	1.02
P8	pVB-GlcA$_{23}$-co-VB-GlcNAc$_{23}$	Statistical Glycocopolymer	35500	4100	1.04
P9	pVBC$_{24}$-alt-TMS PMI$_{24}$	Alternating Copolymer	12800	19500	1.57
P10	pVBAz$_{24}$-alt-TMS PMI$_{24}$	Alternating Copolymer	19900	18300	2.40
P11	pVB-GlcNAc$_{24}$-alt-PMI$_{24}$	Alternating Glycocopolymer	27000	4800	1.02
P12	pVB-GlcNAc$_{24}$-alt-PMI-GlcA$_{24}$	Alternating Glycocopolymer	40000	5700	1.06

[a] ^{1}H NMR (400 MHz, d-DMSO), [b] DMF + 5 mM NH$_4$BF$_4$ eluent, calibrated with PS standards.

4.2.1.1. Viscoelastic Behaviour

HA is used as a viscoelastic supplement in conditions such as osteoarthritis, with injections into the knee to relieve symptoms. In solution, HA acts as a non-Newtonian liquid with viscoelastic properties which arise from the HAs elongated linear structure, aid by the glycosidic bond and reinforced with intramolecular hydrogen bonds (Scheme 4.2) causing the polysaccharide to become semi-flexible. When shear is applied to non-Newtonian fluids, their viscosity decreases with increased in shear rate and this behaviour is known as shear-thinning. Rheological data of natural HA shows a correlation between viscosity and the molecular weight (Figure 4.1A) matching

trends seen in literature[6]. HA with 20 kDa presents an average viscosity of 1.3×10^{-3} Pa·s and the shear-thinning effect is negligible.
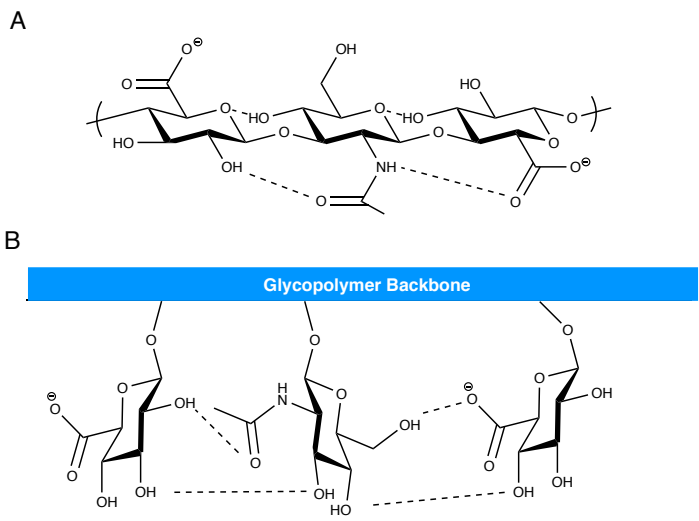
Scheme 4.2. Schematic representation of a HA dimer with an addition GlcA showing the internal hydrogen bonding represented by the dotted lines (A) and purposed hydrogen bonding within P12 (B).

In contrast, the glycopolymers do not bare multiple glycosidic bonds between saccharides, but a single glycosidic bond with an alcohol (e.g. propargyl alcohol and 2-azidoethanol) used to click onto the polymer backbone. While the glycopolymers lack the glycosidic bonds of HA, there is still the possibility for intra and intermolecular hydrogen bonds between the saccharide pendant groups. The lack of glycosidic bonds in the glycopolymers causes a detrimental effect on the viscosity when compared to 20 kDa HA with a four-fold decrease due to the increased flexibility (Figure 4.1B). Comparing the viscosity among the glycopolymers, higher viscosity is seen for P7. This infers that the carboxylic acid group of GlcA in a regular repeating structure is forming stronger intra/intermolecular hydrogen bonding. From the trends observed in the viscosity with increasing molecular weight of HA infers a longer polymer backbone will increase viscoelastic like properties from the mimics.
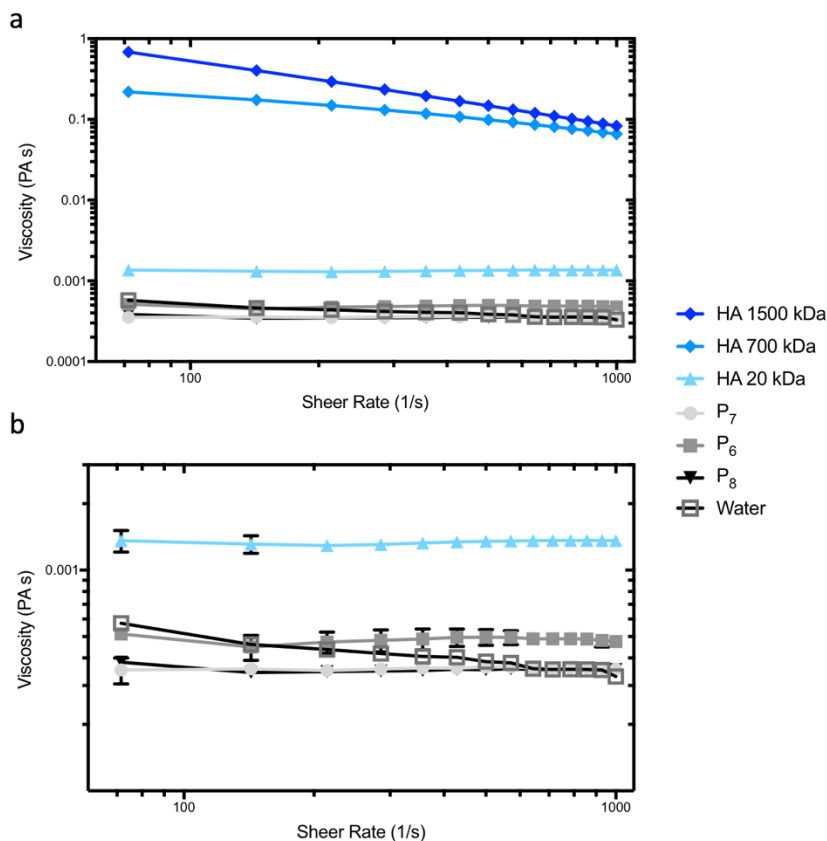
Figure 4.1. Viscosity versus shear rate of HA (1%. wt), glycopolymers solutions (1%. wt) and water (A) with a zoom of the lower viscosity results (B).

The rheology data, as well as the data found in literature, indicates a dependence of viscosity with molecular weight and concentration. By setting one of the parameters as constant and increasing the other, an increase in viscosity of HA solutions is observed[7-8]. Increasing the concentration of the glycopolymers would lead to increase in viscosity but would require concentrations greater than 3%. There is a relation of R^3 dependency on the viscosity (η) in Equation 4.1, where R is root-mean-square end-to-end distance and N is the number of monomers.

$$[\eta] \cong R^3/N$$

Equation 4.1

Since the overall length of the polymer leads to a cubic increase on the viscosity, polymerisation was attempted to create large polymers. By increasing the ratio of monomers to initiator and RAFT agent, large polymers could be produced, but the Đ becomes broader through by this method (Figure 4.2).
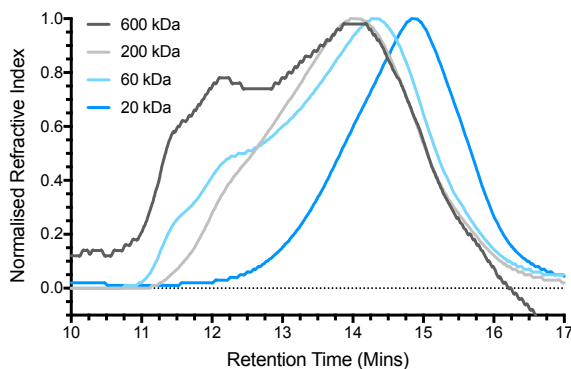
Figure 4.2. Normalised GPC traces of the polymerisation results of various different polymers with increasing Mw to mimic 20, 60, 200 and 600 kDa HA showing a loss in control of dispersity upon scaling the polymerisation.

Consequently, the chain extension was tested over direct polymerisation. Products of RAFT polymerisation retain the reactive C-S bond which can fragment to release the chain for further polymerisation as a macroinitiator. By this method a further degree of control is achieved as there is not a large excess of monomers in the solution. Using an alternating polymer of VBC and TMS PMI with an Mw of 11800, the chain was extended to 21800 while retaining a narrow Đ, from 1.23 to 1.30 (Figure 4.3).
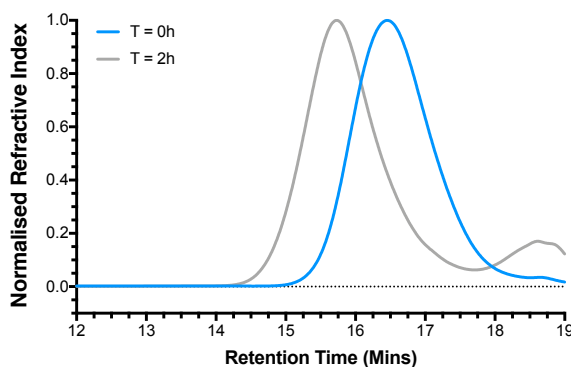
Figure 4.3. Normalised GPC traces of the polymerisation results of VBC and TMS PMI by chain extension.

A small peak was observed at 18.5 minutes from unreacted TMS PMI, which caused the slight broadening in the peak. The ability to chain extend the polymer has the potential to synthesis longer glycopolymers to begin to rival the size of HA whilst maintaining a low Đ. This proof of concept is promising but current controlled radical polymerisation techniques of complex monomers still lags behind the capabilities of enzymes.

4.2.1.2. Polyelectrolyte Behaviour

In aqueous solutions, HA also behaves as a polyelectrolyte (PE) due to the presence of carboxylates 1 nm apart. This negative charge across HA gives a large negative ζ-

potential of -20.08 mV. For the synthetic glycopolymers, a negative ζ-potential is also observed for those polymers containing a GlcA residue. In contrast the homopolymers of P3-6 show a neutral ζ- potential (Figure 4.4).
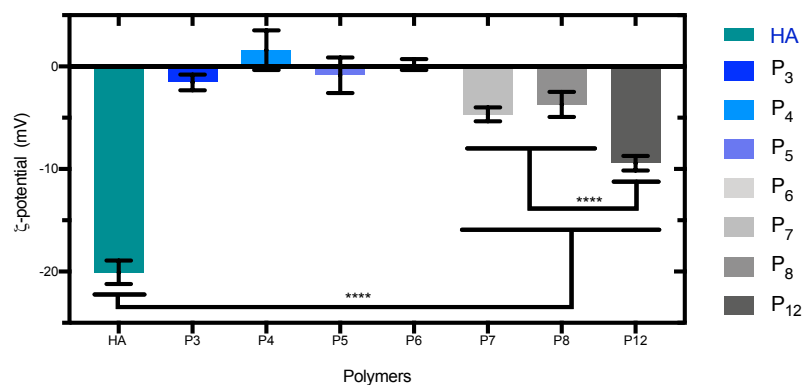
Figure 4.4. ζ-potential of the glycopolymers compared to HA. Analysed by two-way ANOVA analysis, where * significant at $P < 0.0332$, ** significant at $P < 0.0021$, *** significant at $P < 0.0002$ and **** significant at $P < 0.0001$.

The ζ-potential values also provide information on the stability of the aggregates formed. HA has the largest negative potential, due to the regularity of the negative charged is place across the polysaccharide. P7 and P12 also have regular negative charge however due to a smaller proportion of the molecule is charged the ζ-potential is lower compared with HA, which has a higher charge density. P7 and P8 show no significant difference on their negative charge. In P7, GlcA is placed regularly across every unit whereas in P8 the GlcA being placed randomly across the polymer chain. The charge density on P12 is significantly greater than the one for P7 and P8. The even distribution of the GlcA spaced by a GlcNAc in P12 leads to a higher stability of the negative charge. This suggests a low repulsion caused by alternation of a charged saccharides and non-charged saccharide within P12.

The differences between the glycopolymers charge and HA is also evident in their small angle X-ray scattering (SAXS) patterns (Figure 4.5). The scattering pattern of natural HA exhibits a peak at 0.04 A^{-1} which is characteristic for the scattering of salt-free polyelectrolyte solutions. This peak, often referred to as a 'correlation peak', represents an average distance between the charged domains in solution (i.e. the HA chains)[9-10]. Although negative, the scattering patterns of P6, P7, P8 and P12 do not display a correlation peak. A qualitative analysis of the glycopolymers scattering patterns yields a power law dependence of the scattered intensity on q with an exponent of ~ -0.8 indicative of a short cylindrical object.
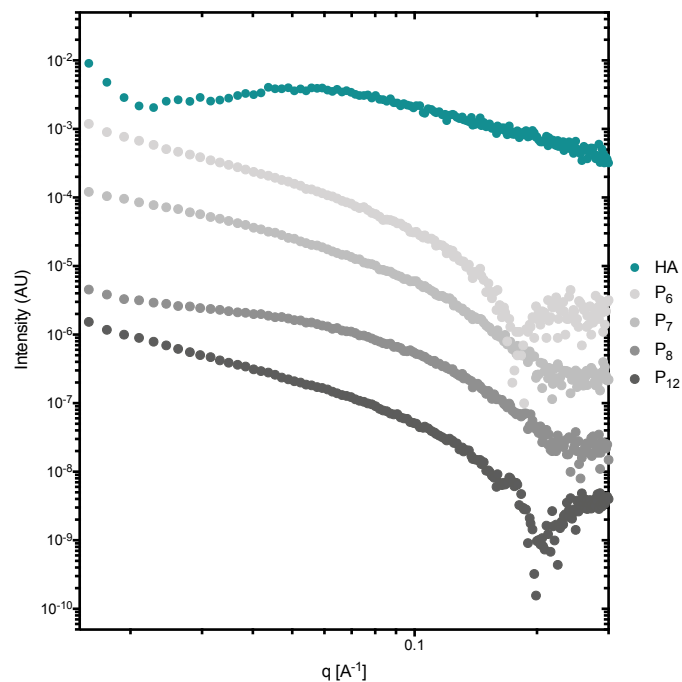
Figure 4.5. SAXS patterns for HA and glycopolymers at 0.2 mM at pH 7 with each line offset by factors of 10.

The scattering of P6, P7, P8 and P12 could be fitted to a semi-flexible chain model[11] Equation 4.2 which describes a chain comprised of a series of locally stiff segments by three parameters b - Kuhn's length, a measure of the chain's flexibility, L - the chain's contour length, and R - radius of the chain's cross section.

$$P(q,b,L,R_{cs}) = P_{exv}(q,b,L) + C(L/b)\frac{b}{15L}\left[4+\frac{7}{u}-\left(11+\frac{7}{u}\right)e^{-u}\right]\cdot\left[2\frac{J_1(q,R_{cs})}{q,R_{cs}}\right]$$

Equation 4.2

The best fit to the model is presented as solid lines in the appendix (Figure A 4.1), and the best-fit parameters are given in Table 4.2. For the different glycopolymers, the Kuhn length (~50 Å) and the radius (~15 Å) parameters are similar suggesting that the flexibility of the chains does not change. The result of the physical studies are summarised in Table 4.3.

Table 4.2. Parameters from the SAXS fitted models for the glycopolymers

Glycopolymer	Kuhn length (Å)	Radius (Å)	Contour Length (Å)
P6	51	16	700
P7	49	16	660
P8	50	15	570
P12	52	15	700

Table 4.3. Summary of properties of glycopolymers

Polymer	R	Type	ζ-potential (mV) [a]	CAC (nM) [a]	PE [b]
HA	GlcNAc & GlcA	Natural Polysaccharide	-20.07 ± 1.44	n/a	Y
P3	Glc	Homo-glycopolymer	-1.55 ± 0.76	550	n.m.
P4	Man	Homo-glycopolymer	1.59 ± 1.93	630	n.m.
P5	Gal	Homo-glycopolymer	-0.86 ± 1.73	< 1	n.m.
P6	GlcNAc	Homo-glycopolymer	0.18 ± 0.53	85	N
P7	GlcA	Homo-glycopolymer	-4.67 ± 0.67	3200	N
P8	GlcNAc & GlcA	Statistical Glycopolymer	-3.70 ± 1.21	2100	N
P12	GlcNAc & GlcA	Alternating Glycopolymer	-9.98 ± 0.71	830	N

R = Side Chain. PE = Polyelectrolyte. n/a = not applicable. n.m. = not measured. [a] measured in H_2O at pH 7. [b] measured by correlation peak on SAXS.

4.2.1.3. Conformation

According to the GPC results (Table 4.1), the glycopolymers showed a reduction in the molecular weight and Đ compared to the polymers before grafting. This may infer degradation of the polymer but there is no sign of degradation seen in the ^{1}H NMR. The GPC measures the size of the polymers by their hydrodynamic volume and using calibrations the molecular weight can be determined. All the glycopolymers showed a CAC point inferring the glycopolymer aggregates forming a hydrophobic pocket (Figure 4.6A). This change in the glycopolymer conformation explains the inconsistent behaviour in the GPC upon the addition of the monosaccharides.

Interestingly, it was not possible to determine the CAC for P5 as the glycopolymer has already formed an aggregate according to the wavelength maxima at 620 nm as well as increased turbidity of the solution (Figure 4.6B), with the highest concentration tested, 0.1 nM, forming a pink solution.
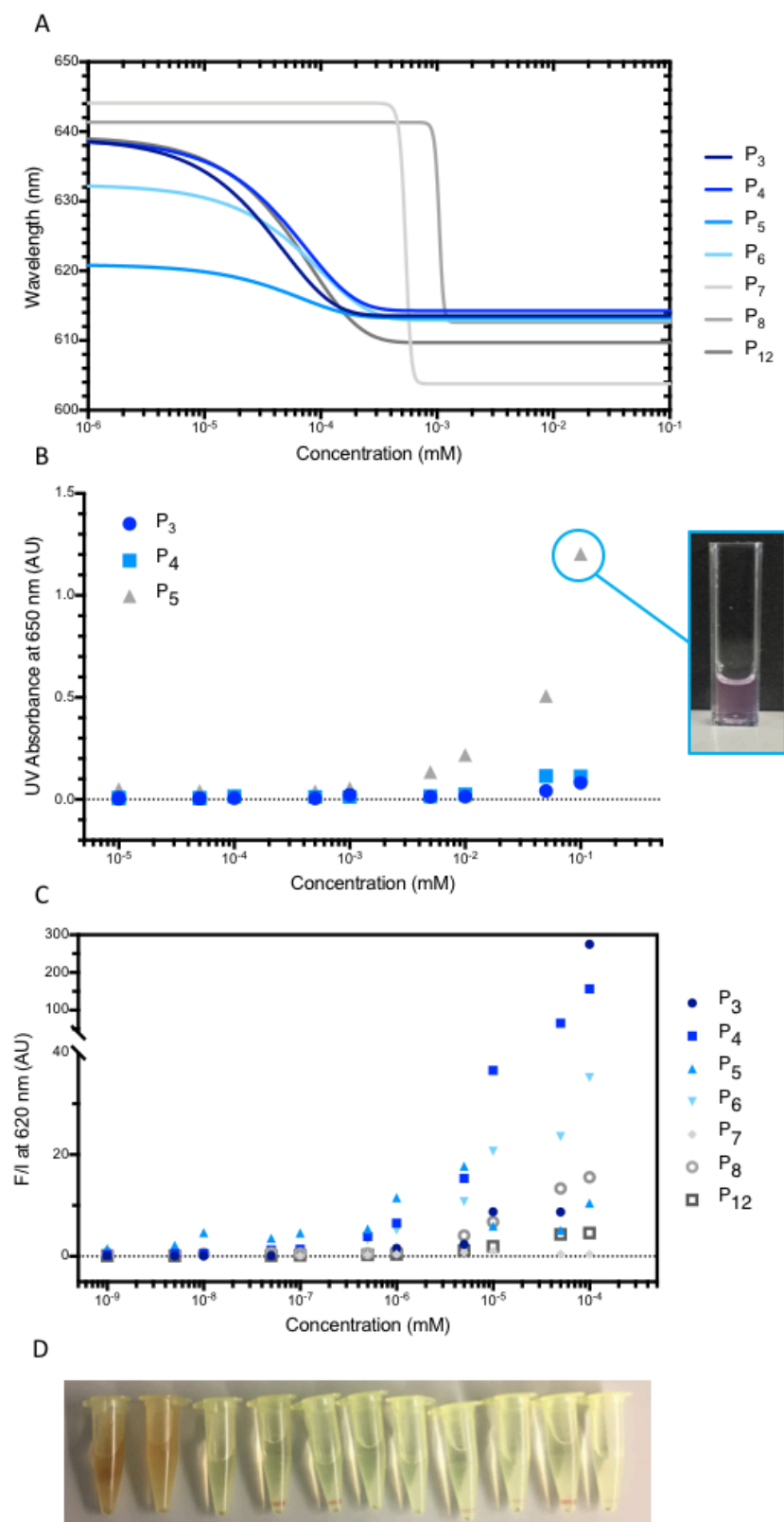
Figure 4.6. Nile Red assay of the glycopolymers (A), turbidity measurements at 650 nm (B) with insert of P5 dyed with Nile Red at 0.1 mM, The fluorescent output of the Nile Red in the glycopolymer solutions at 620 nm (C) and P7 insolubility at pH 3 (D).

For those glycopolymers which bare a GlcA monosaccharide a later CAC point is seen due to the electrostatic repulsion of these monosaccharides as well as an overall decrease in fluorescence output by P7 and P8 (Figure 4.6C). By comparison, the CAC of P12 is reduced compared with P7 and P8 following the trend of the uncharged glycopolymers. The two factors that contribute to the reduction of the CAC. Firstly, increasing the distance between the charged monosaccharides leads to a reduction in repulsion and secondly the benzyl rings are not adjacent leading to a reduction in π-π stacking. These two factors could be the cause for the lowering of the CAC to values seen for the other non-GlcA glycopolymers. Attempts to screen the charge of the polymers containing GlcA using HCl to lower the pH, led to the formation of aggregates, which crashed out of solution (Figure 4.6D).

The glycopolymer aggregates were imaged using TEM (Figure 4.7A-D) at pH 7 and 1 mM to ensure all the glycopolymers were above the CAC. All the glycopolymers tested showed the ability to form spherical aggregates of different sizes (Figure 4.7E). These spherical structures can arise due to the differences in hydrophobicity across the polymer. The styrenic, RAFT group with the alkyl tail and/or maleic anhydride backbone are not water soluble and aggregate through hydrophobic interactions including π-π stacking between the adjacent styrene rings. The aggregates formed by the glycopolymers containing GlcA show a significantly lower mean diameter than those formed by the homopolymer of GlcNAc (P6) when measured using Image J (Figure 4.7E). This trend is also seen by DLS (Figure 4.7F) as P6 maximum is higher than that of any the GlcA-containing glycopolymers. The largest spread of sizes in the DLS was observed for the P6 with the largest error in measurement. This result, together with the values of ζ-potential (Figure 4.4) showing the negative charge of the GlcA-containing glycopolymers can be associated with charge on the surface of the aggregate, but it is also a competition between the hydrophobicity of the backbone against the charge-charge repulsion. This charge-charge repulsion causes the higher CAC observed for P7 and P8 (Figure 4.6A). The charge inhibit aggregation with multiple glycopolymer chains. In the absence of the charge repulsion, the non-charged, P6 can aggregate with multiple glycopolymer chain in solution to form a larger aggregate. This aggregation is not restricted by charge and therefore causes a larger distribution of sizes observed with a large associated error. When screening the charge of the GlcA-containing polymer, P7 shows aggregation which causes the precipitation of the glycopolymer into the solution as the aggregation is no longer governed by charge repulsion (Figure 4.6D).
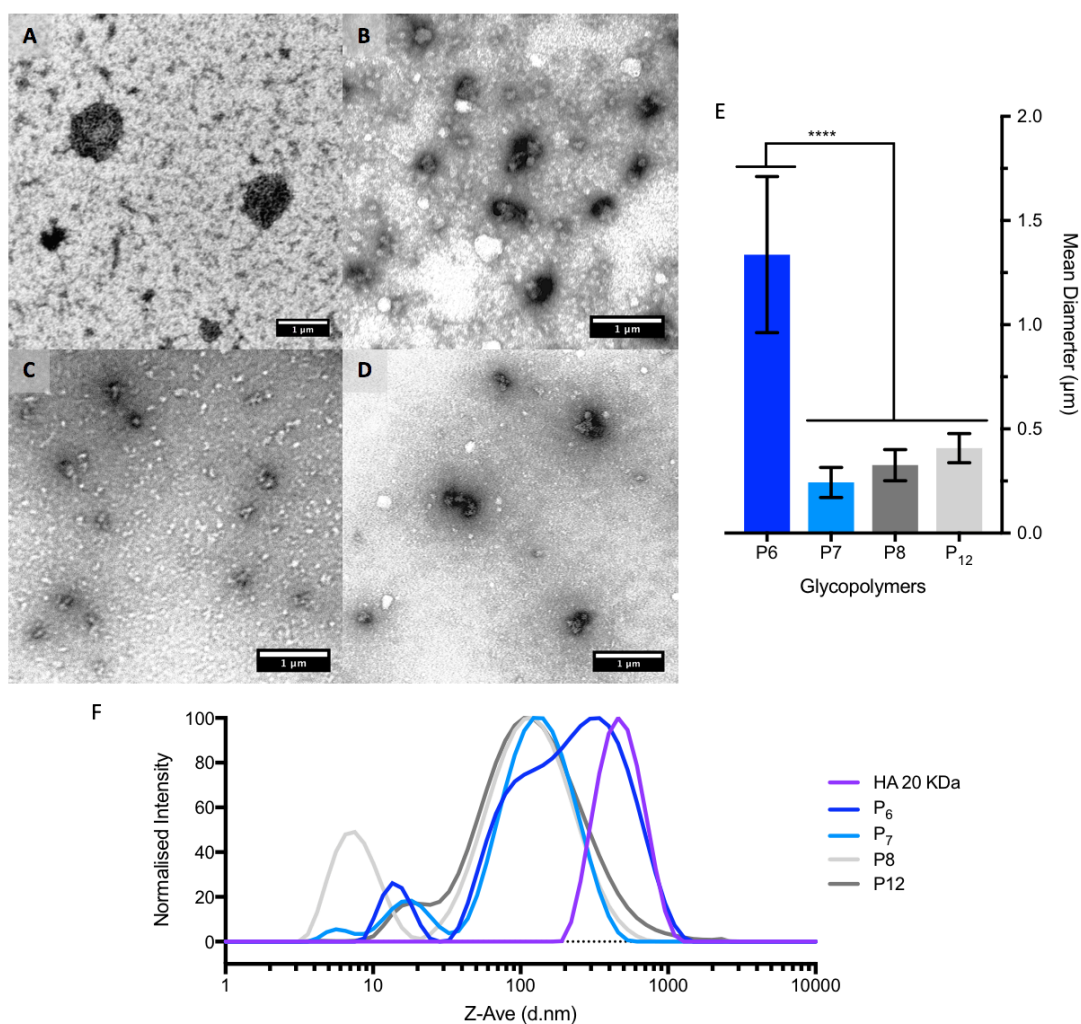
Figure 4.7. TEM images of the glycopolymers at 1 mM and pH 7 for (A) P6, (B) P7, (C) P8 and (D) P12 with the mean size distribution (E) of the formed aggregates measured by ImageJ analysis. DLS (F) of the glycopolymers at 0.1 mM and pH 7. Analysed by two-way ANOVA analysis, where * significant at $P < 0.0332$, ** significant at $P < 0.0021$, *** significant at $P < 0.0002$ and **** significant at $P < 0.0001$.

The size of the glycopolymer aggregates seen in the TEM images is two orders of magnitude higher than those obtained from the SAXS (Figure 4.5). TEM was performed on dried samples while SAXS is done in solution. The drying process in TEM increases the polymer concentration inducing their aggregation into larger particles. Cryo-TEM could be an alternative to obtain images of the glycopolymer aggregates in the solution state through a thin film of vitrified solvent. The styrenic backbone was postulated to be the cause of aggregation seen for the glycopolymers. Therefore, a new class of glycopolymers was synthesised to determine if the backbone was restricting the glycopolymer from acting as a polyelectrolyte.

4.2.2. Acrylate-based Glycopolymers

The acrylate polymerization system presents an alternative to the styrene-based polymers. The acrylate is a monomer two orders of magnitude more reactive than styrene[12] at 30 °C (Table 4.4). The monomer is more flexible when we consider the functionality orthogonal to the polymerisable group compared to the benzene ring of a styrene monomer.

Table 4.4. Propagation rate coefficients of different monomers at 30 °C[12]

Monomer	k_p (mol^{-1} s^{-1})
Dimethyl itaconate	11
Ethene	16
Methacrylonitrile	20
1,3-Butadiene	57
Styrene	160
Methyl methacrylate	390
Chloroprene	500
Vinyl Acetate	3000
Methyl Acrylate	15000

4.2.2.1. Homoglycopolymers

The monomer was synthesised by the coupling of acryloyl chloride with 2-bromoethanol to form bromoethyl acrylate[13] (BEA, **20**) (Scheme 4.3). In the ^{1}H NMR for **20**, a small shift is seen between the conjugated alkene of the acryloyl chloride and the pair doublet of the 2-bromoethanol in the product **20**. The monomer was polymerised using the same RAFT protocol as VBC monomer to form poly bromoethyl acrylate (pBEA, P13) (Table 4.5).

Table 4.5. Polymerisation of acrylate-based glycopolymers

Entry	Polymer	Reaction Type	Time (h)	ρ (%)	$M_{n,}$ (g mol^{-1}) Theo [a]	GPC [b]	Đ [b]
P13	pBEA	RAFT	2	60	10800	9800	1.26
P14	pAEA	Azidation	5	>99	7500	10700	1.40
P15	pEA-GlcNAc	CuAAc	16	>99	32000	3100	1.05
P16	pEA-GlcA	CuAAc	16	>99	32000	2400	1.05

[a] ^{1}H NMR (400 MHz, DMSO), [b] DMF + 5 mM NH$_4$BF$_4$ eluent, calibrated with PS standards.

The GPC traces showed the high molecular weight shoulder similar to the styrene family of glycopolymers on azidation (Figure 4.8A). The azidation caused a shift in the pair of the CH_2's in the pendant group and in the ^1H NMR upfield due to change from an electron withdrawing halide to an electron donating azide (Figure 4.8B), with a peak at 2096 cm^{-1} for the azide on the FT-IR (Figure 4.8C).
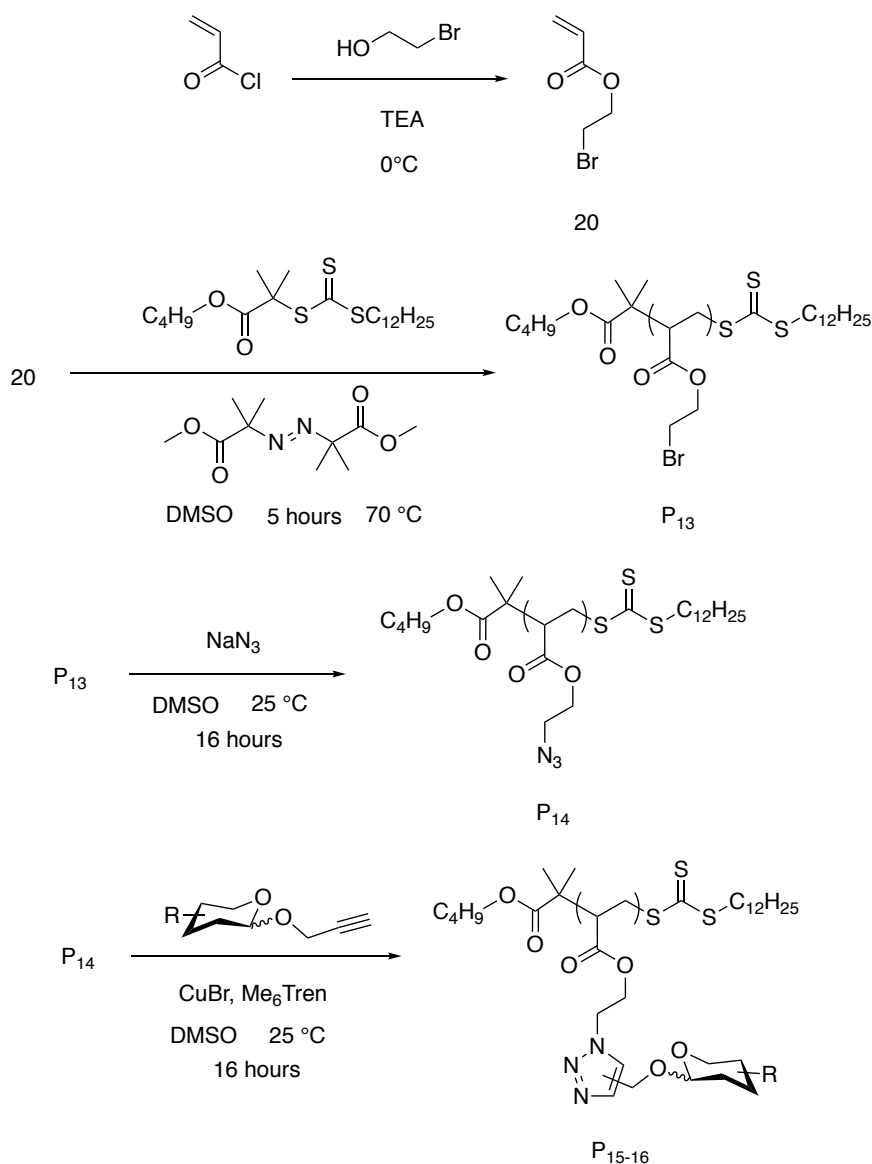
Scheme 4.3. Schematic representation of the synthesized acrylate-based glycopolymer via RAFT polymerisation, azidation and finally CuAAC

Using the CuAAc determined previously, the sugars of **4** and **10** were grafted onto the pendant azide group of P14. In both cases, the ^1H NMR showed the shift of the pair of CH_2 with the change of environment again, as well as the addition of the triazole peak at 8.00 ppm. The FT-IR also shows a loss in the azide peak at 2096 cm^{-1} due to the consumption of this group during the CuAAC reaction.
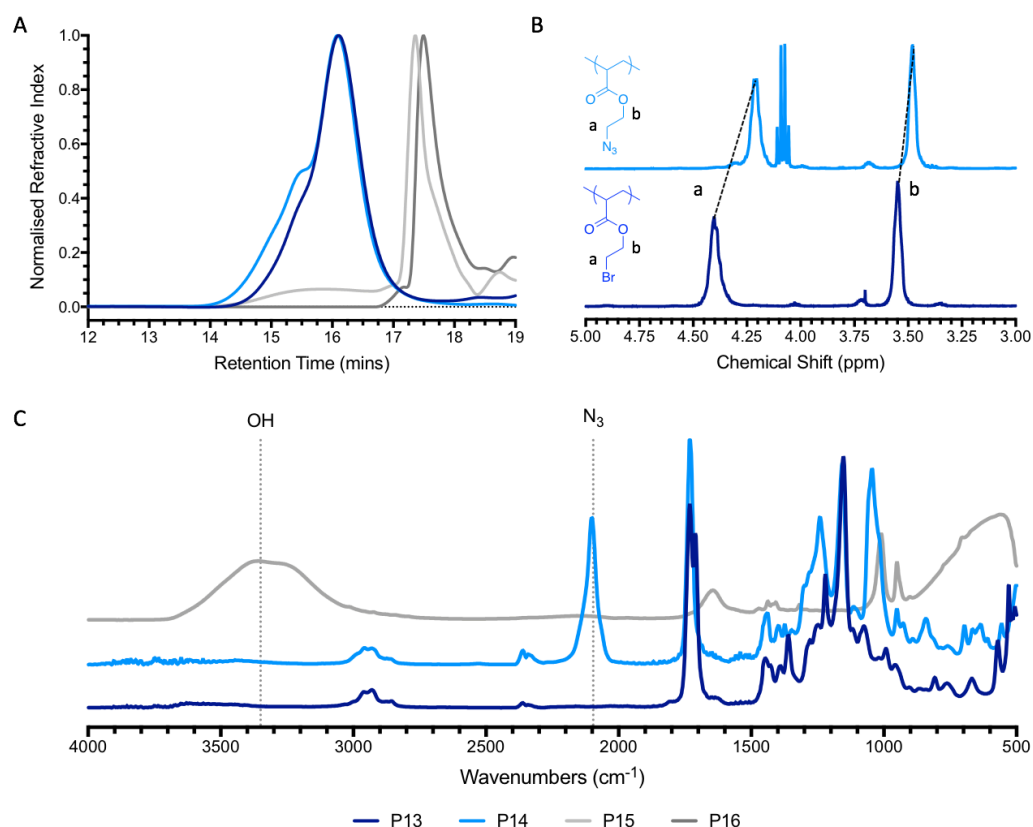
Figure 4.8 Results of the formation of the acrylate glycopolymer P15 and P16 by GPC (A), ^{1}H NMR at 400 MHz in *d*-Acetone (B) monitoring the two CH$_2$ of the ethyl group from P13 to P14 and FT-IR (C) highlighting the azide and OH peaks.

4.2.2.2. Dual Acrylate Glycopolymers

While substantial research has been developed around the styrene-maleic anhydride system, less has been carried out on alternating polymers with acrylates. The monomers reactivity and polarization affects the ability for the co-monomer polymerisation to alternate, as an electron acceptor monomer with a low electron density, such as maleimide, will preferentially react with an electron donating substituent such as a styrene that with itself[14]. Therefore, for an alternating polymer to be successful, rather than producing a statistical polymerisation it must have a low propensity to hompolymerise. The low polarity of the acrylate bond results in being a poor monomer to produce an alternating polymer, unless a Lewis acid[15] or complex reagents[16-17] are present. Instead, the formation of glycomonomer based on an acrylate, which can bare two monosaccharides which would not require any complex alternating acrylate polymerisation is a more suitable approach[18-21]. Examples of this type of acrylate exists for monomers containing the same sugar twice, typically using a thiol-alkyne reaction for a double substitution. Conversely, in this work two different

monosaccharides would be required to be synthesised on the same monomer. Epihydrins are molecules containing a ring stained epoxypropane as well as a halide group. Examples from the literature shows the use of NaN_3 to ring open and form an asymmetric molecule which bares an azide for click chemistry with the potential for a second click reaction (Scheme 4.4).
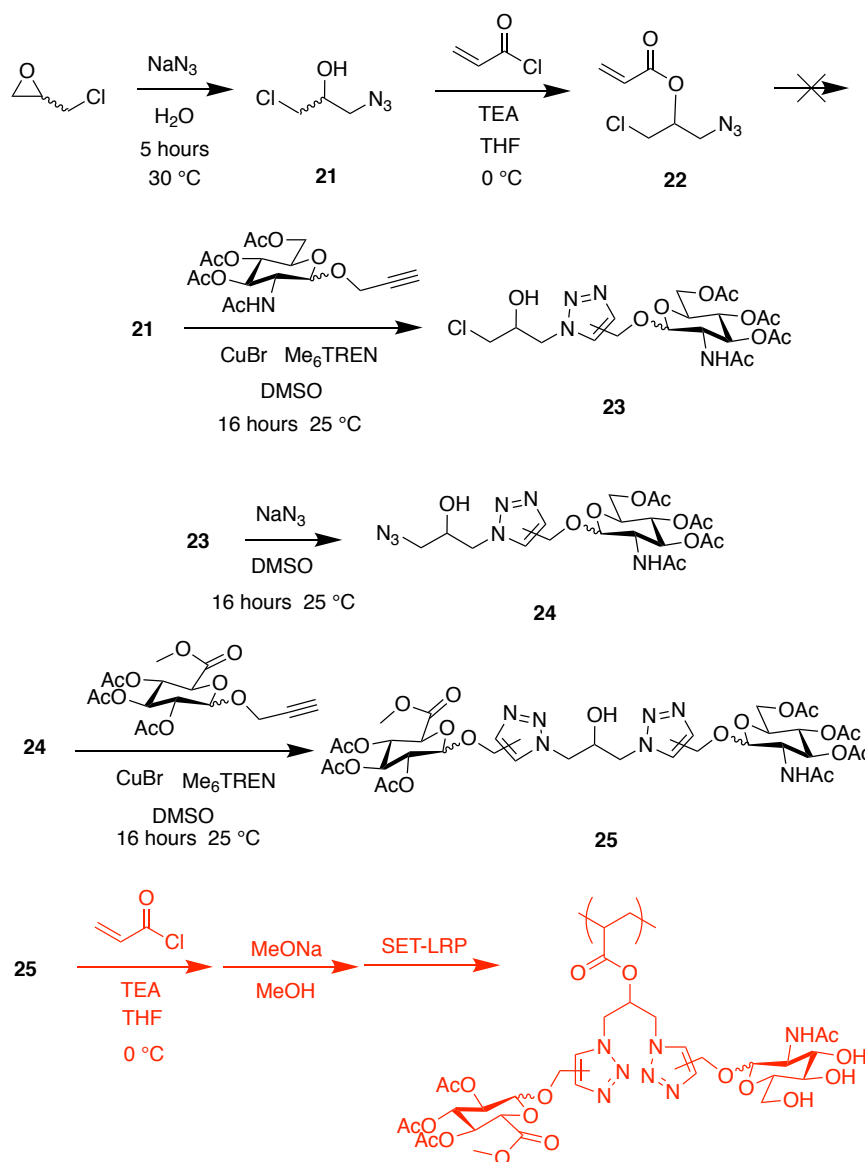
Scheme 4.4. Schematic representation of the synthesized acrylate-based glycopolymer from (±) epichlorohydrin, with (red) synthetic pathway to be verified.

The ring opening of the epibromohydrin can be monitored by ^{1}H NMR and FT-IR as the azide is introduced. The ^{1}H NMR shows an asymmetric splitting in the alkyl hydrogen due to the different groups adjacent to them (Figure 4.9A). Initially, **21** was coupled to acryloyl chloride in the reaction used to synthesise **20**, to form **22** in order to synthesise the monomer without the requirement to protect the hydroxyls of the

saccharides. However, the monomer was unstable and auto-polymerised. The autopolymerisation in the presence of an azide in situ causes a broad uncontrolled polymer, similar to that seen with VBAz (Table 2.5).
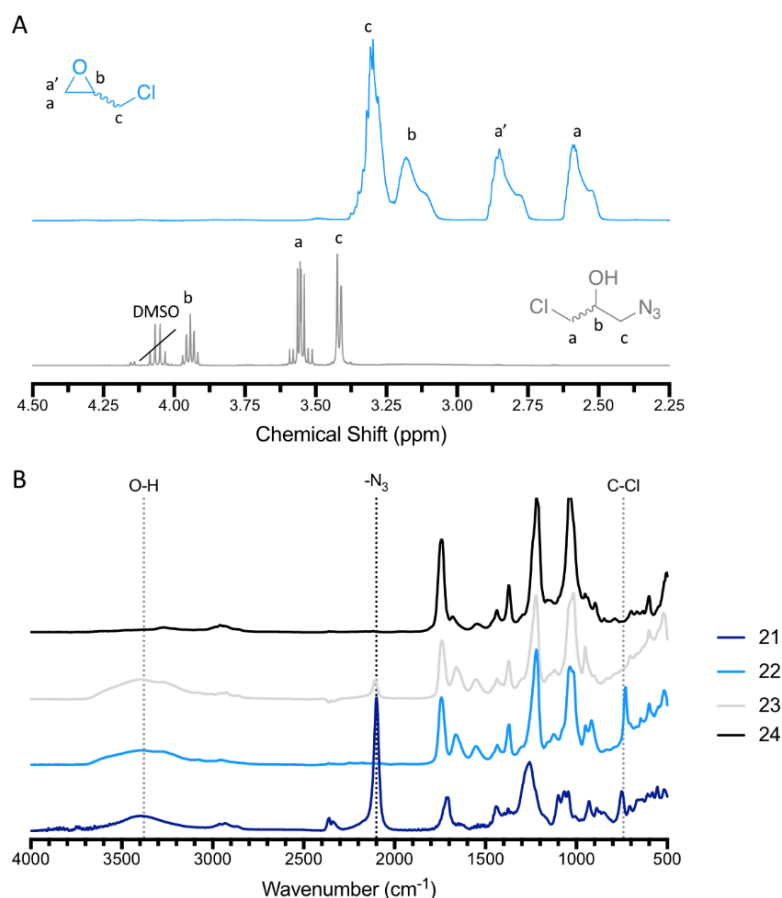
Figure 4.9. Monitoring of the formation of **21** by ^{1}H NMR in *d*-Acetone at 400 MHz (A) of (±) epichlorohydrin (top) and 1-azido-3-chloro-propan-2-ol (bottom) showing the asymmetric product formed by the equivalency of alkyls adjacent to the secondary alcohol and FT-IR (B) of compounds **21** to **24** showing the addition and consumption of the azide at 2098 cm^{-1}.

By reordering the synthesis to incorporate the monosaccharides first, followed by the addition of the polymerisable group, this would avoid any auto-polymerisation. Using FT-IR, the azide production and consumption can be monitored from compound **21** to **24** (Figure 4.9B). The consumption and formation of the azide is clear with a peak at 2098 cm^{-1}. On the formation of the second azide, a loss in the C-Cl is observed at 725 cm^{-1}. Upon the addition of the second acetylated monosaccharide, the broad peak between 3200 – 3600 cm^{-1} is reduced as the hydroxide is blocked from hydrogen bonding due to the sterics around the hydroxide. The ^{1}H NMR becomes challenging as the complexity of increase molecule due to the region between 3.0 ppm to 5.0 ppm being incredibly crowded due to the sugar hydrogens, which upon adding the second

monosaccharide become a large multiplet. The ^{1}H NMR however, does show an increase intensity of the triazole peak upon addition of the second monosaccharide through CuAAc coupling.

Further work needs to be undertaken on the diacrylate monomer in order to verify the successful synthesis of the compound before the addition of the acryloyl chloride and deprotection of the sugar acetyl groups. There is concern over the use of MeONa due to the potential of hydrolysis of the ester bond in the acrylate at the same time.

4.2.2.3. Physical Properties of Acrylate Glycopolymers

Using the acrylate homoglycopolymers, SAXS was used to determine if the polymer backbone was the cause for lack of polyelectrolyte behaviour. The polymers show no sign of a CAC, from 1 nM up to 1 mM, confirming the backbone of the styrene polymers has an effect on the conformation of these glycopolymers in solution. There is a significant increase in the negative ζ-potential of the P16 compared to the styrene based glycopolymer P7 (Figure 4.10).

The increased flexibility of the alkane chain between the polymer, as well as the lack of aggregation, will allow the charge to distribute evenly over the polymer by repelling the monosaccharides which is not available to the rigid styrene homopolymers. Although the charge of the acrylate-based glycopolymers is still significantly lower than HA, the increase in negative charge suggest that the acrylate backbone may be suited better to mimic HA in terms of the larger negative ζ-potential.
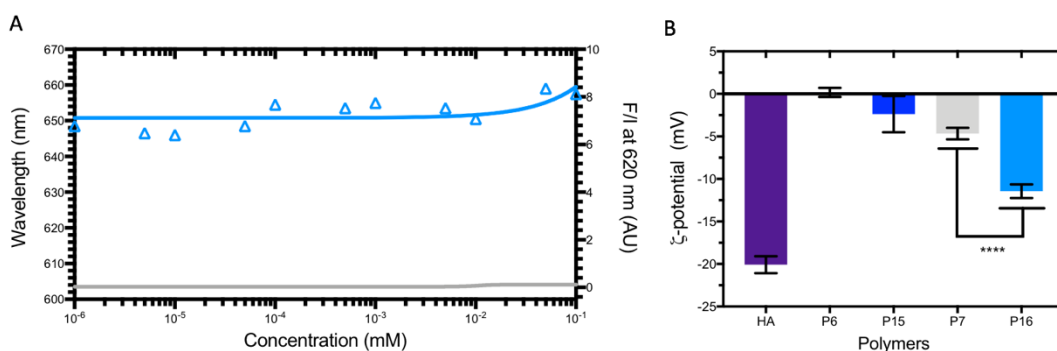
Figure 4.10. Fluorescence output of Nile red (A) with increasing concentrations of P16; ζ-potential (B) of the glycopolymer comparing the styrene homopolymers of P6 and P8 to their acrylate counterparts of P15 and P16. Analysed by two-way ANOVA analysis, where * significant at P < 0.0332, ** significant at P < 0.0021, *** significant at P < 0.0002 and **** significant at P < 0.0001

The more flexible linker between the polymer backbone and the saccharides produces for P16 with higher negative ζ-potential in comparison to the styrene variant P7, as well as displaying the polymer as linear. However, ζ-potential still remains lower than HA with the SAXS showing no evidence of a correlation peak for polyelectrolyte behaviour (Figure 4.11).
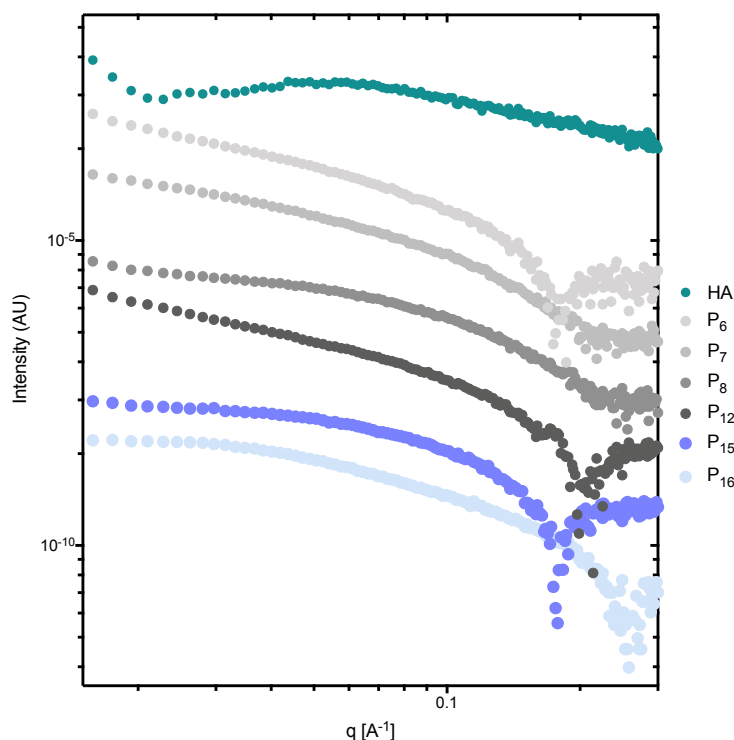
Figure 4.11. SAXS patterns for both the styrene and acrylate glycopolymers and HA at 0.2 mM at pH 7 with each line offset by factors of 10.

4.2.3. Biological Properties

4.2.3.1. Cytotoxicity

Before using the glycopolymers in biological applications, they must first be tested for their cytotoxicity. The monomers of VBC[22], as well as maleimides[23], are known to be toxic compounds, but many glycopolymers reported in the literature are known to be non-toxic. This reduction in toxicity comes from the biocompatibility of the monosaccharide pendant groups. Luc4 cells were used due to their high expression of CD44 on the surface. Using the Luc4 cells, the cytotoxicity of the glycopolymers was assessed by supplementing them into the culture media.

Over a 24-hour period, the normalised fluorescent reading showed that P6, P7 and P12 showed no significance in the reading with the untreated control and in some case the

cell appears to have proliferated more when compared to the untreated cells (control) (Figure 1.12A) P8, the statistical polymer, shows a significant drop in the cell numbers over the 24-hour period. However, analysing the cell death over the same period. P8 does not show a higher number of dead cells, compared to the other glycopolymers and untreated cells (Figure 1.12B).
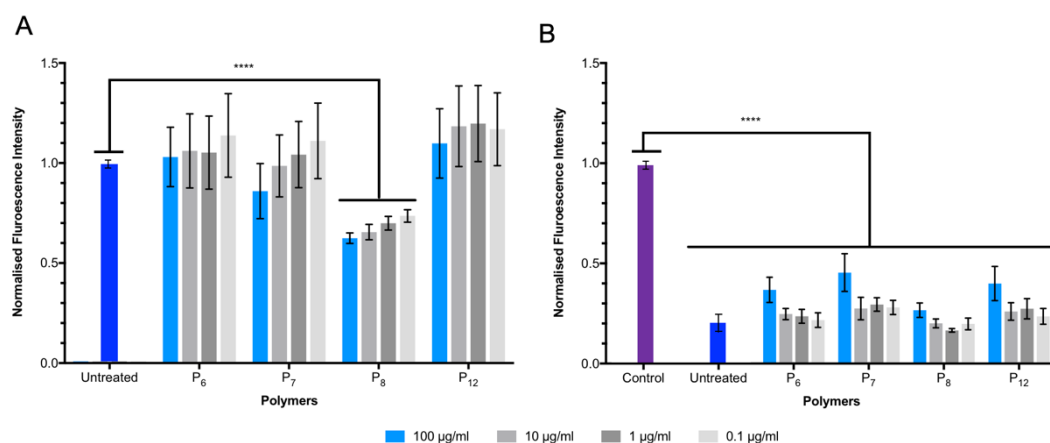
Figure 4.12. Cytotoxicity of glycopolymers at various concentrations by analysis of live cells (A) and dead cells (B) normalised against controls of untreated (live) and methanol (dead). Analysed by two-way ANOVA analysis, where **** significant at $P < 0.0001$.

4.2.3.2. Antimicrobial Properties

Cationic macromolecules such as polylysine have been shown to have antimicrobial activity, by interacting through the positive charge with the negative bacterial cell membrane causing disintegration and cytoplasmic leakage. However, this positive charge also leads to high cytotoxicity towards mammalian cells. The charge can be reduced or balanced by additional functionality such as saccharides[24]. The saccharides can also act as a targeting moiety for binding carbohydrate receptors on the bacteria[25]. The glycopolymers were tested against pathogens found in a hospital environment (Table 4.6).

It is evident from the results that the glycopolymers showed a high degree of toxicity to bacterial pathogens, whereas no inhibition was seen for the fungi tested even at the highest concentration. Since these glycopolymers have a negative ζ-potential, no antibacterial activity was expected due to the surface of many bacteria being negatively charged, causing repulsive interactions. However, due to the low negative potentials (Table 4.3) this repulsion between the glycopolymer aggregates and bacterial membrane appears not to be evident.

Table 4.6. MICs of HA-based glycopolymers against typical pathogens found in hospitals.

Entry	Polymer	MIC (ug/mL)			
		E. Coli*	P. Aeruginosa*	MRSA†	Fungi
P6	pVB-GlcNAc$_{56}$	0.78	6.25	1.56	> 25
P7	pVB-GlcA$_{56}$	0.78	12.50	3.13	> 25
P8	pVB-GlcA$_{23}$-co-VB-GlcNAc$_{23}$	1.56	12.50	3.13	> 25
P12	pVB-GlcNAc$_{24}$-alt-PMI-GlcA$_{24}$	0.78	6.25	1.56	> 25

* Gram Negative † Gram Positive

HA is not known as an bactericidal molecule but, is used as a scaffold for which cationic species such as peptides[26] to be grafted or the incorporation of metal ions[27] to form antibacterial materials. HA however, does display exhibited bacteriostatic affects dependent on the bacteria strain and Mw of HA[28-29]. Reports infer that bacteria produce hyaluronate lyase to break down HA for tissue permeability. Increased concentrations of HA leads to saturation of these enzymes and therefore slow the rate of the bacteria's tissue permeability.

4.2.3.3. Haemolytic Activity

With the glycopolymers showing low toxicity towards mammalian cells, but a high degree of toxicity towards bacteria, a haemolytic assay was carried out to determine the potential toxicity on red blood cells. As shown in Figure 4.13A, haemolysis was observed as the red colour is localised within the cells by comparison to those treated with Triton-X, which showed dispersion of red colour into the supernatant at 450 nm, due to the rupturing of the red blood cell (Figure 4.13B).

Bacteria have a different cellular organization compared to mammalian cells in terms of cell membrane composition and bacteria possess an additional cell wall. The cell membrane is composed by phospholipids, glycolipids, and proteins. In contrast, bacteria possess an addition cell wall made of a thick peptidoglycan for Gram-positive bacteria and thinner peptidoglycans with an additional outer membrane for Gram-negative bacteria. Fungi do not possess a peptidoglycan layer within the fungi cell membrane construct[30] and that only bacteria, which have this peptidoglycan within the membranes layer, showed toxicity to the glycopolymers.
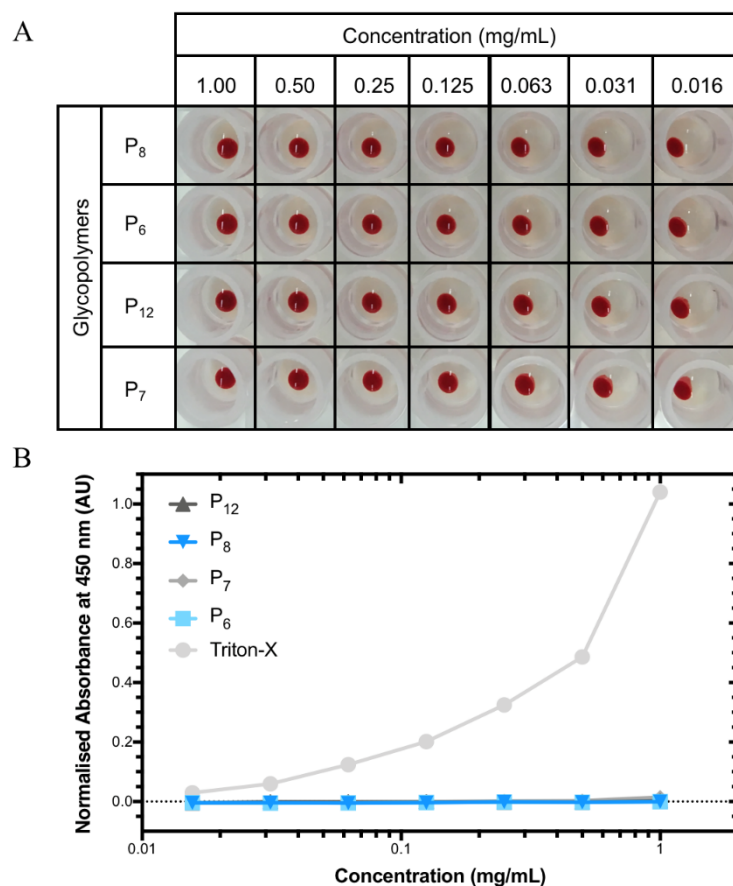
Figure 4.13. Haemolytic test for the glycopolymers with image of the intact red blood cells (A) and absorbance of the supernatant at 450 nm (B) with Triton-X control.

The glycopolymers bactericide properties might arise from their aggregated conformation, possible bacterial uptake or even the bacteria's inability to breakdown the glycopolymers but the mode of action is unclear at this stage with further studies required.

4.2.4. Glycopolymers Binding to Peptide and Proteins

4.2.4.1. Synthesis and Immobilisation of Thiolated HA-binding Peptides

Thiolate peptides enable their direct binding to a gold surface as well as other metallic surfaces without the need to chemically modify the surface. It has been shown previously that the use of cysteine at the N-terminus caused reduced surface density across the gold surface[22]. This is due to the amine of the N-terminus causing repulsive interaction due to sterics and charge repulsions. Mercapto acid terminated peptides can be produced with various lengths, not being restricted by the number of CH_2, compared with cysteine and no amine. Using the 3-mercaptopropionic acid, the thiol can be protected using 4-methoxytriphenylmethyl chloride (Mmt).
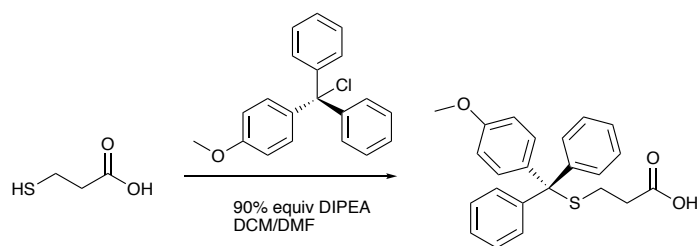
Scheme 4.5. Protection of 3-mercaptopropionic acid. (i) 4-Methoxytrityl chloride, DIPEA, DCM: DMF (1:1 v/v).

The ^{1}H NMR showed the loss of the thiol hydrogen, a shift in the CH$_2$ groups, as well as the change in splitting patterns caused by the loss of the thiol hydrogen. The reaction also showed quantitative conversion of the thiol due to the ratio of 2:2:3 of the two CH$_2$ at 2.2 and 2.6 ppm on the backbone of the mercapto acid and the methoxy CH$_3$ at 3.8 ppm (Figure 4.14).
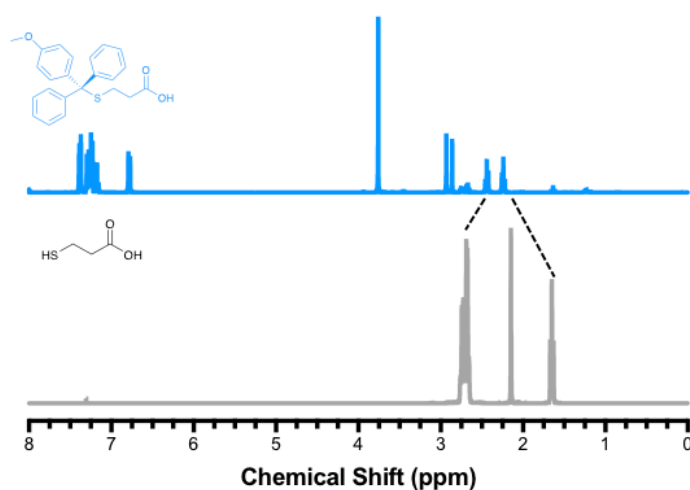
Figure 4.14. ^{1}H NMR spectra in CDCl$_3$ at 400 MHz comparing the 3-mercaptopropionic acid (grey) and the protected thiol product (blue).

This protecting group is acid labile, allowing to be cleaved off in the TFA cleavage of the peptide, thus requiring no extra step in the existing procedures. The thiol variants of the peptides were synthesised by automated peptide synthesis with the final thiol tail coupled by hand (Figure 4.15). The peptides were cleaved using a slightly adjusted cleavage cocktail (90% TFA, 5% thioanisole, 2.5% anisole and 2.5% ethane dithiol) to ensure the thiols remained in their reduced state followed by purification by HPLC.

Thiol-HABPep-1

Thiol-HABPep-2
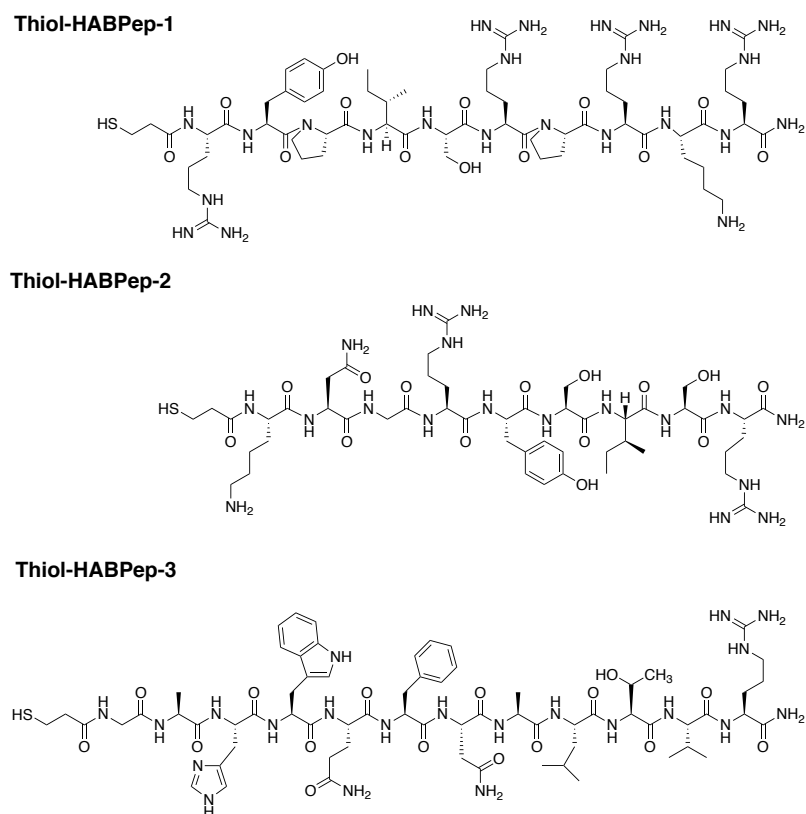
Thiol-HABPep-3

Figure 4.15. Structure of thiolated HABPeps (Thiol-HABPeps) synthesised.

The binding of the peptide to a Au surface was first analysed by measuring the surface contact angle. The bare gold showed a contact angle of 67.6° and a decrease in the contact angle was observed upon incubation of the peptides 16 hours.

Both Thiol-HABPep-1 (40.0°) and Thiol-HABPep-2 (49.4°) produce large change in contact compared to bare Au (P = <0.0001), but the two peptides have similar contact angle with minor significance (P = 0.0132) between one another. Since Thiol-HABPep-3 (67.6°) is very hydrophobic, low significant change in hydrophobicity compared with the native bare Au surface (77.2°) was observed (Figure 4.16).

Thiol-HABPep-1 has a lower surface hydrophobicity compared to that of Thiol-HABPep-2, this is caused by a significantly higher hydrophobicity observed for the three outer amino acid residues of Thiol-HABPep-2. After incubation with HA 1.5 MDa, the contact angle of the droplet on the surface increases for Thiol-HABPep-1 and Thiol-HABPep-2, 61.6° & 58.4° respectively, while decreases for Thiol-HABPep-3 (56.1°).

The lack of significance in contact angle between all three surfaces after the coverage of HA, infers that all three thiol peptides are mediating the binding of HA to the surface. As control, the bare gold was incubated with ethanol in the absence of thiolated peptide followed by immersion in HA solution. In this condition, there is no

significant difference in the contact angle compared to the initial bare Au surface, indicating the inability of the Au to retain HA on the surface and the need for the HABPep to mediate the efficient HA immobilization.
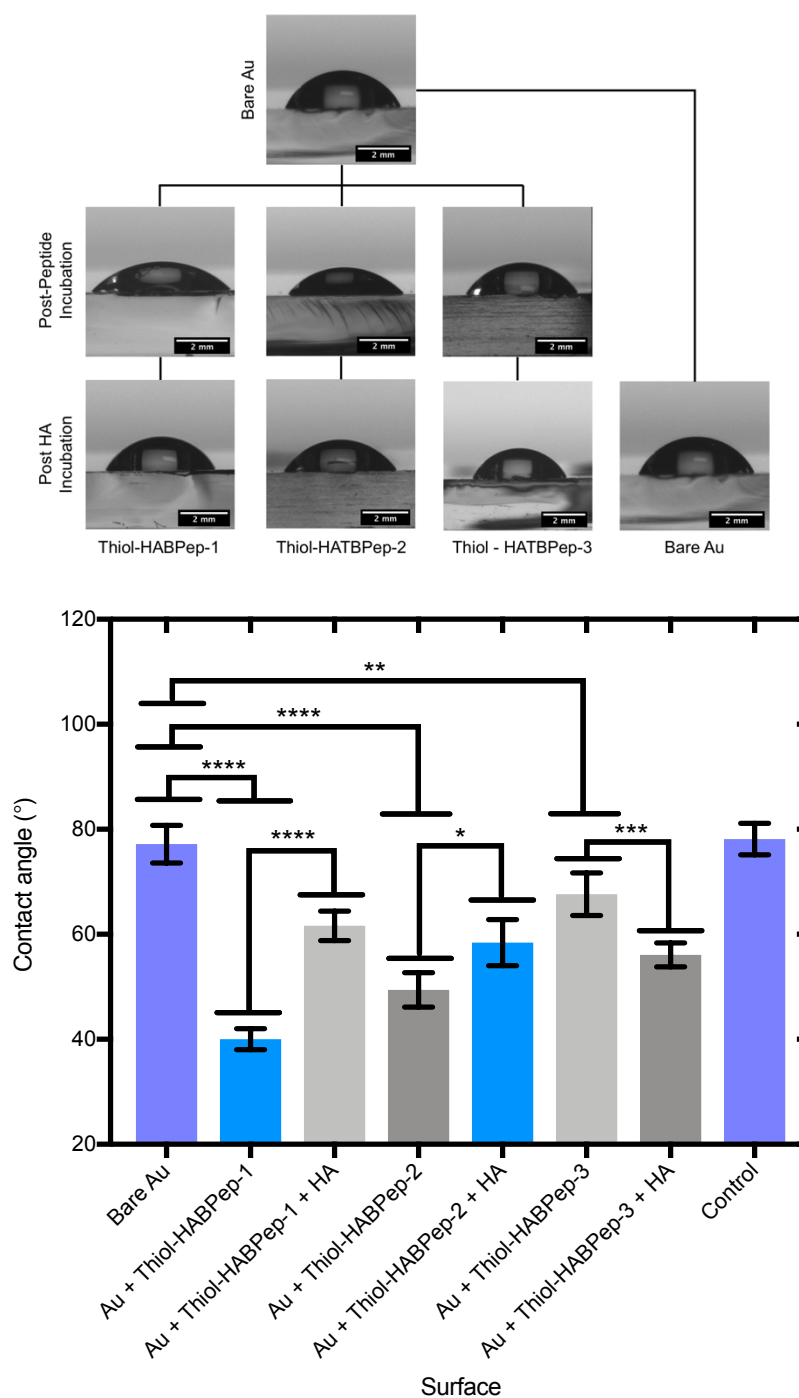
Figure 4.16. Immobilization of HA (1.5 MDa) on a gold surface mediated by Thiol-HABPeps analysed by contact angle measurements. Images of water droplets on the gold surface (top) and contact angle values (below) measured using ImageJ. Data analysis by two-way ANOVA analysis, where * significant at P < 0.0332, ** significant at P < 0.0021, *** significant at P < 0.0002 and **** significant at P < 0.0001.

Binding of thiols to gold is not only limited to planar 2D surfaces, but gold nanoparticles (AuNPs) have also been used. For AuNPs, the larger the particles the higher the wavelength in which they absorb. Therefore, small diameter AuNPs appear red in colour whilst larger appear purple. When binding a thiol to a gold NP, a shift of 2-3 nm is normally observed if the gold NP is stable, any more than that the gold has begun to aggregate causing the AuNP to destabilise. As a proof of concept, Thiol-HABPep-1 was adsorbed onto AuNPs using two different buffer solutions; citrate (Cit) and a stronger solution of Bis(p-Sulfonatophenyl) Phenylphosphine (BSPP). Using first the citrate buffer, the solution of AuNPs appears to become purple in colour even at the lowest concertation of 1 µM (Figure 4.17A); the weaker citrate buffered solution cannot prevent aggregation of the AuNPs. The UV trace of the Au-Cit shows a large shift (> 3 nm) from the maximum of the bare Au at 520 nm.
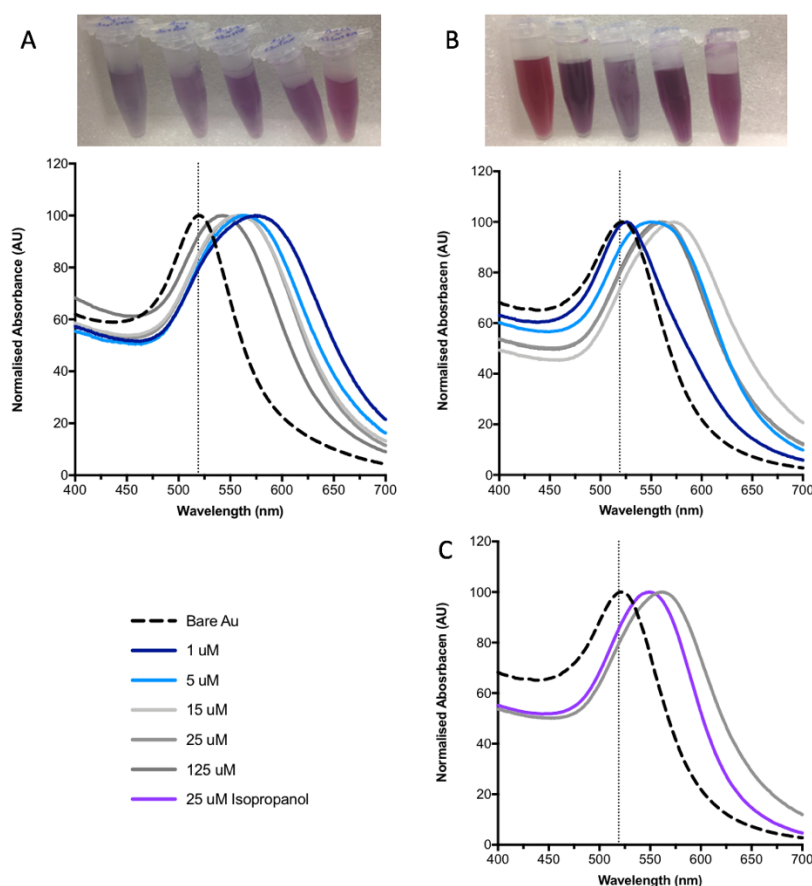
Figure 4.17. Thiol-HABPep-3 adsorbed onto AuNPs (Eppendorf's from left to right: 1, 5, 15, 25 & 125 µM) with two different Au capping agents: citrate (A) and BSPP (B) and corresponding UV spectra (below). UV spectra of BSPP capped AuNP with Thiol-HABPep-3 at 25 mM comparing the UV shift in differing polarity solvents (C).

Comparing the Cit results to BSPP capped AuNPs (Figure 4.17B), 1 uM shows more promise with a shift from 520 to 526 nm, remaining in the blue region of the visible

light spectra, whilst for higher concentration a shift in colour is observed towards purple. The results show the strength of the BSPP to prevent aggregation compared with Cit, but still does not overcome the high hydrophobicity of the peptide sequence. Switching the solvent from H_2O to isopropanol (IPA), a lower polarity solvent, the UV peak of HABP-3 at 25 mM moves from 561 nm in H_2O to 549 nm in isopropanol (Figure 4.17C), but this remains large than 2-3 nm. This in an improvement with a peak shift of 29 nm compared to 41 nm in water, due to the reduction in aggregation caused the use of a more hydrophobic and lower polar solvent of IPA.

TEM images of the AuNPs confirms the formation of aggregates (Figure 4.18), with more aggregation seen in the Cit buffer compared with the BSPP buffer. Both show a reduction in aggregation at lower concentrations of Thiol-HABPep-3.
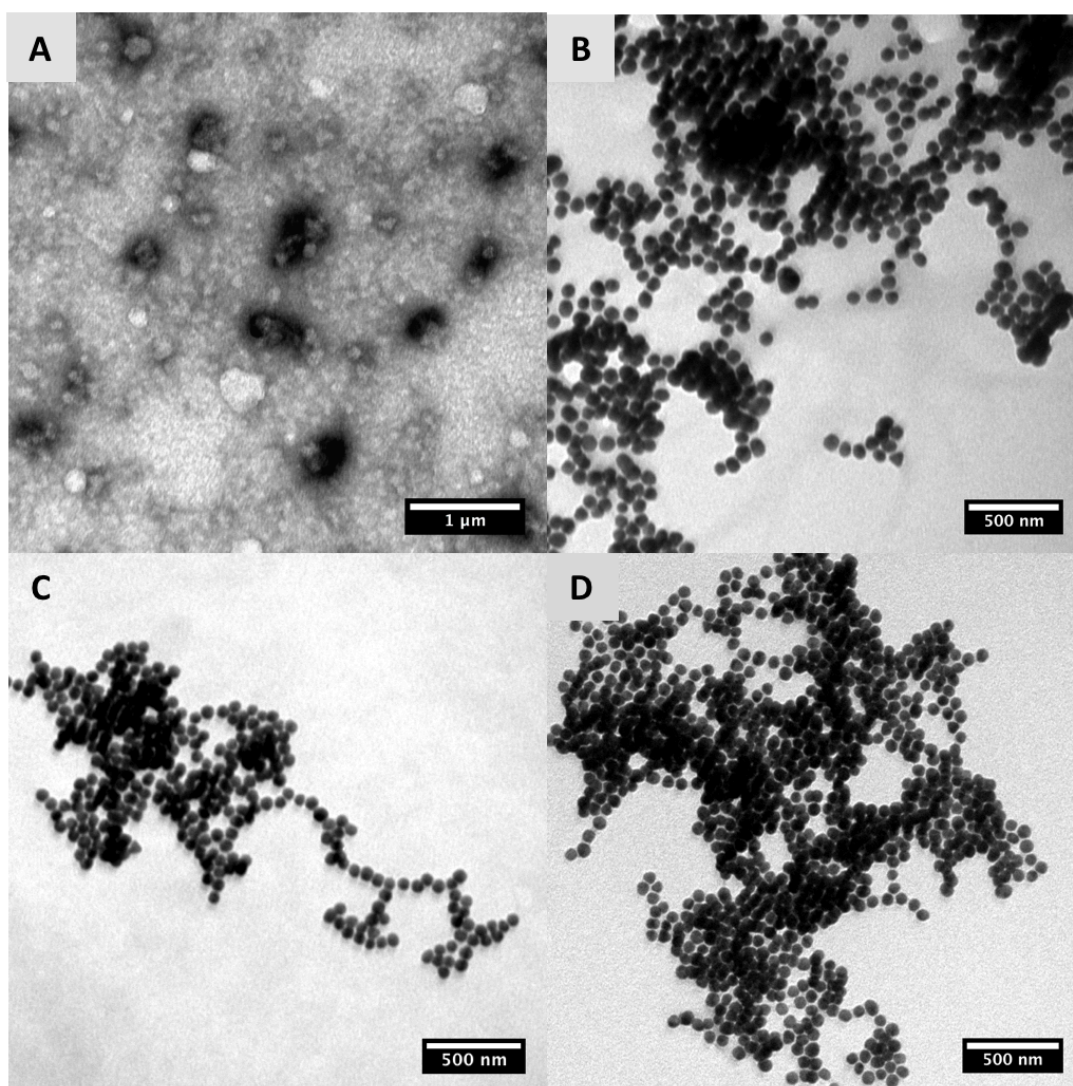
Figure 4.18. TEM images of AuNPs capped with (A, B) Cit and (C, D) BSPP at (A, C) low concentrations (5 μM) and (B, D) high concentrations (25 μM) of Thiol-HABPep-3.

4.2.4.2. Binding of Glycopolymers to HA-Binding Peptides by Surface Plasmon Resonance

To determine the binding of the HA-based glycopolymers to HABPeps the Thiol-HABPeps were bound to a gold SPR chip. SPR is a technique used to measure the binding of an analyte to a ligands bound to a metal surface. This can be done through direct binding to the gold, such in this case, or mediated through modified dextran or Ni chelating coatings on the gold. One advantage of SPR is that it does not require labelling of molecules, but the ligand requires to be bound onto the SPR chip. Light is passed through a prism in order to oscillate the electron of the metal surface at an incident angle to create the surface plasmon. The surface plasmon is very sensitive to change in the surface. Upon binding, the intensity of the light is reduced as well as the angle of light reflected. This leads to a change in the refractive index of the surface, which can be used to measure the binding affinity to the surface. The binding of the thiolate peptide showed a rapid association to the gold surface (Figure 4.19). Once the analyte flow was removed, a small drop off in response was seen, that stabilised once the excess had been washed off from the channel.
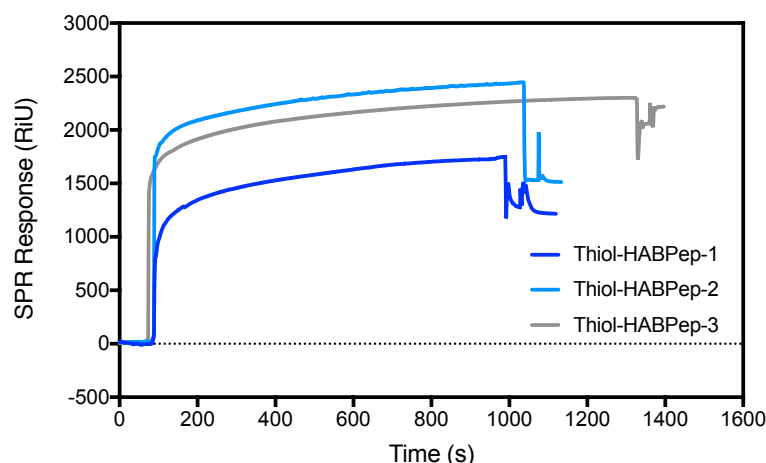
Figure 4.19. SPR sensorgrams of the binding of the Thiol-HABPeps to the gold SPR chip.

SPR was used to study the interaction with Thiol-HABPep-1and Thiol-HABPep-2 with HA and the glycopolymers. The K_D values for both peptides on the gold surface show an overall preference for the P3 and P6, with no binding seen for HA or the other HA-based glycopolymers (Figure 4.20). The peptides appear to have a preference for the glucose epimers as no binding is seen to the other epimers of Man (P4) and Gal (P5). Both peptides similarly show a lack of binding to negatively charged GlcA of P7, P8, P12 even though these peptides carry a large positive charge seen in the ζ-potential. The sensorgrams of P3 and P6 in both systems shows a larger response for these polymers suggesting the N-acetyl plays an important role in the binding to the

peptides. The K_D for P6 shows a tighter binding for Thiol-HABPep-2 over Thiol-HABPep-1. The sequence of HAPep-3 where 4 out of 9 residues are hydrophobic is more hydrophobic than HAPep-2 in which only 2 of the 10 residues are hydrophobic. Since the acetyl CH_3 is hydrophobic, the decreased hydrophobicity of HAPep-2 in Thiol-HABPep-2 will increase the binding with P6.
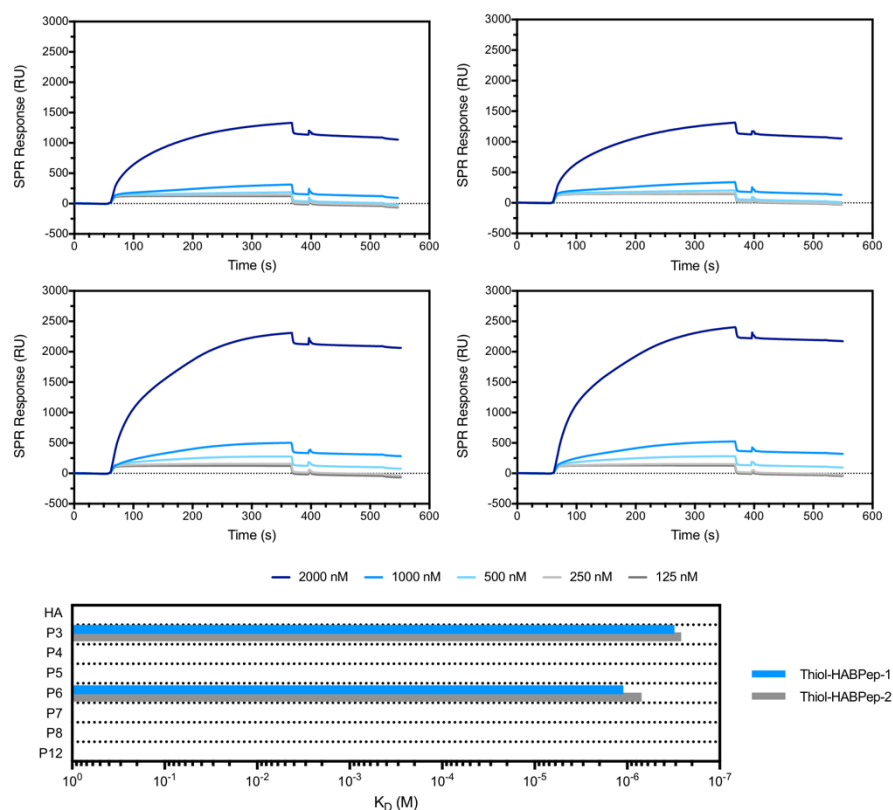
Figure 4.20 SPR sensorgrams of Thiol-HABPep-1 (left) and Thiol-HABPep-2 (right) with the glycopolymers P3 (top), P6 (middle) and K_D overview (bottom).

As seen earlier, HABPep-3 has a $\zeta = + 55.1 \pm 4.1$ mV and would be expected to associate with GlcA-based polymers which have a negative ζ- potential (Figure 4.4). However, through alanine scanning, HABPep-3 sequence was shown to bind to HA through more of the hydrophobic residues[2]. The SPR shows that HA binds to the peptide with a K_D of 9.7 μM, which is within the literature value of 1.65 μM found by radioactive ^{125}I labelled HABPep-3[2].

The SPR also indicates that Thiol-HABPep-3 prefers the HA sugars of GlcNAc (P6) and GlcA (P7) over other monosaccharides of Glc (P3), Man (P4) and Gal (P5) (Figure 4.21). According to the K_D values, the individual sugars have a 100-fold strong binding affinity than the natural HA. Using Equation 4.3, it is easy to see why the K_D of P7 matches that P6. The RU maximums of each of the three sensorgrams (Figure

4.22), P7 has a strong binding affinity due to the low k_a along with an even lower k_d whereas, P6 gives a large response and k_a but gives also a large k_d.

$$K_D = \frac{k_d}{k_a} = \frac{1}{K_A}$$

Where:

k_a = rate of association

k_d = rate of disassociation

K_A = Equilibrium association constant

K_D = Equilibrium disassociation constant
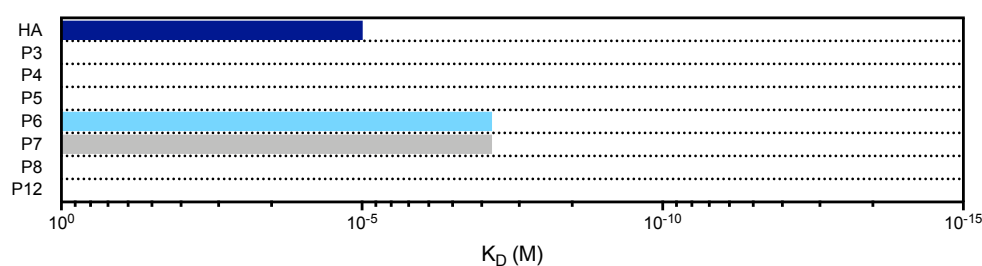
Figure 4.21. K_D values for the binding of the glycopolymers to Thiol-HABPep-3.

Comparing P6 with HA, a similar binding pattern is seen for the top concentration of 2000 nM, but a tighter binding is seen for P6 (Figure 4.22). The k_a is larger giving a higher RU maximum of 2490.1 RU compared to HA with gave a response of 1379.0. P6 also produces a stronger binding, as when the analyte flow is stopped the response decreases by 271.16 RU for HA, but only 195.97 RU for P6. These results indicate that the HABPep-3 prefers the hydrophobic residue of the N-acetyl group on the GlcNAc, rather than the electrostatic interactions of the GlcA.

The SPR however also shows a lack of binding for P8 and P12 which infers the that having the two sugars in the same polymer is inhibiting the binding to the peptide by interacting with each other. Thiol-HABPep-1 and Thiol-HABPep-2 did display binding to some of the glycopolymers despite the lack of binding to HA. These peptides are derived from sequences in the Link Protein and CD44, but they are taken from a much larger protein. The crystal structure gives us an indication of the binding to HA (Figure 4.23). For the link protein[31-32] it is observed that the aromatic residues of Tyr-12, Tyr-59, Tyr-78, and Trp-88 as well as basic and acid residues of Lys-11, Lys-72, Asp-77, Arg-81 and Glu-86 all are required for the binding with the cleft.
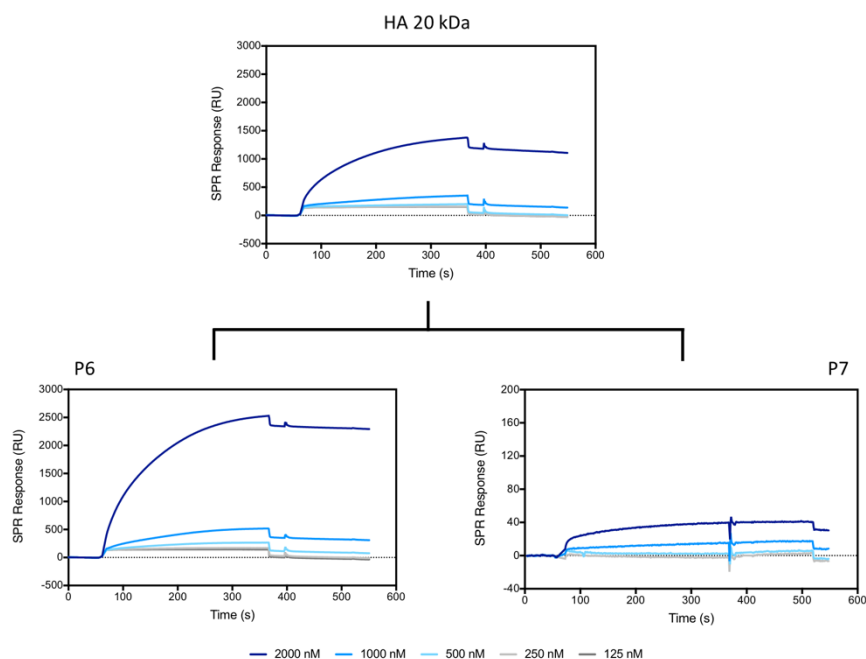
Figure 4.22. SPR sensorgrams for HA 20 kDa and homopolymers mimics of P6 and P7

CD44 is known to bind to 8-mers of HA as shown in the crystal structure[33] (Figure 1.23). Within the groove in CD44, where the 8-mers of HA bind, there are thirteen residues along the channel: Arg45, Tyr46, Cys81, Arg82, Tyr83, Ile92, Asn98, Ile100, Cys101, Ala102, Ala103, His105 and Tyr109. Of these, the aliphatic residues of Ile92, Ile100, Ala102 and Ala103 provide a large contribution to the binding of HA, recognising the N-acetyl group of the GlcNAc as it sits in a hydrophobic pocket. These results support the importance of the N-acetyl group during binding with the HABPs.
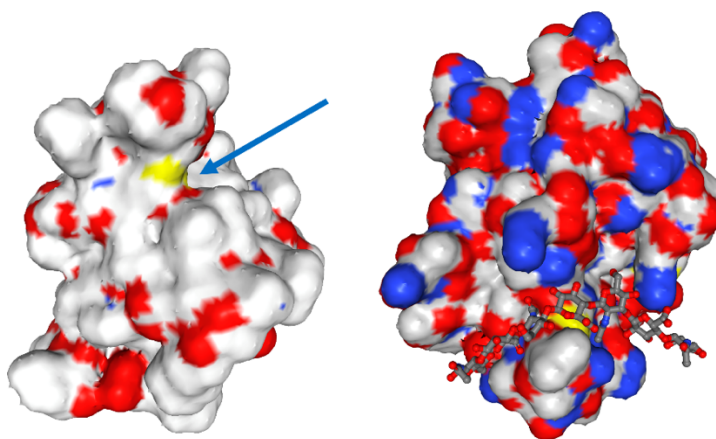
Figure 4.23. Surface crystal structure of HABPs of Link Proteins (left) and CD44 (right) with the grooves highlighted with either an arrow or with 8-mer of HA.

4.2.4.3. Binding of Glycopolymers to CD44 Protein by Surface Plasmon Resonance

Both the Link Protein and CD44 bind HA superficially in a binding "channel" or "cleft" rather than a binding pocket. The limitation of using a peptide sequence taken from a protein is that the peptide will not reproduce the necessary tertiary structure for optimal binding to HA. Using the recombinant protein of the CD44 extracellular domain (24 kDa), SPR was used to monitor the binding of the glycopolymers. The protein is coupled to the surface through amine coupling. The binding is much slower (Figure 4.24) compared to the absorption of the thiol onto the Au surface (Figure 4.19).
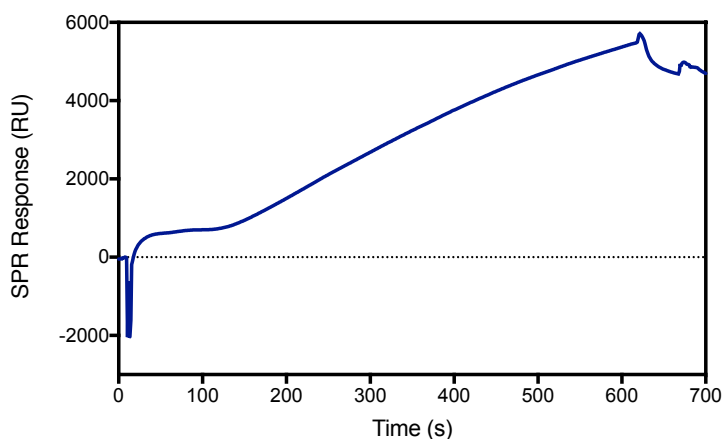
Figure 4.24. SPR sensorgram showing the immobilisation of CD44 onto a CM5 dextran covered SPR chip by amino coupling.

Similarly, to the CD44-derived peptide, the protein shows binding to Glc epimers with P3, P6 as well as P7 (Figure 4.25A-C). The protein shows a high response upon binding towards P3 by comparison to the others glycopolymer. The CD44 protein shows no binding towards P4, P5 of the other monosaccharide epimers, showing a specificity for the Glc epimer. Again, no binding is seen for the copolymers of P8 and P12. This is due to a difference the aggregation of the glycopolymer (Figure 4.7) compared to the elongated structure of HA in solution[34]. The CD44 is shown to bind the saccharides in a cleft region (Figure 4.23). If the glycopolymers are in spherical aggregates, this will impair their binding to CD44, for those with P8 and P12.

Binding to natural HA is not seen for lower HA concentrations (Figure 4.25D). This is caused by irreversible binding of HA at 2 mM, as in the regeneration of the surface the HA does not dissociate in the current buffers and therefore a K_D value is unreliable from the SPR. Examples of HA_8-CD44 complex monitored by SPR have previous been carried out yielding a Kd value of 24.6 μM[35-36].

In comparison, the literature example binds the HA to the surface rather than the CD44 to ensure the protein isn't affected by the binding to the surface. Through this method ligands or modified HA effect on the HA-CD44 complex[36-37] can be studied. The HA-CD44 protein SPR therefore require fine tuning in order to regenerate the surface. The binding of CD44 to the surface via amino coupling lacks control and therefore the addition of CD44 though a C-terminus His-Tag and Ni combination would provide a more control method of binding.
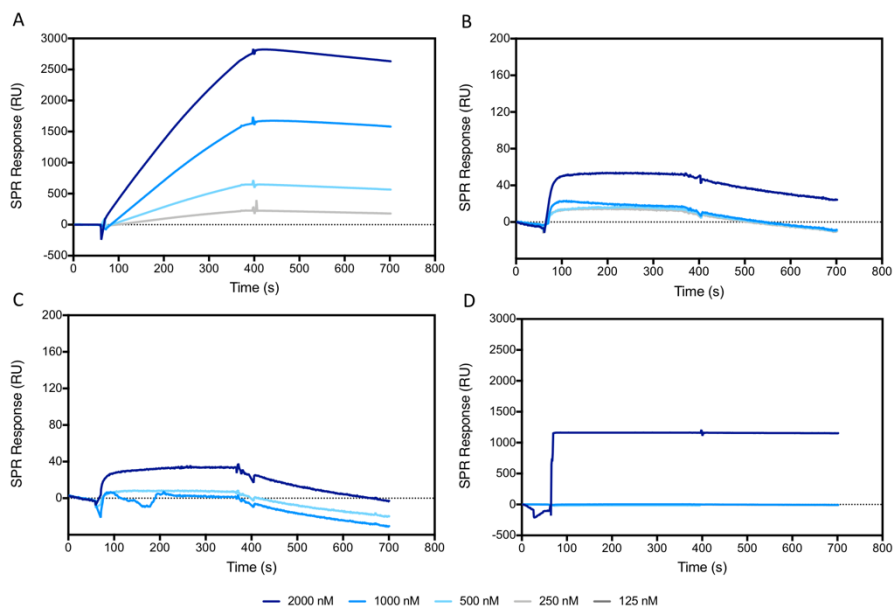
Figure 4.25. SPR sensorgrams of P3 (a), P6 (b), P7 (c) and HA (d) to the extracellular domain of CD44.

4.2.4.4. Binding of Glycopolymers to HA-Binding Peptides by Quartz Crystal Microbalance

As previously mentioned, the limitation in the use of a peptide on the surface of the gold is the surface itself being sterically hindering. It has been shown that several different sulphur containing functional groups will in fact bind to a metal surface[38]. By binding the glycopolymer over the peptide on the gold surface, this could reduce the sterics between surface and the analyte. This is because the peptides used are no longer than 12 mers, whereas the glycopolymers are 56 repeats in length. Therefore, the distance between the end of macromolecule and the gold surface is longer with the glycopolymer, leading to a high degree of freedom in which to interact, by comparison to the peptide. The backbone will limit this degree of freedom as it tends to aggregate as shown by TEM (Figure 4.7), but these are in the dry state so are a result of increasing concentration of the solution as it removed. The RAFT agent has the potential to bind to an Au substrate, but the RAFT agent decomposed during the

azidation (Figure 2.8), using UV-Vis the RAFT agent can be observed with the peak between 240-340 nm corresponds to the RAFT agent (Figure 4.26A).

Alternatively, to SPR, quartz crystal microbalance (QCM) can be used to measure the deposition of the glycopolymer onto gold substrate by monitoring the change of frequency. This change of frequency, through the Sauerbrey Equation 4.4 can be linked to the mass deposition.

$$\Delta f = -\frac{2f_0^2}{A\sqrt{\rho_q \mu_q}} \Delta m \qquad\qquad \text{Equation 4.4}$$

Where:

f_0 Resonant frequency (Hz)

Δf Frequency change (Hz)

Δm Mass change (g)

A   Piezoelectrically active crystal area (cm^2)

ρ_q Density of quartz (g cm^{-3})

μ_q Shear modulus (g cm^{-1} s^{-2})

The QCM (Figure 4.26B) for P7 shows the binding of the glycopolymer onto the gold surface (region I) with minimal mass loss upon washing the system with water (region II). The frequency then decreases again upon injection of acetylated HABPep-3 into the chamber (region III). Once this has stabilised after the water washing (region IV). shows a small decrease in the frequency, but the frequency has still dropped substantially. These results point for the use of different techniques and formats for performing the binding studies. In addition, the QCM can be utilised to investigate both the glycopolymers on the surface binding to the peptide in solution as well as the inverse.

A

B
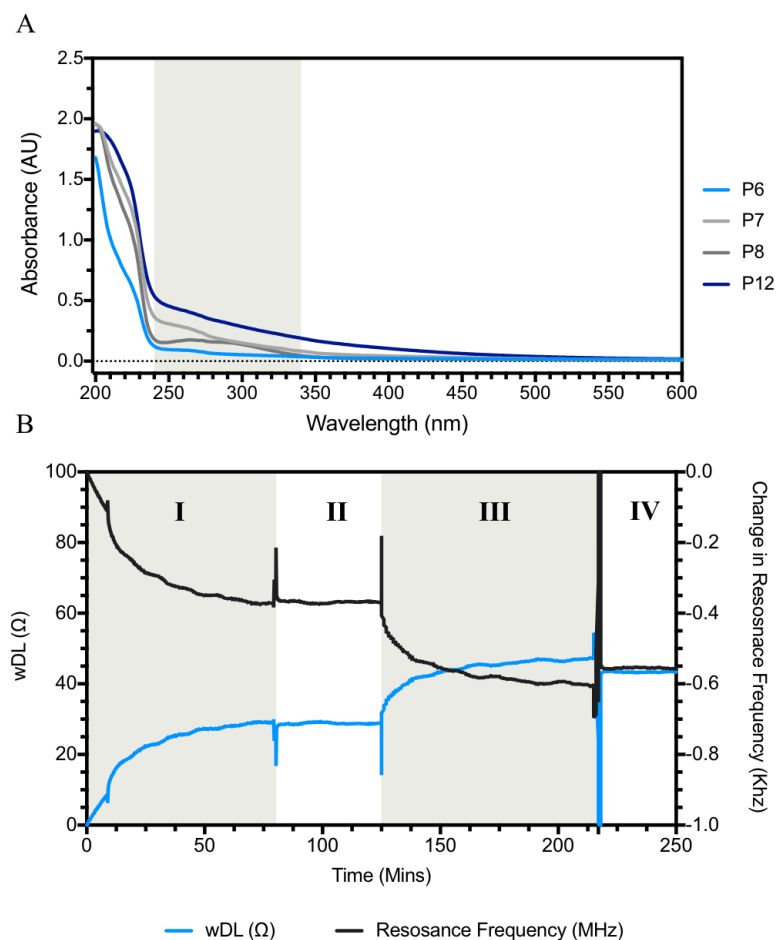
Figure 4.26. UV trace of the glycopolymer highlighting the small peak between 240 – 340 nm (grey) caused by the RAFT agent (A) followed by the QCM (B) showing the 4 regions of the QCM.

4.2.4.5. Binding of Glycopolymers to HA-Binding Peptides by Turbidity Assays

Where SPR and QCM require complex instruments as well as software to analyse the data produced, turbidity can also give an insight to binding through the transparency of solution to opaque as the two components bind. This can be used to screen binding as well as determine molar ratio. An initial screen for P6 and P7 showed that on addition of a 10-fold molar excess HABPep-3 a precipitate formed. This was due to the glycopolymer aggregates (Figure 4.7) binding to the HABPep-3 and forming an insoluble aggregate by the covering of the saccharide epitopes, which provide the glycopolymer with their solubility in water. The interaction between HABPep-3 & HA lead to the formation of membranes as observed previously (Figure 3.5). This precipitation can be seen by looking at the change in turbidity of the glycopolymer in solution with/without HABPep-3 (Figure 4.27A).
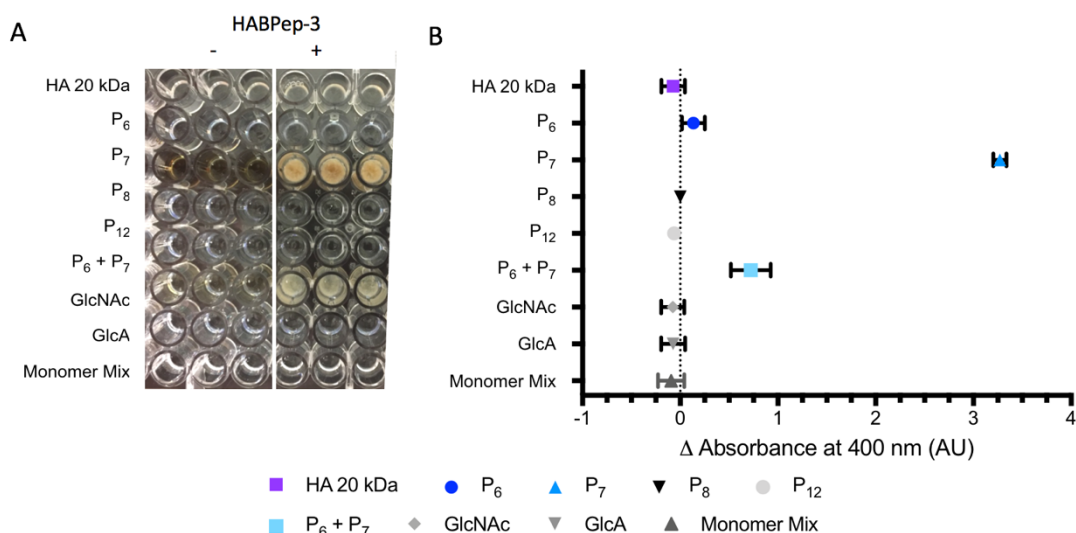
Figure 4.27. Turbidity of 1% (wt%) glycopolymer and monomer solutions with 1% (wt%) of HABPep-3 at pH 7. visual turbidity in 96-well plate (A) quantified by visible light absorbance at 400 nm (B).

A small increase in turbidity is observed between P6 and HABPep-3, suggesting a small amount of binding is occurring. The turbidity was quantified by the transmittance through the sample at 400 nm compared to the sample without HABPep3 (Figure 4.27B). When HABPep-3 is not bound to a surface such as a gold SPR chip, it can self-assemble producing extended positively charged nanofibers to interact with negatively charged GlcA. The turbidity measurements of the 1% solutions also confirm the lack of binding seen by the SPR to P8 and P12. Although these glycopolymers contain the GlcA residue, with no change in turbidity was seen. Interestingly, when placing P6 and P7 in a 50:50 ratio mixture, the absorbance is 0.722 AU of is approximately a fifth of that of P7 alone at 3.271 AU. When considering the Beer-lambert law Equation 4.5, absorbance is linear to concentration if the extinction coefficient and path length are kept constant.

The decreased turbidity in the 50:50 glycopolymer mixture infers the sugars may interact with one another over the peptide, reducing the turbidity. Applying this to P8 and P12 no turbidity is observed inferring the saccharide upon the glycopolymer interact with themselves rather than the HABPep-3.

$$A = \varepsilon c l \qquad \text{Equation 4.5}$$

Where:

A   Absorbance (AU)

ε Extinction Coefficient (mol^{-1} dm^3 cm^{-1})

c   Concentration (mol dm^{-3})

l   path length (cm)

These observations also highlight the importance of the glycosidic bond in the polysaccharide, by reducing intramolecular interaction with HA. For P6 and P7, the binding can be seen as a function of the molar ratio of HABPep-3 (Figure 4.28). Upon increasing the molar ratio above 1, an increase in turbidity is seen for both glycopolymers as the HABPep-3 coats the monosaccharides of the aggregates making the glycopolymer insoluble in water.
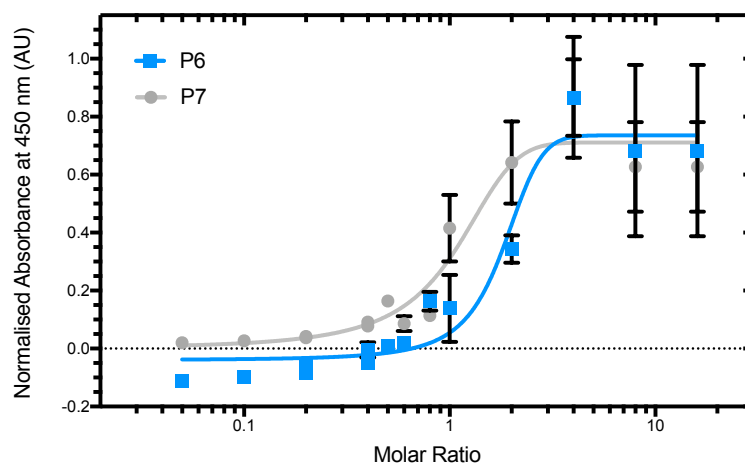
Figure 4.28. Turbidity curve for P6 and P7 at 1 mmol with increasing molar ratio of HABPep-3 at pH 7 monitoring the change in turbidity at 450 nm.

From the results, a clear influence of the surface such as the gold SPR chip or QCM electrode can influence the binding. The binding of HABPep-3 is clearly affected by the self-assembly of the peptide. When self-assembling on a surface, the hydrophobic core is available to bind the GlcNAc residues, whilst when allowing the HABPep-3 to self-assemble into the long nanofibrous structures, the stacking of these hydrophobic sections produce the arginine's of the peptide to be exposed across the surface leading to a charge interaction with the GlcA. In comparison to the peptides, lectins are large proteins and their binding to a surface is expected to have a reduced effect on their binding capabilities.

4.2.4.6. Binding of Glycopolymers to Lectins by Surface Plasmon Resonance

Dendritic cell-specific intercellular adhesion molecule-3-grabbing non-integrin

Dendritic cell-specific intercellular adhesion molecule-3-grabbing non-integrin or more commonly known as DC-SIGN or CD209 is a type II C-type lectin part of the Type-2 receptor family found on the membrane surface[39] of macrophages and dendritic cells (DC) formed as an oligomeric structure (Figure 4.29A & B)[40]. The

multiple domains come together due to the hydrophobic section along the protein assembling together to produce a hydrophobic core.
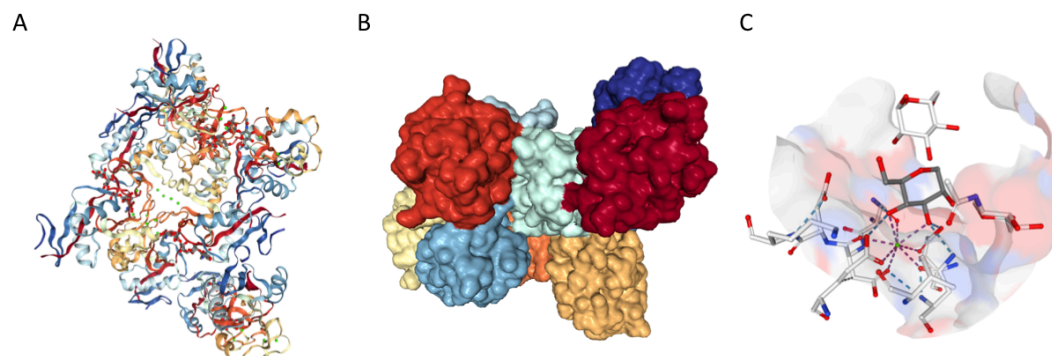
Figure 4.29. Crystal structure of the tetramer of DC-SIGN showing (A) along with the multiple domains (B) and binding pocket of DC-SIGN (C) showing the interactions between mannose and a Ca^{2+} ion.

DC-SIGN is able to recognize mannose-based compounds as well as fructose found on Lewis-type determinants[41] and GlcNAc[39-40]. The binding of these saccharides also facilitates a vast array of pathogens, which possess saccharides on their surface. Several of these diseases bind to DC-SIGN cause the antigens to be taken up leading by T-cells. However, other pathogens, such as human immunodeficiency virus (HIV) and hepatitis C virus (HCV), utilize DC-SIGN in order to go unnoticed to the immune system and to allow HCV and HIV to spread. For this reason, DC-SIGN has been well studied for its interactions with monosaccharides[42-44]. The SPR sensorgrams show a positive response for both P4 as well as P3 with K_D values of 37.9 nM and 0.4 nM, respectively (Figure 4.30A). However, the response from the SPR is much higher for P3 (Figure 4.30B) than P4 (Figure 4.30C) at 2 mM, the k_a is much quicker, 47.3 M^{-1} s^{-1} compared to 2.1 × 10³ M^{-1} s^{-1} for P3 and P4, respectively (Table 4.7). This can be seen by the initial slopes of the SPR sensorgrams.

Once the flow of the analyte is stopped, the k_d of P3 is 1.79 × 10⁻⁶ s^{-1} compared to 8.3 × 10⁻⁷ s^{-1} for P4. The response can also be correlated to a mass change. A mannose glycopolymer, P4, which has a stronger binding affinity is statistically more likely to bind across several saccharides on the same glycopolymer leading to a smaller mass change on the SPR chip. Whereas a low affinity glycopolymer such as glucose, P3 will bind, but with multiple chains. With more chains binding, this causes a significant mass increase leading to a larger response (Scheme 4.6).

Figure 4.30. K_D values (A) and trends of the glycopolymers and HA along with individual SPR sensorgrams of P3 (B), P4 (C), P6 (D) and P7 (E).

Compared to literature examples the mannose polymer is an order of magnitude lower in K_D. However, it is challenging to directly compare literature values to P4 as the composition of the polymers in terms of morphology and polymer backbone are different.

Since this lectin binding is dependent on chelation using the Ca^{2+}, the binding to P5, the Gal epimer, shows no binding to lectin as expected. This is caused by the lack of equatorial hydroxide at C4. HA showed no specific binding to DC-SIGN, this is due to the large polysaccharide structure of HA, which DC-SIGN is unable to bind as the lectin binds terminus monosaccharides (Scheme 4.7). Therefore, the probability for HA to bind is low.

Table 4.7. Kinetic data of DC-SIGN with the various polymers.

Macromolecule	DC-SIGN				
	k_a (1/Ms)	k_d (s)	RU_{Max}	K_a (M)	K_d (1/M)
HA	n.s.	n.s.	n.s.	n.s.	n.s.
P3	47.3	1.8×10^{-6}	1107	2.6×10^{7}	3.8×10^{-8}
P4	2.1×10^{3}	8.7×10^{-7}	166	2.5×10^{9}	4.0×10^{-9}
P5	n.s.	n.s.	n.s.	n.s.	n.s.
P6	259	1.5×10^{-3}	1700	1.8×10^{5}	5.6×10^{-6}
P7	419	3.4×10^{-3}	1100	1.2×10^{6}	8.1×10^{-7}
P8	n.s.	n.s.	n.s.	n.s.	n.s.
P12	n.s.	n.s.	n.s.	n.s.	n.s.

n.s. non-specific binding.

When considering the multivalent effect to stabilise the ligand-lectin binding, HA can never form more than one interaction, with a C-type lectin. The glycopolymers can however form multiple to stabilise the interaction and produce a stronger binding affinity.
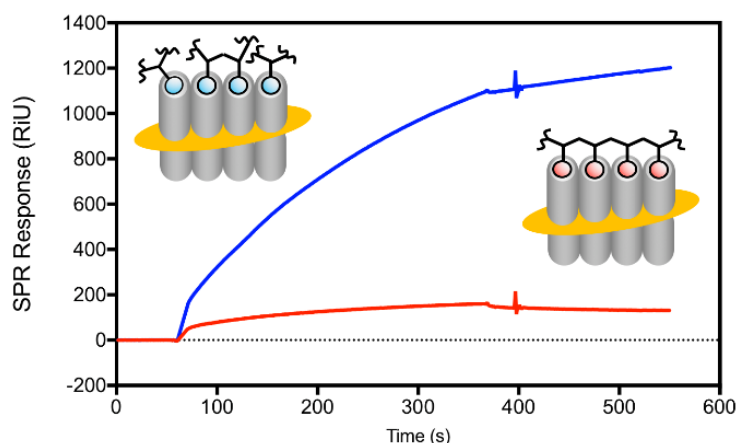
Scheme 4.6. Schematic representation of difference in RU_{Max} caused multiple chains binding (blue) compared with a single chain binding (red) the same number of receptors with mass and SPR directly.

The homopolymers of P6 and P7 showed binding to DC-SIGN (Figure 4.30D-E). Since GlcNAc and GlcA are in the same epimers conformation as Glc, they show a reduced binding compared to the Man-based polymer (P4). What can be inferred is the two-functional groups of the acid at C5 on GlcA and the N-acetyl group at C2 of GlcNAc have caused a reduction in binding. A 100-fold decrease in binding is observed for P6 when comparing to P3. This decrease can be attributed to the steric bulk of the N-acetyl group as well as the loss of a potential hydrogen bonding hydroxide. The addition of a carboxylic acid at C5 for P7 shows a moderate increase compared to P6 but remains weaker than P3. This indicates that the C2 hydroxide is

important, with a preference to be axial, with a destabilising effect seen by the addition of the carboxylate at C5, either sterics or electrostatic repulsion.
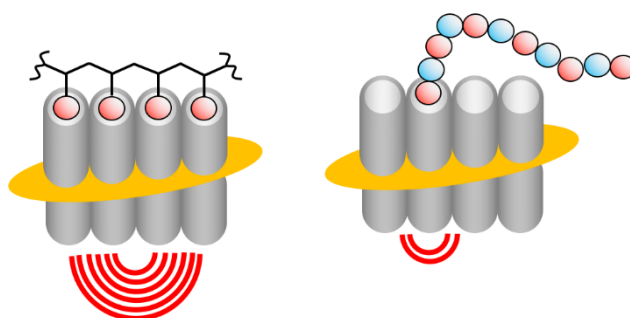
Scheme 4.7. Schematic representation comparing the binding of a C-type lectin, such as DC-SIGN, to a glycopolymer displaying multiple C-3, C-4 equatorial hydroxide (left) and a polysaccharide, such as HA, where only the terminus C-3, C-4 equatorial hydroxide exists (right). Image inspired by ref[4]

When both sugars are present in the same polymer, P8 and P12, the polymers show no specific binding to DC-SIGN. By comparing to P5 and P6, this infers that the monosaccharide in the same polymer again disturbs the binding to the lectin. This could be caused by potential intramolecular hydrogen bonding affecting the conformation of the sugars.

From these results, it was shown the C4 and C3 hydroxides should remain as equatorial, whilst C5 and C2 functionality reduces the K_D when binding to DC-SIGN. To further investigate the binding properties of this lectin, the use of sugars such as N-acetyl-D-mannose (ManNAc) and mannuronic acid (ManA) would be useful to look at the binding once the C2 stereochemistry is inverted to the mannose epimer.

Mannose Binding Lectin

The mannose binding lectin (MBL) or mannose-binding protein is a soluble lectin type III and part of the collectin family[45-46]. The MBL is formed of a tetramer of 250 kDa with these tetramers linked together by disulphide bonds (Figure 4.31). As part of the immune system found within the blood, it recognises a large range of microbial saccharides which coat yeast, bacteria and viruses.
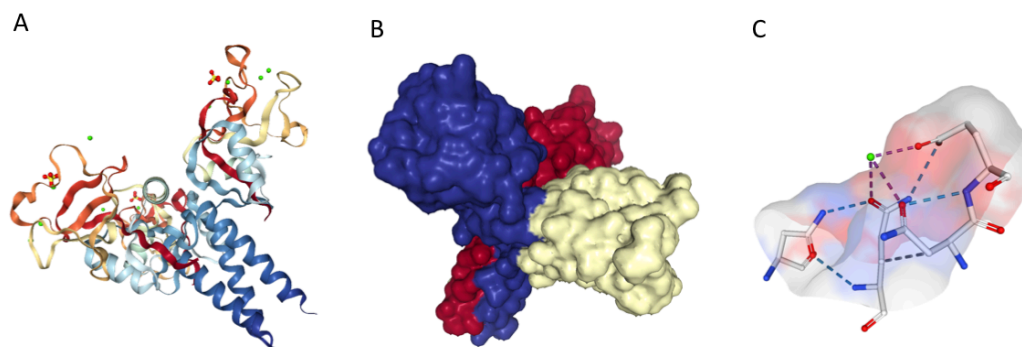
Figure 4.31. Crystal structure of the tetramer of MBL (A) showing the Ca^{2+} ions (green) along with the trimeric structure of which forms MBL (B) and binding pocket (C) where Ca^{2+} ions are found on the surface of the lectin.

Upon binding to pathogens, the lectin associates with the MBL-associated serine protease (MASP) leading to the destruction of pathogen. The lectin has been observed to bind to Man and GlcNAc, but can also bind nucleic acids through the Ca^{2+} dependency[47]. This Ca^{2+} dependency can be seen in the sensorgrams due to the non-specific binding seen for P5. Similarly, to DC-SIGN, the lectin has a specificity for C4 and C3 equatorial hydroxides (Table 4.8).

Table 4.8. Kinetic data of MBL with the various polymers.

Macromolecule	MBL				
	k_a (1/Ms)	k_d (s)	RU_{Max}	K_a (M)	K_d (1/M)
HA	n.s.	n.s.	n.s.	n.s.	n.s.
P3	13.8	2.8×10^{-4}	1342	5.0×10^4	9.4×10^{-5}
P4	7.6×10^2	1.2×10^{-6}	155	6.3×10^8	1.6×10^{-9}
P5	n.s.	n.s.	n.s.	n.s.	n.s.
P6	1.0×10^4	9.5×10^{-4}	417	1.1×10^{12}	9.4×10^{-13}
P7	n.s.	n.s.	n.s.	n.s.	n.s.
P8	n.s.	n.s.	n.s.	n.s.	n.s.
P12	n.s.	n.s.	n.s.	n.s.	n.s.

n.s. non-specific binding.

Comparing P3 and P4, the data shows MBL to be mannose specific, due to the 10,000-fold decrease in K_D from P3 to P4 (Figure 4.32A). Again, the larger response is seen from the glucose glycopolymer (Figure 4.32B), however the larger k_a is seen from mannose glycopolymer (Figure 4.32C). Similarly, to DC-SIGN, a change of stereochemistry at C4 position inhibits the binding to P5 due to the Ca^{2+} dependency. P6, whilst being a glucose epimer, shows a further 10,000-fold decrease in K_D compared to P4. Though the addition of GlcA onto the polymer backbone showed no binding in the homopolymer, P7, it also leads to inhibition of the P8 and P12, which

possess equal quantities of GlcA and GlcNAc. This infers for MBL is a mannose receptor, but with an increased significance of the functionality and stereochemistry at the C2 and C5 position.
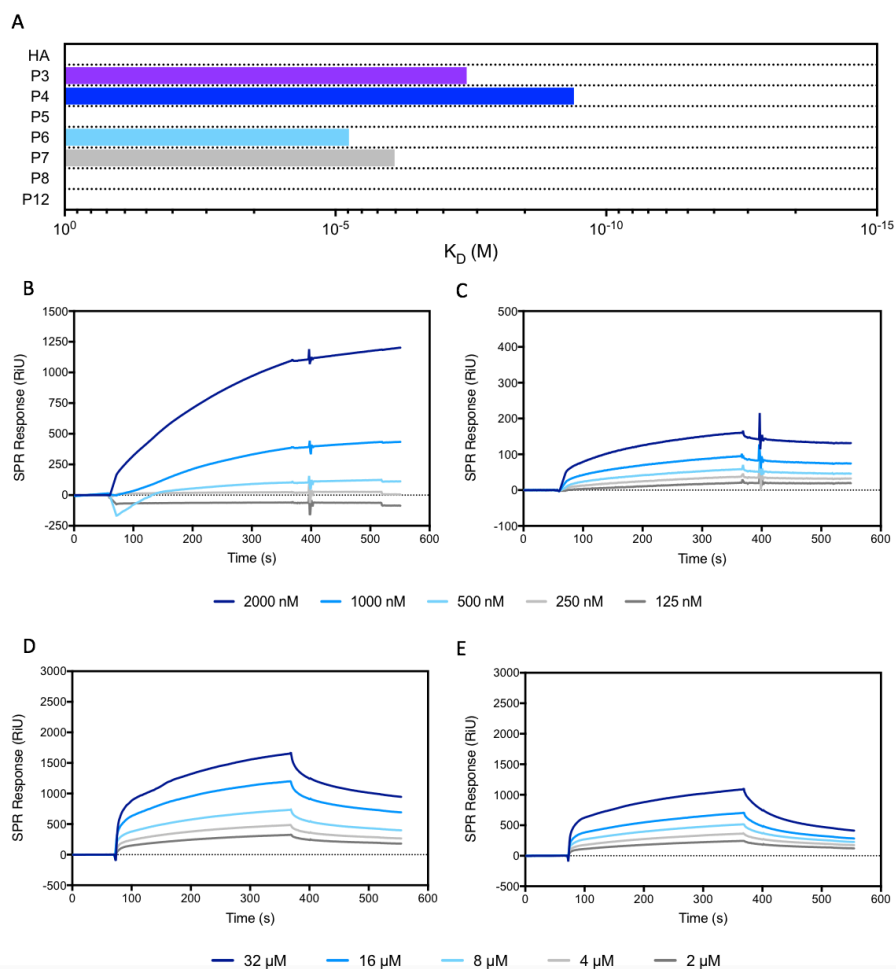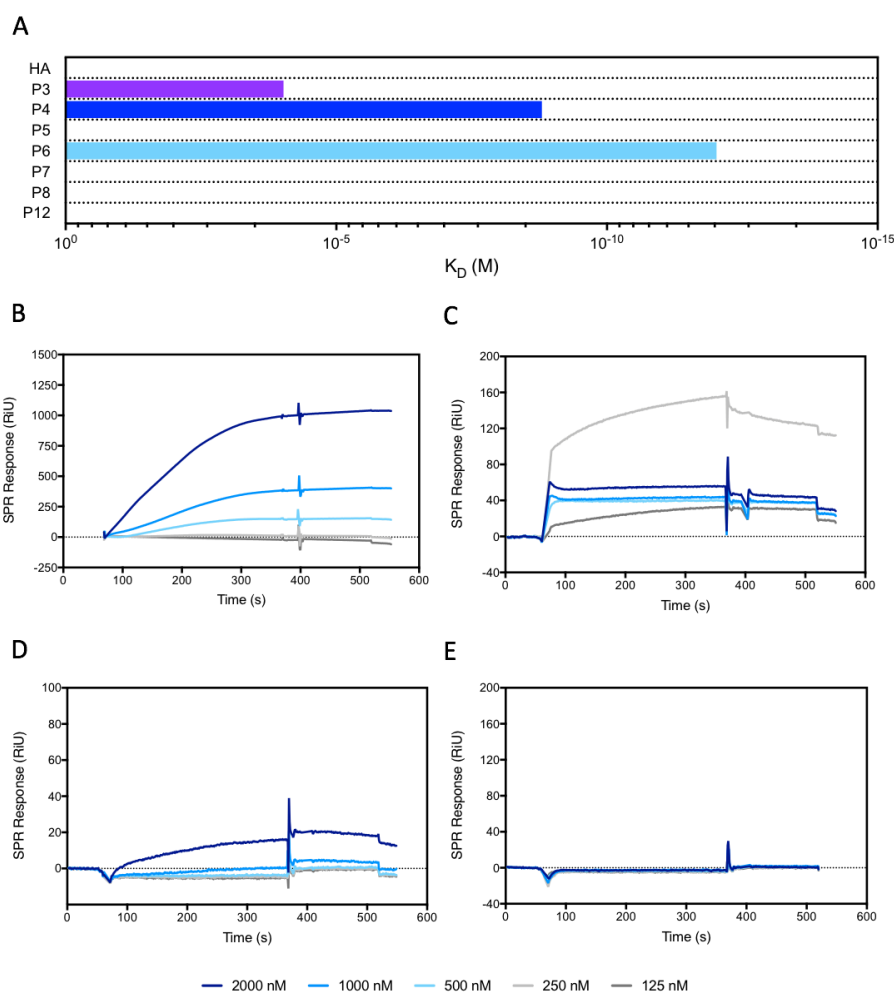

Figure 4.32. K_D values (A) and trends of the glycopolymers and HA along with individual SPR Sensorgrams of P3 (B), P4 (C), P6 (D) and P7 (E).

The MBL binding results show, as expected, that the lectin requires the C3 and C4 position for chelation using the Ca^{2+}. The lectin has been shown to prefer hydrophobicity at the C2 position due to the increase in binding with P6 whereas charge and/or functionality at the C5 position leads to inhibition of the binding. To further investigate the preference for ligand sugars, ManNAc should be used to test the hydrophobicity being placed in the axial position as well as Iduronic acid (IdoA). By using IdoA, the position of the charge can be tested to determine whether there is a steric effect or an intolerance to negative charge at the C5 position. The carboxylate can easily be esterified to screen the charge of the glycopolymers to test without the charge.

Surfactant protein-D

Surfactant protein-D (SP-D) (Figure 4.33A) is another C-type lectin found predominately within the lungs but also found in gastrointestinal and genitourinary tracts. This soluble C-type lectin, like MBL, is part of the Collectin Family and a Group III lectin. SP-D is divided in 3 main components, a triple-helical collagen, an α-helical coiled-coil neck and a C-type lectin domain.
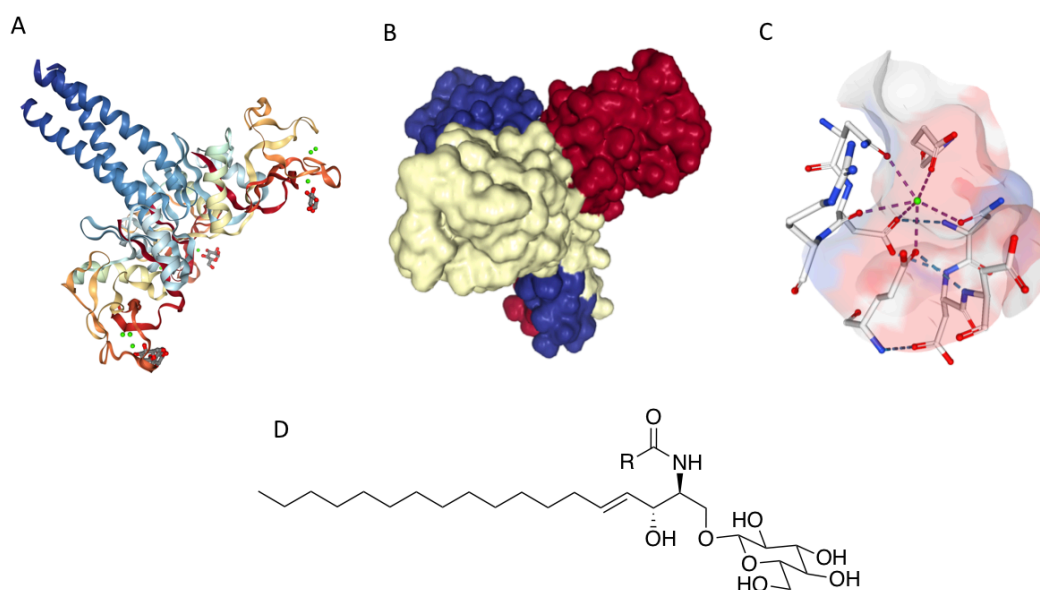
Figure 4.33. SP-D crystal structure (A) bound to 3 Glc units, the trimer subunits (B), the binding of Glc (C) by Ca^{2+} held within the binding pocket and natural ligand of SP-D, glucosylceramides (D), a glucose-based cerebroside.

The C-type domain is found at the C-terminus of the protein whilst the other two domains are found towards the N-terminus. The SP-D is formed of 3 of these units to make a trimeric structure (Figure 4.33B) by the linking of the cysteine rich N-terminuss. SP-D binds to glucosylceramide, a glucose-based ceramide by coordination with Ca^{2+} (Figure 4.33C) but has also shown binding to phosphatidylinositol and lipopolysaccharides. Glucosylceramides are cerebrosides which is the common name for glycosphingolipids (Figure 4.33D). These molecules are sugars which have a glycosidic linkage to a ceramide. These glycosphingolipids exist as only glucose and galactose based epimers. SP-A, an analogue of SP-D, binds to the galactose-based ceramides, galactocerebroside. Within the lungs, both SP-A and SP-D are potent innate immune molecules which bind to lipopolysaccharides found on various pathogens, such as bacteria, yeast and fungi. The binding of these pathogens to SP-A/D leads to their destruction, as SP-A/D are also able to bind to phagocytic cells (white bloods cells) which envelope the protein-microbe complex. Since SP-D binds

glucose-based ceramides, upon testing with the glycopolymers it is evident that this lectin is exclusive for the glucose polymer (P3) with binding seen with a K_D of 265 nM, whereas the other epimers P4 and P5 show no binding, showing specificity for the glucose epimer (Figure 4.34A).
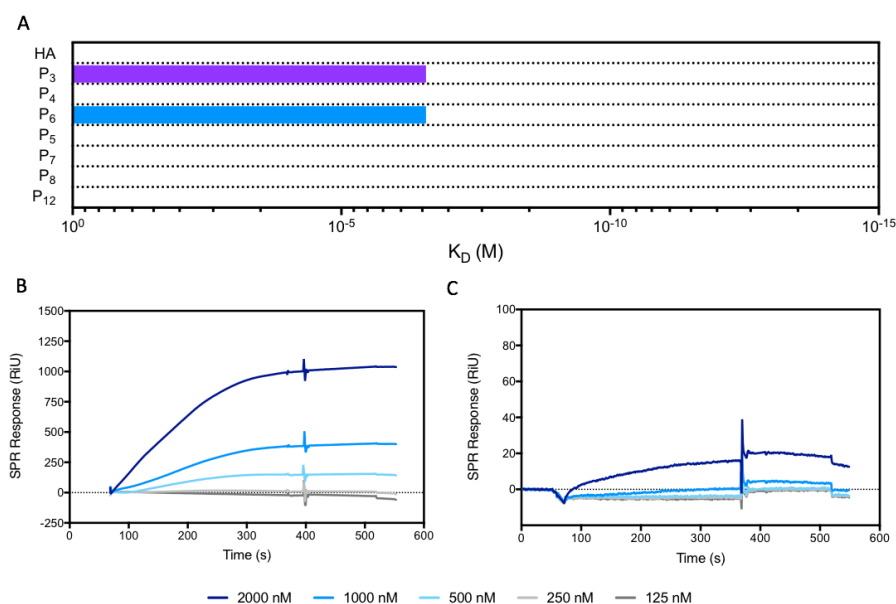
Figure 4.34. K_D values for the binding to SP-D (A) with individual SPR sensorgrams of P3 (B) and P6 (C).

Binding of free galactose to SP-D has been reported[48] and this is due to the ability of the molecule to rotate and bind through the C1 and C2 hydroxide, which in both the glycopolymers and glucosylceramides, the C1 is used to connect the monosaccharide. Compared to P3 (Figure 4.34B), P6 shows a lower affinity to SP-D (Figure 4.34C) reflected by smaller RU seen in the SPR sensorgrams. Although the two glycopolymers show small k_a values, 5.95 $M^{-1}s^{-1}$ and 19.2 $M^{-1}s^{-1}$ for P3 and P6 respectively, they differ in the dissociation, k_d, where there is a 1,000-fold difference (1.57×10^{-3} s^{-1} compared to 5.09×10^{-6} s^{-1}) (Table 4.9).

Due to the mechanism in which SP-D binds saccharides through the Ca^{2+} with the C3 & 4 hydroxyls, HA does not exhibit binding, as well as any glycopolymer containing a GlcA unit also does not bind inferring an intolerance for C5 modification or electrostatic repulsion, similar to MBL. To further investigate this lectin, the use of 2-deoxy-D-glucose and 6-deoxy-D-glucose would provide a valuable insight to the binding. By removing these two hydroxides and comparing to P3, Glc glycopolymer, the stabilities of the lectin-saccharide without the hydroxide can be tested.

Table 4.9. Kinetic data of SP-D with the various polymers.

Macromolecule	SP-D				
	k_a (1/Ms)	k_d (s)	RU_{Max}	K_a (M)	K_d (1/M)
HA	n.s.	n.s.	n.s.	n.s.	n.s.
P3	19.2	5.1×10^{-6}	1004	3.8×10^{6}	9.4×10^{-5}
P4	n.s.	n.s.	n.s.	n.s.	n.s.
P5	n.s.	n.s.	n.s.	n.s.	n.s.
P6	6.0	1.6×10^{-3}	16.3	3.8×10^{3}	9.4×10^{-13}
P7	n.s.	n.s.	n.s.	n.s.	n.s.
P8	n.s.	n.s.	n.s.	n.s.	n.s.
P12	n.s.	n.s.	n.s.	n.s.	n.s.

n.s. non-specific binding.

Dectin-1

Found on the cell membrane surface, Dectin-1 is a group V lectin and is part of the natural killer (NK) cell receptor[49-50]. Unlike DC-SIGN, MBL and SP-D, it binds saccharides without the requirement of a Ca^{2+} ion. This can be seen in the crystal structure (Figure 4.35A). Upon binding to the lectin, the carbohydrate sits within a recess/cleft rather than a binding pocket formed between the two dimers (Figure 4.35B-C)[51]. This binding cleft is similar to that seen in the link protein and CD44 (Figure 4.23). Dectin-1 binds to carbohydrates with a β(1-3) but this is enhanced by the addition of a β(1-6) bond upon the saccharide. Dectin-1 binds to polysaccharides such as zymosan, laminarin and pustulan. However, it will not recognise carbohydrates which solely possess a β(1-6) bond[52]. Compared to a binding pocket, the cleft accepts a longer carbohydrate leading to the inability to bind individual monosaccharides as the lectin binds weakly to several of the saccharides in a carbohydrate.

With HA possessing β(1-3) linkages, it meets the criteria for Dectin-1 binding. Whilst the response is low from the sensorgrams, the actual k_a is large with the steep increase upon the addition of HA. The kinetic data acquired from the SPR sensorgrams shows the HA binding to Dectin-1 with a K_D of 150 nM (Figure 4.36A). The K_D of HA is similar to a known β-glycan of laminarin which has a K_D of 200 nM[53]. These β-glycans are based on glucose linked together by β(1-3) linkages, yet for P3 the data cannot be fitted as there is lack of binding with only the 1 μM solution producing a typical SPR

sensorgram. The lectin shows selectivity towards the other glucose epimers of HA-based glycopolymer with P4 and P5 showing no specific binding.
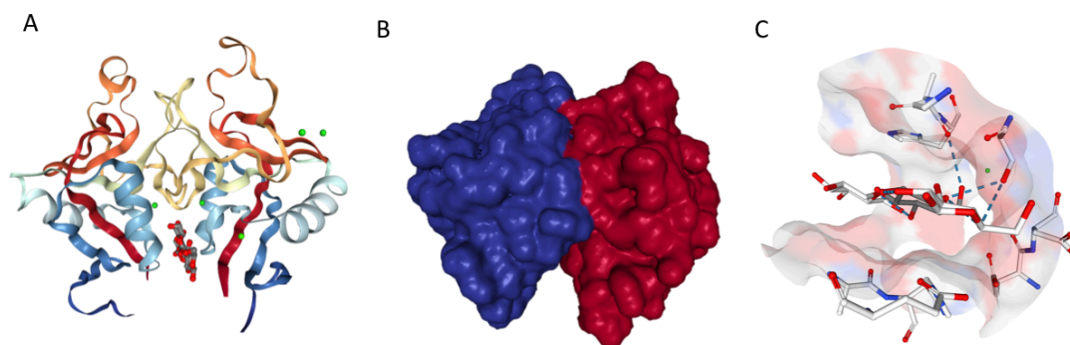
Figure 4.35. Dectin-1 crystal structure (A) with a bound β-glycan trimer, the dimer subunits (B) and the binding of Glc (C) by Ca^{2+} held within the binding pocket.

Of the two monosaccharides found in HA, a clear preference is seen for P7, due to the non-specific binding to P6 once the analyte flow is stopped. When examining the crystal structure of the binding site within the lectin, several hydrophilic residues line on the surface of the binding cleft, including histidine's and arginine's which can interact electrostatically with the carboxylic acid of GlcA, whilst other residues such as serine and aspartic acids can interact through hydrogen bonding. When comparing the K_D of the GlcA-containing glycopolymers, the largest K_D is seen for that of P7 with a K_D of 2 pM, due to the low dissociation constant (Figure 4.36B). The K_D is affected by the organisation of the charge, whereas the k_a for P8 is the fastest of the three, the binding is the weakest as the irregularity of the charge destabilises the interactions leading to the largest k_d (Figure 4.36C) of the 3-GlcA glycopolymers.

From this it can be inferred that the lectin has a preference for regular charge spacing in order to bind, with a preference for charge every monosaccharide unit. The largest response is however seen from P12 (Figure 4.36D) with 186 RU compared with 125 RU (P7) and 52 RU (P8) indicating a higher number of interactions between the lectin and the polymer (Table 4.10). Those glycopolymer with a controlled GlcA sequence (P7, P12) produced the tightest binding and highest response, inferring the necessity for the controlled localisation of negative charge in this lectin.
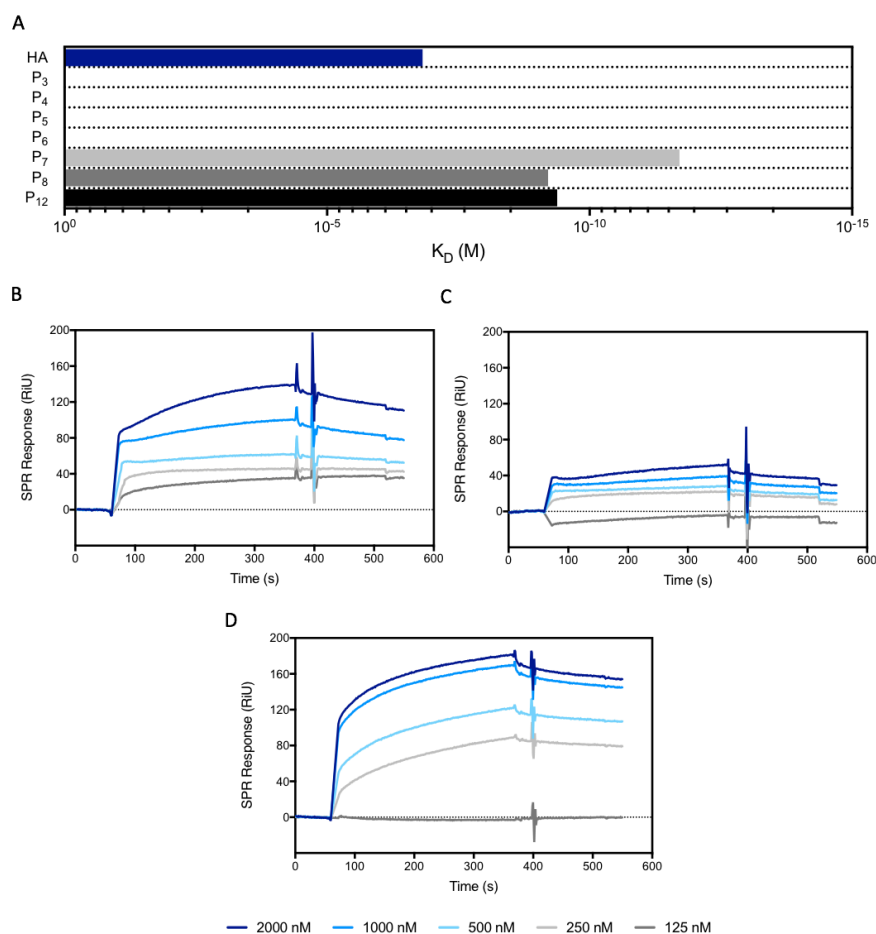
Figure 4.36. K_D values for the binding to Dectin-1 (A) with individual SPR sensorgrams of GlcA containing glycopolymers of P7 (B), P8 (C) and P12 (D).

To further investigate this hypothesis of the charge on the glycopolymers, variants with iduronic acid (IdoA) should be tested to determine whether the stereochemistry of the sugar is necessary for the binding as well as natural alginate. Alginate is a polymer of mannose epimers of GlcA and IdoA and the polysaccharide consists of carboxylates on every unit, similar to P7. Additionally, the alternating polymers, P12, showed the largest response from the SPR. Since GlcA appears to be the crucial residue on the glycopolymer, other alternating glycopolymers are required where a different non-charged monosaccharide such as Glc could be inserted instead of GlcNAc to determine if a different disaccharide creates a stronger binding to this lectin.

Table 4.10. Kinetic data of Dectin-1 with the various polymers.

Macromolecule	Dectin-1				
	k_a (1/Ms)	k_d (s)	RU_{Max}	K_a (M)	K_d (1/M)
HA	5.4×10^3	8.2×10^{-4}	58	6.6×10^6	1.5×10^{-7}
P3	n.s.	n.s.	n.s.	n.s.	n.s.
P4	n.s.	n.s.	n.s.	n.s.	n.s.
P5	n.s.	n.s.	n.s.	n.s.	n.s.
P6	n.s.	n.s.	n.s.	n.s.	n.s.
P7	5.0×10^2	9.8×10^{-9}	125	5.1×10^{11}	2.0×10^{-12}
P8	3.7×10^3	2.3×10^{-6}	52	1.6×10^9	6.3×10^{-10}
P12	7.4×10^2	3.0×10^{-6}	186	2.4×10^9	4.2×10^{-10}

n.s. non-specific binding.

DEC-205

DEC-205[54-55] is a multi-lectin receptor and has been suggested to be a homologous to that of other mannose receptors. It has a c-type lectin domain but no natural ligands have been discovered[56]. Its crystal structure is currently not available with signalling pathways still not fully determined, but it has been shown to play a role in sensing of cell-death[57-58].

Other mannose receptors, such as DC-SIGN, MBL and SP-D, bind terminus saccharides, DEC-205 shows binding to HA of 1.89×10^{-7} M suggesting that this lectin behaves more closely to Dectin-1 and CD44 (Figure 4.37A). The literature suggests that Dectin-1 is thought to be a mannose binding lectin, but when studying the individual monosaccharides on the glycopolymers, no specific binding is seen for P4 or P5, but in contrast P3 showed specific binding with a K_D of 91 nM, inferring this lectin is actually a glucose specific lectin. Since P5 shows no binding and HA shows specific binding to DEC-205, binding is likely to be Ca^{2+} independent, as the C4 hydroxide of both of these polymers is unavailable for binding. This hypothesis is extended by the binding of P6 and P7, which are glucose-based epimers (Figure 4.37B-C). When comparing the binding affinities of P6 and P7, an order of magnitude difference is observed with a K_D of 100 n M and 17 nM, respectively, similarly to Dectin-1, inferring potential interaction with amino acid residues of DEC-205 and the carboxylic acid of GlcA, but as yet there is no crystal structure of DEC-205. The binding affinities are enhanced by the formation of a statistical copolymer containing both monosaccharides. A 2 orders of magnitude decrease in K_D is observed for P8 (K_D

= 910 pM). This is due to the steep, rapid association as well as a lower dissociation compared to individual homoglycopolymers (Figure 4.37D, Table 4.11).
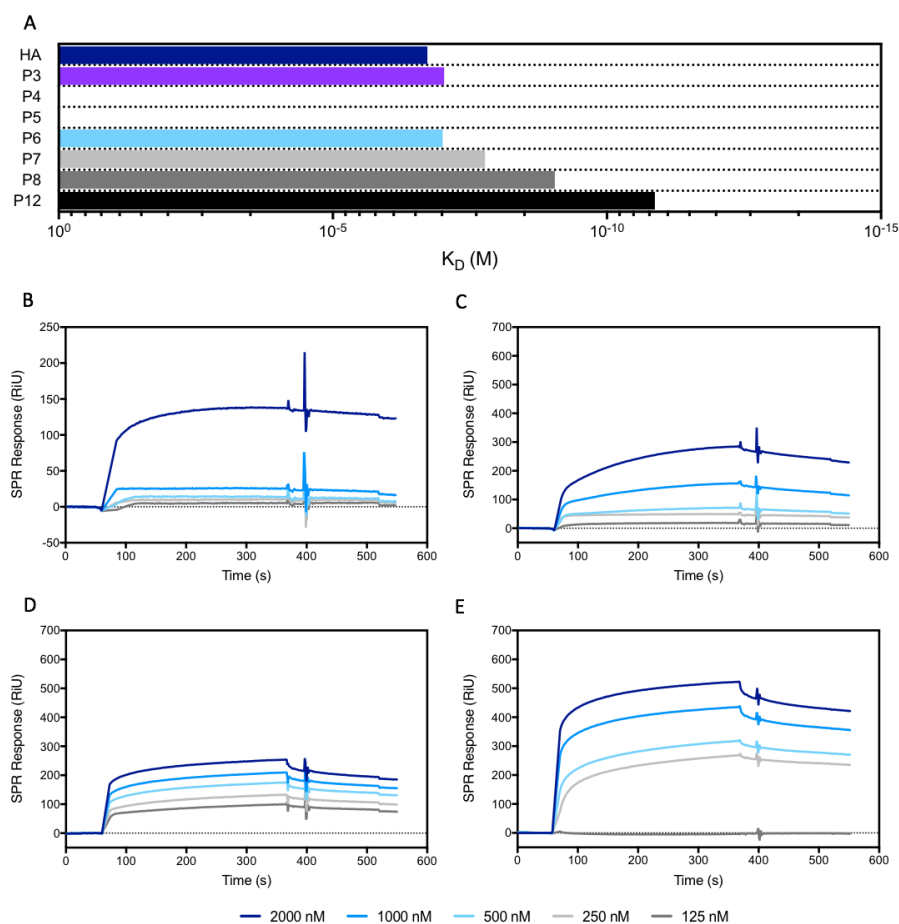
Figure 4.37. K_D values for the binding to DEC-205 (A) with individual SPR sensorgrams of HA-based glycopolymers of P6 (B), P7 (C), P8 (D) and P12 (E).

The binding is further enhanced by an order of magnitude for P12 with a K_D of 13 pM, with k_a of 7.7×10^2 M^{-1}s^{-1} which is half that of P8 at 1.4×10^3 M^{-1}s^{-1} (Figure 4.37A). Although the association is slow, the dissociation is tighter with a k_d of 1.0×10^{-7} s compared to 1.3×10^{-6} s. This indicates the glycopolymers are associating through hydrogen bonding enhanced by the carboxylate at C5. This binding process is slower however, the additional time to adjust into the binding site leads to a stronger binding. By spacing the carboxylic acid out with units of GlcNAc, the glycopolymer is in a superior conformation for favourable interactions with the lectin compared to random positioning of the GlcA, inferring the binding site has periodic residues in which to interact with. With DEC-205 also being referred to as cluster of differentiation-205 (CD-205) similarities can be drawn from other CDs including CD44[33] and CD168 (or RHAMM)[59] which are well known for binding HA.

Table 4.11. Kinetic data of DEC-205 with the various polymers.

Macromolecule	DEC-205				
	k_a (1/Ms)	k_d (s)	RU_{Max}	K_a (M)	K_d (1/M)
HA	5.4×10^3	1.0×10^{-3}	77	5.3×10^6	1.9×10^{-7}
P3	5.6×10^2	5.3×10^{-6}	635	1.1×10^7	9.1×10^{-8}
P4	n.s.	n.s.	n.s.	n.s.	n.s.
P5	n.s.	n.s.	n.s.	n.s.	n.s.
P6	6.5×10^2	6.5×10^{-6}	523	1.0×10^7	1.0×10^{-7}
P7	5.6×10^2	9.3×10^{-6}	303	6.0×10^7	1.7×10^{-8}
P8	1.4×10^3	1.3×10^{-6}	254	1.1×10^9	9.1×10^{-10}
P12	7.7×10^2	1.0×10^{-7}	523	7.5×10^{10}	1.3×10^{-11}

n.s. non-specific binding

From the results of glycopolymers with DEC-205, to better understand the binding to DEC-205 new probes are required. The glycopolymer suggested for Dectin-1 would also be beneficial for DEC-205 due to the apparent similarities in binding between these two lectins. To interpret the lectin binding, the crystal structure would help to define the amino acid residues which line the binding site, to better assess the residues available to bind.

4.3. Conclusion

HA-based glycopolymers showed distinct properties from those of natural HA. These can be seen in the measurements collect for rheology where the polymers show minimal viscoelastic properties by comparison to those of the natural HA. This is linked to the TEM images seen for the formation of aggregates compared to HA which forms long elongated structures in water. Not only is there a physical structural difference, but also a difference in the potentials of the polymers compare to HA. No correlation peak was seen in SAXS to show a polyelectrolyte behaviour and a significant difference observed in the ζ-potential between P12 and HA. All the difference seen between the glycopolymers and HA is based on the lack of a glycosidic bond which ensures that semirigid structure which aids to a small extent the rheological properties, but to the periodicity of the negative charge producing a large negative charge on HA, compare those glycopolymers baring GlcA units. The glycosidic bond aided with the increased M_w is the key driving force for the viscoelastic properties of large Da HA. Though, at this moment glycopolymer by this methodology would struggle to remain at a low polydispersity as the M_w increases in the polymer backbone.

However, the various versions of the glycopolymers synthesized offer insight into the role of HA with a far simpler methodology than conventional carbohydrate synthesis. As probes the glycopolymers have been shown to be non-cytotoxic towards human cell lines and red blood cells, therefore making them potentially applicable to use *in vivo or in vitro*. Their preliminary antimicrobial activity shows potential for future applications, these going against the trends seen by antimicrobial peptide which are positively charged, therefore opening an interesting avenue, with HA being bacteriostatic, whilst the glycopolymers go one step further to be bactericidal. Glycopolymers also offered insights into the binding of HA to peptides and proteins, revealing potential new binders such as lectins by SPR, but it has also been shown through the RAFT group to applicable to other techniques such as SAMs and SPR measurements. Whilst these glycopolymers need fine tuning as HA mimics, there is a vast amount of potential for them.

4.4. Experimental

4.4.1. Materials

Fmoc-amino acids, Mueller Hinton (MH) and 4-methylbenzhydrylamine (MBHA) rink amide resin were purchased from Novabiochem. 3-mercaptopropionic acid, 4-methoxytriphenylmethyl chloride (Mmt), 1-hydroxybenzotriazole hydrate (HOBt), N,N′-diisopropylcarbodiimide (DIC), piperidine, dimethylformamide (DMF), dichloromethane (DCM), trifluoroacetic acid (TFA), anisole, thioanisole, 1,2-ethanedithiol (EDT) triisopropylsilane (TIS), diethyl ether, acetonitrile (ACN), acryloyl chloride, triethylamine (TEA), tetrahydrofuran (THF), copper bromide (CuBr), dimethyl sulfoxide (DMSO), phosphate buffer saline (PBS), bromoethanol and the Kaiser Test Kit were purchased from Sigma-Aldrich and were used without further purification. Sodium azide (NaN_3), magnesium sulfate ($MgSO_4$), sodium phosphate was purchased from VWR. Triton-X purchased from Alfa Aesar and LIVE/DEAD™ viability/cytotoxicity Kit for mammalian cells from Invitrogen. Recombinant Human CD44 24 kDa was purchased Cambridge Bioscience. The lectins are purchased from R and D System.

4.4.2. Instruments and Analysis

4.4.2.1. Rheology

Rheology measurements for HA and glycopolymer solutions were carried out in a HAAKE RS150 rheometer equipped with 30 mm cone and plate set 0.19 mm apart with angle of 5° between the surface the conical surface of the cone. The viscosity was measured at 37 °C regulated by a water bath connected to the plate. The viscosity was monitored at fourteen different shear rates increasing linearly from 70 s^{-1} to 1000 s^{-1}. The average was taken from 20 measurements, using the Rheowin software.

4.4.2.2. Small Angle X-ray Scattering (SAXS)

Small angle x-ray scattering patterns of glycopolymer solutions were obtained with a SAXSLAB GANESHA 300-XL. CuK$_\alpha$ radiation was generated by a Genix 3D Cu-source with an integrated monochromator, 3-pinhole collimation and a two-dimensional Pilatus 300K detector. The scattering intensity q was recorded at intervals of $0.012 < q < 0.3$ Å^{-1} (corresponding to lengths of 10-800 Å). Measurements were performed under vacuum at ambient temperature. The scattering curves were

corrected for counting time and sample absorption. The solution under study was sealed in thin-walled quartz capillaries with about 1.5 mm in diameter and 0.01 mm wall thickness. The scattering spectra of the solvent were subtracted from the corresponding solution data using the Irena package for analysis of small-angle scattering data[60] Data analysis was based on fitting the scattering curve to an appropriate model by software provided by NIST (NIST SANS analysis version 7.0 on IGOR) [61].

Model fitting of small-angle scattering pattern

The form factor of a semiflexible chain with excluded volume effects is expressed by equations Equation 4.6 & Equation 4.7[11, 62].

$$P(q,b,L,R_{cs}) = P_{exv}(q,b,L) + C(L/b)\frac{b}{15L}\left[4 + \frac{7}{u} - \left(11 + \frac{7}{u}\right)e^{-u}\right] \cdot \left[2\frac{J_1(q,R_{cs})}{q,R_{cs}}\right]$$
<div align="right">Equation 4.6</div>

$$P_{exv}(q,b,L) = \left[1 - w(qR_g)\right] \cdot P_{Debye}(q.b.L) + w(qR_g)\left[C_1(qR_g)^{-1/v}C_2(qR_g)^{-2/v}C_3(qR_g)^{-3/v}\right]$$
<div align="right">Equation 4.7</div>

4.4.2.3. Visible Light Spectroscopy

Visible light spectroscopy was carried out on a Lambda35 Ultraviolet-Visible Light Spectrometer (Perkin Elmer), with turbidity measurements done at a fixed wavelength of 650 nm, while visible light scans were run between 400-700 nm. Turbidity measurements were performed by dissolving the glycopolymer in water at pH 7.0 from 0.1 mM to 1.0 nM by serial dilution. The resulting solution transmittance was measured at 650 nm and compared to a control of water.

4.4.2.4. Critical Aggregation Concentration (CAC)

The CAC for the glycopolymers was determined by producing a serial dilution of peptide solutions from 0.1 mM to 1 nM. These solutions were added to Eppendorf's containing Nile Red, with the samples being left 16 hours to allow the incorporation of the Nile Red into any aggregates formed by the peptides. The fluorescence emission spectrum was measured on an LS55 fluorescence spectrometer (PerkinElmer) ranging from 580 to 720 nm with an excitation wavelength at 550 nm.

4.4.2.5. Dynamic Light Scattering (DLS)

Dynamic light scattering of the glycopolymers was measured on a Nano-ZS Zetasizer (Malvern Instruments). The solutions were prepared above the CAC (1 mM) at pH 7 and allowed to stand for 48 hours to ensure aggregation. The solutions were diluted 10-fold and passed through a 0.2 µm filter. The cell and the machine were cleaned using compressed air to ensure removal of large dust particles, before reading.

4.4.2.6. Cell Viability

Cell viability was assessed using the LIVE/DEAD™ viability/cytotoxicity kit for mammalian cells (Invitrogen) and following the manufacturer's instructions. Briefly, LuC4 cells were seeded at 5,000 cells per well into a 96 well plate and grown in a humidified atmosphere at 37 °C, 5% CO_2 for 48 hours. Cells were treated with glycopolymers at a range of concentrations, 0.1, 1, 10, 100, µg/mL, and incubated for 24 hours. Media was removed, and Live/dead stains of Calcein and Ethidium homodimer-1 were added in PBS and incubated for 1 hour. Fluorescence was measured using in Synergy HT (BioTek) plate reader at 494 nm excitation & 517 nm emission for Calcein and 528nm excitation & 617 nm emission for Ethidium homodimer-1. The number of live and dead cells was calculated as a percentage of the fluorescent output compared to the controls of untreated for the live control and methanol fixed cells for the dead assay with an untreated cell negative for dead assay.

4.4.2.7. Minimum Inhibitory Concentration (MIC)

The MIC of the glycopolymers was determined by plating the glycopolymers in Mueller Hinton (MH) broth (100 µL), which was serially diluted down the wells. The bacteria concentration was determined by OD_{600} measurement and diluted to a concentration of cells of 6×10^6. The cells (50 µL) were added to the wells to make a final concertation of 3×10^6 cells. The plates were incubated for 16 hours at 37 °C and then inspected for turbidity.

4.4.2.8. Haemolytic Assay

Ethics Disclaimer: Fresh blood was obtained from St Georges Hospital Blood Testing department and transported in vacutainers containing citrate. No ethical approval

was required, due to the blood not being stored and only being used by the researcher themselves.

Blood was centrifuged (2998 rpm, 5 mins) in 2 ml microfuge. The supernatant was removed, and PBS (pH 7.4) was added before re-centrifugation, this was repeat three time. The red blood cells (RBCs) were diluted in PBS to form 4% suspension. The 4% untreated was used as a negative control, whilst the 4% RBC suspension (90 µL) was plated with the glycopolymers (40 µL) and serial diluted across the plate. Triton-X (0.1%) was used as positive control, PBS and untreated cells as negative controls. The plate was incubated for 1 hour at 37 °C. Plates were centrifuged (2998 rpm, 5 minutes at 4 ˚C). After formation of the red blood cell pellets, 70 µl of supernatant was removed from each well and transferred into clear, flat, round bottom 96 well plate, ensuring the pellets were not disturbed. The absorbance plates were measured in a Tecan INFINITE pro 2000 (Tecan, USA) plate reader at 450 nm.

4.4.2.9. Self-Assembled Monolayers (SAMs) of Thiol-HABPeps on Gold

The formation of the SAMs was performed on gold, cleaned with basic piranha mixture before use. The clean gold surfaces were placed in an ethanoic solution of Thiol-HABPep-3 (1% w/v) for 24 hours at 37 ºC, after which the surface was washed with water and dried under nitrogen stream.

Surface Analysis

The contact angle was measured using water (2 µL) a Drop Shape Analyzer – DSA100 (Kurss, Germany). The incubation process was repeated in an aqueous solution of 1.5 MDa HA (0.5% w/v). The contact angle was again measured and compared to a control of a bare gold surface which had been treated in a similar way but with no peptide or HA in the incubation solutions.

3D Analysis

UV-visible spectra of colloidal gold nanoparticles were collected over the range from 400 to 800 nm using a Cary 100 UV-Vis spectrophotometer. TEM images were obtained on a FEI Tecnai transmission electron 3S microscope operating at a bias voltage of 80 kV. All samples (~10 µL) were deposited and evaporated on carbon film 400 mesh copper grids.

4.4.2.10. Surface Plasmon Resonance (SPR)

Surface plasmon resonance (SPR) was used for investigating the interaction of the polymers with peptides and protein. This was performed on a BIAcore 2000 system (GE Healthcare, UK). Lectins (0.025 mg/ml) were immobilized *via* a standard amino coupling protocol onto a CM5 sensor chip (carboxymethylated dextran covalently attached to a gold surface) that was activated by flowing a 1:1 mixture of 0.1 M *N*-hydroxysuccinimide and 0.1 M *N*-ethyl-*N'*-(dimethylaminopropyl)carbodiimide over the chip for 5 min at 25 °C at a flow rate of 5 µL/min after the system equilibration with HEPES filtered buffer (10 mM HEPES pH 7.4, 150 mM NaCl, 5 mM $CaCl_2$). Subsequently, channels 1 (blank), 2, 3 and 4 were blocked by flowing a solution of ethanolamine (1 M, pH 8.5) for 10 min at 5 µL/min to remove remaining reactive groups on the channels.

For the immobilization of peptides, a blank CM5 sensor chip (gold surface without any modification) was used and each thiolated peptide (1 mg/ml) was run at a flow rate of 2 µL/min for 15 min at 25 °C to allow attachment of peptide on the gold surface.

Glycopolymer solutions were prepared at varying concentrations (2000 nM-125 nM) in the same HEPES buffer to calculate the binding kinetics. Sensorgrams for each glycopolymer concentration were recorded with a 300 seconds injection of polymer solution (*on period*) followed by 150 seconds of buffer alone (*off period*). Regeneration of the sensor chip surfaces was performed using 10 mM HEPES pH 7.4, 150 mM NaCl, 10 mM EDTA, 0.01% P20 surfactant solution. Kinetic data was evaluated using a single set of sites (1:1 Langmuir Binding) model in the BIA evaluation 3.1 software.

4.4.3. Methods

4.4.3.1. Bromoethyl acrylate
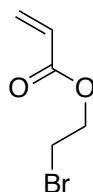
The synthesis has been modified from a previously reported method[13]. Briefly, 2-bromoethanol (10 mL, 141 mmol) was dissolved in DCM (50 mL) followed by the addition of TEA (23.5 mL, 170 mmol) under a nitrogen atmosphere. The reaction was cooled to 0 °C after which point acryloyl chloride (9.2 mL, 113 mmol) was added

dropwise over an hour. The reaction was then allowed to warm to room temperature and stirred for 16 hours. The resulting solid was filtered off and washed with DCM. The organic layer was washed with water (2 × 100 mL) followed by brine (2 × 100 mL). The organic layer was dried with MgSO$_4$, filtered and reduced under reduced pressure to give the product as a colourless oil.

^{1}H NMR (CDCl$_3$, 400 MHz)	δ: 6.41 (d, 1H, 16 Hz C=C**H$_2$** trans), 6.11 (dd, 1 H, 16 Hz, 9.8 Hz 1H, HC=C), 5.85 (d, 9.8 Hz, C=C**H$_2$** cis), 4.42 (t, 2H, 6.1 Hz, C**H$_2$**Br), 3.51 (t, 2H, 6.1 Hz, OC**H$_2$**).

4.4.3.2. poly bromoethyl acrylate (P13)
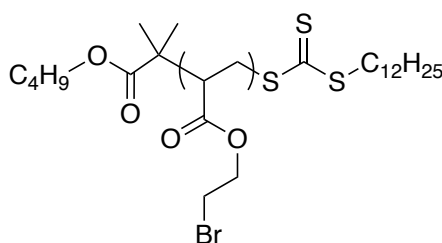
^{1}H NMR ((CD$_3$)$_2$CO, 400 MHz)	δ: 4.40 (br, 2H, CH$_2$Br), 3.55 (br, 2H, CH$_2$O), 2.45 (br, 1H, CH), 1.76 (br, 2H, CH$_2$), 1.53 (br, RAFT-CH$_2$), 0.84 (br, RAFT-CH$_3$)
FT-IR (ATR):	2950.5 (C-H), 1731.6, 1710.4 (C=O), 1360.9, 1220.6, 1152.6, 570.4, 529.3

4.4.3.3. poly azidoethyl acrylate (P14)
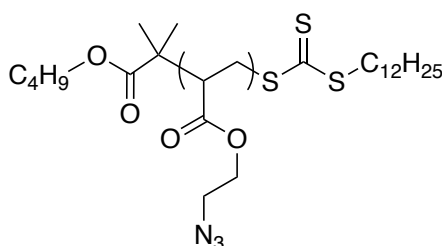
^{1}H NMR ((CD$_3$)$_2$CO, 400 MHz)	δ: 4.20 (br, 2H, CH$_2$Br), 3.48 (br, 2H, CH$_2$O), 2.41 (br, 1H, CH), 1.73 (br, 2H, CH$_2$), 1.53 (br, RAFT-CH$_2$), 0.84 (br, RAFT-CH$_3$)
FT-IR (ATR):	2952.4 (C-H), 2101.2 (N$_3$), 1730.8 (C=O), 1360.9, 1240.6, 1156.7, 1044.7

4.4.3.4. 1-azido-3-chloropropan-2-ol (21)

The synthesis has been modified from previously reported method[63]. Briefly, epibromohydrin (5 mL, 63.3 mmol) was suspended in water (20 mL) with acetic acid (2.5 mL). Sodium azide (5 g, 75.7 mmol) was added to the solution and stirred for 5 hours at 30 °C. The resulting solution was cooled to room temperature and washed with diethyl ether (3 × 15 mL). The organic layer was collected and washed with sodium phosphate buffer (50 mM) (15 mL) followed by the organic layer dried over MgSO$_4$, filtered and reduced under reduced pressure to produce a yellow oil.

^{1}H NMR ((CD$_3$)$_2$CO, 400 MHz)	δ: 3.97 (q, 5.4 Hz, 1H, C**H**OH), 3.48 (dd, 5.1 Hz, 4.4 Hz, 2H, CH$_2$N$_3$), 3.44 (d, 5.0 Hz, 2H, CH$_2$N$_3$), 1.73 (br, 2H, CH$_2$), 1.53 (br, RAFT-CH$_2$), 0.84 (br, RAFT-CH$_3$)
FT-IR (ATR):	3367.1 (OH), 2904.3 (CH), 2098.8 (N$_3$), 1707.22, 1257.5, 1044.8, 929.7, 750.5, 554.7

4.4.3.5. 1-azido-3-chloropropan-2-acryalte (22)


The synthesis has been modified from previously reported method[13]. Briefly, **21** (5 g, 27 mmol) was dissolved in DCM (30 mL) followed by the addition of TEA (4.5 mL, 32 mmol) under a nitrogen atmosphere. The reaction was cooled to 0 °C after which point acryloyl chloride (2.9 mL, 21.6 mmol) was added dropwise over an hour. The reaction was then allowed to warm to room temperature and was stirred for 16 hours. The resulting solid was filtered off and washed with DCM. The organic layer was washed with water (2 ×100 mL) followed by brine (2 ×100 mL). The organic layer was dried with MgSO$_4$, filtered and reduced under reduced pressure to give the product as a yellow oil.

FT-IR (ATR):	2952.4 (C-H), 2104.1 (N$_3$), 1732.5 (C=O), 1372.5, 1237.2, 1042.8, 607.4, 503.0

4.4.3.6. General procedure for CuAAc click reaction on small molecules

The monomer (1 equiv with respect to azide), acetylated alkyne sugar (1.5 equiv), Me_6TREN (2 equiv) were suspended in DMSO (2 ml/g of solid) and degassed by gentle bubbling of Ar gas for 30 minutes. CuBr was charged into a Schlenk tube and degassed by gentle bubbling of Ar gas for 30 minutes. The degassed solution was cannulated into the Schlenk tube, with the solution and catalyst being stirred. The reaction was stirred at 25 ºC for 48 hours. The resulting solution was diluted by water (v/v) and washed with DCM (3 × 20 mL). The organic later were combined, dried over $MgSO_4$, filtered and reduced under reduced pressure.

4.4.3.6.40. 1-GlcNAc-3-chloropropan-2-ol (23)
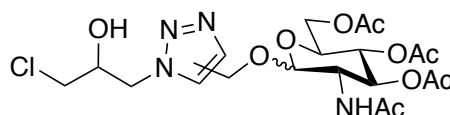
FT-IR (ATR):	3395.4 (OH), 1741.6 (CO), 1661.8, 1552.6, 1435.0, 1370.6, 1218.3, 1123.6, 1017.3, 949.9

4.4.3.7. General procedure for azidation of small molecule.

The synthesis has been modified from previously reported method[64]. Briefly, the chloride functionalised compound was suspended in DMSO followed by the addition of NaN_3 (1.5 equiv per halide) and stirred for 16 hours at 25 ºC. The resulting solution was diluted into water and extracted in EtOAc (3 × 50 mL). The organic layers were combined, dried over $MgSO_4$, filtered and reduced under reduced pressure to give the crude product.

4.4.3.7.41. 1-GlcNAc-3-azidoopropan-2-ol (24)
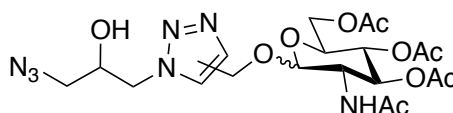
FT-IR (ATR):	3395.2 (OH), 2106.4 (N_3), 1739.3 (CO), 1660.4, 1552.6, 1436.0, 1371.4, 1221.8, 1120.1, 1016.3, 951.3

4.4.3.7.42. 1-GlcNAc-3-GlcA-propan-2-ol (25)
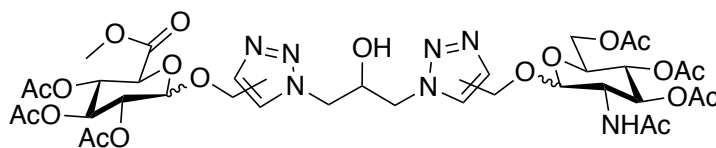
FT-IR (ATR):	3270.4 (OH), 2657.7 (CH), 1741.5 (CO), 1661.5, 1542.7, 1436.9, 1371.5, 1214.6, 1158.9, 1036.6, 951.4, 897.1, 788.3, 698.2, 666.9, 634.5, 600.0

4.4.3.8. 3-(((4-methoxyphenyl)diphenylmethyl)thio)propanoic acid

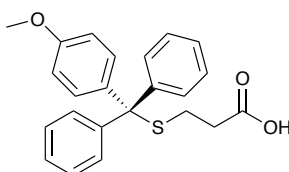To a stirring solution of Mmt-Chloride (3.5 g, 11.33 mmol) in 1:1 DCM/DMF (30 mL) and DIPEA (2.8 mL), the mercapto acid (0.82 mL, 9.4 mmol) was added dropwise. The reaction was allowed to stir for 16 hours. The reaction mixture was concentrated and then suspended in H_2O (50 mL) which was washed with ether (3 × 50 mL). The organic layer was washed with brine (100 mL), dried over $MgSO_4$ and reduced under reduced pressure. The oil was dried under high vac leaving a white powder (1.71 g, 4.5 mmol, 48%).

^{1}H NMR (CDCl$_3$, 400 MHz)	δ: 7.49 (d, 4H, 7.5 Hz, *m*-C**H)**, 7.39 (d, 2H, 8.9 Hz, *o*-C**H)**, 7.35 (t, 4H, 7.1 Hz, *o*-C**H)**, 7.29 (d, 2H, 7.1 Hz, *p*-C**H)**, 6.89 (d, 2H, 8.9 Hz, *m*-C**H)**, 3.86 (s, C**H**$_3$), 2.54 (t, 5.1 Hz, 2H, SC**H₂)**, 2.34 (t, 5.1 Hz, 2H, C**H₂**COOH)
^{13}C NMR (CDCl$_3$, 133 MHz)	177.52 (1C, **C**OOH), 158.23 (1C, H$_3$CO**C)**, 145.00 (1C, **C**C), 136.78, 130.87 (2C, o-C**H)**, 129.58 (4C, *m*-C**H)**, 128.04 (4C, o-C**H)**, 126.79 (2C, *p*-C**H)**, 113.32 (2C, *m*-C**H)**, 66.56 (1H **C**S), 55.35 (1C, C**H**$_3$), 33.53 (1C, **C**H$_2$COOH), 26.72 (1C, SC**H**$_2$)
FT-IR (ATR):	2833.0 (CH), 1708.7 (CO), 1592.9, 1508.1, 1430.9, 1249.7, 1027.9, 817.7, 740.5, 700.0, 580.5, 534.2

4.4.3.9. Thiol Peptide Capping

The peptide bound to the resin was removed from the peptide synthesiser with the 3-(((4-methoxyphenyl) diphenylmethyl)thio)propanoic acid coupled manually using HOBt and DIC in 4 times excess. The mixture was shaken for 2 hours. After the capping cycle, the resin was subsequently washed with DMF followed by DCM with Kaiser test confirming the coupling.

4.4.3.10. Thiol Peptide Cleavage

Once positive coupling was achieved, the peptide and acid-labile side groups were cleaved by TFA/thioanisole/anisole/EDT (90:5:2.5:2.5) for 3 hours. The solution was collected, concentrated by reduced pressure and precipitated in cold ether. The resulting suspension was collected by centrifugation and decanting the supernatant, followed by lyophilisation to obtain a white solid.

4.4.3.11. Peptide Characterization and Purification

The crude peptides were passed through a 0.2 μm filter and then purified on an Auto Purification System (Waters) using a preparative reverse-phase C18 column (XBridge, 130 Å, 5 μm, 30×150 mm, Waters) at 25 °C with a gradient running from 98:2 to 0:100 of water/acetonitrile supplemented with 0.1% TFA over a 30-minute period at 20 mL/min. The fractions were collected by the SQ Mass Detector (Waters), combined, reduced under reduced pressure and then lyophilised to produce a white powder.

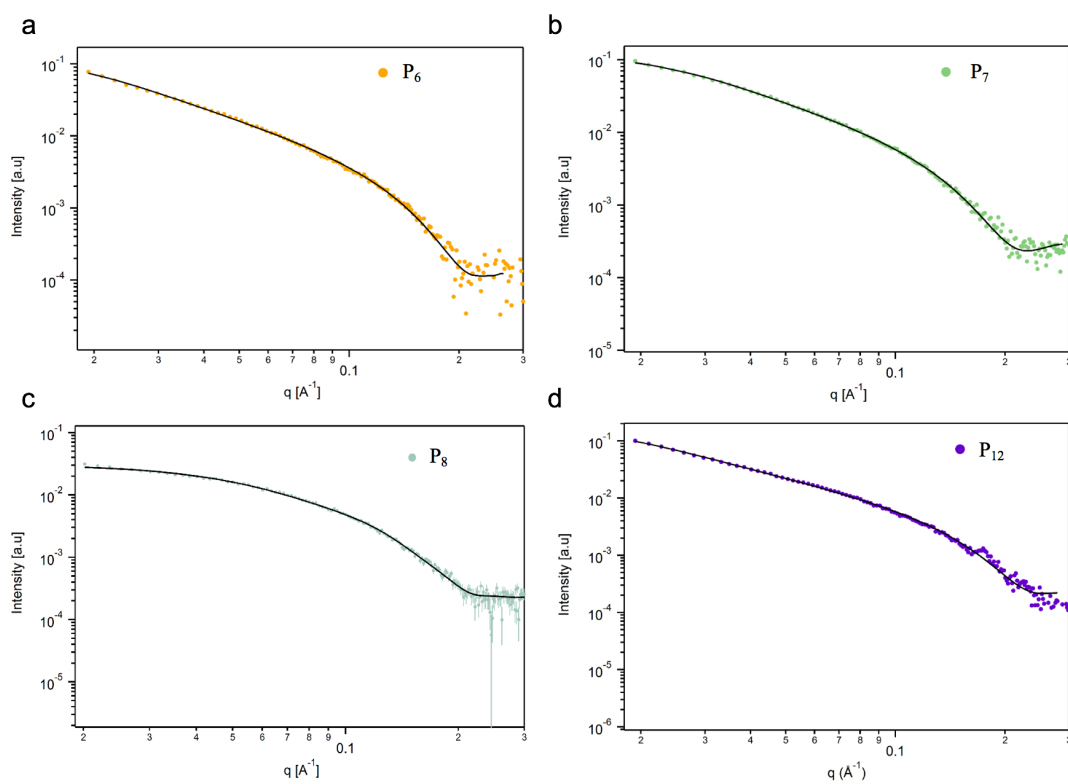## 4.5. Appendix

4.5.1. SAXS of the Glycopolymers

Figure A 4.1. SAXS data of the glycopolymers at 0.2 mM at pH 7 fitted to a model shown in the black line

4.5.2. Peptide Analysis

4.5.2.1. HS-RYPISRPRKR-CONH₂ (Thiol-HABPep-1)

Figure A 4.2. HPLC trace of purified Thiol-HABPep-1 running a gradient of 98: 2 to 0: 100 (H_2O + 0.1 % TFA: ACN + 0.1 % TFA) over a 30-minute period at a flow rate of 1 ml/min

Figure A 4.3. ESI Mass spectrum of Thiol-HABPep-1 measured in the positive ion channel

RP-HPLC (mins)	10.08
Purity (%)	> 99%
ESI-MS (m/z)	1416.7 [Expected], 724.9 [M+2H]²⁺, 473.4 [M+3H]³⁺, 355.5 [M+4H]⁴⁺

4.5.2.2. HS-KNGRYSISR-CONH₂ (Thiol-HABPep-2)
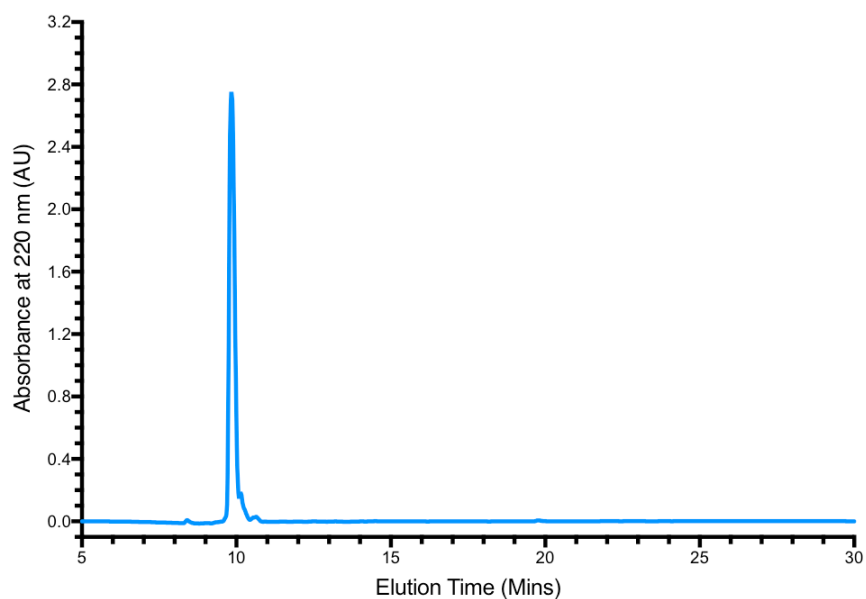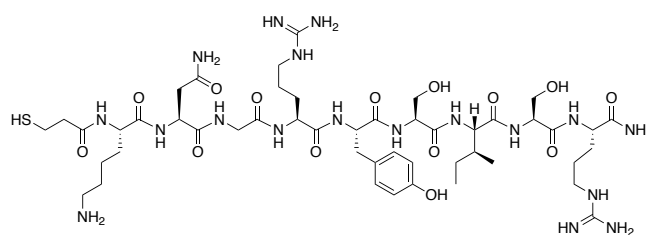
Figure A 4.4. HPLC trace of purified Thiol-HABPep-2 running a gradient of 98: 2 to 0: 100 (H₂O + 0.1 % TFA: ACN + 0.1 % TFA) over a 30-minute period at a flow rate of 1 ml/min.
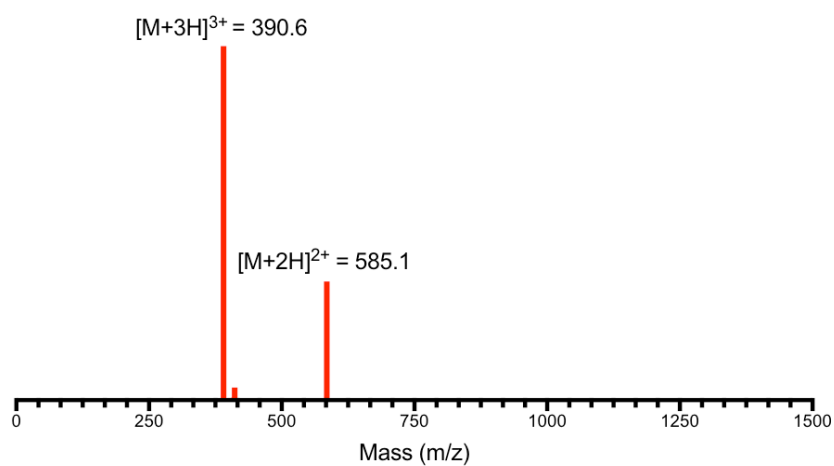
Figure A 4.5. ESI Mass spectrum of Thiol-HABPep-2 measured in the positive ion channel.

RP-HPLC (mins)	9.87
Purity (%)	> 98%
ESI-MS (m/z)	1167.4 [Expected], 585.1 [M+2H]$^{2+}$, 390.6 [M+3H]$^{3+}$

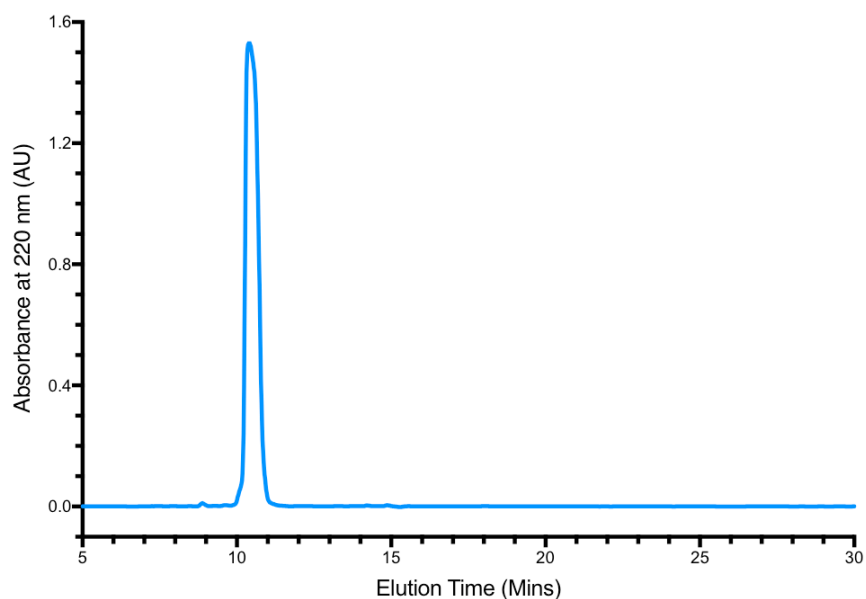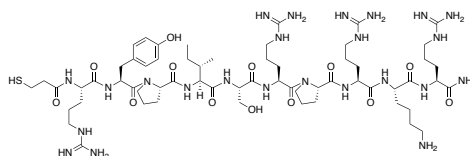*4.5.2.3. HS-GAHWNFQALTVR-CONH$_2$ (Thiol-HABPep-3)*
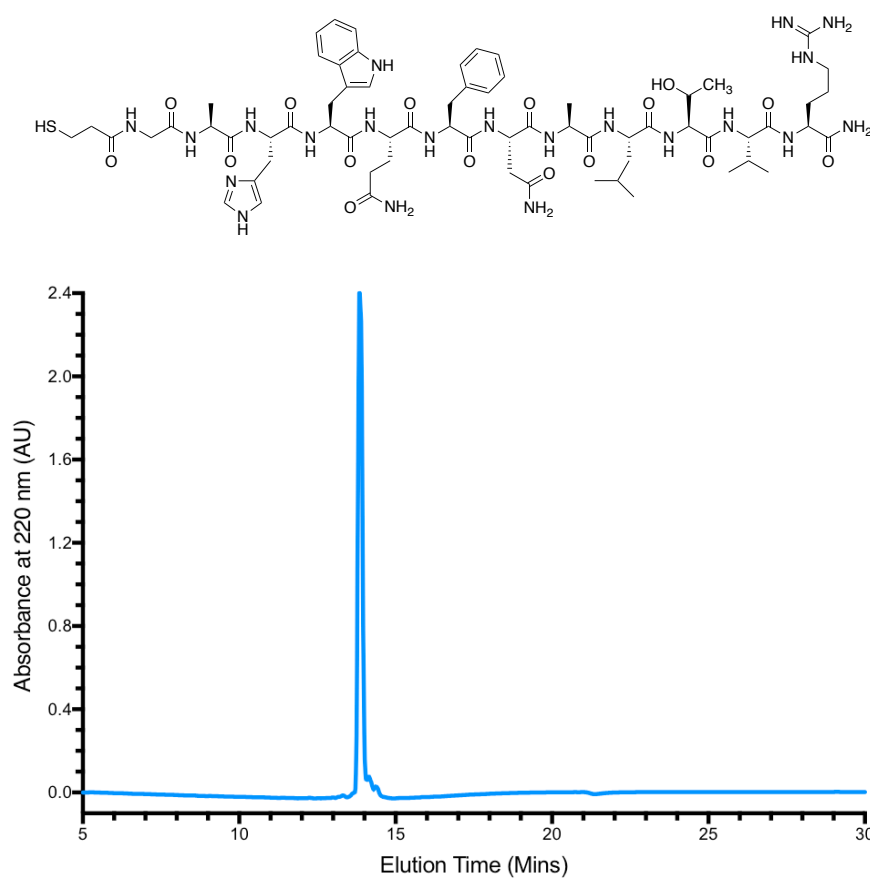
Figure A 4.6. HPLC trace of purified Thiol-HABPep-3 running a gradient of 98: 2 to 0: 100 (H$_2$O + 0.1 % TFA: ACN + 0.1 % TFA) over a 30-minute period at a flow rate of 1 ml/min.
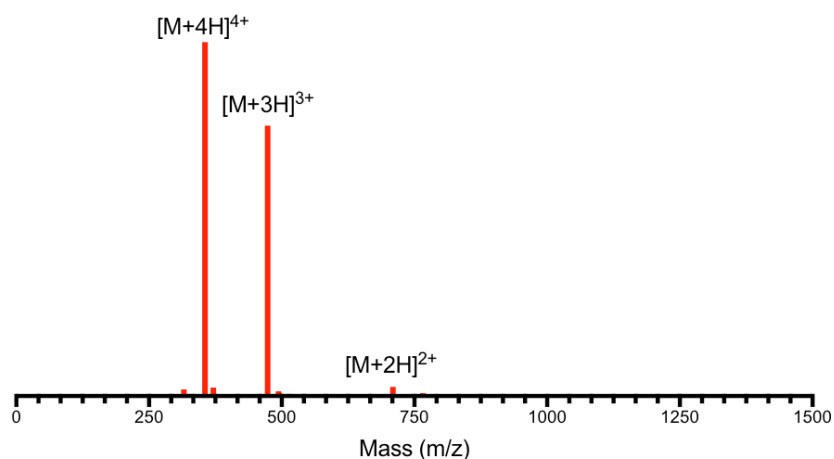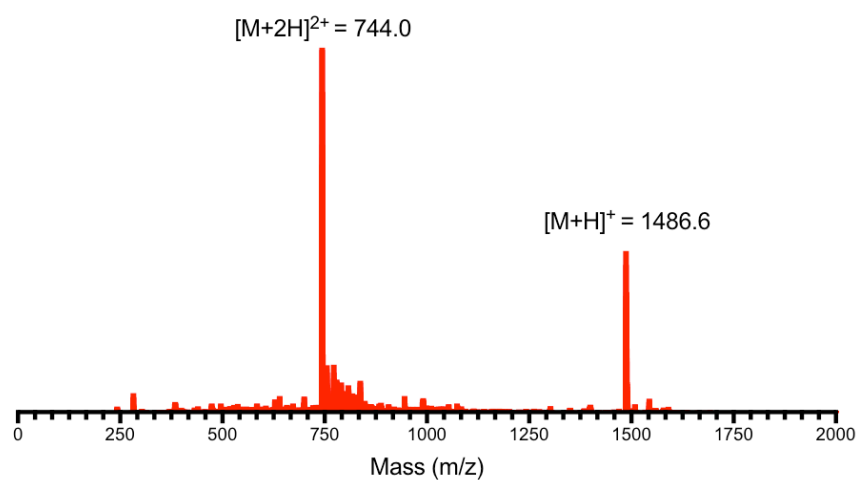

Figure A 4.7. ESI Mass spectrum of Thiol-HABPep-3 measured in the positive ion channel.

RP-HPLC (mins)	13.88
Purity (%)	> 97%
ESI-MS (m/z)	1486 [Expected], 1486.6 [M+H]$^+$, 744.0 [M+2H]$^{2+}$

4.5.3. Nile Red Assay
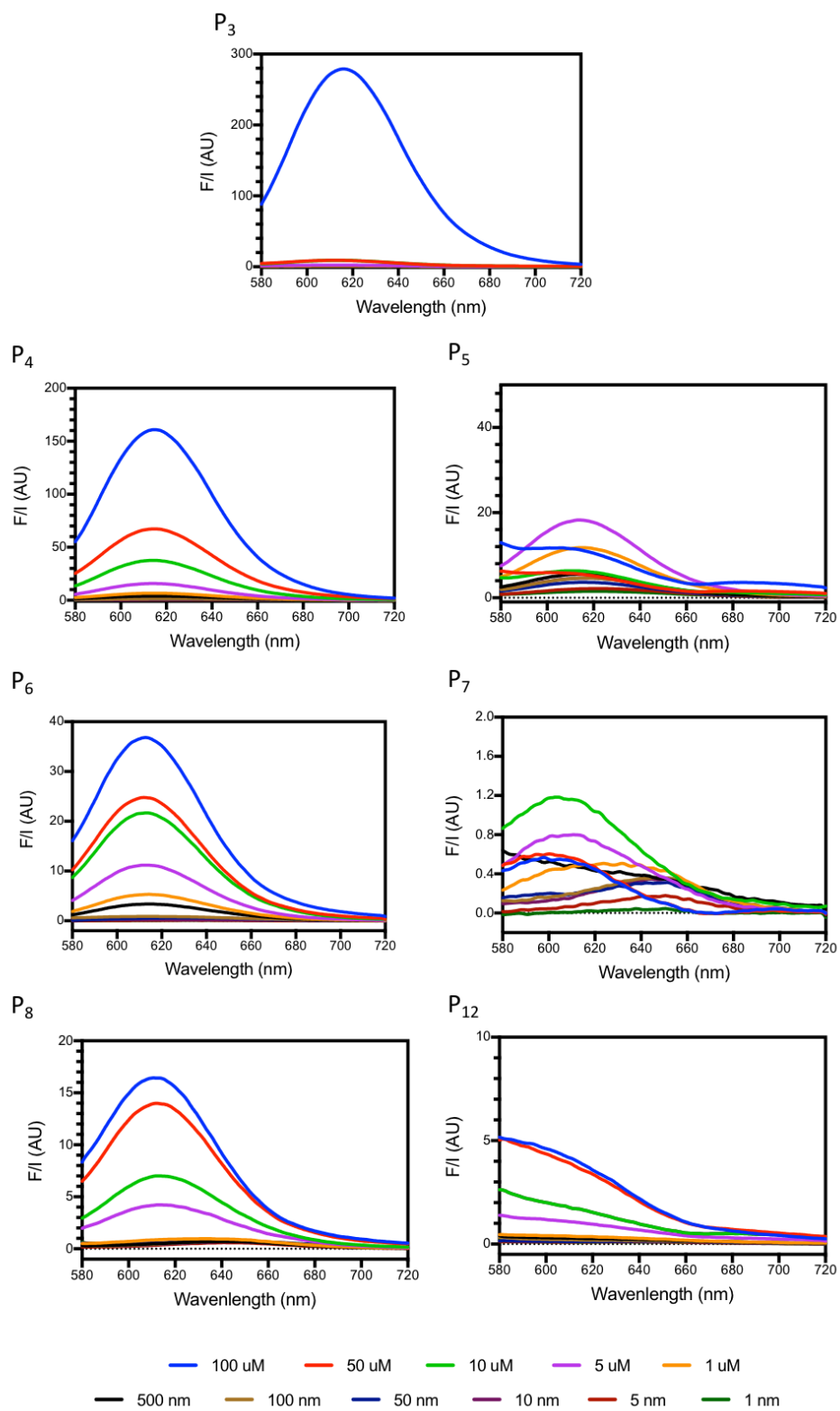
Figure A 4.8. Nile Red emission when excited at 550 nm at increasing concentrations of the glycopolymers in H_2O

4.5.4. SPR
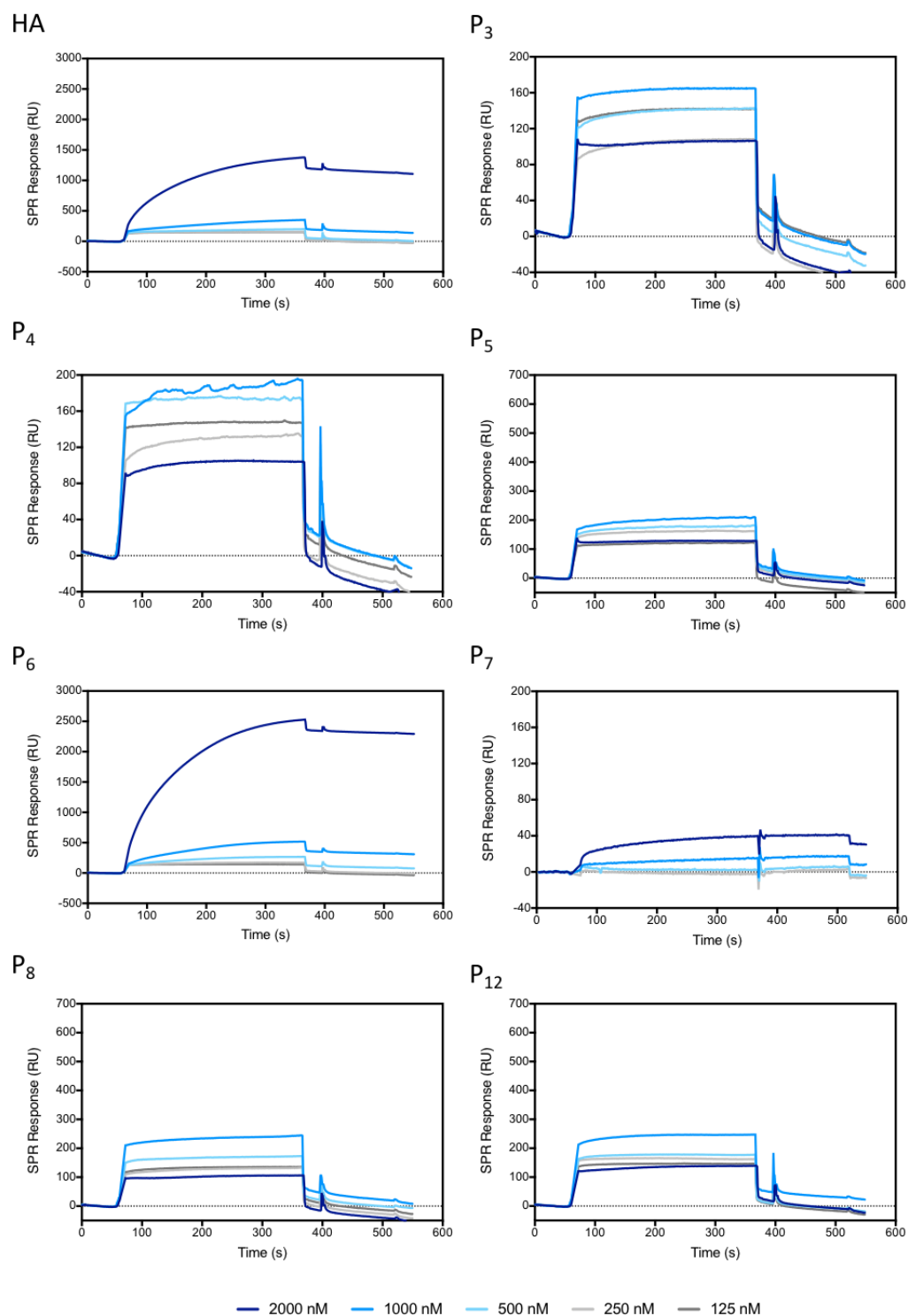
Figure A 4.9. SPR sensorgrams showing the binding of the various polymers on Thiol-HABPep-3.
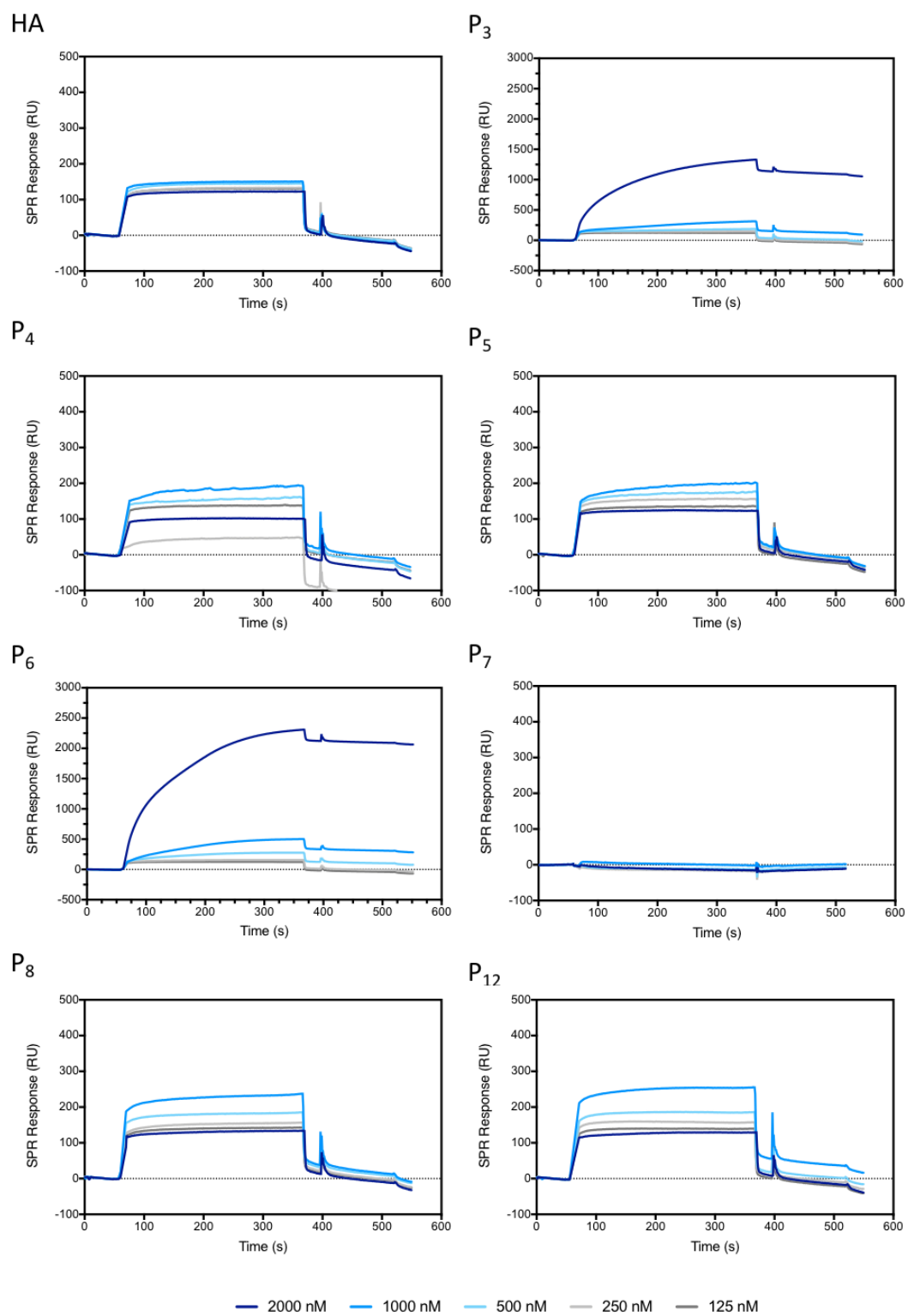
Figure A 4.10. SPR sensorgrams showing the binding of the various polymers on HABTPep-1.
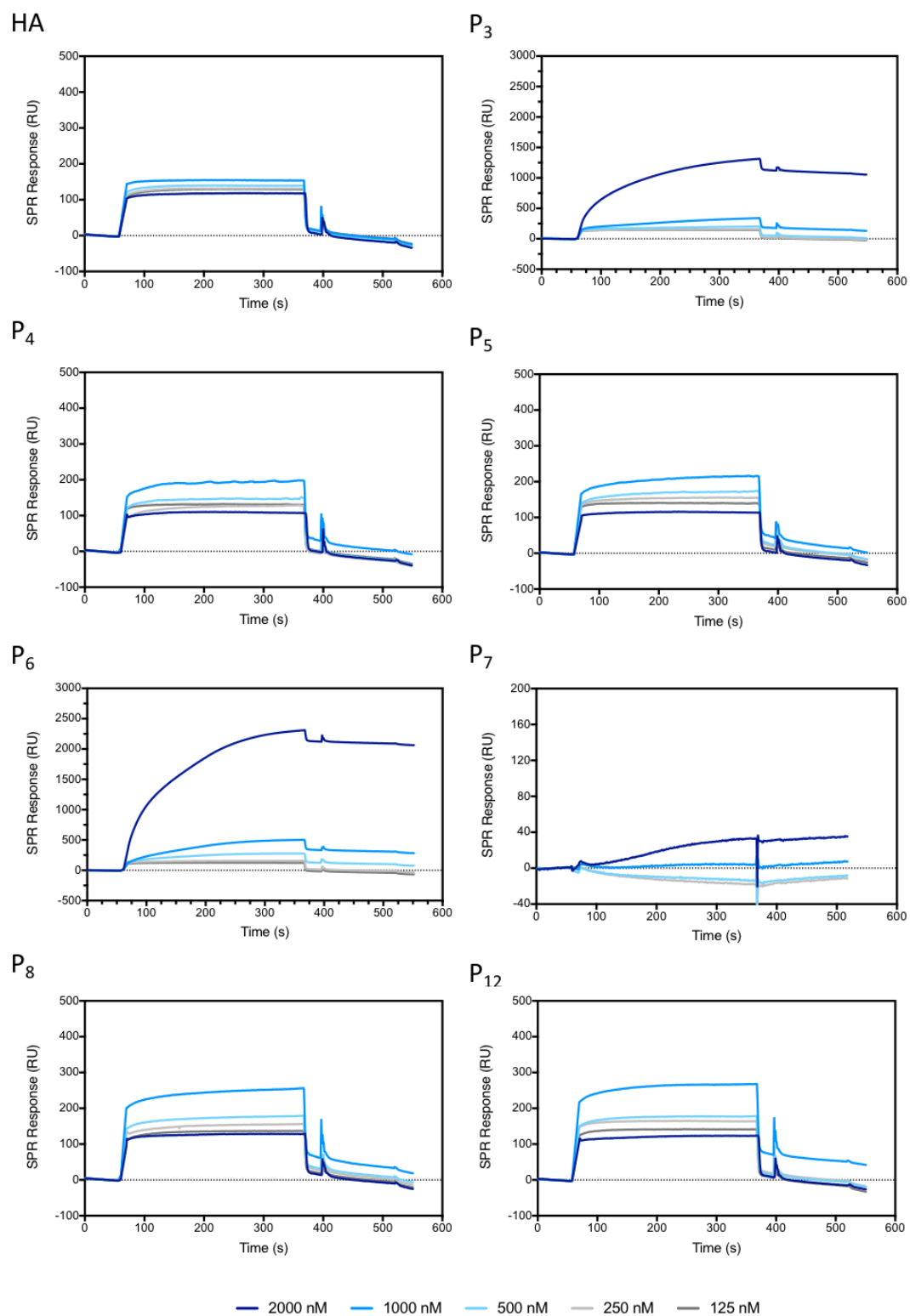
Figure A 4.11. SPR sensorgrams showing the binding of the various polymers on Thiol-HABPep-2.
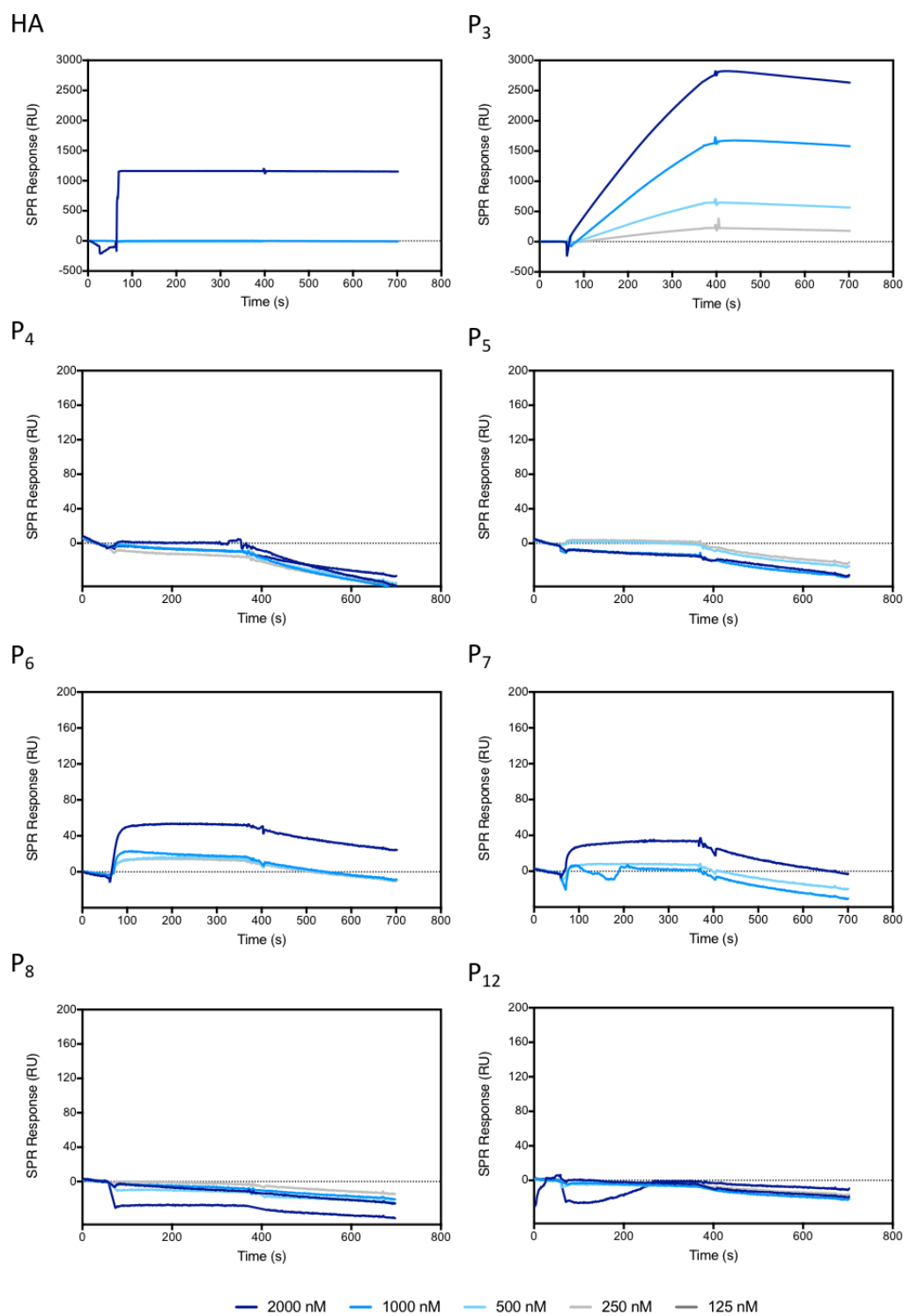
Figure A 4.12. SPR sensorgrams showing the binding of the various polymers on the. extracellular domain of CD44 protein.
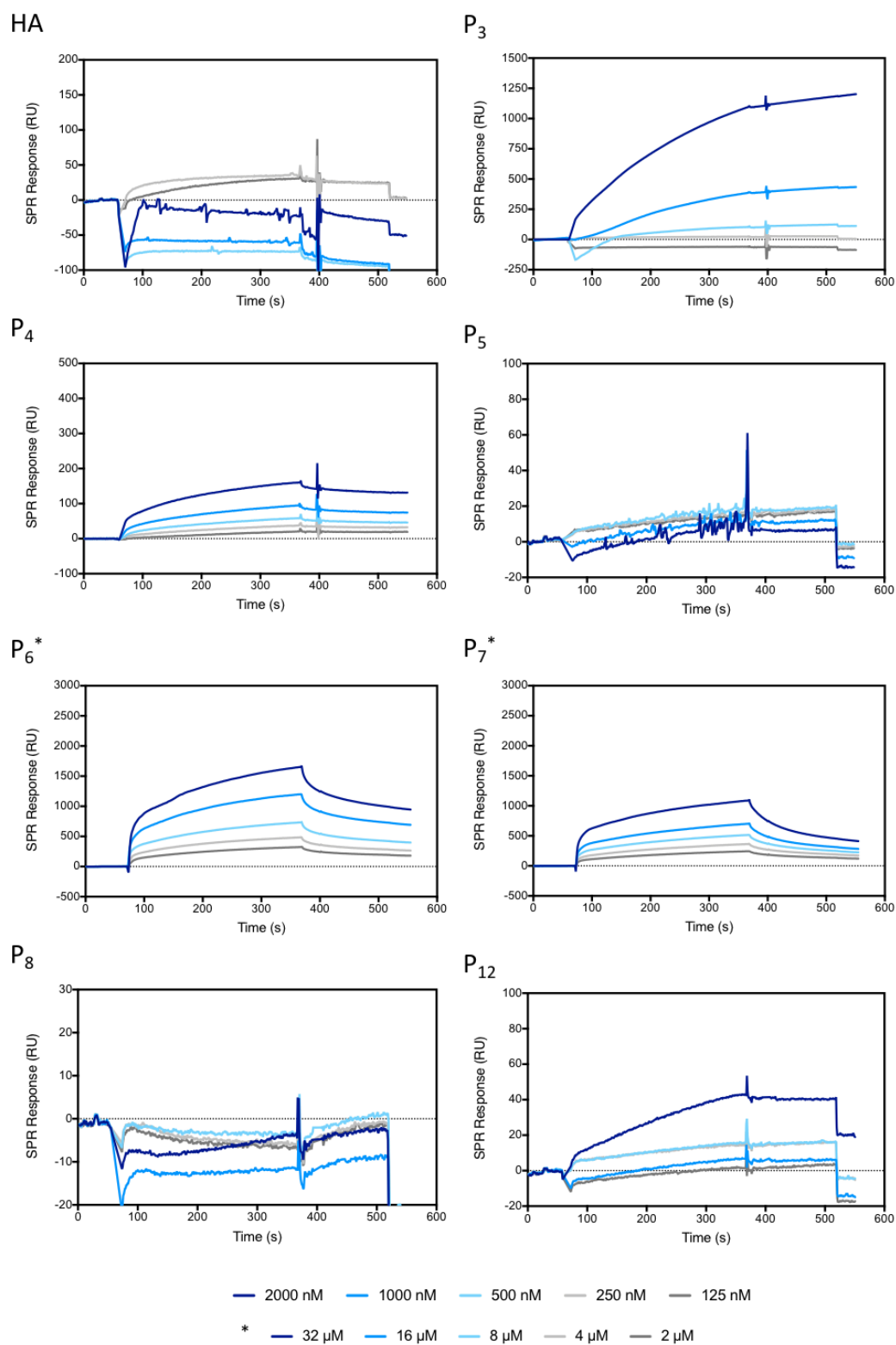
Figure A 4.13. SPR sensorgrams showing the binding of the various polymers on DC-SIGN with increased concentration used for P6 and P7 denoted by *.
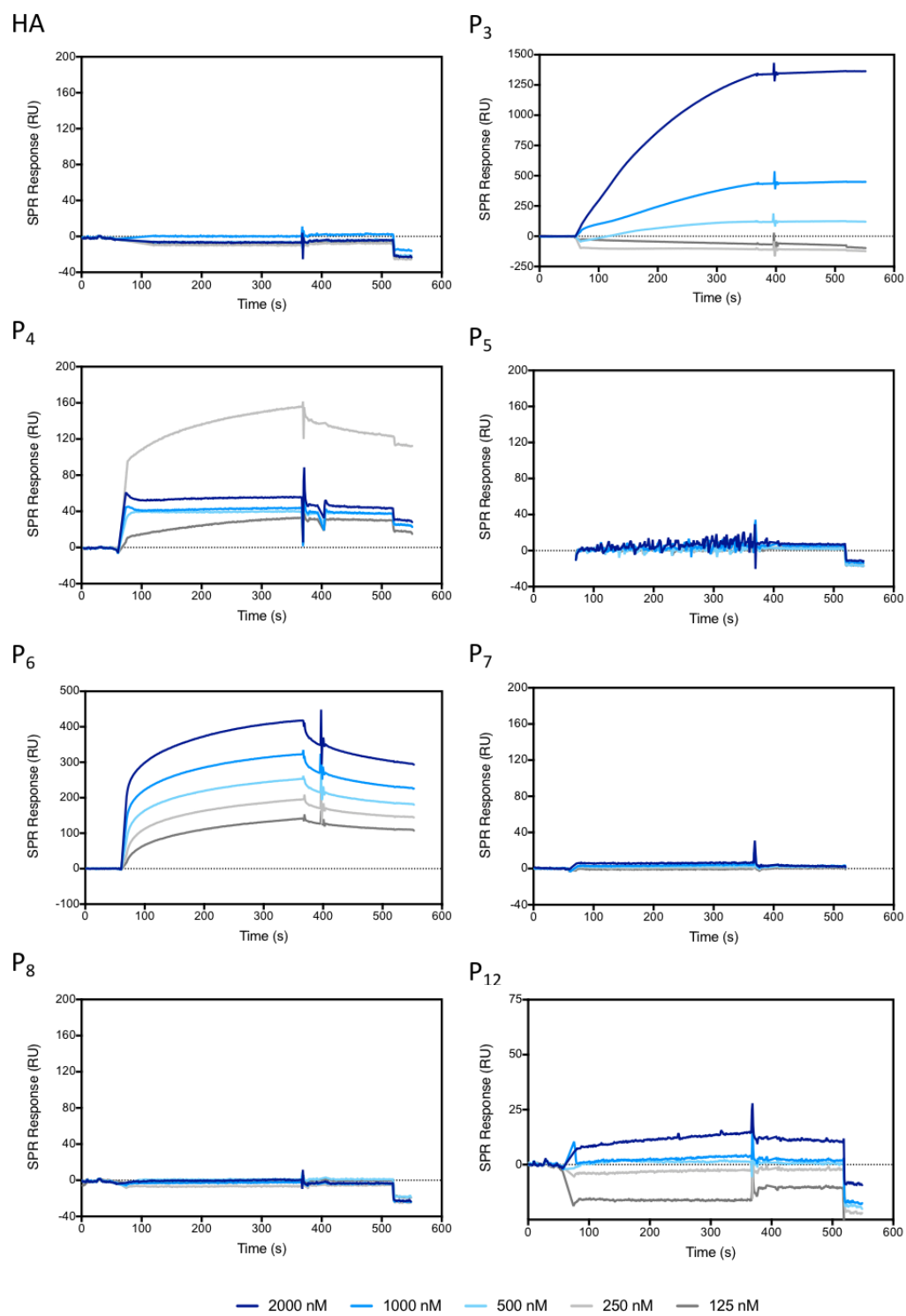
Figure A 4.14. SPR sensorgrams showing the binding of the various polymers on MBL.
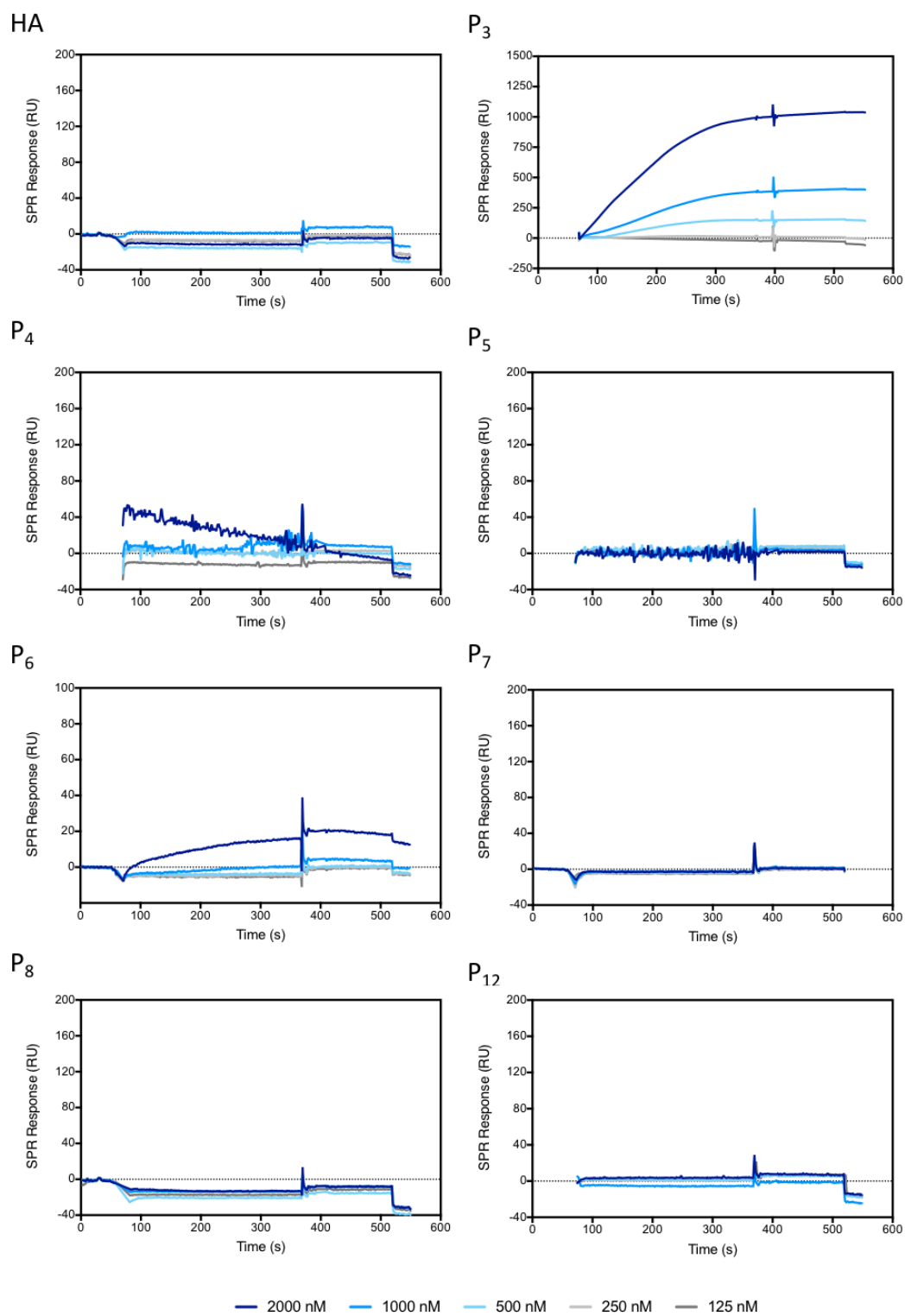
Figure A 4.15. SPR sensorgrams showing the binding of the various polymers on SP-D.
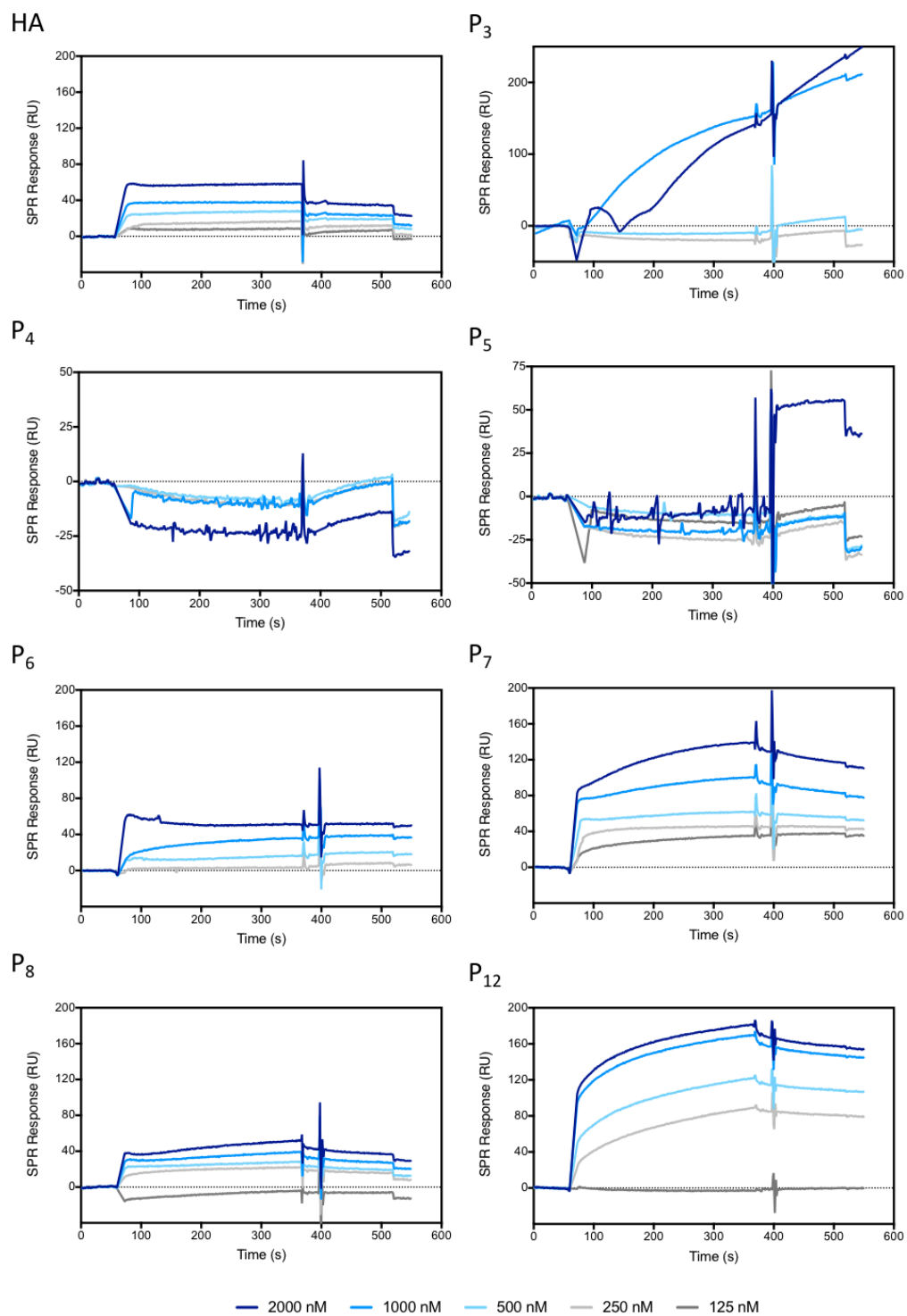
Figure A 4.16. SPR sensorgrams showing the binding of the various polymers on Dectin-1.
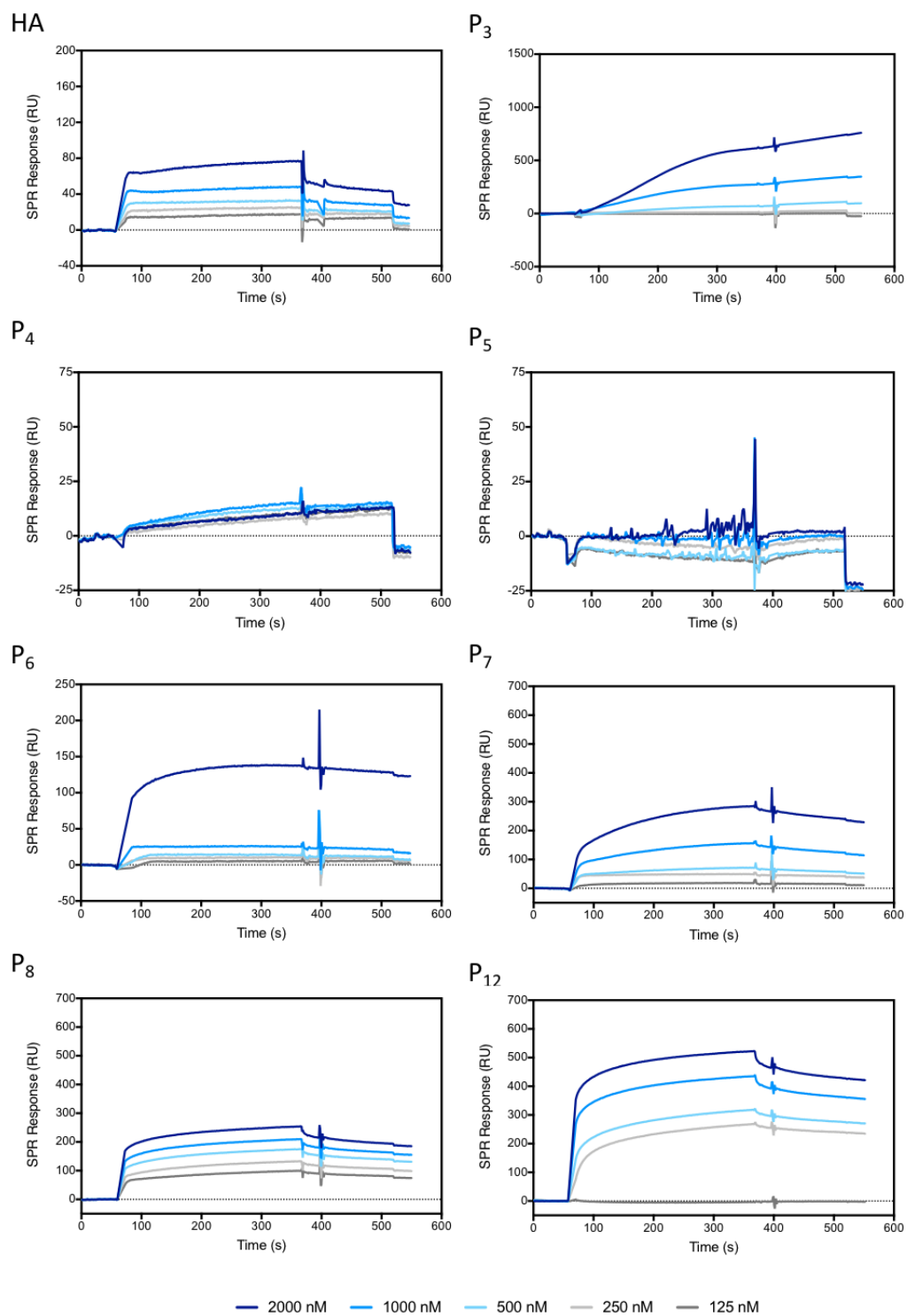
Figure A 4.17. SPR sensorgrams showing the binding of the various polymers on DEC-205.

References

1. Dicker, K.T., et al., *Hyaluronan: A Simple Polysaccharide with Diverse Biological Functions.* Acta Biomater, 2014. **10**(4): p. 1558-70.
2. Mummert, M.E., et al., *Development of a peptide inhibitor of hyaluronan-mediated leukocyte trafficking.* Journal of Experimental Medicine, 2000. **192**(6): p. 769-779.
3. Yang, B., et al., *Identification of a common hyaluronan binding motif in the hyaluronan binding proteins RHAMM, CD44 and link protein.* The EMBO Journal, 1994. **13**(2): p. 286-296.
4. Kiessling, L.L. and J.C. Grim, *Glycopolymer probes of signal transduction.* Chemical Society Reviews, 2013. **42**(10): p. 4476-4491.
5. Zelensky, A.N. and J.E. Gready, *The C-type lectin-like domain superfamily.* FEBS J, 2005. **272**(24): p. 6179-217.
6. Cowman, M.K., et al., *Viscoelastic Properties of Hyaluronan in Physiological Conditions.* F1000Research, 2015.
7. Falcone, S.J., D.M. Palmeri, and R.A. Berg, *Rheological and cohesive properties of hyaluronic acid.* J Biomed Mater Res A, 2006. **76**(4): p. 721-8.
8. Krause, W.E., E.G. Bellomo, and R.H. Colby, *Rheology of Sodium Hyaluronate under Physiological Conditions.* Biomacromolecules, 2001. **2**(1): p. 65-69.
9. J. Roe, R., *In Methods of X-Ray and Neutron Scattering in Polymer Science.* Vol. 3. 2000.
10. Walenta, E., *Small angle x-ray scattering. Von O. GLATTER und O. KRATKY. London: Academic Press Inc. Ltd. 1982. ISBN 0-12-286280-5. X, 515 Seiten, geb. £ 43,60; US $ 81.00.* Acta Polymerica, 1985. **36**(5): p. 296-296.
11. Pedersen, J.S. and P. Schurtenberger, *Scattering Functions of Semiflexible Polymers with and without Excluded Volume Effects.* Macromolecules, 1996. **29**(23): p. 7602-7612.
12. Beuermann, S. and M. Buback, *Rate coefficients of free-radical polymerization deduced from pulsed laser experiments.* Progress in Polymer Science, 2002. **27**(2): p. 191-254.
13. Barlow, T.R., J.C. Brendel, and S. Perrier, *Poly(bromoethyl acrylate): A Reactive Precursor for the Synthesis of Functional RAFT Materials.* Macromolecules, 2016. **49**(17): p. 6203-6212.
14. Lutz, J.-F., B. Kirci, and K. Matyjaszewski, *Synthesis of Well-Defined Alternating Copolymers by Controlled/Living Radical Polymerization in the Presence of Lewis Acids.* Macromolecules, 2003. **36**(9): p. 3136-3145.
15. Bataille, P., N. Sharifi-sanjani, and H. Rahmani, *Copolymerization of 2-Ethyl Hexyl Acrylate with Styrene in the Presence of Zncl2.* Journal of Macromolecular Science, Part A, 1994. **31**(6): p. 761-774.
16. Mishima, E. and S. Yamago, *Controlled alternating copolymerization of (meth)acrylates and vinyl ethers by using organoheteroatom-mediated living radical polymerization.* Macromolecular Rapid Communications, 2011. **32**(12): p. 893-8.
17. Banerjee, S., et al., *Organometallic-Mediated Alternating Radical Copolymerization of tert-Butyl-2-Trifluoromethacrylate with Vinyl Acetate and Synthesis of Block Copolymers Thereof.* Macromolecular Rapid Communications, 2017. **38**(15).
18. Kumar, J., A. Bousquet, and M.H. Stenzel, *Thiol-alkyne chemistry for the preparation of micelles with glycopolymer corona: dendritic surfaces versus linear glycopolymer in their ability to bind to lectins.* Macromol Rapid Commun, 2011. **32**(20): p. 1620-6.
19. Semsarilar, M., V. Ladmiral, and S.b. Perrier, *Highly Branched and Hyperbranched Glycopolymers via Reversible Addition−Fragmentation Chain Transfer Polymerization and Click Chemistry.* Macromolecules, 2010. **43**(3): p. 1438-1443.
20. Hoyle, C.E., A.B. Lowe, and C.N. Bowman, *Thiol-click chemistry: a multifaceted toolbox for small molecule and polymer synthesis.* Chemical Society Reviews, 2010. **39**(4): p. 1355-87.

21.   Lowe, A.B., C.E. Hoyle, and C.N. Bowman, *Thiol-yne click chemistry: A powerful and versatile methodology for materials synthesis.* Journal of Materials Chemistry, 2010. **20**(23): p. 4745.

22.   Aldrich, S. *VInylbenzyl Chloride SDS*. 2018   [cited 2018 23/09/2018]; Available from: https://www.sigmaaldrich.com/MSDS/MSDS/DisplayMSDSPage.do?country=GB& language=en&productNumber=436887&brand=ALDRICH&PageToGoToURL=htt ps%3A%2F%2Fwww.sigmaaldrich.com%2Fcatalog%2Fproduct%2Faldrich%2F43 6887%3Flang%3Den.

23.   Aldrich, S. *Maleimide SDS*. 2018   [cited 2018 23/09/2018]; Available from: https://www.sigmaaldrich.com/MSDS/MSDS/DisplayMSDSPage.do?country=GB& language=en&productNumber=129585&brand=ALDRICH&PageToGoToURL=htt ps%3A%2F%2Fwww.sigmaaldrich.com%2Fcatalog%2Fsearch%3Fterm%3Dmalei mide%26interface%3DAll%26N%3D0%26mode%3Dmatch%2520partialmax%26l ang%3Den%26region%3DGB%26focus%3Dproduct.

24.   Pranantyo, D., et al., *Increasing bacterial affinity and cytocompatibility with four-arm star glycopolymers and antimicrobial α-polylysine.* Polymer Chemistry, 2017. **8**(21): p. 3364-3373.

25.   Eissa, A.M., et al., *Glycosylated Nanoparticles as Efficient Antimicrobial Delivery Agents.* Biomacromolecules, 2016. **17**(8): p. 2672-9.

26.   Lequeux, I., et al., *Addition of antimicrobial properties to hyaluronic acid by grafting of antimicrobial peptide.* European Polymer Journal, 2014. **51**: p. 182-190.

27.   Cárdenas-Triviño, G., et al., *Synthesis and Bactericidal Properties of Hyaluronic Acid Doped with Metal Nanoparticles.* Journal of Nanomaterials, 2017. **2017**: p. 1-9.

28.   Pirnazar, P., et al., *Bacteriostatic Effects of Hyaluronic Acid.* Journal of Periodontology, 1999. **70**(4): p. 370-374.

29.   Carlson, G.A., et al., *Bacteriostatic properties of biomatrices against common orthopaedic pathogens.* Biochem Biophys Res Commun, 2004. **321**(2): p. 472-8.

30.   Brown, L., et al., *Through the wall: extracellular vesicles in Gram-positive bacteria, mycobacteria and fungi.* Nature Reviews Microbiology, 2015. **13**(10): p. 620-30.

31.   Kohda, D., et al., *Solution Structure of the Link Module: A Hyaluronan-Binding Domain Involved in Extracellular Matrix Stability and Cell Migration.* Cell, 1996. **86**(5): p. 767-775.

32.   Higman, V.A., et al., *Plasticity of the TSG-6 HA-binding loop and mobility in the TSG-6-HA complex revealed by NMR and X-ray crystallography.* Journal of Molecular Biology, 2007. **371**(3): p. 669-84.

33.   Banerji, S., et al., *Structures of the Cd44-hyaluronan complex provide insight into a fundamental carbohydrate-protein interaction.* Nature Structural & Molecular Biology, 2007. **14**(3): p. 234-9.

34.   Dicker, K.T., et al., *Hyaluronan: A Simple Polysaccharide with Diverse Biological Functions.* Acta Biomaterialia, 2014. **10**(4): p. 1558-70.

35.   Baggio, C., et al., *The cell surface receptor CD44: NMR based characterization of putative ligands.* ChemMedChem, 2016. **11**(10): p. 1097-1106.

36.   Bhattacharya, D., et al., *Impact of structurally modifying hyaluronic acid on CD44 interaction.* Journal of Materials Chemistry B, 2017. **5**(41): p. 8183-8192.

37.   Liu, L.K. and B.C. Finzel, *Fragment-based identification of an inducible binding site on cell surface receptor CD44 for the design of protein-carbohydrate interaction inhibitors.* Journal of Medicinal Chemistry, 2014. **57**(6): p. 2714-25.

38.   Love, J.C., et al., *Self-Assembled Monolayers of Thiolates on Metals as a Form of Nanotechnology.* Chemical Reviews, 2005. **105**(4): p. 1103-1170.

39.   Garcia-Vallejo, J.J. and Y. van Kooyk, *The physiological role of DC-SIGN: a tale of mice and men.* Trends Immunology, 2013. **34**(10): p. 482-6.

40.   Feinberg, H., et al., *Structural basis for selective recognition of oligosaccharides by DC-SIGN and DC-SIGNR.* Science, 2001. **294**(5549): p. 2163-6.

41.   Pederson, K., D.A. Mitchell, and J.H. Prestegard, *Structural characterization of the DC-SIGN-Lewis(X) complex.* Biochemistry, 2014. **53**(35): p. 5700-9.

42. Becer, C.R., et al., *High-Affinity Glycopolymer Binding to Human DC-SIGN and Disruption of DC-SIGN Interactions with HIV Envelope Glycoprotein.* Journal of the American Chemical Society, 2010. **132**(43): p. 15130-15132.

43. Yilmaz, G., et al., *The effect of linker length on ConA and DC-SIGN binding of S-glucosyl functionalized poly(2-oxazoline)s*. Vol. 9. 2017.

44. Zhang, Q., et al., *Sequence-Controlled Multi-Block Glycopolymers to Inhibit DC-SIGN-gp120 Binding.* Angewandte Chemie International Edition, 2013. **125**(16): p. 4531-4535.

45. Brown, G.D., J.A. Willment, and L. Whitehead, *C-type lectins in immunity and homeostasis.* Nat Rev Immunol, 2018. **18**(6): p. 374-389.

46. Turner, M.W., *Mannose-Binding Lectin (MBL) in Health and Disease.* Immunobiology, 1998. **199**(2): p. 327-339.

47. Takahashi, M., et al., *Mannose-Binding Lectin (MBL)-Associated Serine Protease (MASP)-1 Contributes to Activation of the Lectin Complement Pathway.* The Journal of Immunology, 2008. **180**(9): p. 6132-6138.

48. Shrive, A.K., et al., *Structural characterisation of ligand-binding determinants in human lung surfactant protein D: influence of Asp325.* Journal of Molecular Biology, 2009. **394**(4): p. 776-88.

49. Brown, G.D., *Dectin-1: a signalling non-TLR pattern-recognition receptor.* Nature Reviews Immunology, 2006. **6**(1): p. 33-43.

50. Ariizumi, K., et al., *Identification of a novel, dendritic cell-associated molecule, dectin-1, by subtractive cDNA cloning.* Journal of Biological Chemistry, 2000. **275**(26): p. 20157-67.

51. Brown, J., et al., *Structure of the fungal beta-glucan-binding immune receptor dectin-1: implications for function.* Protein Science, 2007. **16**(6): p. 1042-52.

52. Brown, G.D. and S. Gordon, *A new receptor for β-glucans.* Nature, 2001. **413**: p. 36.

53. Rapaka, R.R., et al., *Enhanced Defense against Pneumocystis carinii Mediated by a Novel Dectin-1 Receptor Fc Fusion Protein.* The Journal of Immunology, 2007. **178**(6): p. 3702-3712.

54. Shrimpton, R.E., et al., *CD205 (DEC-205): a recognition receptor for apoptotic and necrotic self.* Mol Immunol, 2009. **46**(6): p. 1229-39.

55. Lahoud, M.H., et al., *DEC-205 is a cell surface receptor for CpG oligonucleotides.* Proceedings of the National Academy of Sciences, 2012. **109**(40): p. 16270.

56. Guo, M., et al., *A monoclonal antibody to the DEC-205 endocytosis receptor on human dendritic cells.* Human Immunology, 2000. **61**(8): p. 729-738.

57. Sancho, D. and C. Reis e Sousa, *Sensing of cell death by myeloid C-type lectin receptors.* Curr Opin Immunol, 2013. **25**(1): p. 46-52.

58. Nickel, T., et al., *oxLDL uptake by dendritic cells induces upregulation of scavenger-receptors, maturation and differentiation.* Atherosclerosis, 2009. **205**(2): p. 442-50.

59. Nedvetzki, S., et al., *RHAMM, a receptor for hyaluronan-mediated motility, compensates for CD44 in inflamed CD44-knockout mice: A different interpretation of redundancy.* Proceedings of the National Academy of Sciences of the United States of America, 2004. **101**(52): p. 18081-18086.

60. Ilavsky, J. and P.R. Jemian, *Irena: tool suite for modeling and analysis of small-angle scattering.* Journal of Applied Crystallography, 2009. **42**(2): p. 347-353.

61. Kline, S.R., *Reduction and analysis of SANS and USANS data using IGOR Pro.* Journal of Applied Crystallography, 2006. **39**(6): p. 895-900.

62. Chen, W.-R., P.D. Butler, and L.J. Magid, *Incorporating Intermicellar Interactions in the Fitting of SANS Data from Cationic Wormlike Micelles.* Langmuir, 2006. **22**(15): p. 6539-6548.

63. Lutje Spelberg, J.H., et al., *Enzymatic dynamic kinetic resolution of epihalohydrins.* Tetrahedron: Asymmetry, 2004. **15**(7): p. 1095-1102.

64. Ting, W.-H., et al., *Facile synthetic route toward poly(vinyl benzyl amine) and its versatile intermediates.* Polymer, 2008. **49**(6): p. 1497-1505.

Chapter 5 Conclusion and Future Work

In this final chapter the aims laid out in chapter 1 are reviewed, recognizing the limitations of the work undertaken and identifying opportunities for further research.

"Synthesis of hyaluronic acid (HA)-based glycopolymers using alternating polymers"

Chapter 2 described the synthesis of HA-based glycopolymers using RAFT polymerisation followed by click reactions to graft the HA monosaccharides on the polymer backbone. This approach was shown to be effective and versatile, allowing the synthesis of glycopolymers based on other GAGs by sulfonation of grafted monosaccharide.

The main limitations of this approach are the RAFT end group used and the length of the polymers produced. As described in Chapter 2, the RAFT end group using NaN_3 caused some degree of disulphide bridging between the polymers. These bonds could not be reduced by PPh_3 as this would cause reduction of the azide formed upon the polymer. Controlled $NaBH_4$ reduction of the RAFT end group to a free thiol and clicking of a maleimide through thiol-ene reaction to the terminus thiol, could be a method to remove the end group and then inhibit the shoulder formation. The formation of disulphide bonds at the omega terminus of two polymers could in principle be used to form large polymers by linking them together (doubling the M_w), since the polymerisation showed lack of control at higher DPs. In Chapter 4, chain extension showed a promising route to form larger polymer backbones and this could be investigated to produce > 100 kDa polymers with Đ < 1.3.

"Engineering HA-binding peptides for self-Assembly with HA"

In chapter 3, several HA-binding peptides, derived by phage display (Pep-1) and taken from natural hyaladherins (CD44 and link protein), were exploited to create defined and controlled self-assembling nanostructures. It was shown that HABPep-3 formed stable complexes with HA, as the peptide formed elongated nanofibers. By contrast, the sequences derived from the HABPep-1 and HABPep-2 did not form stable complexes, due to their high-water solubility. Using a PA design, the HA-binding sequence could be displayed on the surface of spherical (micelle) or cylindrical (fibre-like) nanostructures, depending on the pH. The incorporation of HABPep-3 in a PA design (HABPA-3) led to the formation of shorter nanofibers compared to the elongated fibres before modification. HABPA-3 lacks the self-assembly structure of long elongated fibres in order to produce gel structures. The next steps in the design

of self-assembling versions of Pep-1 would be to include V_3A_3 domain close to the alkyl tail to promote the formation of elongated fibres able to interact with HA in a controlled manner. Other possibilities to explore would be to use other sequences from HA-binding proteins (Table 1.7), as the variations in peptide sequence could lead to unique self-assemblies.

"Comparing the properties of HA synthetic analogues with natural HA"

The results presented in chapter 4 showed that the glycopolymers produced do not exhibit physical properties similar to those of natural HA. The differences arise mainly from the lack of a glycosidic bond and shorter polymer length. The polymer backbone does not give the rigidity of the glycosidic bond between the monosaccharides, compare to HA. These will lead to different internal hydrogen bonding interaction causing changes in the HA properties in solution. The glycopolymers showed the ability to aggregate as seen through the CAC measurements and TEM imaging. The low cytotoxicity towards different cell types suggest their potential use in biomedical applications, such as a drug delivery vehicle. Hydrophobic drugs can be incorporated within the core of the glycopolymer aggregates, similarly to the CAC assay using the hydrophobic nile red dye.

"HA glycopolymers as probes to elucidate HA binding processes"

In the later section of chapter 4, the ability of HA glycopolymers to interact with the HA-binding Pep-1 (HABPep-1), described in chapter 4, was investigated by SPR with the binding results showing patterns and trends in the structure of the saccharide and the sequence of the glycopolymer (Table 5.1). This allowed us to probe which HA sugar might be involved in the binding process. These studies were extended to HA-binding proteins (CD44) as well as to other (non-specific) carbohydrate-binding proteins (lectins: Dectin-1 and DEC-205).

Table 5.1. Summary table of binding hits (blue) of the glycopolymers and the lectins.

Lectin	Glycopolymers								Monosaccharide to test
	HA	P3	P4	P5	P6	P7	P8	P12	
DC-SIGN		blue	blue		blue	blue			ManNAc, ManA
MBL		blue	blue		blue				ManNAc, IdoA
SP-D		blue			blue				6-deoxy-D-glucose & 2-deoxy-D-glucose
Dectin-1	blue					blue		blue	Swap GlcNAc in P8 and P12
DEC-205	blue		blue		blue			blue	Swap GlcNAc in P8 and P12

In the SPR measurements, the HABPep-3 was attached to the chip surface rather than the glycopolymer. The peptide used is at most 12 mers away of the gold surface whereas the glycopolymers are roughly 50 repeats (Figure 5.1). Through the RAFT end group of the trithioester, the glycopolymers could bind to the gold surface. Whilst the glycopolymer have shown to aggregate in solution, the gold surface will restrict to a degree this aggregation to display the monosaccharides across the surface of the gold.
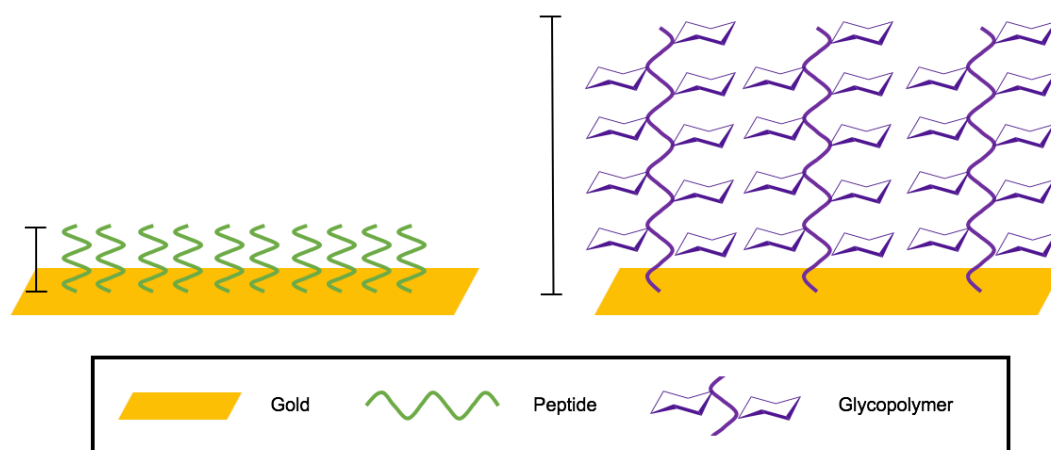

Figure 5.1. Schematic representation showing the potential limitation of the peptide bound onto the gold surface (left) compared to the glycopolymers (right) due to the distance from the surface.

QCM showed the binding of P7 to the surface of the gold crystal followed by the binding of HABPep-3 to the glycopolymer as seen by the positive mass increase upon every addition. The QCM will provide further validation of the SPR results. From the binding results of this first generation of HA glycopolymers, a second generation can be obtained as different combinations of statistical and alternating glycopolymers could provide a key insight the binding to lectins. By building up a large library of glycopolymers with the binding to the lectins, structural similarities can be determined to find glycopolymers that produce a strong K_D as either potential inhibitors or agonists for the lectins.

An alternative method to measure the binding affinity is isothermal titration calorimetry (ITC). By measuring small heat changes between a reference cell and the reaction cell in which the ligand is being titrated into the cell the heat of binding can be quantified. Preliminary ITC experiments with HA and HABPep-3 showed that the interactions were masked by the heat of dilution of HABPep-3 in water rather than as heat of binding between HABPep-3 and HA (Figure 5.2). HABPep-3 was shown to have a low CAC of 6.7×10^{-5} M and dilution of HABPep-3 below the CAC, generates

heat that is entropic rather than enthalpic. Based on these results, SPR and QCM were considered more adequate methods.
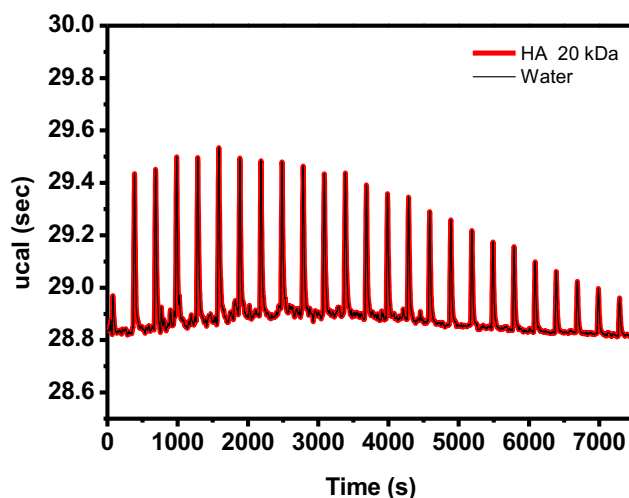

Figure 5.2. ITC graph of Pep-1 (30 μM) titrated with HA 20 kDa (300 μM) (red) and against water (black) showing the overlay between the two graphs.

The ability of the glycopolymers to bind to a gold surface opens the possibility to explore their attachment to gold nanoparticles (NPs). The RAFT group possess at C_{16} tail which would help the stabilization of the gold NPs with the monosaccharides displayed from the central gold core. This method will allow to exploit of their biological effects of the glycopolymers were shown to be non-toxic. The gold can be imaged by TEM to track the glycopolymers in vitro.

Since the acrylate polymers did not show any CAC, compared to the styrene-based glycopolymers, it can be concluded that the polymer backbone affects the conformation of the glycopolymers in water. By completing the synthesis of the dual acrylate glycopolymer synthesis, (Scheme 4.4) as well as the statistical, a complete comparison can be undertaken for the styrenic and acrylate-based glycopolymers.

This work has shown for the first time the synthesis of alternating glycopolymers based on the structure of HA. The same polymer backbone can be used as an interchangeable platform to create glycopolymers of sulfonated GAGs. If the biological properties of these new GAG glycopolymers are comparable to other sulfonated glycomimetics reported in the literature, the synthetic route to obtain GAG-based glycopolymers can be greatly simplified.